DAA/LANGLEY
P-FILE
35266
P. 390
NAG1-713

PLATES AND SHELLS CONTAINING A SURFACE CRACK UNDER GENERAL LOADING CONDITIONS

by

Paul F. Joseph

and

Fazil Erdogan

Lehigh University

Bethlehem, Pennsylvania

July 1987

(NASA-CR-181052) PLATES AND SHELLS CONTAINING A SURFACE CRACK UNDER GENERAL LOADING CONDITIONS (Lehigh Univ.) 390 p CSCL 20K
Avail: NTIS HC A17/MF A01
N87-27226
Unclas
G3/39 0085266

THE NATIONAL AERONAUTICS AND SPACE ADMINISTRATION

GRANT NAG-1-713

CONTENTS

	Page
Abstract	1
Chapter 1. Introduction, Literature Survey, and Overview	3
1.1 Introduction	3
1.2 Literature Survey	5
1.3 Overview	11
Chapter 2. The Line-Spring Model	13
2.1 Introduction	13
2.2 Derivation of the Compliance Functions	15
2.3 Endpoint Behavior	21
Chapter 3. Through Cracks in Plates	37
3.1 Formulation	37
3.2 Symmetric Loading, Mode 1	47
3.2.1 Tension	48
3.2.2 Bending	51
3.2.3 Thin Plate Bending	57
3.3 Skew-Symmetric Loading, Modes 2 & 3	60
Chapter 4. Part-Through Cracks in Plates	85
4.1 Mode 1	85
4.1.1 Contact Bending	88
4.1.2 Using the LSM to Calculate SIFs at the Corners	89
4.1.3 Double Cracks	94
4.2 Modes 2 & 3	95
Chapter 5. Through Cracks in Shallow Shells	168
5.1 Formulation	168
5.2 Symmetric Loading, Mode 1	177
5.3 Symmetric Loading, Mode 1 Results	182
5.4 Skew-Symmetric Loading, Modes 2 & 3	184
5.5 Skew-Symmetric Loading, Modes 2 & 3 Results	189
Chapter 6. Part-Through Cracks in Shells	211
6.1 Mode 1	213
6.2 Modes 2 & 3	215
Chapter 7. Conclusions and Future Work	270
List of References	274
Appendices	281
Vita	382

APPENDICES

		Page
Appendix A.	Non-Dimensional Variables and Useful Formulae ...	281
A.1	Non-Dimensional Plate and Shell Quantities	281
A.2	Some Useful Properties of Modified Bessel Functions	281
A.3	Chebychev Polynomials	282
A.4	Finite-Part, Cauchy Principal Value, and Log Integrals	283
Appendix B.	Finite-Part Integrals	287
Appendix C.	The Compliance Functions	293
C.1	Governing Equations for in-Plane Loading	293
C.1.1	Mode 1	294
C.1.2	Mode 2	300
C.2	Anti-Plane Shear	304
C.3	Edge Crack SIF Curve Fitting	308
C.4	Line-Spring Model SIF Normalization	310
Appendix D.	Determination of the Weight Functions	314
Appendix E.	Numerical Methods for the Solution of Singular Integral Equations	318
E.1	Quadrature	318
E.2	Collocation	321
Appendix F.	Short Crack Analysis of the Compliance Functions	330
Appendix G.	Stress Intensity Factors	336
G.1	Elasticity Theory	336
G.2	Plate and Shell Theory	339
Appendix H.	Thin Plate Bending Limit of Fredholm Kernel	349
Appendix I.	Log Integrals	354
Appendix J.	Asymptotic Analysis of the Shell Infinite Integrals	360
J.1	Asymptotic Expansions for the Roots of the Characteristic Equation	360
J.2	Symmetric Asymptotic Analysis	362
J.3	Skew-Symmetric Asymptotic Analysis	371

LIST OF TABLES

		Page
Tables 2.1,2	Approximate crack profiles for use with the LSM to improve numerical convergence.	27
Tables 2.3,4	Normalized SIFs for the approximate profiles given in table 2.1.	28
Tables 2.5,6	Normalized SIFs for the approximate profiles given in table 2.2.	29
Table 3.1	The effect of Poisson's ratio ν and crack length to plate thickness ratio a/h on the normalized bending stress intensity factor.	65
Table 3.2	The ratio of the crack surface rotation for Reissner's theory to that of the classical theory at the center of a cracked plate subjected to bending.	66
Table 3.3	Bending stress intensity factors for a plate with two collinear cracks.	67
Tables 3.4-6	The effect of crack length to plate thickness ratio a/h on the normalized stress intensity factors for out-of-plane shear and for twisting.	68-70
Tables 3.7a,b	Stress intensity factors for a plate with two collinear cracks subjected to out-of-plane shear loading (a) and to twisting (b).	71,72
Tables 4.1-10a,b	Normalized SIF distribution for rectangular (a) and semi-elliptical surface cracks in a plate under tension and bending loads.	99-118
Table 4.11	Normalized SIF at the center of a semi-elliptical crack subjected to tension and to bending.	119
Table 4.12	The effect of Poisson's ratio on the normalized SIF at the center of a semi-elliptical crack subjected to tension and to bending.	120
Tables 4.13-14a,b	The effect of normalization on the SIFs for the LSM for deep semi-elliptical cracks.	121,122

Table 4.15	Contact curve for crack closure in bending.	123
Table 4.16	Normalized SIFs for two interacting semi-elliptical surface cracks.	124
Table 4.17	The normalized SIF at the maximum penetration point of two interacting surface cracks.	125
Tables 4.18-21a,b	Normalized SIF distribution for rectangular (a) and semi-elliptical surface cracks in a plate under out-of-plane shear, in-plane shear, and twisting loads.	126-149
Table 4.22	Normalized SIF at the center of a semi-elliptical crack subjected to out-of-plane shear, in-plane shear, and twisting loads.	150
Table 4.23	Poisson's ratio effect of the center value of the SIF.	151
Table 4.24	The LSM approximation of the corner SIF of a semi-elliptical crack for out-of-plane shear, in-plane shear, and twisting loading.	152
Tables 5.1-8	Mode 1 SIFs for symmetric collinear through cracks in a cylinder.	191-198
Tables 5.9-14	Modes 2 & 3 SIFs for symmetric collinear through cracks in a cylinder.	199-204
Tables 6.1-5	Normalized SIFs at the center of a semi-elliptical surface crack in a sphere, Mode 1.	219-223
Table 6.6	Distribution of the mode 1 SIF along a semi-elliptical surface crack in a toroidal shell.	224
Tables 6.7-22	Normalized mode 1 SIFs for the center of a semi-elliptical surface crack in a toroidal shell.	225-240
Tables 6.23-34	Normalized SIFs for the skew-symmetric loading of a cylinder with a semi-elliptical surface crack.	241-252
Tables 6.35-46	Normalized mode 2&3 SIFs for the center a semi-elliptical surface crack in a toroidal shell.	253-264

Table C.1	Stress intensity factors in an edge-cracked strip.	311
Table C.2,3	Coefficients for the Compliance Functions.	312
Table E.1	Convergence comparison of Chebychev Polynomials and power series.	327
Table E.2	Convergence of expansion coefficients.	328
Table E.3	The effect of the collocation points on convergence.	329
Table G.1	Benthem's results for the strength of the stress singularity at the free surface.	347
Table I.1	Convergence of log integrals.	357
Table I.2	The effect of log integrals on the calculation of SIFs for bending.	358
Table I.3	The effect of log integrals on the calculation of SIFs for out-of-plane shear and twisting.	359

LIST OF FIGURES

Figure		Page
Figure 2.1	The shell geometry.	30
Figure 2.2	Representation of the two-dimensional stress state in the net ligament with stress resultants for the mode 1 problem.	31
Figure 2.3a-c	Force and Displacement quantities as defined by plate or shell theory that are used in the mode 1 line-spring model.	32-34
Figure 2.4	The superposition used to solve part-through crack problems with the line-spring model. All solutions are obtained for the problem in the lower right (the perturbation problem) where the only loads are applied to the crack surfaces.	35
Figure 2.5	The corresponding plane strain problem.	36
Figure 3.1a-d	Normalized stress intensity factors in a plate with two identical collinear cracks of half length a/h=1 loaded in tension (a), bending (b), out-of-plane shear (c), and twisting (d).	73
Figure 3.2	Normalized stress intensity factors in a plate for bending.	74
Figure 3.3a-c	Plots of the Fredholm integral term from Reissner's theory of plate bending (Eqns. 3.129, 140) for a/h=10 (a), a/h=100 (b), a/h=1000 (c), (solid lines), compared to the limit from Appendix E, (dashed lines).	75-77
Figures 3.4,5	Plots of the normalized rotation for plate bending for a/h=10,100,1000 from Reissner's theory compared to classical theory, ν=.3,	78,79
Figure 3.6	The ratio of crack surface rotation for Reissner's theory to that of the classical theory at the center of a cracked plate subjected to bending, ν=.3.	80
Figure 3.7	Bending stresses in front of the crack tip for a/h=.5,10. ν=.3	81
Figure 3.8a,b	Geometry of the double crack for (a) unequal length and (b) equal length cracks.	82

Figure 3.9a,b	Stresses in front of the crack tip resulting from out-of-plane shear loading (a), and from twisting (b). ν=.3	83,84
Figures 4.1-4	Comparison of mode 1 line spring model with and without transverse shear deformation to Newman's and Raju's finite element solution.	153-156
Figure 4.5	Geometry of the bending contact problem.	157
Figure 4.6	Line-spring model approximation to the stress intensity factor at the corner of a rectangular surface crack.	158
Figure 4.7	Line-spring model approximation to the stress intensity factor at the corner of 1/4 power "semi-elliptical" surface crack.	159
Figure 4.8	Line-spring model approximation to the stress intensity factor at the corner of a through crack subjected to bending allowing for contact stresses as compared to the value assuming no contact.	160
Figure 4.9	The LSM approximation to the stress intensity factor at the corner of a semi-elliptical surface crack.	161
Figures 4.10-4.15	Normalized stress intensity factor profiles for the mode 2,3 line-spring model for rectangular and semi-elliptical surface cracks subjected to out-of-plane shear, in-plane shear and twisting.	162-167
Figures 5.1-4	Stresses ahead of a crack in a cylinder subjected to membrane and bending loads.	205-208
Figures 5.5,6	Out-of-plane displacement $w(0^+,y)$ as measured from y=0 in the deformed position for a cylinder with a through crack.	209,210
Figures 6.1,2	Comparison of the mode 1 LSM with results from Refs. [33,40] for the normalized SIF along an axial, internal, semi-elliptical surface crack in a pressurized cylinder.	265,266
Figures 6.3,4	Out-of-plane displacement $w(0^+,y)$ as measured from y=0 in the deformed position for a cylinder with a surface crack.	267,268
Figure 6.5	The geometry of the toroidal shell.	269

Figure C.1	The geometry and superposition of the cracked strip.	313
Figure G.1	Crack surface displacement for the different modes of fracture.	348

ABSTRACT

In this study various through and part-through crack problems in plates and shells are considered. The line-spring model of Rice and Levy is generalized to the skew-symmetric case to solve surface crack problems involving mixed-mode, coplanar crack growth. New compliance functions are introduced which are valid for crack depth to thickness ratios at least up to .95. This includes expressions for tension and bending originally used by the model for symmetric loading as well as new expressions for in-plane shear, out-of-plane shear, and twisting for the skew-symmetric case. Transverse shear deformation is taken into account in the plate and shell theories and this effect is shown to be important in comparing stress intensity factors obtained from the plate theory with three-dimensional surface crack solutions. Stress intensity factor results for cylinders obtained by the line-spring model also compare well with the three-dimensional solutions.

By using the line-spring approach, for a given crack length to thickness ratio, stress intensity factors can be obtained for the through crack and for part-through cracks of any crack front shape, without need for recalculating integrals that take up the bulk of the computer time. Therefore, parameter studies involving crack length, crack depth, shell type, and shell curvature are made in some detail. The results presented are believed to be useful in brittle fracture, and more importantly, in fatigue crack propagation studies.

The line-spring model is also used to solve the contact problem in plate bending. Investigations into stress intensity factors for

crack growth in the length direction (as opposed to growth in the thickness direction), are also made by using the model. The endpoint behavior of the results given by the line-spring model is considered in detail.

In addition to part-through crack problems, some results for single and double through cracks are presented. The thin plate bending limit of Reissner's theory and its relationship to the classical theory are reconsidered.

All problems considered in this study are of the mixed boundary value type and are reduced to strongly singular integral equations which make use of the finite-part integrals of Hadamard. These equations are obtained by using displacement quantities as the unknowns, rather than the more commonly used displacement derivatives which lead to integral equations with Cauchy singularities. The equations are solved numerically in a manner that is believed to be very efficient.

CHAPTER 1

Introduction, Literature Survey and Overview

1.1 Introduction

Pressure vessels, pipelines, containers, ship hulls, etc. are all shell-like structures which can fail by fracture. The designers of these components must take this into account as such failures are often catastrophic, endangering lives and the environment. The fracture process typically starts with a small material defect or weld imperfection that grows in fatigue which is driven by mechanical or environmental conditions. Eventually the flaw may be characterized as a macroscopic surface crack. This surface or part-through crack then continues its growth through the thickness, leading to failure by leaking or to unstable fracture.

In the discipline of fracture mechanics one usually assumes an initial flaw configuration, and then seeks to obtain certain fracture parameters that are believed to govern the tendency of the crack to grow. In the case of brittle fractures and more importantly, fractures by fatigue, the stress intensity factor (SIF) is the most commonly used parameter.

The analysis of through cracks in thin structures was first performed within the theory of plates and shells, which allows for a straightforward analytical solution for practical geometries such as cylinders, spheres, and pipe elbows. The problem is of the mixed boundary value type and is reduced to a system of dual integral equations or a system of singular integral equations (SIE), most often

the latter. It is usually assumed that the curvatures are constant and the shell has constant thickness, the material is homogeneous, isotropic, or perhaps specially orthotropic, and behaves in a linear elastic manner. Three-dimensional effects due to the interaction between the free surface and the crack plane are neglected. Benthem [1] has investigated these effects for a crack in a half space. To date no research has included this surface layer behavior in a problem with a practical geometry.

The surface crack has a three-dimensional geometry which seems accessible only to either analytical or numerical techniques from the theory of elasticity. Rice in 1972 [2,3] introduced the so-called line-spring model (LSM) which transformed the part-through crack into a through crack problem by making use of the edge-cracked strip plane strain solution. This model has been shown to give very good results in spite of its simplicity. Therefore, within the limitations of this model, both through and part-through crack problems can be solved with the same plate or shell theory formulation.

It is important to point out that for a through crack the primary interest is in the behavior of the stress state at and near the crack tip. Whereas, for surface cracks the most important point is the deepest penetration point of the crack front. The model in its original form is limited to symmetric (mode 1) fracture, and cannot predict behavior at the endpoint where the crack front meets the free surface (again neglecting the free surface effect).

1.2 Literature Survey

The problem of determining the singular stress field in an infinitely large plate of thickness h, containing a finite crack of half-length a, subjected to tension was studied by Williams [4] in 1957. In a 1960 paper [5] Williams also investigated the problem of plate bending by using the classical plate theory. Although in the bending problem the stress singularity was observed to be the same as in the plane elasticity case, (namely $r^{-1/2}$), the angular variation of the stresses around the crack tip was found to be different. Shortly after this paper was published, Knowles and Wang [6] showed that this discrepancy could be removed if the 6th order Reissner plate theory [7,8], which includes transverse shear deformation, was used. This theory allows for the satisfaction of all three crack surface boundary conditions ($M_{xy}=0$, $V_x=0$, $N_{xy}=0$), instead of combining these three conditions into two as did the previous theory by use of the Kirchhoff condition, ($N_{xy}=0$, $V_x+\frac{\partial M_{xy}}{\partial y}=0$). The work of Knowles and Wang was later made more complete by Hartranft and Sih [9] and by Wang [10]. In these papers the SIF solution is given for various crack length to plate thickness ratios, i.e. (a/h).

In the paper by Knowles and Wang it was observed that Reissner's theory approaches classical theory in the limit as $h/a \to 0$, or as the plate gets thin. This limit is well behaved except at the crack tip where boundary layer behavior in the SIF is indicated by graphical solutions [9,10]. This "discontinuous" behavior was discussed by Civelek and Erdogan [11] with the aid of more complete and more precise numerical results, but not proven. Also it was pointed out by

Hartranft [12] that this limit should not be used. For more discussion of this problem see Sih [13].

In all of the preceeding papers the solution was limited to symmetric (mode 1) loading, which includes tension and bending. Wang in 1970 [14] was the first to consider twisting, again with Reissner's plate theory. The asymptotic stress field was shown to be compatible with 2-D elasticity, therefore mode 2 and 3 SIFs had the same elasticity definition. This problem is not approachable by the classical theory for the same reasons that apply to plate bending. The results of Wang [14] were extended by Delale and Erdogan [15] to include specially orthotropic materials.

The first analysis of cracks in shells was presented by Folias in 1965 for a cracked sphere [16,17] and for an axially cracked cylinder [18]. The circumferentially cracked cylinder was investigated in 1967 [19]. The results in these papers are asymptotic in nature for short cracks. A shallow shell theory was also used which linearizes the governing equations. The full curvature problem is non-linear and has not yet been solved by analytical techniques although Sanders [20,21] has used a thin shell theory which is linear yet valid for a complete cylinder to obtain energy release rates (not SIFs) for long cracks. The validity of shallow shell analysis can be summarized as follows: for a given shell radius, the smaller the thickness h, the more appropriate the shell assumption; the shorter the crack length 2a, the more appropriate the shallow shell assumption.

In the late 1960's Erdogan and Kibler [22] and Copley and Sanders [23] provided a more complete solution to the problems studied by

Folias. Although the same approximate, shallow shell equations are employed, the numerical techniques for the solution of the singular integral equations are exact (to any reasonable specified degree of accuracy).

The major shortcoming of these early shell solutions, including the work of Sanders [20-21], was the neglect of transverse shear deformation as in the early plate bending problem. In shells, since extension and bending are coupled, the elasticity concept of the SIF cannot be used with these 8th order theories without redefinition. As bending becomes more of a factor in the geometry and loading considered, the results become less accurate. Also the contribution from extension is affected. It was Sih and Hagendorf [24] in 1974 who first solved cracked shell problems with transverse shear accounted for; see also a second paper by Sih [25]. Later papers, which used the shallow shell governing equations due to Naghdi [26], provided more exact and extensive results for the axially cracked cylinder, see Krenk [27], and for the circumferentially cracked cylinder, see Delale and Erdogan [28]. It was shown in these papers that the asymptotic stress field obtained is compatible with the solution from the theory of elastic fracture mechanics; therefore standard fracture parameters such as the SIF could be used. The skew-symmetric shell problem was studied by Delale [29] and it was shown that the mode 2 and 3 stress intensity factors also have the same elasticity definition. Therefore it appears that the simplest shell theory that may be used to study cracks in plates and shells to obtain SIFs is one that includes transverse shear deformation, [7,8,26]. In 1983 Yashi and Erdogan

[30] solved the shallow shell problem for a crack arbitrarily oriented with respect to a principal line of curvature. They used the same formulation as was used by Delale and Erdogan [28], but the analysis involved ten unknowns instead of two [28] or three [29] because of the loss of symmetry.

In all the previous shell solutions which included transverse shear deformation, the assumption of shallowness has been applied. Barsoum, Loomis, and Stewart [31] were the first to publish results to the complete through crack problem in a cylinder by using finite elements which took into account transverse shear deformation. There is good agreement between these results and the results from the shallow shell theories [22,27], even for relatively long cracks. More recent finite element calculations by Ehlers [32] disagree with the work of Barsoum, et. al. However these calculations are limited to $a/R > .5$, which for a "shallow shell", is a very long crack. More work must be done to determine the error due to the shallow shell assumption for increasing a/R. This theory may be regarded as an asymptotic solution for small a/R.

The study of surface cracks in plates and shells has a more detailed history involving three-dimensional numerical techniques because it is both more important and more difficult. In addition to the finite element method [33,34], there is the alternating method [35,36], the boundary integral equation method [37], the finite element alternating method [38-40], the method of weight functions [41,42], and the body force method [43]. The standard solution for plates is that of Newman and Raju [33]. The more recent work of

Isida, Noyuchi, and Yoshida [43] have verified these results and perhaps slightly improved upon them. For reviews of the various solutions and methods see [44-46].

The previous studies for surface cracks deal only with mode 1 loading, which is the most important mode for crack extension. However there are situations that involve twisting and shearing that cannot be neglected. For instance, depending on the geometry, when these loadings are primary, a secondary mode 1 contribution can result. The body force method [47] has recently been applied to an inclined surface crack in a half space which involved all modes of fracture. This problem has not received much attention in the literature, because it is less important than mode 1, and also more expensive to solve.

As mentioned previously the line-spring model allows for the solution of the 3-D surface crack problem within the 2-D theory of plates and shells. This reduces the computational effort considerably. Therefore more extensive parameter studies can be made once the model has been verified by the more accurate three-dimensional methods.

Since the introduction of the model in 1972 [2], there have been numerous papers suggesting improvements and modifications. As with the through crack problem the use of a Reissner plate theory has improved the results [48,49], especially for realistic crack lengths on the order of $a/h=1$. The classical theory gives good results for $a/h\geq 2$, and in the limit as $a/h\to\infty$ the two theories are the same (for the LSM). The initial suggestions of Rice [3] concerning the use of

the model to study plasticity effects have been advanced by Parks [50] and more recently by Miyoshi, Shiratori, and Yoshida [51] who used the model with thick shell finite elements to predict crack growth. Other researchers [49,52] have devised techniques that implement a numerical plate or shell solution instead of the original singular integral equation procedure. This is an advantage in shell analysis, because to date, the analytical techniques are limited to the shallow shell theory which is not valid for long cracks. However the long surface crack is not a practical geometry, and if needed, can usually be approximated by a plane strain solution.

Yang in a recent paper [53] has considered crack surface loading in the form of a polynomial to solve problems of residual or thermal stress. The original LSM used only the constant and linear terms associated with tension and bending plate variables respectively. Theocaris and Wu [54,55] have suggested a way to determine the SIF at the corner of a surface crack. This method seems inappropriate since they have used the classical theory of plate bending which is unable to predict this value for the much simpler through crack case. The finite width plate has been solved by Boduroglu and Erdogan [56,57]. All previous LSM solutions were for an "infinitely large" plate. Erdogan and Aksel have considered the cavity in a plate [58] and Wu and Erdogan have extended the LSM to an orthotropic plate [59]. Delale and Erdogan [60] have used the model with a shallow shell formulation to predict SIFs for surface cracks in cylinders for axial, circumferential, inner and outer cracks.

1.3 Overview

The primary interests in this study are to extend the LSM to the mixed-mode case and to use the model to approximate crack growth tendencies in the length direction as opposed to the depth direction for which it already applies. In Chapter 2 the line-spring model for mixed-mode loading conditions is derived. Furthermore, the mode 1 compliance relations [61-63,48] are improved by using the recent edge-cracked strip solution of Kaya [64]. The curves are fit to data for $0 \leq (L_0/h) \leq .95$ and may be used for the entire range of values as the curves have the proper asymptotic behavior for $(L_0/h) \to 1$ [65]. Also the necessary solutions for modes 2 and 3 are obtained.

In Chapter 3 some unsolved through crack problems in plates are considered and the thin plate limit for Reissner's theory is investigated to better understand the validity of the classical plate theory when applied to the LSM. In Chapter 4 the LSM, with and without including the transverse shear deformation, is compared to finite element surface crack solutions. SIF comparisons are also made for the corner of a semi-elliptical surface crack. The contact bending or crack closure problem, a difficult unsolved 3-D problem, is solved in a straightforward manner. Also extensive SIF results are given for both rectangular and semi-elliptical crack shapes under all five loading conditions, i.e. tension, bending, out-of-plane shear, in-plane shear, and twisting.

Crack problems in shells are considered in Chapters 5 and 6. Comparisons of surface crack solutions obtained with the model are made with 3-D solutions from the literature [34,40]. Various unsolved

through and part-through problems are considered and the effect of curvature is studied for both the symmetric and the skew-symmetric cases.

All integral equations are derived with displacement quantities as unknowns. The resulting equations are, therefore, strongly singular and make use of the finite-part integrals of Hadamard [66], see also Kaya [67]. Finite-part integrals as used in this study are defined in Appendix B. The numerical techniques used to solve these equations are presented in Appendix E.

The definition of stress intensity factors (SIFs) that are referred to throughout this dissertation is given in Appendix G.

CHAPTER 2

The Line-Spring Model

2.1 Introduction.

A surface or part-through crack in a pipe, pressure vessel, or any other shell-like structure is a common and important flaw geometry to analyze, see Fig. 2.1. Because the elasticity problem is three-dimensional, many solutions involve expensive numerical techniques such as the Finite Element Method [33,34], the Alternating Method [35,36], the Boundary Integral Method [37], the finite element alternating method [38-40], the method of weight functions [41,42], and the body force method [43]. This problem has also been formulated analytically for a flat plate or strip in terms of two-dimensional integral equations, but has not been solved [67].

The line-spring model, proposed by Rice and Levy [2], and incorporated in a plate or shell theory that allows for transverse shear deformation [7,8,26], competes with these methods because of its simplicity and surprising accuracy. See Figs. 4.1-4, 6.1,2, for comparisons with the Finite Element Method and for the effect of transverse shear for various geometries in mode 1 loading.

Briefly, the model allows one to use a plate or shell theory to formulate the problem by removing the "net ligament", and replacing it by unknown, thickness averaged stress resultants which are treated as crack surface loads in a through crack problem. See Fig. 2.2 for a mode 1 illustration of this process. This reduces by one dimension the complexity of the analysis. The force resultant and displacement

variables used in both plates and shells are given below and are defined in Figs. 2.3a-c. Also the corresponding fracture modes are included in the figures.

$$\{F\}^T = \left\{ F_1, F_2, F_3, F_4, F_5 \right\} , \tag{2.1}$$

$$= \left\{ N_{xx}, M_{xx}, V_x, N_{xy}, M_{xy} \right\} , \tag{2.2}$$

$$= \left\{ h\sigma_1, \frac{h^2}{6}\sigma_2, \frac{2h}{3}\sigma_3, h\sigma_4, \frac{h^2}{6}\sigma_5 \right\} , \tag{2.3}$$

$$\{u\}^T = \left\{ u_1, u_2, u_3, u_4, u_5 \right\} = \left\{ u_x, \beta_x, u_z, u_y, \beta_y \right\} , \tag{2.4}$$

$$\delta_i = u_i^+ - u_i^- \qquad i=1,\ldots,5 . \tag{2.5}$$

The two-dimensional formulation of through and part-through crack problems in plates and shells as a mixed boundary value problem makes use of the superposition illustrated in Fig. 2.4. With regard to these figures, $\overset{\infty}{F}_i$ are the constant applied loads at "infinity" or away from the crack region and N and M are unknown stress resultants which are due to the net ligament of the part-through crack. In the case of a through crack, the crack surfaces are stress-free so N=M=0. For the solution of the mode 1 perturbation problem in a plate shown in Fig. 2.4, the following singular integral equations must be solved:

$$\frac{1}{2\pi} \fint_a^b \frac{u(t)}{(t-y)^2}\, dt = -(\overset{\infty}{N}_{xx} - N_{xx}) , \tag{2.6}$$

$$\frac{\gamma(1-\nu^2)}{2\pi} \fint_a^b \frac{\beta(t)}{(t-y)^2}\, dt + \frac{1}{2\pi} \int_a^b K_{22}(y,t)\beta(t)\, dt = -(\overset{\infty}{M}_{xx} - M_{xx}) . \tag{2.7}$$

For the derivation of Eqns. 2.6,7 and for the expression for $K_{22}(y,t)$,

γ, and ν see Chapter 3. Also see Appendix B for the interpretation of the strongly singular integrals appearing in these equations. The unknowns in the equations are N, M, u, and β. Since there are four unknowns and only two equations more information is needed. In the derivation that follows N and M are linearly related to u and β in the manner of a spring. After substitution of these relationships into Eqns. 2.6,7, u and β can be numerically determined from which all quantities of interest can be calculated.

2.2 Derivation of the Compliance Relationships.

The line-spring model is based on two assumptions. The first, previously stated, and illustrated in Fig. 2.2, involves replacing the net ligament (in which the state of stress is two-dimensional), by resultant forces which are functions of y only. The second assumption is that the stress intensity factors along the crack front may be obtained from these resultant forces as though the stress state were one of plane strain. The restriction at the ends of the crack and the crack front curvature, both act against this assumption. Therefore the model is most accurate in the center of the crack and improves as the crack gets longer for a given crack depth, i.e. as plane strain conditions are approached.

In order to make use of this analogy, the plane strain stress intensity factor solution for an edge-cracked strip must be available for the five possible loading conditions in a shell on a given surface, see Eqns. 2.2,3 and Fig. 2.3a-c. These solutions are presented in Appendix C along with a curve fit in the form,

$$g_i(\xi) = \frac{k_j}{\sigma_i\sqrt{L}} = \frac{K_j}{\sigma_i\sqrt{\pi L}} = \frac{1}{(1-\xi)^{\lambda}} \sum_{k=1}^{n_i} C_{ik}\xi^k , \tag{2.8}$$

where L is the crack depth, and the variable ξ is the ratio of the depth L to the strip thickness h, i.e. ξ=L/h. From Fig. 2.3a-c, when i=1 or 2, j=1, when i=3, j=2 and when i=4 or 5, j=3. The exponent λ is 3/2 when i=1,2 (mode 1), and 1/2 when i=3,4,5 (modes 2,3). The constants n_i and C_{ik} are given in Appendix C. From this follows

$$K_1 = \sqrt{\pi\xi h}\,[\,\sigma_1 g_1 + \sigma_2 g_2\,] , \tag{2.9}$$

$$K_2 = \sqrt{\pi\xi h}\,\sigma_3 g_3 , \tag{2.10}$$

$$K_3 = \sqrt{\pi\xi h}\,[\,\sigma_4 g_4 + \sigma_5 g_5\,] . \tag{2.11}$$

In these expressions $\sigma_i=\sigma_i(y)$ represents the net ligament stresses according to the relations given in Fig. 2.3. Note that $\xi=\xi(y)$.

The derivation is based on expressing the energy available for fracture along the crack front in two different ways. First we generalize Irwin's relation [68,69] for the potential energy release rate,

$$\frac{d}{dL}(U-V) = G = \frac{1-\nu^2}{E}\left\{ K_1^2 + K_2^2 + \frac{1}{1-\nu} K_3^2 \right\} , \tag{2.12}$$

where U is the work done by external loads and V is the strain energy. The use of the relation,

$$G_2 = \frac{(1-\nu^2)K_2^2}{E} \tag{2.13}$$

involves the assumption that the crack will grow in its own plane. This would apply to structures that are made of composite materials

that may have a weak cleavage plane [70]. If the crack deviates from a straight path, G_2 in Eqn. 2.13 is not the energy dissipated by incremental crack growth, and therefore Eqn. 2.12 would not be valid.

With the assumption of coplanar crack growth, Eqns. 2.9-11 are substituted into Eqn. 2.12 to obtain,

$$\frac{d}{dL}(U-V) = h\frac{1-\nu^2}{E}\left\{ \sigma_1^2 g_1^2 + 2\sigma_1\sigma_2 g_1 g_2 + \sigma_2^2 g_2^2 + \sigma_3^2 g_3^2 + \frac{1}{1-\nu}\left[\sigma_4^2 g_4^2 + 2\sigma_4\sigma_5 g_4 g_5 + \sigma_5^2 g_5^2 \right]\right\} . \tag{2.14}$$

Next consider the crack to extend from L to L+ΔL under "fixed load" conditions. The changes in U and V are as follows (refer to Fig. 2.5 for the notation used),

$$\Delta U = F_i \Delta\delta_i , \tag{2.15}$$

$$\Delta V = \frac{1}{2} F_i(\delta_i+\Delta\delta_i) - \frac{1}{2} F_i\delta_i = \frac{1}{2} F_i\delta_i , \tag{2.16}$$

where F_i and δ_i are defined in Eqns. 2.1-5.

After writing

$$\Delta\delta_i = \frac{\partial\delta_i}{\partial L}\Delta L , \tag{2.17}$$

due to the force F_i,

$$\frac{d}{dL}(U-V) = \frac{1}{2} F_i \frac{\partial\delta_i}{\partial L} . \tag{2.18}$$

The sum of all five loadings is,

$$\frac{d}{dL}(U-V) = \frac{1}{2}\sum_{i=1}^{5} F_i \frac{\partial\delta_i}{\partial L} . \tag{2.19}$$

Define the following matrices,

$$\{\delta'\}^T = \left\{ \delta_1', \delta_2', \delta_3', \delta_4', \delta_5' \right\} = \left\{ \delta_1, \frac{h}{6}\delta_2, \frac{2}{3}\delta_3, \delta_4, \frac{h}{6}\delta_5 \right\} , \tag{2.20}$$

$$[G] = \begin{bmatrix} g_1^2 & g_1 g_2 & 0 & 0 & 0 \\ g_1 g_2 & g_2^2 & 0 & 0 & 0 \\ 0 & 0 & g_3^2 & 0 & 0 \\ 0 & 0 & 0 & \frac{1}{1-\nu} g_4^2 & \frac{1}{1-\nu} g_4 g_5 \\ 0 & 0 & 0 & \frac{1}{1-\nu} g_4 g_5 & \frac{1}{1-\nu} g_5^2 \end{bmatrix} . \tag{2.21}$$

Now equate Eqn. 2.14 to 2.19 using Eqns. 2.3,20,21 for substitution to obtain,

$$h \frac{1-\nu^2}{E} \{\sigma\}^T [G] \{\sigma\} = \frac{1}{2} h \{\sigma\}^T \frac{\partial}{\partial L} \{\delta'\} , \tag{2.22}$$

or

$$\frac{\partial}{\partial L} \{\delta'\} = \frac{2(1-\nu^2)}{E} [G] \{\sigma\} . \tag{2.23}$$

Integrate and observe that $\sigma \neq \sigma(L)$,

$$\{\delta'\} = \frac{2(1-\nu^2)}{E} \left\{ \int_0^L [G] \, dl \right\} \{\sigma\} + \{ \overset{0}{\delta} \}|_{L=0} . \tag{2.24}$$

Next define

$$[B] = [\alpha_{ij}] = \frac{1}{h} \int_0^L [G] \, dl = \int_0^\xi [G] \, d\xi , \quad \xi = L/h , \tag{2.25}$$

where

$$\alpha_{ij} = \int_0^\xi g_i g_j \, d\xi , \quad i,j=1,2,3 \tag{2.26}$$

and

$$\alpha_{ij} = \frac{1}{1-\nu} \int_0^\xi g_i g_j \, d\xi , \quad i,j=4,5 . \tag{2.27}$$

Because of the form chosen for the functions g_i (see Eqn. 2.8), α_{ij} are determined numerically. When the matrix [B] is substituted into Eqn. 2.24 and the equation is solved for the stresses, the result is

$$\{\sigma\} = \frac{E}{2h(1-\nu^2)} [B]^{-1}\{\delta'\} , \tag{2.28}$$

where

$$[B]^{-1} = \begin{bmatrix} \alpha_{22}/\Delta_1 & -\alpha_{12}/\Delta_1 & 0 & 0 & 0 \\ -\alpha_{12}/\Delta_1 & \alpha_{11}/\Delta_1 & 0 & 0 & 0 \\ 0 & 0 & 1/\alpha_{33} & 0 & 0 \\ 0 & 0 & 0 & \alpha_{55}/\Delta_2 & -\alpha_{45}/\Delta_2 \\ 0 & 0 & 0 & -\alpha_{45}/\Delta_2 & \alpha_{44}/\Delta_2 \end{bmatrix} , \tag{2.29}$$

and

$$\Delta_1 = \alpha_{11}\alpha_{22} - \alpha_{12}^2 , \quad \Delta_2 = \alpha_{44}\alpha_{55} - \alpha_{45}^2 . \tag{2.30}$$

Eqn. 2.28 has the information that is needed for substitution into integral equations of the form of Eqns. 2.6,7. First it must be non-dimensionalized. This is done according to the definitions in Appendix A. Since all problems in this dissertation are either symmetric or skew-symmetric we have $\delta_i = 2u_i$, i.e. $|u^+| = |u^-| = u_i$. The final non-dimensional result is:

$$\begin{aligned} \sigma_1 &= \gamma_{11}u_1 + \gamma_{12}u_2 , \\ \sigma_2 &= 6[\gamma_{21}u_1 + \gamma_{22}u_2] , \\ \sigma_3 &= \frac{5}{8(1+\nu)} \gamma_{33}u_3 , \\ \sigma_4 &= \gamma_{44}u_4 + \gamma_{45}u_5 , \\ \sigma_5 &= 6[\gamma_{54}u_4 + \gamma_{55}u_5] , \\ u_1 &= (1-\nu^2)[\alpha_{11}\sigma_1 + \alpha_{12}\sigma_2] , \\ u_2 &= 6(1-\nu^2)[\alpha_{12}\sigma_1 + \alpha_{22}\sigma_2] , \end{aligned} \tag{2.31}$$

$$u_3 = \frac{3}{2}\,(1-\nu^2)\;\alpha_{33}\sigma_3 \;,$$

$$u_4 = (1-\nu^2)\,[\;\alpha_{44}\sigma_4 + \alpha_{45}\sigma_5\;] \;,$$

$$u_5 = 6(1-\nu^2)\,[\;\alpha_{45}\sigma_4 + \alpha_{55}\sigma_5\;] \;, \tag{2.32}$$

where

$$\gamma_{11} = \frac{1}{1-\nu^2}\,\frac{\alpha_{22}}{\Delta_1} \;, \qquad \gamma_{12} = \frac{-1}{6(1-\nu^2)}\,\frac{\alpha_{12}}{\Delta_1} \;,$$

$$\gamma_{21} = \gamma_{12} \;, \qquad \gamma_{22} = \frac{1}{36(1-\nu^2)}\,\frac{\alpha_{11}}{\Delta_1} \;,$$

$$\gamma_{33} = \frac{16}{15(1-\nu)}\,\frac{1}{\alpha_{33}} \;,$$

$$\gamma_{44} = \frac{1}{1-\nu^2}\,\frac{\alpha_{55}}{\Delta_2} \;, \qquad \gamma_{45} = \frac{-1}{6(1-\nu^2)}\,\frac{\alpha_{45}}{\Delta_2} \;,$$

$$\gamma_{54} = \gamma_{45} \;, \qquad \gamma_{55} = \frac{1}{36(1-\nu^2)}\,\frac{\alpha_{44}}{\Delta_2} \;. \tag{2.33}$$

If these equations are now substituted into Eqns. 2.6,7, the result is,

$$\frac{1}{2\pi}\fint_a^b \frac{u(t)}{(t-y)^2}\,dt - \gamma_{11}u - \gamma_{12}\beta = -\overset{\infty}{N}_{xx} = -\overset{\infty}{\sigma}_1 \;, \tag{2.34}$$

$$\frac{\gamma(1-\nu^2)}{2\pi}\fint_a^b \frac{\beta(t)}{(t-y)^2}\,dt + \frac{1}{2\pi}\int_a^b K_{22}(y,t)\beta(t)\,dt$$

$$- \gamma_{21}u - \gamma_{22}\beta = -\overset{\infty}{M}_{xx} = -\overset{\infty}{\sigma}_2/6 \;. \tag{2.35}$$

The compliance coefficients γ_{ij} are indirectly functions of y

through the variable ξ which is the non-dimensional crack depth. Note that for a through crack the γ_{ij} are zero. In this case the equations uncouple and respectively correspond to tension and bending loadings.

Since the model is most accurate in the central portion of the crack, it is best applied to problems where failure occurs when the surface crack grows through the thickness leading either to leaking or to the development of a through crack which then grows in length to critical size. Because of the plane strain assumption, the model becomes less applicable near the ends of the crack. Although the model unexpectedly gives reasonable results here (see Figs. 4.1-4 and 6.1,2 where curves are drawn up to y/a = .98), the use of the solution in this region for anything other than general trends is not justified. Even though the solution at the ends is not used, the behavior of the solution here plays a role in the convergence of the method over the entire range, and therefore should be examined.

2.3 Endpoint behavior.

In the case of the through crack it is known that the behavior of the displacement quantities are of the form (see Appendix D),

$$u_i(t) = f_i(t)(1-t^2)^{1/2} , \tag{2.36}$$

where the square root is referred to as the weight function (of the integral equation) and $f_i(t)$ is a simple function which can be represented by a polynomial that is easily obtained numerically. Note that the crack domain has been normalized to (-1,1). If $u_i(t)$ were determined without extracting the endpoint behavior given by the

weight function, convergence of $u_i(t)$ towards the ends (i.e. -1,1) would be unacceptably slow. Also in the through crack problem the stress intensity factors are proportional to f(-1) and f(+1), and therefore can only be found if the weight is extracted. The addition of the line-spring terms into the integral equation has an effect on this asymptotic analysis only if the net ligament stresses are unbounded, which is unreasonable. If these stresses are assumed to be finite at the ends, Eqns. 2.32 and 2.36 show that,

$$u_1 = (1-\nu^2)[\ \alpha_{11}\sigma_1 + \alpha_{12}\sigma_2\ ] = f_1(t)(1-t^2)^{1/2}\ ,$$

$$u_2 = 6(1-\nu^2)[\ \alpha_{12}\sigma_1 + \alpha_{22}\sigma_2\ ] = f_2(t)(1-t^2)^{1/2}\ ,$$

$$u_3 = \frac{3}{2}\ (1-\nu^2)\ \alpha_{33}\sigma_3 = f_3(t)(1-t^2)^{1/2}\ ,$$

$$u_4 = (1-\nu^2)[\ \alpha_{44}\sigma_4 + \alpha_{45}\sigma_5\ ] = f_4(t)(1-t^2)^{1/2}\ ,$$

$$u_5 = 6(1-\nu^2)[\ \alpha_{45}\sigma_4 + \alpha_{55}\sigma_5\ ] = f_5(t)(1-t^2)^{1/2}\ . \qquad (2.37)$$

For finite, non-zero net ligament stresses, α_{ij} in Eqns. 2.32 must carry the square root behavior as t approaches -1 and 1. Recall that α_{ij} are functions of t through the crack shape variable ξ. If the crack depth of the surface crack is non-zero at the ends as in the case of a rectangular crack, α_{ij} will be constant at the endpoints. The solution will then require σ_i to be zero at the endpoints, a condition that does not seem reasonable. If the crack depth, ξ is zero at the ends, the behavior of α_{ij} will depend on how ξ goes to zero. For small ξ we may write

$$g_i \simeq \sum_{j=0}^{N} c_{ij}\xi^j \ , \tag{2.38}$$

from which we obtain from Eqns. 2.26,27,

$$\alpha_{11} = \frac{\pi}{2} c_{10}^2\xi^2 + \frac{2\pi}{3} c_{10}c_{11}\xi^3 + 0(\xi^4) \ ,$$

$$\alpha_{12} = \alpha_{21} = \frac{\pi}{2} c_{10}c_{20}\xi^2 + \frac{\pi}{3} [c_{20}c_{11} + c_{10}c_{21}]\xi^3 + 0(\xi^4) \ ,$$

$$\alpha_{22} = \frac{\pi}{2} c_{20}^2\xi^2 + \frac{2\pi}{3} c_{20}c_{21}\xi^3 + 0(\xi^4) \ ,$$

$$\alpha_{33} = \frac{\pi}{4} c_{31}^2\xi^4 + 0(\xi^5) \ ,$$

$$(1-\nu)\alpha_{44} = \frac{\pi}{2} c_{40}^2\xi^2 + \frac{2\pi}{3} c_{40}c_{41}\xi^3 + 0(\xi^4) \ ,$$

$$(1-\nu)\alpha_{45} = (1-\nu)\alpha_{54} = \frac{\pi}{2} c_{40}c_{50}\xi^2 + \frac{\pi}{3} [c_{40}c_{51} + c_{50}c_{41}]\xi^3 + 0(\xi^4),$$

$$(1-\nu)\alpha_{55} = \frac{\pi}{2} c_{50}^2\xi^2 + \frac{2\pi}{3} c_{50}c_{51}\xi^3 + 0(\xi^4) \ , \tag{2.39}$$

where from Eqn 2.8 the c_{ij} in terms of the C_{ij} are,

$$c_{i0} = C_{i0} \ ,$$

$$c_{i1} = C_{i1} + \lambda C_{i0} \ . \tag{2.40}$$

More terms in this series are given in Appendix F.

In order for Eqn. 2.37 to be true for bounded, non-zero stresses, Eqn. 2.39 (except for α_{33}) suggest that:

$$\alpha_{ij} \sim (1-t^2)^{1/2} \ , \tag{2.41}$$

or

$$\xi^2 \sim (1-t^2)^{1/2} \ . \tag{2.42}$$

Therefore if the crack shape is chosen in the form

$$\xi = \xi_0(1-t^2)^{1/4} \ , \tag{2.43}$$

convergence will be good for $|t| \leq 1$. Rice [2] made this point. Any other crack shape will impose either unbounded or zero endpoint behavior on the net ligament stresses and the solution will not converge at the endpoints in a satisfactory manner. If one considers the semi-ellipse for example, σ_i will be of the order $(1-t^2)^{-1/2}$ as $|t|$ approaches 1.

There is one exception. In the case of α_{33} in Eqn. 2.37 the stress σ_3 will be zero. This should be expected because the assumed form of the out-of-plane shear stress is parabolic, i.e. zero at the surface of the shell. Therefore as the crack depth goes to zero so does σ_3.

It should be pointed out that regardless of what form of the crack is chosen, satisfactory convergence can be obtained in the central portion where the line-spring model is most applicable. The results in this dissertation were thus obtained for the semi-ellipse. But if a solution is desired for (-1,1), it is necessary to have the crack shape at the ends asymptotically behave like Eqn. 2.43. A procedure to get this function utilizes a simple expansion about zero and for some typical shapes is as follows. Let

$$\xi = \xi_0 \ (1-t^2)^n \tag{2.44}$$

be the desired shape. Note that a rectangle is given by n=0, and a semi-ellipse results from n=1/2. Next we write

$$\xi = \xi_0 \ (1-t^2)^n \simeq \xi_0 \ (1-t^2)^{1/4} g(t) \ , \tag{2.45}$$

where

$$g(t) \simeq (1-t^2)^{n-1/4} \simeq \sum_{i=0}^{M} a_i t^{2i} \quad . \tag{2.46}$$

M is chosen so that an adequate representation of the crack front is given over most of the domain, and the coefficients a_i, are given as follows,

$$a_0 = 1$$

$$a_1 = -(n-1/4)$$

$$a_2 = \frac{(n-1/4)[(n-1/4)-1]}{2!}$$

$$a_3 = -\frac{(n-1/4)[(n-1/4)-1][(n-1/4)-2]}{3!} \quad , \text{ etc.} \tag{2.47}$$

The convergence of Eqn. 2.46 is demonstrated for n=0 and n=1/2 in tables 2.1,2, respectively. Stress intensity factor results of Eqns. 2.6,7 for the crack shapes in these tables are given in tables 2.3-6. The stress intensity factors in Eqns. 2.9-11 are normalized with respect to the value of K from Eqn. 2.8 for ξ in the center of the crack and for the corresponding loading, see section C.4 of Appendix C. This technique however, is of limited use.

Semi-elliptic crack shapes are chosen for most mode 1 analysis because of their general resemblance to surface cracks. Most experiments however show that cracks grown by fatigue tend to have a blunter shape at the ends, see for example [55,71]. Note that the 1/4 power represents this better than 1/2.

One further point to make before concluding this chapter is that for small ξ the inverse of the B matrix (Eqn. 2.29) is singular and the asymptotic behavior of relations 2.32 is of the form,

$$\gamma_{ij} = (\text{constant})\ \xi^{-4} + O(\xi^{-3}) \ . \tag{2.48}$$

The constants are defined in Appendix F. It would seem that the contribution of the stress terms (Eqn. 2.31) for the case of a semi-ellipse where $u \sim \xi \sim (1-t^2)^{1/2}$ would be unbounded and to the -3/2 power rather than -1/2 as predicted by Eqn. 2.37. However when the terms of Eqn. 2.31 are combined, the two leading order terms cancel and we are left with the singular nature predicted by Eqn. 2.37, see Appendix F.

Table 2.1 Crack profiles approximating a constant depth using Eqns. 2.46,47.

Rectangular Profile (ξ = .6)

t \ M	1	3	5	10	20	exact
.0	.6000	.6000	.6000	.6000	.6000	.6000
.1	.5985	.6000	.6000	.6000	.6000	.6000
.2	.5939	.6000	.6000	.6000	.6000	.6000
.3	.5860	.6000	.6000	.6000	.6000	.6000
.4	.5744	.5997	.6000	.6000	.6000	.6000
.5	.5584	.5987	.5999	.6000	.6000	.6000
.6	.5367	.5958	.5996	.6000	.6000	.6000
.7	.5070	.5882	.5980	.6000	.6000	.6000
.8	.4648	.5689	.5906	.5993	.6000	.6000
.9	.3961	.5170	.5579	.5900	.5992	.6000
.95	.3353	.4536	.5037	.5585	.5898	.6000
.98	.2677	.3705	.4200	.4862	.5440	.6000

Table 2.2 Crack profiles approximating a semi-ellipse using Eqns. 2.46,47.

Semi-Elliptic profile, ($\xi = .6(1-t^2)^{1/2}$)

t \ M	1	3	5	10	20	exact
.0	.6000	.6000	.6000	.6000	.6000	.6000
.1	.5985	.5970	.5970	.5970	.5970	.5970
.2	.5939	.5879	.5879	.5879	.5879	.5879
.3	.5860	.5724	.5724	.5724	.5724	.5724
.4	.5744	.5501	.5499	.5499	.5499	.5499
.5	.5584	.5202	.5196	.5196	.5196	.5196
.6	.5367	.4818	.4801	.4800	.4800	.4800
.7	.5070	.4335	.4292	.4285	.4285	.4285
.8	.4648	.3726	.3630	.3601	.3600	.3600
.9	.3961	.2915	.2736	.2636	.2617	.2615
.95	.3353	.2304	.2122	.1954	.1888	.1873
.98	.2677	.1802	.1587	.1387	.1267	.1194

Table 2.3 Normalized stress intensity factors for the crack profiles given in table 2.1 for applied tension.

Rectangular Profile (ξ = .6), Tension

t \ M	1	3	5	10	20	∞
.0	.258	.271	.272	.273	.273	.273
.1	.258	.270	.272	.272	.272	.273
.2	.256	.268	.269	.270	.270	.270
.3	.253	.263	.265	.265	.266	.266
.4	.249	.256	.258	.259	.259	.259
.5	.243	.246	.250	.249	.249	.250
.6	.236	.235	.237	.238	.238	.239
.7	.225	.219	.220	.221	.222	.222
.8	.210	.199	.197	.197	.198	.199
.9	.185	.172	.166	.161	.161	.163
.95	.163	.151	.145	.136	.130	.132
.98	.138	.128	.124	.117	.107	.098

Table 2.4 Normalized stress intensity factors for the crack profiles given in table 2.1 for pure bending.

Rectangular Profile (ξ = .6), Bending

t \ M	1	3	5	10	20	∞
.0	.144	.152	.153	.153	.153	.153
.1	.145	.151	.152	.152	.152	.152
.2	.146	.148	.149	.149	.149	.149
.3	.148	.144	.144	.145	.145	.145
.4	.151	.136	.137	.137	.137	.137
.5	.154	.126	.126	.126	.126	.128
.6	.158	.116	.114	.114	.114	.114
.7	.162	.103	.097	.958	.096	.096
.8	.165	.093	.077	.071	.071	.071
.9	.166	.087	.060	.040	.034	.033
.95	.161	.089	.060	.029	.012	.006
.98	.150	.091	.066	.034	.009	-.013

Table 2.5 Normalized stress intensity factors for the crack profiles given in table 2.2 for applied tension.

Semi-elliptic Profile (ξ_0 = .6), Tension

t \ M	1	3	5	10	20	∞
.0	.258	.246	.245	.245	.244	.244
.1	.258	.246	.245	.244	.244	.244
.2	.256	.245	.244	.243	.243	.243
.3	.253	.243	.243	.242	.242	.242
.4	.249	.241	.240	.240	.239	.239
.5	.243	.238	.236	.236	.236	.236
.6	.236	.234	.232	.231	.231	.231
.7	.225	.228	.226	.225	.225	.225
.8	.210	.218	.218	.217	.217	.217
.9	.185	.201	.206	.208	.208	.207
.95	.163	.184	.193	.201	.204	.203
.98	.138	.162	.173	.189	.200	.205

Table 2.6 Normalized stress intensity factors for the crack profiles given in table 2.2 for pure bending.

Semi-elliptic Profile (ξ_0 = .6), Bending

t \ M	1	3	5	10	20	∞
.0	.144	.135	.134	.133	.133	.133
.1	.145	.136	.135	.135	.135	.134
.2	.146	.141	.140	.139	.139	.139
.3	.148	.149	.148	.147	.147	.147
.4	.151	.160	.159	.158	.158	.158
.5	.154	.176	.175	.174	.174	.172
.6	.158	.191	.190	.189	.189	.189
.7	.162	.209	.210	.209	.209	.208
.8	.165	.227	.233	.233	.232	.231
.9	.166	.239	.253	.261	.261	.259
.95	.161	.236	.257	.274	.281	.280
.98	.150	.219	.244	.273	.293	.302

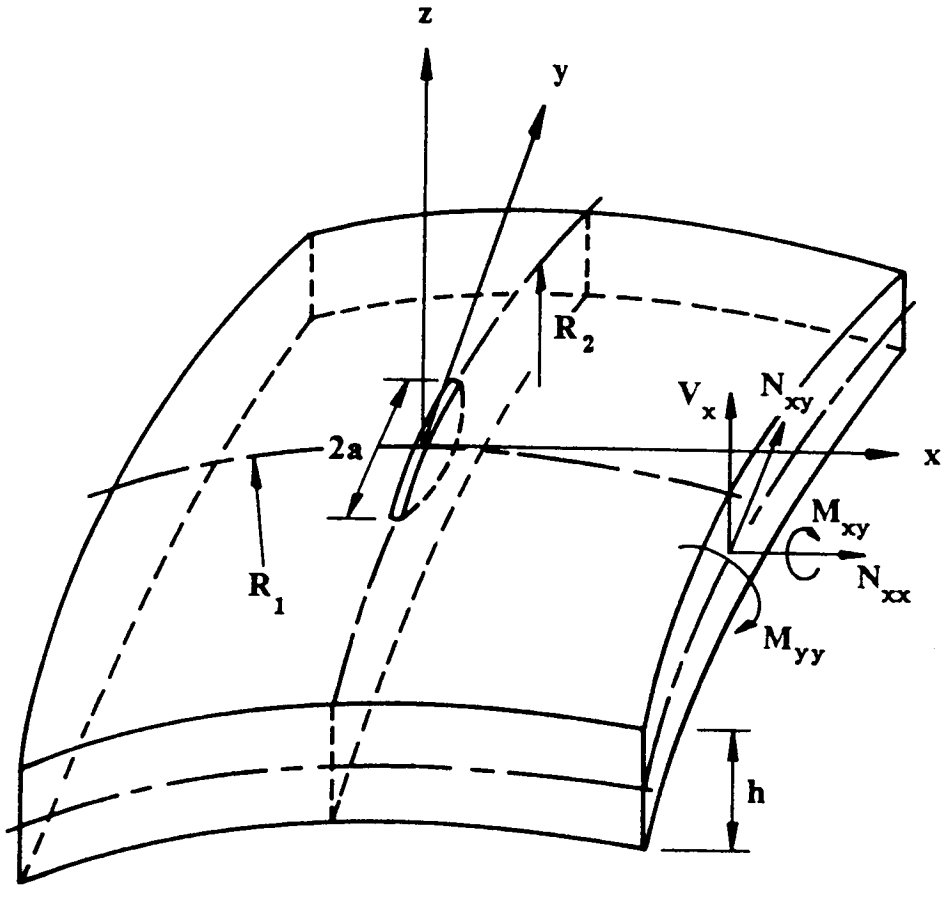

Figure 2.1 The shell geometry.

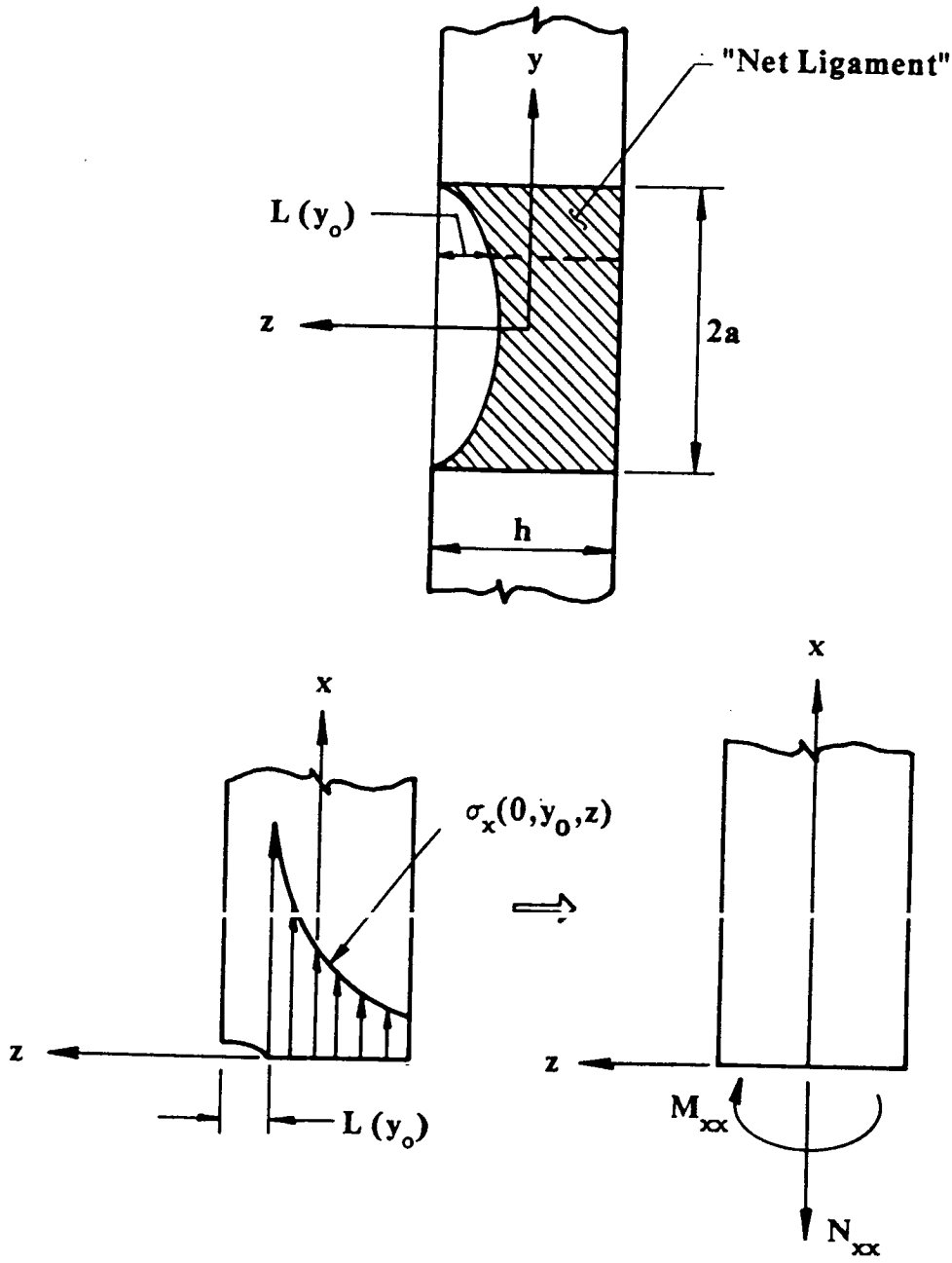

Figure 2.2 Representation of the two-dimensional stress state in the net ligament with stress resultants for the mode 1 problem.

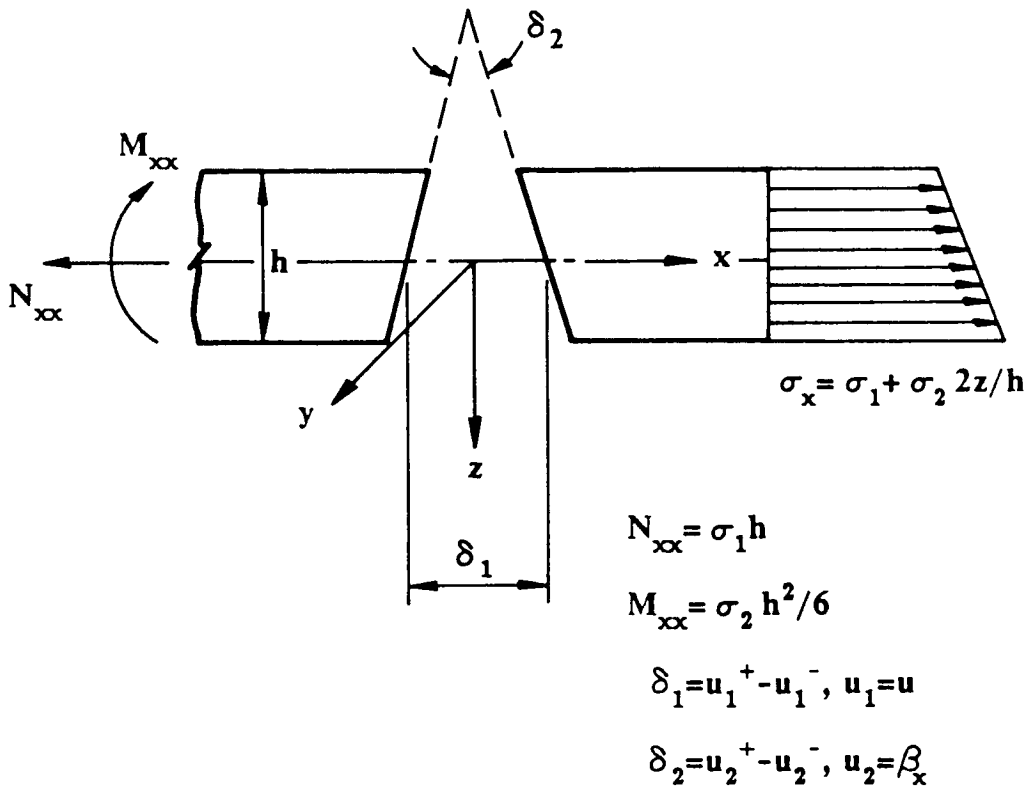

(a)

Figure 2.3a Force and Displacement quantities as defined by plate or shell theory that are used in the mode 1 line-spring model.

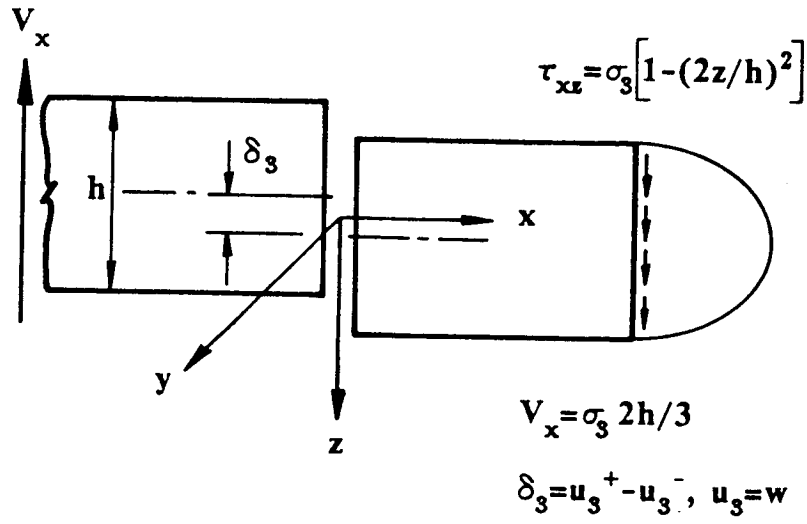

(b)

Figure 2.3b Force and Displacement quantities as defined by plate or shell theory that are used by the line-spring model for mode 2 loading.

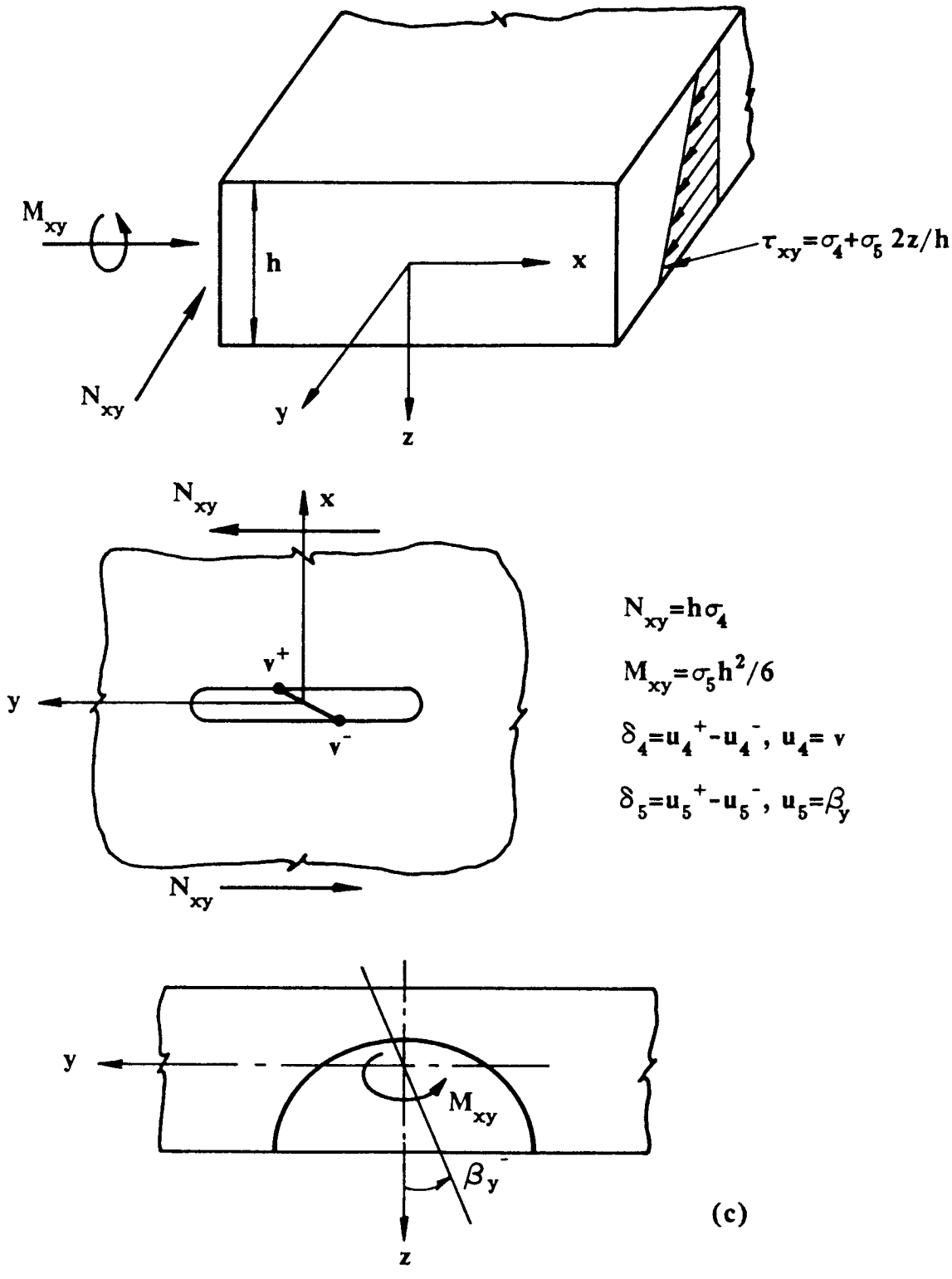

Figure 2.3c Force and Displacement quantities as defined by plate or shell theory that are used by the line-spring model for mode 3 loading.

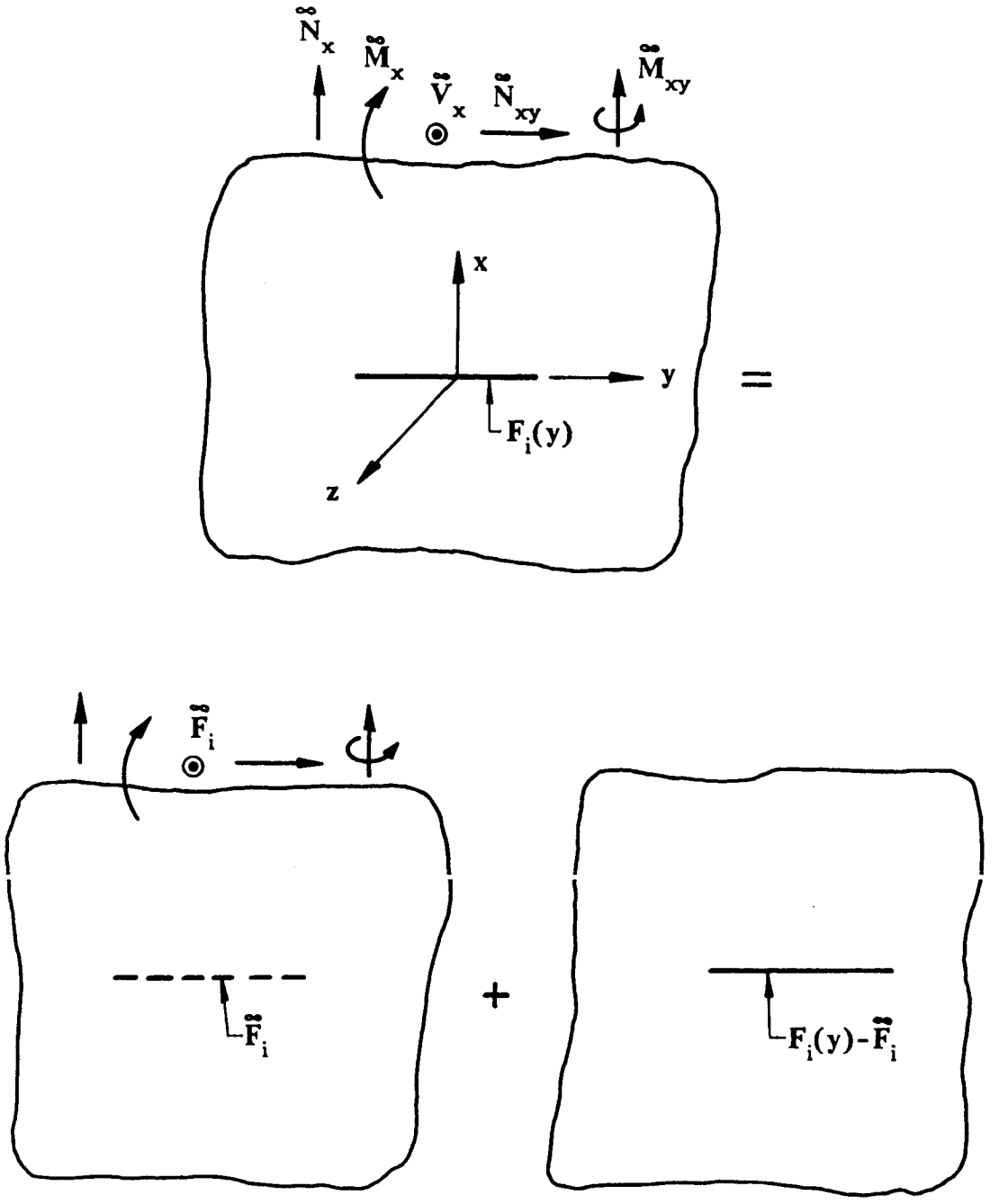

Figure 2.4 The superposition used to solve part-through crack problems with the line-spring model. All solutions are obtained for the problem in the lower right (the perturbation problem) where the only loads are applied to the crack surfaces.

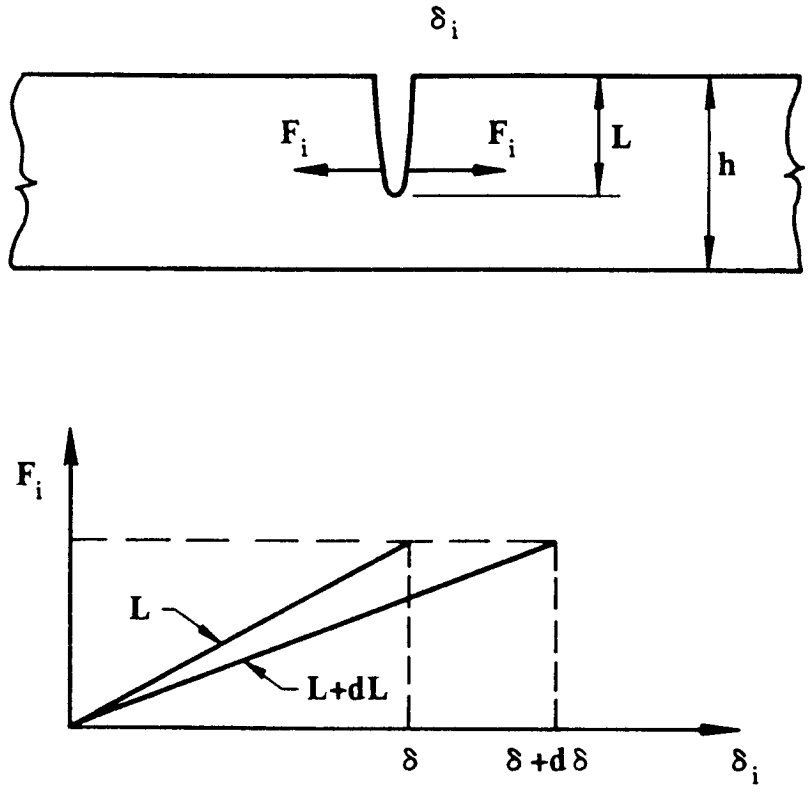

Figure 2.5 The corresponding plane strain problem.

CHAPTER 3

Through Cracks in Plates

In this chapter the singular integral equations for a cracked plate under both symmetric (mode 1) and skew-symmetric (modes 2,3) loadings will be derived. The plate theory includes transverse shear deformation. For mode 1 loading there is very little to add to the existing literature [6,9-13]. The thin plate limit examined in these papers will be reconsidered. For the skew-symmetric case stress intensity factor solutions found in Refs. [14,15] for a single crack will be supplemented. Also some results for the double crack case will be presented.

3.1 Formulation

The governing equations, both dimensional (Eqns. 3.1a-16a, 18a, 19a) and non-dimensional (Eqns. 3.1b-16b,18b,19b) are listed below. The dimensional relationships are defined in Appendix A. From equilibrium

$$\frac{\partial N_{11}}{\partial x_1} + \frac{\partial N_{12}}{\partial x_2} = 0 \quad , \quad \frac{\partial N_{xx}}{\partial x} + \frac{\partial N_{xy}}{\partial y} = 0 \quad , \tag{3.1a,b}$$

$$\frac{\partial N_{12}}{\partial x_1} + \frac{\partial N_{22}}{\partial x_2} = 0 \quad , \quad \frac{\partial N_{xy}}{\partial x} + \frac{\partial N_{yy}}{\partial y} = 0 \quad , \tag{3.2a,b}$$

$$\frac{\partial V_1}{\partial x_1} + \frac{\partial V_2}{\partial x_2} + \bar{q}(x_1,x_2) = 0 \quad ,$$

$$\frac{\partial V_x}{\partial x} + \frac{\partial V_y}{\partial y} + \frac{12(1+\nu)}{5}\, q(x,y) = 0 \quad , \tag{3.3a,b}$$

$$\frac{\partial M_{11}}{\partial x_1} + \frac{\partial M_{12}}{\partial x_2} - V_1 = 0 \quad ,$$

$$\frac{\partial M_{xx}}{\partial x} + \frac{\partial M_{xy}}{\partial y} - \frac{5}{12(1+\nu)} V_x = 0 \quad , \tag{3.4a,b}$$

$$\frac{\partial M_{12}}{\partial x_1} + \frac{\partial M_{22}}{\partial x_2} - V_2 = 0 \quad ,$$

$$\frac{\partial M_{xy}}{\partial x} + \frac{\partial M_{yy}}{\partial y} - \frac{5}{12(1+\nu)} V_y = 0 \quad , \tag{3.5a,b}$$

where q(x,y) is normal loading to the plate surface. The other variables are standard plate quantities (see Fig. 2.3). From kinematical considerations,

$$\epsilon_{11} = \frac{\partial u_{1D}}{\partial x_1} \quad , \quad \epsilon_{xx} = \frac{\partial u}{\partial x} \quad , \tag{3.6a,b}$$

$$\epsilon_{22} = \frac{\partial u_{2D}}{\partial x_2} \quad , \quad \epsilon_{yy} = \frac{\partial v}{\partial y} \quad , \tag{3.7a,b}$$

$$\epsilon_{12} = \frac{1}{2}\left[\frac{\partial u_{1D}}{\partial x_2} + \frac{\partial u_{2D}}{\partial x_1} \right] \quad , \quad \epsilon_{xy} = \frac{1}{2}\left[\frac{\partial u}{\partial y} + \frac{\partial v}{\partial x} \right] \quad , \tag{3.8a,b}$$

$$\theta_1 = \frac{\partial u_{3D}}{\partial x_1} + \beta_1 \quad , \quad \theta_x = \frac{\partial w}{\partial x} + \beta_x \quad , \tag{3.9a,b}$$

$$\theta_2 = \frac{\partial u_{3D}}{\partial x_2} + \beta_2 \quad , \quad \theta_y = \frac{\partial w}{\partial y} + \beta_y \quad , \tag{3.10a,b}$$

where θ_1 and θ_2 are the total rotations of the normals. For classical plate theory they are zero showing that normals to the plate surface stay normal, i.e. there is no deformation transversely. The constitutive relations (Hooke's law) are,

$$h\epsilon_{11} = \frac{1}{E}\,(N_{11} - \nu N_{22}) \quad , \quad \epsilon_{xx} = N_{xx} - \nu N_{yy} \quad , \tag{3.11a,b}$$

$$h\epsilon_{22} = \frac{1}{E}\,(N_{22} - \nu N_{11}) \quad , \quad \epsilon_{yy} = N_{yy} - \nu N_{xx} \quad , \tag{3.12a,b}$$

$$h\epsilon_{12} = \frac{1}{2\mu}\,N_{12} \quad , \quad \epsilon_{xy} = (1+\nu)N_{xy} \quad , \tag{3.13a,b}$$

where E is Young's modulus and ν is Poisson's ratio. From plate bending,

$$M_{11} = D\left[\frac{\partial\beta_1}{\partial x_1} + \nu\frac{\partial\beta_2}{\partial x_2}\right] \quad ,$$

$$M_{xx} = \frac{1}{12(1-\nu^2)}\left[\frac{\partial\beta_x}{\partial x} + \nu\frac{\partial\beta_y}{\partial y}\right] \quad , \tag{3.14a,b}$$

$$M_{22} = D\left[\frac{\partial\beta_2}{\partial x_2} + \nu\frac{\partial\beta_1}{\partial x_1}\right] \quad ,$$

$$M_{yy} = \frac{1}{12(1-\nu^2)}\left[\nu\frac{\partial\beta_x}{\partial x} + \frac{\partial\beta_y}{\partial y}\right] \quad , \tag{3.15a,b}$$

$$M_{12} = \frac{D(1-\nu)}{2}\left[\frac{\partial\beta_1}{\partial x_2} + \frac{\partial\beta_2}{\partial x_1}\right] \quad ,$$

$$M_{xy} = \frac{1}{24(1+\nu)}\left[\frac{\partial\beta_x}{\partial y} + \frac{\partial\beta_y}{\partial x}\right] \quad , \tag{3.16a,b}$$

where,

$$D = \frac{Eh^3}{12(1-\nu^2)} \quad . \tag{3.17}$$

The linear transverse shear stress-strain relationships are,

$$\theta_1 = \frac{1}{hB}\,V_1 \quad , \quad \theta_x = V_x \quad , \tag{3.18a,b}$$

$$\theta_2 = \frac{1}{hB}\,V_2 \quad , \quad \theta_y = V_y \quad , \tag{3.19a,b}$$

where

$$B = \frac{5E}{12(1+\nu)} \quad . \tag{3.20}$$

From here on only the non-dimensional variables will be used. Define $\phi(x,y)$ such that

$$N_{xx} = \frac{\partial^2\phi}{\partial y^2} \quad , \quad N_{yy} = \frac{\partial^2\phi}{\partial x^2} \quad , \quad N_{xy} = -\frac{\partial^2\phi}{\partial x\partial y} \quad , \tag{3.21}$$

and Eqns. 3.1b,2b are satisfied. Next combine Eqns. 3.6b,7b with 3.11b,12b to obtain,

$$\frac{\partial u}{\partial x} = N_{xx} - \nu N_{yy} \quad , \quad \frac{\partial v}{\partial y} = N_{yy} - \nu N_{xx} \quad . \tag{3.22}$$

Next use Eqns. 3.8b,13b to write,

$$(1+\nu)N_{xy} = \frac{1}{2}\left[\frac{\partial u}{\partial y} + \frac{\partial v}{\partial x}\right] \quad , \tag{3.23}$$

or

$$(1+\nu)\frac{\partial^2}{\partial x\partial y}N_{xy} = \frac{1}{2}\left[\frac{\partial^3 u}{\partial x\partial y^2} + \frac{\partial^3 v}{\partial y\partial x^2}\right] \quad . \tag{3.24}$$

After substituting 3.22 into 3.24 we obtain,

$$(1+\nu)\frac{\partial^2}{\partial x\partial y}N_{xy} = \frac{1}{2}\left\{\left[\frac{\partial^2 N_{xx}}{\partial y^2} - \nu\frac{\partial^2 N_{yy}}{\partial y^2}\right] + \left[\frac{\partial^2 N_{yy}}{\partial x^2} - \nu\frac{\partial^2 N_{xx}}{\partial x^2}\right]\right\} \quad . \tag{3.25}$$

Using 3.21 this becomes,

$$\nabla^4\phi = 0 \quad , \tag{3.26}$$

where

$$\nabla^2 = \frac{\partial^2}{\partial x^2} + \frac{\partial^2}{\partial y^2} \quad . \tag{3.27}$$

Next using 3.3b-5b we can write,

$$\frac{\partial^2 M_{xx}}{\partial x^2} + 2\frac{\partial^2 M_{xy}}{\partial x \partial y} + \frac{\partial^2 M_{yy}}{\partial y^2} + q(x,y) = 0 \quad . \tag{3.28}$$

Substitute Eqns. 3.14b-16b into 3.28 to obtain,

$$\frac{\partial^3 \beta_x}{\partial x^3} + \frac{\partial^3 \beta_y}{\partial x^2 \partial y} + \frac{\partial^3 \beta_y}{\partial y^3} + \frac{\partial^3 \beta_x}{\partial y^2 \partial x} + 12(1-\nu)^2 q(x,y) = 0 \quad . \tag{3.29}$$

Look at the following expression from the first two terms of Eqn. 3.29,

$$\frac{\partial^3 \beta_x}{\partial x^3} + \frac{\partial^3 \beta_y}{\partial x^2 \partial y} = \frac{\partial^2}{\partial x^2}\left[\frac{\partial \beta_x}{\partial x} + \frac{\partial \beta_y}{\partial y} \right] \quad . \tag{3.30}$$

Substitute for β_x and β_y according to Eqns. 3.9b,10b together with 3.18b,19b,

$$\frac{\partial^3 \beta_x}{\partial x^3} + \frac{\partial^3 \beta_y}{\partial x^2 \partial y} = \frac{\partial^2}{\partial x^2}\left[\frac{\partial V_x}{\partial x} - \frac{\partial^2 w}{\partial x^2} + \frac{\partial V_y}{\partial y} - \frac{\partial^2 w}{\partial y^2} \right] \quad . \tag{3.31}$$

Next use Eqns. 3.3b and 3.27 for substitution into 3.31 to obtain,

$$\frac{\partial^3 \beta_x}{\partial x^3} + \frac{\partial^3 \beta_y}{\partial x^2 \partial y} = \frac{\partial^2}{\partial x^2}\left[\frac{12(1+\nu)}{5} q(x,y) - \nabla^2 w \right] \quad . \tag{3.32}$$

Similarly,

$$\frac{\partial^3 \beta_y}{\partial y^3} + \frac{\partial^3 \beta_x}{\partial y^2 \partial x} = \frac{\partial^2}{\partial y^2}\left[\frac{12(1+\nu)}{5} q(x,y) - \nabla^2 w \right] \quad . \tag{3.33}$$

Eqns. 3.32,33 are now substituted back into Eqn. 3.29 to obtain,

$$\nabla^4 w = \left\{ \frac{12(1+\nu)}{5} \nabla^2 + 12(1-\nu^2) \right\} q(x,y) \quad . \tag{3.34}$$

Next use Eqn. 3.4b with substitutions from 3.14b,3.16b and 3.18b with 3.9b to write,

$$\beta_x + \frac{\partial w}{\partial x} = \frac{1}{12(1-\nu)^2}\left\{\frac{12(1+\nu)}{5}\nabla^2\beta_x + \frac{1+\nu}{2}\frac{\partial}{\partial y}\left[\frac{\partial\beta_y}{\partial x} - \frac{\partial\beta_x}{\partial y}\right]\right\} . \quad (3.35)$$

Similar substitutions with Eqn. 3.5b leads to,

$$\beta_y + \frac{\partial w}{\partial y} = \frac{1}{12(1-\nu)^2}\left\{\frac{12(1+\nu)}{5}\nabla^2\beta_y + \frac{1+\nu}{2}\frac{\partial}{\partial x}\left[\frac{\partial\beta_x}{\partial y} - \frac{\partial\beta_y}{\partial x}\right]\right\} . \quad (3.36)$$

After defining the constants,

$$\kappa = \frac{1}{5(1-\nu)} , \quad \gamma = \frac{1}{12(1-\nu^2)} , \quad (3.37)$$

and the new unknowns,

$$\Omega(x,y) = \frac{\partial\beta_x}{\partial y} - \frac{\partial\beta_y}{\partial x} , \quad (3.38)$$

$$\psi(x,y) = \kappa\left[\frac{\partial\beta_x}{\partial x} + \frac{\partial\beta_y}{\partial v}\right] - w , \quad (3.39)$$

Eqns. 3.26,34,35,36 become,

$$\nabla^4\phi = 0 , \quad (3.40)$$

$$\nabla^4 w = 0 , \quad (3.41)$$

$$\kappa\nabla^2\psi - \psi - w = 0 , \quad (3.42)$$

$$\kappa\frac{1-\nu}{2}\nabla^2\Omega - \Omega = 0 , \quad (3.43)$$

where $q(x,y)$ has been assumed to be zero. To solve Eqns. 3.40-43 we introduce the Fourier transform,

$$\bar{\phi}(x,\alpha) = \int_{-\infty}^{+\infty}\phi(x,y)e^{i\alpha y}dy , \quad (3.44)$$

$$\phi(x,y) = \frac{1}{2\pi}\int_{-\infty}^{+\infty}\bar{\phi}(x,\alpha)e^{-i\alpha y}d\alpha \quad , \tag{3.45}$$

with identical definitions for $w(x,y)$, $\psi(x,y)$ and $\Omega(x,y)$. After making use of the relationships,

$$\int_{-\infty}^{+\infty}\nabla^2 f(x,y)e^{i\alpha y}dy = \frac{\partial^2\bar{f}}{\partial x^2} - \alpha^2\,\bar{f} \quad ,$$

$$\int_{-\infty}^{+\infty}\nabla^4 f(x,y)e^{i\alpha y}dy = \frac{\partial^4\bar{f}}{\partial x^4} - 2\alpha^2\frac{\partial^2\bar{f}}{\partial x^2} + \alpha^4\,\bar{f} \quad , \tag{3.46}$$

Eqns. 3.40-43 are reduced to the following ordinary differential equations,

$$\frac{\partial^4\bar{\phi}}{\partial x^4} - 2\alpha^2\frac{\partial^2\bar{\phi}}{\partial x^2} + \alpha^4\bar{\phi} = 0 \quad , \tag{3.47}$$

$$\frac{\partial^4\bar{w}}{\partial x^4} - 2\alpha^2\frac{\partial^2\bar{w}}{\partial x^2} + \alpha^4\bar{w} = 0 \quad , \tag{3.48}$$

$$\kappa\left\{\frac{\partial^2\bar{\psi}}{\partial x^2} - \alpha^2\bar{\psi}\right\} - \bar{\psi} - \bar{w} = 0 \quad , \tag{3.49}$$

$$\kappa\,\frac{1-\nu}{2}\left\{\frac{\partial^2\bar{\Omega}}{\partial x^2} - \alpha^2\bar{\Omega}\right\} - \bar{\Omega} = 0 \quad . \tag{3.50}$$

Assuming symmetry of loading and geometry with respect to x, the transformed solution for x>0 of Eqns. 3.47-50 is,

$$\phi(x,y) = \frac{1}{2\pi}\int_{-\infty}^{+\infty}\left[A_1(\alpha)e^{-|\alpha|x} + A_2(\alpha)xe^{-|\alpha|x}\right]e^{-i\alpha y}d\alpha \quad , \tag{3.51}$$

$$w(x,y) = \frac{1}{2\pi}\int_{-\infty}^{+\infty}\left[A_3(\alpha)e^{-|\alpha|x} + A_4(\alpha)xe^{-|\alpha|x}\right]e^{-i\alpha y}d\alpha \quad , \tag{3.52}$$

$$\psi(x,y) = \frac{1}{2\pi}\int_{-\infty}^{+\infty}\Big\{\Big[-A_3(\alpha) + (2|\alpha|\kappa - x)A_4(\alpha)\Big]e^{-|\alpha|x} +$$

$$C(\alpha)\exp\left[-x\left(\frac{\kappa\alpha^2+1}{\kappa}\right)^{1/2}\right]\Big\}e^{-i\alpha y}d\alpha \quad , \tag{3.53}$$

$$\Omega(x,y) = \frac{1}{2\pi}\int_{-\infty}^{+\infty} A_5(\alpha)e^{-Rx}\ e^{-i\alpha y}d\alpha \quad , \tag{3.54}$$

where

$$R = \left[\ \alpha^2 + \frac{2}{\kappa(1-\nu)}\ \right]^{1/2} \quad . \tag{3.55}$$

For either the symmetric or the skew-symmetric problem there are five conditions with which to determine six constants, $A_i(\alpha)$, $i=1,\ldots,5$, and $C(\alpha)$. This shows that one constant is extra and we take

$$C(\alpha) = 0 \quad , \tag{3.56}$$

and proceed to show that the problem can be uniquely solved without it. Now that the four unknowns, w,ϕ,ψ, and Ω are known in terms of the five unknown coefficients, the other plate variables are expressed in terms of them. N_{xx}, N_{yy}, and N_{xy} are already expressed in this form in Eqn. 3.21. The other important expressions are,

$$\beta_x = \kappa\frac{1-\nu}{2}\frac{\partial\Omega}{\partial y} + \frac{\partial\psi}{\partial x} \quad , \tag{3.57}$$

$$\beta_y = -\kappa\frac{1-\nu}{2}\frac{\partial\Omega}{\partial x} + \frac{\partial\psi}{\partial y} \quad , \tag{3.58}$$

$$M_{xx} = \gamma\left\{\ \kappa\frac{(1-\nu)^2}{2}\frac{\partial^2\Omega}{\partial x\partial y} + \frac{\partial^2\psi}{\partial x^2} + \nu\frac{\partial^2\psi}{\partial y^2}\ \right\} \quad , \tag{3.59}$$

$$M_{yy} = \gamma\left\{\ \kappa\frac{(1-\nu)^2}{2}\frac{\partial^2\Omega}{\partial x\partial y} + \frac{\partial^2\psi}{\partial y^2} + \nu\frac{\partial^2\psi}{\partial x^2}\ \right\} \quad , \tag{3.60}$$

$$M_{xy} = \frac{1}{24(1+\nu)}\left\{\kappa\frac{1-\nu}{2}\left[\ \frac{\partial^2\Omega}{\partial y^2} - \frac{\partial^2\Omega}{\partial x^2}\ \right] + 2\frac{\partial^2\psi}{\partial x\partial y}\ \right\} \quad , \tag{3.61}$$

$$V_x = \frac{\partial w}{\partial x} + \kappa\frac{1-\nu}{2}\frac{\partial\Omega}{\partial y} + \frac{\partial\psi}{\partial x} \quad , \tag{3.62}$$

$$V_y = \frac{\partial w}{\partial y} - \kappa\frac{1-\nu}{2}\frac{\partial \Omega}{\partial x} + \frac{\partial \psi}{\partial y} \quad , \tag{3.63}$$

$$\frac{\partial^2 u}{\partial y^2} = -(2+\nu)\frac{\partial^3 \phi}{\partial y^2 \partial x} - \frac{\partial^3 \phi}{\partial x^3} \quad , \tag{3.64}$$

$$\frac{\partial v}{\partial y} = \frac{\partial^2 \phi}{\partial x^2} - \nu\frac{\partial^2 \phi}{\partial y^2} \quad . \tag{3.65}$$

Now if Eqns. 3.51-54 are substituted into Eqns. 3.21,57-65 the result is,

$$N_{xx} = -\frac{1}{2\pi}\int_{-\infty}^{+\infty} \alpha^2\left[A_1(\alpha) + xA_2(\alpha)\right]e^{-|\alpha|x}e^{-i\alpha y}\, d\alpha \quad , \tag{3.66}$$

$$N_{yy} = \frac{1}{2\pi}\int_{-\infty}^{+\infty}\left[\alpha^2 A_1(\alpha) + A_2(\alpha)(\alpha^2 x - 2|\alpha|)\right]e^{-|\alpha|x}e^{-i\alpha y}\, d\alpha \quad , \tag{3.67}$$

$$N_{xy} = \frac{i}{2\pi}\int_{-\infty}^{+\infty} \alpha\left[-|\alpha|A_1(\alpha) + (1-x|\alpha|)A_2(\alpha)\right]e^{-|\alpha|x}e^{-i\alpha y}\, d\alpha \quad , \tag{3.68}$$

$$\beta_x = \kappa\frac{1-\nu}{2}\frac{-i}{2\pi}\int_{-\infty}^{+\infty} \alpha A_5(\alpha)e^{-Rx}\, e^{-i\alpha y} d\alpha \; +$$

$$\frac{1}{2\pi}\int_{-\infty}^{+\infty}\left[|\alpha|A_3(\alpha) - (2\alpha^2\kappa - x|\alpha| + 1)A_4(\alpha)\right]e^{-|\alpha|x}e^{-i\alpha y} d\alpha \quad , \tag{3.69}$$

$$\beta_y = \kappa\frac{1-\nu}{2}\frac{1}{2\pi}\int_{-\infty}^{+\infty} RA_5(\alpha)e^{-Rx}e^{-i\alpha y} d\alpha \; -$$

$$\frac{i}{2\pi}\int_{-\infty}^{+\infty} \alpha\left[-A_3(\alpha) + (2|\alpha|\kappa - x)A_4(\alpha)\right]e^{-|\alpha|x}e^{-i\alpha y} d\alpha \quad , \tag{3.70}$$

$$M_{xx} = \frac{\gamma}{2\pi}\int_{-\infty}^{+\infty}\Big\{(1-\nu)\alpha^2\left[(2\kappa|\alpha| - x)A_4(\alpha) - A_3(\alpha)\right] +$$

$$2|\alpha|A_4(\alpha)\Big\}e^{-|\alpha|x}e^{-i\alpha y}\, d\alpha \; +$$

$$+ \frac{\gamma\kappa}{2}(1-\nu)^2 \frac{i}{2\pi} \int_{-\infty}^{+\infty} \alpha R A_5(\alpha) e^{-Rx} e^{-i\alpha y} \, d\alpha \quad , \tag{3.71}$$

$$M_{yy} = \frac{-\gamma}{2\pi} \int_{-\infty}^{+\infty} \Big\{ (1-\nu)\alpha^2 \Big[(2\kappa|\alpha|-x) A_4(\alpha) - A_3(\alpha) \Big] +$$

$$2\nu|\alpha| A_4(\alpha) \Big\} e^{-|\alpha|x} e^{-i\alpha y} \, d\alpha -$$

$$- \frac{\gamma\kappa}{2}(1-\nu)^2 \frac{i}{2\pi} \int_{-\infty}^{+\infty} \alpha R A_5(\alpha) e^{-Rx} e^{-i\alpha y} \, d\alpha \quad , \tag{3.72}$$

$$M_{xy} = -\gamma(1-\nu)\frac{i}{2\pi} \int_{-\infty}^{+\infty} \alpha \Big[(x|\alpha| - 2\kappa\alpha^2 - 1) A_4(\alpha) + |\alpha| A_3(\alpha) \Big] e^{-|\alpha|x} e^{-i\alpha y} \, d\alpha$$

$$-\frac{\gamma\kappa}{4}(1-\nu)^2 \frac{1}{2\pi} \int_{-\infty}^{+\infty} (\alpha^2 + R^2) A_5(\alpha) e^{-Rx} e^{-i\alpha y} \, d\alpha \quad , \tag{3.73}$$

$$V_x = -\frac{\kappa}{\pi} \int_{-\infty}^{+\infty} \alpha^2 A_4(\alpha) e^{-|\alpha|x} e^{-i\alpha y} \, d\alpha -$$

$$- \frac{\kappa}{2}(1-\nu)\frac{i}{2\pi} \int_{-\infty}^{+\infty} \alpha A_5(\alpha) e^{-Rx} e^{-i\alpha y} \, d\alpha \quad , \tag{3.74}$$

$$V_y = -i\frac{\kappa}{\pi} \int_{-\infty}^{+\infty} \alpha|\alpha| A_4(\alpha) e^{-|\alpha|x} e^{-i\alpha y} \, d\alpha +$$

$$+ \frac{\kappa}{2}(1-\nu)\frac{1}{2\pi} \int_{-\infty}^{+\infty} R A_5(\alpha) e^{-Rx} e^{-i\alpha y} \, d\alpha \quad , \tag{3.75}$$

$$\frac{\partial^2 u}{\partial y^2} = \frac{1}{2\pi} \int_{-\infty}^{+\infty} \alpha^2 \Big[-(1+\nu)|\alpha| A_1(\alpha) + A_2(\alpha)(-1+\nu-|\alpha|x(1+\nu)) \Big] e^{-|\alpha|x} e^{-i\alpha y} d\alpha \tag{3.76}$$

$$\frac{\partial v}{\partial y} = \frac{1}{2\pi} \int_{-\infty}^{+\infty} \Big[(1+\nu)\alpha^2 A_1(\alpha) + A_2(\alpha)(-2|\alpha| + x\alpha^2 + \nu\alpha^2 x) \Big] e^{-|\alpha|x} e^{-i\alpha y} d\alpha \tag{3.77}$$

3.2 Symmetric loading, Mode 1.

The symmetry conditions are,

$$N_{xy}(0,y) = 0 \quad , \tag{3.78}$$

$$M_{xy}(0,y) = 0 \quad , \tag{3.79}$$

$$V_x(0,y) = 0 \quad . \tag{3.80}$$

After using this information in Eqns. 3.68,73,74 we obtain

$$A_1(\alpha) = \frac{1}{|\alpha|} A_2(\alpha) \quad , \tag{3.81}$$

$$A_3(\alpha) = \frac{\kappa(\alpha^2+R^2)+1}{|\alpha|} A_4(\alpha) \quad , \tag{3.82}$$

$$A_5(\alpha) = \frac{4\alpha i}{1-\nu} A_4(\alpha) \quad . \tag{3.83}$$

This eliminates three of the five unknown constants leaving only $A_2(\alpha)$ and $A_4(\alpha)$. The following two mixed boundary conditions will determine them.

$$N_{xx}(0^+,y) = -f_1(y) \quad , \quad y \text{ in } L_n \quad , \tag{3.84}$$

$$u(0^+,y) = 0 \quad , \quad y \text{ outside of } L_n \quad , \tag{3.85}$$

$$M_{xx}(0^+,y) = -f_2(y) \quad , \quad y \text{ in } L_n \quad , \tag{3.86}$$

$$\beta_x(0^+,y) = 0 \quad , \quad y \text{ outside of } L_n \quad , \tag{3.87}$$

where

$$L_n = (a_1,b_1),\ (a_2,b_2),\ \ldots\ ,\ (a_n,b_n) \quad , \tag{3.88}$$

each section (a_i,b_i) defining a crack on x=0. Note that since all length quantities are normalized with respect to the plate thickness h, each section is actually $(a_i/h,b_i/h)$. After using Eqns. 3.81-83 in

Eqns. 3.66,76,71 and 69 we obtain the following,

$$N_{xx}(0,y) = \lim_{x\to 0} \frac{-1}{2\pi} \int_{-\infty}^{+\infty} |\alpha| A_2(\alpha) e^{-|\alpha|x} e^{-i\alpha y} \, d\alpha \quad , \tag{3.89}$$

$$\left.\frac{\partial^2 u}{\partial y^2}\right|_{x=0} = \lim_{x\to 0} \frac{-1}{2\pi} \int_{-\infty}^{+\infty} 2A_2(\alpha)\alpha^2 e^{-|\alpha|x} e^{-i\alpha y} \, d\alpha \quad , \tag{3.90}$$

$$M_{xx}(0,y) = \lim_{x\to 0} \frac{\gamma\kappa(1-\nu)}{2\pi} \int_{-\infty}^{+\infty} \left\{ \left[2\alpha^2|\alpha| + \frac{\alpha\ (3+\nu)}{|\alpha|\kappa(1-\nu)} \right] e^{-|\alpha|x} \right.$$

$$\left. - 2\alpha^2 R e^{-Rx} \right\} A_4(\alpha) e^{-i\alpha y} \, d\alpha \quad , \tag{3.91}$$

$$\beta_x(0,y) = \lim_{x\to 0} \frac{-1}{2\pi} \int_{-\infty}^{+\infty} A_4(\alpha) \left[2\kappa\alpha^2 e^{-Rx} - \kappa(\alpha^2+R^2) e^{-|\alpha|x} \right] e^{-i\alpha y} \, d\alpha \quad . \tag{3.92}$$

Note that Eqns. 3.89,90 are uncoupled from 3.91,92 for simple $f_i(y)$ in the mixed boundary conditions 3.84,86.

3.2.1 Tension.

The singular integral equation for tension will be derived first. Consider Eqn. 3.90.

$$\left.\frac{\partial^2 u}{\partial y^2}\right|_{x=0} = \frac{1}{2\pi} \int_{-\infty}^{+\infty} -2A_2(\alpha)\alpha^2 e^{-i\alpha y} \, d\alpha \quad . \tag{3.93}$$

From Eqns. 3.44,45 we invert 3.93,

$$-2\alpha^2 A_2(\alpha) = \int_{-\infty}^{+\infty} \left.\frac{\partial^2 u}{\partial t^2}\right|_{x=0} e^{i\alpha t} dt \quad , \tag{3.94}$$

and then integrate by parts twice noting that $u(t)$ is zero at infinity.

$$-2\alpha^2 A_2(\alpha) = -i\alpha \int_{-\infty}^{+\infty} \left.\frac{\partial u}{\partial t}\right|_{x=0} e^{i\alpha t} dt \quad , \tag{3.95}$$

$$= -\alpha^2 \int_{-\infty}^{+\infty} u(t) e^{i\alpha t} dt \quad , \tag{3.96}$$

or

$$A_2(\alpha) = \frac{1}{2} \int_{L_n} u(t) e^{i\alpha t} dt \quad , \tag{3.97}$$

where use has been made of Eqn. 3.85. Now $A_2(\alpha)$ is substituted into Eqn. 3.89 and the displacement u(t) becomes the only unknown in the problem. After defining

$$u_1(t) = u(t) \quad ,$$

we have,

$$N_{xx}(0,y) = \lim_{x \to 0} \frac{-1}{2\pi} \int_{-\infty}^{+\infty} \frac{|\alpha|}{2} \int_{L_n} u_1(t) e^{i\alpha t} dt \; e^{-|\alpha| x} e^{-i\alpha y} d\alpha \quad , \tag{3.98}$$

or

$$N_{xx}(0,y) = \lim_{x \to 0} \frac{-1}{2\pi} \int_{L_n} u_1(t) \int_{-\infty}^{+\infty} \frac{|\alpha|}{2} e^{-|\alpha| x} e^{i\alpha(t-y)} \, d\alpha \, dt \quad . \tag{3.99}$$

Next using

$$\lim_{x \to 0} \int_0^{+\infty} \alpha \cos\alpha(t-y) e^{-\alpha x} d\alpha = \frac{-2}{(t-y)^2} \quad , \tag{3.100}$$

Eqn. 3.99 becomes,

$$N_{xx}(0,y) = \frac{1}{2\pi} \int_{L_n} \frac{u_1(t)}{(t-y)^2} dt \quad , \quad \text{for all } y \quad , \tag{3.101}$$

or

$$-f_1(y) = \frac{1}{2\pi} \oint_{L_n} \frac{u_1(t)}{(t-y)^2} dt \quad , \quad \text{for } y \text{ in } L_n \quad . \tag{3.102}$$

For a single crack in tension Eqn. 3.102 becomes,

$$\frac{1}{2\pi} \fint_{-a}^{+a} \frac{u_1(t)}{(t-y)^2}\, dt = f_1(y) = \overset{\infty}{N}_{xx} = \frac{\overset{\infty}{N}_{11}}{hE} = \frac{\overset{\infty}{\sigma}_1}{E} \quad . \tag{3.103}$$

The solution is

$$u_1(y) = 2\,\frac{\overset{\infty}{\sigma}}{E}\,(a^2-y^2)^{1/2} \quad . \tag{3.104}$$

If we substitute this back into Eqn. 3.101, the stress in front of the crack is,

$$\frac{\sigma_1(y)}{E} = \frac{1}{2\pi} \int_{-a}^{+a} 2\,\frac{\overset{\infty}{\sigma}}{E}\,\frac{(a^2-y^2)^{1/2}}{(t-y)^2}\, dt = \frac{\overset{\infty}{\sigma}}{E}\left\{ \frac{|y|}{(y^2-a^2)^{1/2}} - 1 \right\} \quad . \tag{3.105}$$

To determine the stress intensity factor, we use Eqn. G.10,

$$k_1 = \lim_{y\to a} [2(y-a)]^{1/2}\sigma_1(y) \quad , \tag{3.106}$$

$$= \lim_{y\to a} \frac{\overset{\infty}{\sigma} y [2(y-a)]^{1/2}}{(y+a)^{1/2}(y-a)^{1/2}} = \overset{\infty}{\sigma}\sqrt{a} \quad . \tag{3.107}$$

Therefore

$$\frac{k_1}{\overset{\infty}{\sigma}_1\sqrt{a}} = 1 \quad . \tag{3.108}$$

Now determine the stress intensity factor using Eqn. G.11.

$$k_1 = \frac{4\mu}{K+1} \lim_{y\to a} \frac{u_1(t)}{\sqrt{2(y-a)}} = \frac{E}{2} \lim_{y\to a} 2\,\frac{\overset{\infty}{\sigma}}{E}\,\frac{(a^2-y^2)^{1/2}}{\sqrt{2(y-a)}} = \overset{\infty}{\sigma}\sqrt{a} \quad , \tag{3.109}$$

where the following substitutions have been made,

$$K = \frac{3-\nu}{1+\nu} \quad , \quad \mu = \frac{E}{2(1+\nu)} \quad . \tag{3.110}$$

Therefore using either stress or displacement the result is the same. This should not be taken for granted because the equations predicting

stress and displacement are from plate theory, while the stress intensity factor is defined in terms of elasticity theory. It is important to note that the classical plate theory is identical to Reissner's theory for tension, Eqn. 3.101.

In Fig. 3.1a at the end of the chapter the stress intensity factors for two identical cracks with a/h=1 are plotted for varying separation distance.

3.2.2 Bending.

For the bending problem from Eqn. 3.91

$$\beta_x(0,y) = u_2(y) = \frac{1}{2\pi}\int_{-\infty}^{+\infty} A_4(\alpha)\kappa(\alpha^2-R^2)e^{-i\alpha y}d\alpha \quad . \tag{3.111}$$

After inversion, making use of Eqn. 3.55, $A_4(\alpha)$ in terms of the new unknown, $u_2(t)$ is,

$$A_4(\alpha) = \frac{1-\nu}{-2}\int_{L_n} u_2(t)e^{i\alpha t}dt \quad . \tag{3.112}$$

This is substituted into Eqn. 3.91,

$$M_{xx}(0,y) = \lim_{x\to 0}\frac{\gamma\kappa(1-\nu)}{2\pi}^2\int_{L_n} u_2(t)\int_{-\infty}^{+\infty}\left\{\left[2\alpha^2|\alpha|+\frac{\alpha\ (3+\nu)}{|\alpha|\kappa(1-\nu)}\right]e^{-|\alpha|x}\right.$$

$$\left. - 2\alpha^2 Re^{-Rx}\right\}e^{i\alpha(t-y)}d\alpha\ dt \quad . \tag{3.113}$$

After using Eqn. 3.100 and the following integrals,

$$\lim_{x\to 0}\int_0^{+\infty}\alpha^3\cos\alpha(t-y)e^{-\alpha x}d\alpha = \frac{6}{(t-y)^4} \quad , \tag{3.114}$$

$$\lim_{x\to 0}\int_0^{+\infty}\alpha^2 Re^{-Rx}\cos\alpha(t-y)\ d\alpha = \frac{1}{2\gamma\kappa(1-\nu)^2}\left\{\frac{4\gamma}{\kappa}\left[K_2(\beta|t-y|)-\right.\right.$$

$$K_0(\beta|t-y|)\Big] + \frac{12\gamma(1-\nu)}{(t-y)^2}K_2(\beta|t-y|)\Big\} \quad , \tag{3.115}$$

where

$$\beta = \left(\frac{2}{\kappa(1-\nu)}\right)^{1/2} = (10)^{1/2} \quad , \tag{3.116}$$

we obtain

$$M_{xx}(0,y) = \frac{1}{2\pi}\int_{L_n} u_2(t)\Big\{\frac{-12\gamma\kappa(1-\nu)^2}{(t-y)^4} + \frac{\gamma(1-\nu)(3+\nu)}{(t-y)^2} +$$

$$\frac{4\gamma}{\kappa}\Big[K_2(\beta|t-y|)-K_0(\beta|t-y|)\Big] + \frac{12\gamma(1-\nu)}{(t-y)^2}K_2(\beta|t-y|)\Big\}dt \quad , \tag{3.117}$$

which is valid for all y. K_2 and K_0 are modified Bessel functions of the second kind. If y is in L_n, we use Eqn. 3.87 to write,

$$-f_2(y) = \frac{\gamma(1-\nu^2)}{2\pi}\fint_{L_n}\frac{u_2(t)}{(t-y)^2}\,dt + \frac{1}{2\pi}\int_{L_n} u_2(t)K_{22}(y,t)\,dt \quad , \tag{3.118}$$

where

$$K_{22}(y,t) = \frac{\gamma}{\kappa}\ln(\beta|t-y|) + \Big\{\frac{2\gamma(1-\nu)}{(t-y)^2} - \frac{12\gamma\kappa(1-\nu)^2}{(t-y)^4} + \frac{4\gamma}{\kappa}\Big[K_2(\beta|t-y|)-$$

$$K_0(\beta|t-y|)\Big] + \frac{12\gamma(1-\nu)}{(t-y)^2}K_2(\beta|t-y|) - \frac{\gamma}{\kappa}\ln(\beta|t-y|)\Big\} \quad . \tag{3.119}$$

It is convenient to write this Fredholm kernel in terms of a single variable,

$$K_{22}(y,t) = \frac{5K(z)}{12(1+\nu)} \quad , \quad z = \beta|t-y| \quad , \tag{3.120}$$

where

$$K(z) = \Big\{\frac{-48}{z^4} + \frac{4}{z^2} - 4K_0(z) + 4K_2(z) + \frac{24}{z^2}K_2(z)\Big\} \quad . \tag{3.121}$$

To show that K(z) is a Fredholm kernel, the small z expansions for the Bessel functions are,

$$K_0(z) \sim -\ln(z/2) - \gamma_e - (z/2)^2\ln(z/2) + O(z^2) \ . \tag{3.122}$$

$$K_2(z) \sim 2/z^2 - 1/2 - 1/2(z/2)^2\ln(z/2) - 1/2(z/2)^2(\gamma_e+5/4)$$

$$- 1/6(z/2)^4\ln(z/2) + O(z^4) \quad , \tag{3.123}$$

where Euler's constant, $\gamma_e = .5772157....$ Substitution of these expansions into Eqn. 3.121 leads to the following behavior for K(z),

$$\lim_{z\to 0} K(z) \sim \left\{\ln(z/2)+(\gamma_e-23/4)+(z/2)^2\ln(z/2)+...\right\} \ . \tag{3.124}$$

For simple plate bending,

$$f_2(y) = \overset{\infty}{M}_{xx} = \frac{\overset{\infty}{M}_{11}}{h^2E} = \frac{\overset{\infty}{\sigma}_2}{6E} \quad . \tag{3.125}$$

The log singularity has been separated from the Fredholm kernel, see Eqn. 3.119. In such a case it was found helpful to handle this part in closed form. However it is possible that the contribution of the log term is nearly equal to, but of opposite sign as the rest of the kernel. Separate treatment here could lead to convergence problems especially for geometries (a/h approaching ∞ for Eqn. 3.118) where the coefficient of the log term gets large. In many problems this coefficient is small and a closed form analysis of the log is not necessary. See Appendix I for the effect of this log behavior on the numerical convergence. It should be noted that if the unknown were the derivative of the rotation, this log term would be replaced by,

$$(t-y)\ln(\beta|t-y|) \quad , \tag{3.126}$$

which is non-singular and easier to integrate (see. Appendix I). This is the least desirable feature of the strongly singular formulation. The Fredholm kernel is essentially divided by (t-y), or alternatively, the infinite integrals which determine the Fredholm kernel decay more slowly by a factor of α, see Appendix J, section 4. This means more asymptotic analysis for equal decay between the two methods. For example the infinite integral for the tension problem, Eqn. 3.100 would be replaced by,

$$\lim_{x\to 0} \int_0^{+\infty} \sin\alpha(t-y)e^{-\alpha x}d\alpha = \frac{1}{t-y} \quad . \tag{3.127}$$

In most problems the infinite integrals must be evaluated numerically so this factor of α becomes important, see Chapter 5.

For a single crack of half length a, Eqn. 3.118 may be written as

$$\frac{h}{24a\pi} \fint_{-1}^{+1} \frac{u_2(\frac{a}{h}r)}{(r-s)^2}\, dr + \frac{5a}{12h(1+\nu)} \frac{1}{2\pi} \int_{-1}^{+1} u_2(\tfrac{a}{h}r)K(\tfrac{a}{h}\beta|r-s|)\, dr = -\overset{\infty}{M}_{xx},$$

$$-1<s<1 \quad . \tag{3.128}$$

If we define

$$u_2(t) = \frac{24a}{h} \overset{\infty}{M}_{xx}\, g(r) \quad , \quad \varsigma = \frac{a}{h}\beta|r-s| = z = \beta|t-y| \quad , \tag{3.129}$$

the equation becomes,

$$\frac{1}{\pi} \fint_{-1}^{+1} \frac{g(r)}{(r-s)^2}\, dr + \frac{5}{\pi(1+\nu)}(a/h)^2 \int_{-1}^{+1} g(r)K(\varsigma)\, dt = -1 \ , \tag{3.130}$$

This equation must be solved numerically, see Appendix E for an explanation of the collocation method. From section 2 of Appendix G, and Eqn. 3.130 the stress intensity factor (actually the maximum value at the plate surface) will be given by,

$$\frac{k_1}{\overset{\infty}{\sigma}_2\sqrt{a}} = f(1) = f(-1) \quad , \tag{3.131}$$

where

$$g(r) = f(r)(1-r^2)^{1/2} \quad , \quad -1 \leq r \leq 1 \quad . \tag{3.132}$$

The stress intensity factor of Eqn. 3.131 is predicted by either stresses (Eqn. G.10) or displacements (Eqn. G.11).

The governing equations for classical plate bending are identical to 3.1-20 with the exception that the transverse shear deformation, θ_i in Eqns. 3.18,19 are zero, or B (Eqn. 3.20) is infinite. The symmetry conditions, Eqns. 3.78-80, cannot be separately satisfied. For classical plate bending,

$$N_{xy}(0,y) = 0 \quad , \tag{3.133}$$

$$\frac{\partial M_{xy}}{\partial y} + V_x(0,y) = 0 \quad . \tag{3.134}$$

The result of this formulation for the determination of the rotation is,

$$\frac{3+\nu}{1+\nu}\,\frac{h}{24a}\,\frac{1}{\pi}\,\fint_{-1}^{+1}\frac{u_2(\frac{a}{h}r)}{(r-s)^2}\,dr = -\overset{\infty}{M}_{xx} \quad , \quad -1<s<1 \quad , \tag{3.135}$$

or in terms of g(r),

$$\frac{3+\nu}{1+\nu}\,\frac{1}{\pi}\,\fint_{-1}^{+1}\frac{g(r)}{(r-s)^2}\,dt = -1 \quad . \tag{3.136}$$

This equation can be solved in closed form.

$$\frac{\sigma_2(y)}{6E} = \frac{\overset{\infty}{\sigma}_2}{6E}\left\{\frac{|y|}{[y^2-(a/h)^2]^{1/2}} - 1\right\} \quad , \tag{3.137}$$

$$u_2(y) = \frac{1+\nu}{3+\nu}\,\frac{24a}{h}\,\frac{\overset{\infty}{\sigma}_2}{6E}\sqrt{1-\left(\frac{h}{a}y\right)^2} \quad , \qquad -a/h<y<a/h \quad . \tag{3.138}$$

Eqn. 3.137 predicts

$$\frac{k_1}{\overset{\infty}{\sigma}_2\sqrt{a}} = 1 \quad , \tag{3.139}$$

while Eqn. 3.138 predicts

$$\frac{k_1}{\overset{\infty}{\sigma}_2\sqrt{a}} = \frac{1+\nu}{3+\nu} \quad . \tag{3.140}$$

This inconsistency shows that the classical plate theory is inadequate to solve for crack tip SIFs for bending. It is also true for out-of-plane shear and for twisting.

In Fig. 3.2 the normalized stress intensity factor as a function of crack length to plate thickness ratio is plotted for Reissner's theory. Table 3.1 lists some values. Note that for large h/a the limit is one, the same as the classical prediction using the stress intensity factor defined in terms of stress, Eqn. 3.139. The other limit, the thin plate limit, is not so clear. It has been reported by [6] that in the limit as h/a goes to zero, the stress intensity factor for the Reissner plate, (Eqn. 3.131) approaches the value $(1+\nu)/(3+\nu)$ as predicted by Eqn. 3.140 from the classical theory, (note that h=0 is not valid for Reissner's theory). Another way of putting this is that Eqn. 3.130 becomes 3.136. The evidence provided by table 3.1 for a/h = 1000 seems to indicate that this is not the case. Numerically it is very difficult to obtain convergent results in the long crack/thin plate domain using the methods of Appendix E, and for

further results some kind of asymptotic analysis with a specially suited numerical scheme seems appropriate. As an aside, for this geometry, a power series (Eqn. E.29) was not adequate using single precision (14 digits). The coefficients were as high as $1.\times 10^{15}$, for example see table E.1. The problem was solved using Chebychev polynomials. The following analysis is provided to support the claim that the curve in Fig. 3.2 does not "reach" the value $(1+\nu)/(3+\nu)$.

3.2.3 Thin Plate Bending.

We consider the large a/h limit of Eqn. 3.130. Only the Fredholm kernel need be analyzed. First define

$$I(s,a/h) = \frac{5}{\pi(1+\nu)}(a/h)^2 \int_{-1}^{+1} g(r)K(\varsigma)\, dr$$

$$= \frac{\rho^2}{2\pi(1+\nu)} \int_{-1}^{+1} g(r)K(\varsigma)\, dr \quad , \tag{3.141}$$

where $\rho=\beta(a/h)$ is introduced for convenience. From Appendix H,

$$\lim_{\rho\to\infty} I(s,a/h) = \frac{2}{\pi(1+\nu)} \fint_{-1}^{+1} \frac{g(r)}{(r-s)^2}\, dr = \frac{2}{\pi(1+\nu)} \fint_{-1}^{+1} \frac{g'(r)}{r-s}\, dr \ , |s|<1, \tag{3.142}$$

$$= \frac{2}{\pi(1+\nu)} \int_{-1}^{+1} \frac{g(r)}{(r-s)^2}\, dr = \frac{2}{\pi(1+\nu)} \int_{-1}^{+1} \frac{g'(r)}{r-s}\, dr \ , \ |s|>1 \ , \tag{3.143}$$

$$= ? \quad , \ y \text{ "near" } 1, \text{ ie. } \rho(1-y) = O(1) \ . \tag{3.144}$$

If Eqn. 3.142 were valid for $|s|=h/a|y|\leq 1$ then in the limit as ρ approaches infinity, Eqn. 3.130 would be identical to Eqn. 136 and therefore the stress intensity factor would be $(1+\nu)/(3+\nu)$. But this is not the case. Figs. 3.3a-c compare I(s,a/h) to the limiting

integrals above. The numerically determined function for g(r) was used to compute these integrals. See Figs. 3.4-5 for plots of g(r),f(r) as defined in Eqn. 3.132, and Fig. 3.6 for the ratio of g(0) from Reissner's theory to g(0) from the classical theory. Also see table 3.2 for numerical values of this ratio. This table shows that in the limit as $h \to 0$, Reissner's theory behaves like the classical theory away from the crack tip. With regard to Fig. 3.3, the distinct difference between I(s,a/h) and the limiting integrals is that I(s,a/h) is continuous at s=1. The "spike" created when I(s,a/h) goes from 1^- to 1^+ gives a contribution to the stress intensity factor that makes it different from $(1+\nu)/(3+\nu)$. This contribution is of significance because it is located at the crack tip. In order to proceed further in the analysis, the area of the spike, which would represent a normalized force (or couple), must be determined. Consider the following:

$$M = \lim_{\rho\to\infty} \int_0^{+1} \left\{ \frac{\rho^2}{2\pi(1+\nu)} I(s,a/h) + \frac{2}{3+\nu} \right\} ds \ , \tag{3.145}$$

$$= \lim_{\rho\to\infty} \frac{\rho^2}{2\pi(1+\nu)} \int_{-1}^{+1} g(r) \int_0^{+1} K(\varsigma) ds \, dr + \frac{2}{3+\nu} \ , \tag{3.146}$$

$$= \lim_{\rho\to\infty} \frac{\rho}{2\pi(1+\nu)} \int_{-1}^{+1} g(r) \left\{ \frac{-16}{u^3} + \frac{4}{u} + \frac{8}{u} K_2(u) \right\} dr + \frac{2}{3+\nu} \ , \quad u=\rho(1-r) \ . \tag{3.147}$$

Again the behavior of this integral near r=1 makes it difficult to analyze. Note that the order one contribution to M coming from the "outer solution" of g(r), Eqns. 3.129,138, drops out.

The limiting value of the stress intensity factor was not found but we can make the following conclusion. Since I(s,a/h) for $|s|>1$ has the behavior of Eqn. 3.143,

$$\lim_{\rho\to\infty} \lim_{s\to 1^+} I(s,a/h) \sim \frac{1}{\sqrt{1-s}} \quad , \tag{3.148}$$

where from Eqn. 3.143, it may be stated that

$$\lim_{\rho\to\infty} \lim_{s\to 1^+} I(s,a/h) \sim \sqrt{\rho} \quad . \tag{3.149}$$

This order analysis is supported by Fig. 3.3. This tells us that the magnitude of the integrated Fredholm kernel, i.e. I(s,a/h), which represents a normalized stress resultant term, (actually a couple), becomes infinite according to Eqn. 3.149. Again since we are dealing with a region where $\rho(1-s)$ is of order one, the "thickness" or support of the spike is of order (1-s) or ρ^{-1}. Therefore the area under the spike, given by eqn 3.147, which represents normalized force, should go to zero as $\rho^{-1/2}$. In order to determine the stress intensity factor for h/a approaching zero the coefficient of this leading order term must be known. If the area were of order one, the contribution to the stress intensity factor would be of order $(1-s)^{-1/2}$, see Sih [72]. If the value of stress resultant were of order one, the area would be zero and there would be no contribution. But the limit is between these two cases and the contribution is finite, probably resulting in a stress intensity factor that can be drawn within the space provided by the lower plot of Fig. 3.2.

Some other results for the bending problem are given at the end of the chapter. In Fig. 3.7 the normalized bending stresses ahead of the crack tip are plotted for a/h=1 and 10 (Eqn. 3.117). In table 3.3

some results for crack interaction are listed for four different crack length ratios, (this table may also be found in [59]). Fig. 3.1 provides a plot of the interaction of equal length cracks where a/h=1 for tension, bending, out-of-plane shear and twisting to compare how strong the interaction is for the various loadings. In-plane-shear is identical to tension, (shown later in this chapter).

3.3 Skew-Symmetric loading, Modes 2 & 3

The symmetry conditions are

$$N_{xx}(0,y) = 0 \quad , \tag{3.150}$$

$$M_{xx}(0,y) = 0 \quad . \tag{3.151}$$

After using this information in Eqns. 3.66,71 we obtain,

$$A_1(\alpha) = 0 \ , \tag{3.152}$$

$$A_3(\alpha) = \left\{2\kappa|\alpha| + \frac{2}{(1-\nu)|\alpha|}\right\}A_4(\alpha) + \frac{i\kappa}{2\alpha}(1-\nu)RA_5(\alpha) \quad . \tag{3.153}$$

This eliminates two of the five unknown constants leaving only $A_2(\alpha), A_4(\alpha)$ and $A_5(\alpha)$. The following mixed boundary conditions will determine them.

$$V_x(0^+,y) = -f_3(y) \quad , \quad y \text{ in } L_n \quad , \tag{3.154}$$

$$w(0^+,y) = 0 \quad , \quad y \text{ outside of } L_n \quad , \tag{3.155}$$

$$N_{xy}(0^+,y) = -f_4(y) \quad , \quad y \text{ in } L_n \quad , \tag{3.156}$$

$$v(0^+,y) = 0 \quad , \quad y \text{ outside of } L_n \quad , \tag{3.157}$$

$$M_{xy}(0^+,y) = -f_5(y) \quad , \quad y \text{ in } L_n \quad , \tag{3.158}$$

$$\beta_y(0^+,y) = 0 \quad , \quad y \text{ outside of } L_n \quad . \tag{3.159}$$

If Eqns. 3.152,153 are substituted into Eqns. 3.52,68,70,73,74 and 77, the quantities appearing in 3.154-159 may be expressed in terms of the unknowns as follows:

$$V_x(x,y) = \frac{-\kappa}{\pi}\int_{-\infty}^{+\infty} \alpha^2 A_4(\alpha) e^{-|\alpha|x} e^{-i\alpha y} d\alpha$$

$$- \frac{\kappa}{2}(1-\nu)\frac{i}{2\pi}\int_{-\infty}^{+\infty} \alpha A_5(\alpha) e^{-Rx} e^{-i\alpha y} d\alpha \quad , \tag{3.160}$$

$$w(x,y) = \frac{1}{2\pi}\int_{-\infty}^{+\infty}\Big\{A_4(\alpha)\Big[2\kappa|\alpha| + \frac{2}{(1-\nu)|\alpha|} + x\Big]$$

$$+ A_5(\alpha)\frac{i\kappa}{2\alpha}(1-\nu)R\Big\} e^{-|\alpha|x} e^{-i\alpha y} d\alpha \quad , \tag{3.161}$$

$$N_{xy}(x,y) = \frac{i}{2\pi}\int_{-\infty}^{+\infty} \alpha(1-x|\alpha|)A_2(\alpha) e^{-|\alpha|x} e^{-i\alpha y} d\alpha \quad , \tag{3.162}$$

$$\frac{\partial v}{\partial y} = \frac{1}{2\pi}\int_{-\infty}^{+\infty} A_2(\alpha)\Big[\alpha^2 x - 2|\alpha| + \nu x\alpha^2\Big] e^{-|\alpha|x} e^{-i\alpha y} d\alpha \quad , \tag{3.163}$$

$$M_{xy}(x,y) = -\gamma(1-\nu)\frac{i}{2\pi}\int_{-\infty}^{+\infty}\Big\{A_4(\alpha)\Big[x\alpha|\alpha| - \alpha + \frac{2\alpha}{1-\nu}\Big]$$

$$+ \frac{i\kappa}{2}(1-\nu)R|\alpha|A_5(\alpha)\Big\} e^{-|\alpha|x} e^{-i\alpha y} d\alpha$$

$$- \frac{\gamma\kappa}{4}(1-\nu)^2\frac{1}{2\pi}\int_{-\infty}^{+\infty}(\alpha^2+R^2)A_5(\alpha) e^{-Rx} e^{-i\alpha y} d\alpha \quad , \tag{3.164}$$

$$\beta_y(x,y) = \frac{i}{2\pi}\int_{-\infty}^{+\infty}\Big\{A_4(\alpha)\Big[x + \frac{2}{(1+\nu)|\alpha|}\Big] +$$

$$- \frac{i\kappa}{2\alpha}(1-\nu)RA_5(\alpha)\Big\} e^{-|\alpha|x} e^{-i\alpha y} d\alpha + \frac{\kappa}{2}(1-\nu)\frac{1}{2\pi}\int_{-\infty}^{+\infty} RA_5(\alpha) e^{-Rx} e^{-i\alpha y} d\alpha \quad . \tag{3.165}$$

Note that N_{xy} is uncoupled from M_{xy} and V_x. The integral equation for N_{xy} can be seen to be the same as for tension, compare Eqns. 3.89,90 with 3.162,163. The result for

$$u_4(t) = v(0^+,t) \quad , \tag{3.166}$$

is

$$N_{xy}(0,y) = \frac{1}{2\pi} \int_{L_n} \frac{u_4(t)}{(t-y)^2}\, dt \quad , \quad \text{for all } y \quad , \tag{3.167}$$

or

$$-f_4(y) = \frac{1}{2\pi} \fint_{L_n} \frac{u_4(t)}{(t-y)^2}\, dt \quad , \quad \text{for } y \text{ in } L_n \quad . \tag{3.168}$$

For in-plane-shear,

$$f_4(y) = \overset{\infty}{N}_{xy} = \frac{\overset{\infty}{N}_{12}}{hE} = \frac{\overset{\infty}{\sigma}_4}{E} \quad . \tag{3.169}$$

All through crack results for tension are also valid for in-plane-shear. To solve the coupled problem of M_{xy} and V_x, first define

$$u_3(t) = w(0^+,t) \quad , \quad u_5(t) = \beta_y(0^+,t) \quad . \tag{3.170}$$

The unknowns $A_4(\alpha)$ and $A_5(\alpha)$ can then be expressed as,

$$A_4(\alpha) = \frac{-i(1-\nu)|\alpha|}{2\alpha} \int_{L_n} u_5(t) e^{i\alpha t}\, dt \quad , \tag{3.171}$$

$$A_5(\alpha) = \frac{-2i\alpha}{\kappa R(1-\nu)} \int_{L_n} u_3(t) e^{i\alpha t}\, dt$$

$$+ \left[\frac{2\alpha^2}{R} + \frac{2}{\kappa R(1-\nu)}\right] \int_{L_n} u_5(t) e^{i\alpha t}\, dt \quad . \tag{3.172}$$

It remains only to substitute these expressions into Eqns. 3.160 and 164 and to evaluate the infinite integrals in a way similar to the bending problem. The equations become,

$$V_x(0,y) = \frac{1}{2\pi}\int_{L_n}\left\{u_3(t)\left[\frac{2}{(t-y)^2} + K_{33}(z)\right] + u_5(t)K_{35}(z)\right\}dt \ , \tag{3.173}$$

$$M_{xy}(0,y) = \frac{1}{2\pi}\int_{L_n}\left\{u_5(t)\left[\frac{\gamma(1-\nu^2)}{(t-y)^2} + K_{55}(z)\right] + u_3(t)K_{53}(z)\right\}dt \ , \tag{3.174}$$

where

$$K_{33}(z) = \beta^2\left\{-\ln(z) + \left[K_2(z) - \frac{2}{z^2}\right] + \left[K_0(z) + \ln(z)\right]\right\} \ , \tag{3.175}$$

$$K_{35}(z) = \beta\left\{\frac{8}{z^3} - \left[z + \frac{4}{z}\right]K_2(z) + zK_0(z)\right\} \ , \tag{3.176}$$

$$K_{55}(z) = \frac{5}{12(1+\nu)}\left\{\ln(z) + \left[\frac{48}{z^4} - \frac{4}{z^2} + 4K_0(z) - 4K_2(z) - \frac{24}{z^2}K_2(z) + \ln(z)\right] - \left[2K_0(z) + 2\ln(z)\right]\right\} \ , \tag{3.177}$$

$$K_{53}(z) = \frac{5\beta}{12(1+\nu)}\left\{\frac{-8}{z^3} + \left[z + \frac{4}{z}\right]K_2(z) - zK_0(z)\right\} \ . \tag{3.178}$$

If Eqns. 3.154,158 are applied to 3.173,174 the singular integral equations become,

$$\frac{1}{2\pi}\fint_{L_n}\frac{2u_3(t)}{(t-y)^2}\,dt + \frac{1}{2\pi}\int_{L_n}\left\{u_3(t)K_{33}(z) + u_5(t)K_{35}(z)\right\}dt = -f_3(y) \tag{3.179}$$

$$\gamma(1-\nu^2)\frac{1}{2\pi}\fint_{L_n}\frac{u_5(t)}{(t-y)^2}\,dt + \frac{1}{2\pi}\int_{L_n}\left\{u_5(t)K_{55}(z) + u_3(t)K_{53}(z)\right\}dt = -f_5(y) \ . \tag{3.180}$$

The through crack loading for out-of-plane shear is,

$$f_3(y) = \overset{\infty}{V}_x = \frac{12(1+\nu)}{5Eh}\overset{\infty}{V}_1 = \frac{8(1+\nu)}{5E}\overset{\infty}{\sigma}_3 \quad , \tag{3.181}$$

and for twisting,

$$f_5(y) = \overset{\infty}{M}_{xy} = \frac{\overset{\infty}{M}_{12}}{h^2E} = \frac{\overset{\infty}{\sigma}_5}{6E} \quad . \tag{3.182}$$

For small z,

$$K_{33}(z) \sim \beta^2\left\{-\ln(z/2)-(1/2+\gamma_e)-3/2(z/2)^2\ln(z/2)+\ldots\right\} \quad , \tag{3.183}$$

$$K_{35}(z) \sim \beta\left\{-z/2\ln(z/2)+(9/8-\gamma_e/2)z-2/3(z/2)^3\ln(z/2)+\ldots\right\} \quad , \tag{3.184}$$

$$K_{55}(z) \sim \frac{5}{12(1+\nu)}\left\{\ln(z/2)+(\gamma_e+23/4)-(z/2)^2\ln(z/2)+\ldots\right\} \quad , \tag{3.185}$$

$$K_{53}(z) \sim \frac{5\beta}{12(1+\nu)}\left\{(z/2)\ln(z/2)+(\gamma_e/2-9/8)z+2/3(z/2)^3\ln(z/2)+\ldots\right\} \quad . \tag{3.186}$$

The effect of this behavior on convergence is shown in Appendix I.

The collocation method was used to solve Eqns. 3.179,180 with f(y) given by 3.181,182 for a single crack, (tables 3.4-6, see also Ref. [15]), for two identical interacting cracks, (Figs. 3.1c,d), and for two interacting cracks of different size, (table 3.7a,b). The notation for the double crack is given in Fig. 3.8a,b. For a single crack, the stresses ahead of the crack tip are plotted in Figs. 3.9a,b.

Table 3.1 The effect of Poisson's ratio ν and crack length to plate thickness ratio a/h on the normalized bending stress intensity factor. See also Figure 3.2. $\sigma=6M/h^2$.

$$\frac{k_1(h/2)}{\sigma\sqrt{a}}$$

a/h	ν=0	ν=.3	ν=.5
.05	.9851	.9885	.9900
.1	.9583	.9676	.9717
.25	.8735	.8992	.9111
.5	.7804	.8193	.8383
1.	.7020	.7475	.7707
2.	.6518	.6997	.7247
4.	.6211	.6701	.6960
6.	.6091	.6446	.6847
10.	.5984	.6481	.6746
100.	.5803	.6306	.6575
200.		.6292	
1000.		.6276	

Table 3.2 The ratio of crack surface rotation for Reissner's theory to that of the classical theory at the center of a cracked plate subjected to bending, ν=.3. See also Figure 3.6.

a/h	$\beta_R(0)/\beta_c(0)$
$\to 0$	$2.538 \to (3+\nu)/(1+\nu)$
.5	1.892
1.0	1.551
1.5	1.394
2.0	1.309
2.5	1.255
3.0	1.219
4.0	1.172
5.0	1.142
6.0	1.122
7.0	1.107
8.0	1.095
10.0	1.079
100.0	1.011
200.0	1.006
1000.0	1.000
$\to\infty$	1.

Table 3.3 Bending stress intensity factors for a plate with two collinear cracks. $\sigma=6M/h^2$, $\nu=.3$

$$\left(a = \frac{b_1-a_1}{2} = 1,\ c = \frac{b_2-a_2}{2},\ d = a_2-b_1 \right)$$

PLATE BENDING

	c/a \ d/a	0.1	0.25	0.5	1	2	∞
$\frac{k_1(a_1)}{\sigma\sqrt{a}}$	1	.8799	.8551	.8313	.8045	.7798	.7475
	0.5	.8071	.7938	.7821	.7698	.7593	.7475
	0.25	.7711	.7647	.7598	.7551	.7513	.7475
	0.1	.7532	.7512	.7500	.7490	.7482	.7475
$\frac{k_1(b_1)}{\sigma\sqrt{a}}$	1	1.294	1.076	.9599	.8697	.8049	.7475
	0.5	1.063	.9143	.8458	.7995	.7698	.7475
	0.25	.9161	.8220	.7863	.7663	.7550	.7475
	0.1	.8088	.7678	.7563	.7514	.7498	.7475
$\frac{k_1(a_2)}{\sigma\sqrt{a}}$	1	1.294	1.076	.9599	.8697	.8049	.7475
	0.5	1.012	.8405	.7498	.6786	.6261	.5794
	0.25	.7990	.6595	.5867	.5297	.4872	.4496
	0.1	.5647	.4577	.4037	.3627	.3325	.3060
$\frac{k_1(b_2)}{\sigma\sqrt{a}}$	1	.8799	.8551	.8313	.8045	.7798	.7475
	0.5	.7395	.7071	.6771	.6434	.6132	.5794
	0.25	.6275	.5867	.5507	.5135	.4816	.4496
	0.1	.4817	.4293	.3917	.3577	.3308	.3060

Table 3.4 The effect of crack length to plate thickness ratio a/h on the normalized stress intensity factors for out-of-plane shear and for twisting. $\sigma_3=3V/(2h)$, $\sigma_5=6M/h^2$, $\nu=.3$.

	OUT-OF-PLANE SHEAR		TWISTING	
	$\frac{k_2(h/2)}{\sigma_3\sqrt{a}}$	$\frac{k_3(0)}{\sigma_3\sqrt{a}}$	$\frac{k_2(h/2)}{\sigma_5\sqrt{a}}$	$\frac{k_3(0)}{\sigma_5\sqrt{a}}$
a/h				
.01	.0000	1.0009	.9991	-.0000
.05	.0007	1.0138	.9862	-.0003
.1	.0039	1.0398	.9587	-.0018
.25	.0336	1.1402	.8557	-.0121
.5	.1400	1.3223	.7056	-.0359
1.0	.4656	1.6760	.5218	-.0697
1.5	.8510	2.0142	.4186	-.0850
2.0	1.2615	2.3425	.3527	-.0913
3.0	2.1201	2.9800	.2732	-.0934
4.0	3.0067	3.6007	.2268	-.0910
5.0	3.9100	4.2099	.1961	-.0876
6.0	4.8249	4.8107	.1742	-.0840
8.0	6.6784	5.9938	.1448	-.0776
10.0	8.5539	7.1592	.1257	-.0722

Table 3.5 The effect of crack length to plate thickness ratio a/h on the normalized stress intensity factors for out-of-plane shear and for twisting. $\sigma_3=3V/(2h)$, $\sigma_5=6M/h^2$, $\nu=0$.

	OUT-OF-PLANE SHEAR		TWISTING	
	$\frac{k_2(h/2)}{\sigma_3\sqrt{a}}$	$\frac{k_3(0)}{\sigma_3\sqrt{a}}$	$\frac{k_2(h/2)}{\sigma_5\sqrt{a}}$	$\frac{k_3(0)}{\sigma_5\sqrt{a}}$
a/h				
.01	.0000	1.0009	.9989	-.0000
.1	.0039	1.0397	.9471	-.0022
.5	.1368	1.3232	.6530	-.0422
1.0	.4442	1.6831	.4669	-.0770
1.5	.8005	2.0321	.3696	-.0910
2.0	1.1765	2.3739	.3095	-.0959
3.0	1.9578	3.0431	.2388	-.0960
4.0	2.7609	3.6992	.1982	-.0925
5.0	3.5770	4.3463	.1716	-.0883
6.0	4.4022	4.9867	.1527	-.0843
8.0	6.0709	6.2529	.1274	-.0773
10.0	7.7568	7.5048	.1109	-.0716

Table 3.6 The effect of crack length to plate thickness ratio a/h on the normalized stress intensity factors for out-of-plane shear and for twisting. $\sigma_3=3V/(2h)$, $\sigma_5=6M/h^2$, $\nu=.5$

	OUT-OF-PLANE SHEAR		TWISTING	
	$\frac{k_2(h/2)}{\sigma_3\sqrt{a}}$	$\frac{k_3(0)}{\sigma_3\sqrt{a}}$	$\frac{k_2(h/2)}{\sigma_5\sqrt{a}}$	$\frac{k_3(0)}{\sigma_5\sqrt{a}}$
a/h				
.01	.0000	1.0009	.9992	-.0000
.1	.0039	1.0397	.9640	-.0015
.5	.1414	1.3219	.7326	-.0327
1.0	.4761	1.6725	.5523	-.0655
1.5	.8765	2.0051	.4469	-.0814
2.0	1.3051	2.3263	.3782	-.0884
3.0	2.2049	2.9470	.2939	-.0916
4.0	3.1364	3.5486	.2441	-.0899
5.0	4.0870	4.1372	.2111	-.0869
6.0	5.0506	4.7164	.1874	-.0836
8.0	7.0049	5.8542	.1555	-.0775
10.0	8.9840	6.9720	.1348	-.0724

Table 3.7a Stress intensity factors for a plate with two collinear cracks subjected to out-of-plane shear loading. $\sigma = 3V/(2h)$, $\nu=.3$.

$$\left(a = \frac{b_1-a_1}{2} = 1,\ c = \frac{b_2-a_2}{2},\ d = a_2-b_1 \right)$$

PLATE, OUT-OF-PLANE SHEAR

	c/a \ d/a	0.1	0.25	0.5	1	2	∞
$\frac{k_3(a_1)}{\sigma\sqrt{a}}$	1	1.763	1.702	1.675	1.669	1.673	1.676
	0.5	1.736	1.699	1.682	1.675	1.675	1.676
	0.25	1.708	1.688	1.679	1.676	1.676	1.676
	0.1	1.687	1.680	1.677	1.676	1.676	1.676
$\frac{k_3(b_1)}{\sigma\sqrt{a}}$	1	2.909	2.124	1.812	1.694	1.677	1.676
	0.5	2.349	1.906	1.745	1.687	1.677	1.676
	0.25	2.028	1.783	1.706	1.680	1.676	1.676
	0.1	1.804	1.707	1.684	1.677	1.676	1.676
$\frac{k_3(a_2)}{\sigma\sqrt{a}}$	1	2.909	2.124	1.812	1.694	1.677	1.676
	0.5	1.348	.9231	.7425	.6719	.6613	.6611
	0.25	.6723	.4362	.3319	.2908	.2849	.2850
	0.1	.2835	.1741	.1254	.1065	.1039	.1040
$\frac{k_3(b_2)}{\sigma\sqrt{a}}$	1	1.763	1.702	1.675	1.669	1.673	1.676
	0.5	.7705	.7059	.6722	.6596	.6598	.6611
	0.25	.4039	.3387	.3020	.2863	.2846	.2850
	0.1	.2015	.1474	.1180	.1056	.1039	.1040
$\frac{k_2(a_1)}{\sigma\sqrt{a}}$	1	-.5879	-.5348	-.5040	-.4844	-.4739	-.4656
	0.5	-.5214	-.4936	-.4791	-.4711	-.4676	-.4656
	0.25	-.4906	-.4767	-.4703	-.4672	-.4661	-.4656
	0.1	-.4731	-.4684	-.4667	-.4659	-.4657	-.4656
$\frac{k_2(b_1)}{\sigma\sqrt{a}}$	1	.0737	.1550	.2512	.3596	.4333	.4656
	0.5	.4199	.3945	.4087	.4365	.4573	.4656
	0.25	.4979	.4566	.4521	.4579	.4635	.4656
	0.1	.4914	.4677	.4639	.4643	.4653	.4656
$\frac{k_2(a_2)}{\sigma\sqrt{a}}$	1	-.0737	-.1550	-.2512	-.3596	-.4333	-.4656
	0.5	.2489	.1600	.0827	.0035	-.0480	-.0700
	0.25	.2065	.1438	.0917	.0391	.0056	-.0084
	0.1	.1052	.0739	.0483	.0225	.0062	-.0004
$\frac{k_2(b_2)}{\sigma\sqrt{a}}$	1	.5879	.5348	.5040	.4844	.4739	.4656
	0.5	.2177	.1717	.1352	.1028	.0818	.0700
	0.25	.1442	.1087	.0748	.0409	.0189	.0084
	0.1	.0839	.0628	.0419	.0202	.0063	.0004

Table 3.7b Stress intensity factors for a plate with two collinear cracks subjected to twisting.

$\sigma = 6M/h^2$, $\nu = .3$.

$$\left(a = \frac{b_1 - a_1}{2} = 1,\ c = \frac{b_2 - a_2}{2},\ d = a_2 - b_1 \right)$$

PLATE, TWISTING

	c/a \ d/a	0.1	0.25	0.5	1	2	∞
$\frac{k_2(a_1)}{\sigma\sqrt{a}}$	1	.5058	.5081	.5110	.5147	.5181	.5218
	0.5	.5131	.5144	.5160	.5182	.5200	.5218
	0.25	.5183	.5188	.5195	.5204	.5212	.5218
	0.1	.5210	.5211	.5213	.5215	.5217	.5218
$\frac{k_2(b_1)}{\sigma\sqrt{a}}$	1	.6748	.5826	.5432	.5239	.5192	.5218
	0.5	.6526	.5726	.5404	.5252	.5210	.5218
	0.25	.6104	.5524	.5322	.5238	.5216	.5218
	0.1	.5590	.5319	.5248	.5224	.5218	.5218
$\frac{k_2(a_2)}{\sigma\sqrt{a}}$	1	.6748	.5826	.5432	.5239	.5192	.5218
	0.5	.4484	.3878	.3631	.3521	.3503	.3527
	0.25	.2737	.2349	.2195	.2130	.2122	.2139
	0.1	.1269	.1065	.0986	.0955	.0951	.0959
$\frac{k_2(b_2)}{\sigma\sqrt{a}}$	1	.5058	.5081	.5110	.5147	.5181	.5218
	0.5	.3532	.3505	.3490	.3489	.3502	.3527
	0.25	.2253	.2184	.2141	.2121	.2123	.2139
	0.1	.1105	.1019	.0973	.0953	.0951	.0959
$\frac{k_3(a_1)}{\sigma\sqrt{a}}$	1	.1035	.0958	.0877	.0792	.0732	.0697
	0.5	.0905	.0856	.0805	.0752	.0716	.0697
	0.25	.0792	.0768	.0744	.0720	.0704	.0697
	0.1	.0721	.0714	.0708	.0702	.0699	.0697
$\frac{k_3(b_1)}{\sigma\sqrt{a}}$	1	.0054	-.0052	-.0234	-.0462	-.0619	-.0697
	0.5	-.0349	-.0337	-.0424	-.0559	-.0655	-.0697
	0.25	-.0605	-.0554	-.0580	-.0638	-.0680	-.0697
	0.1	-.0702	-.0669	-.0671	-.0684	-.0693	-.0697
$\frac{k_3(a_2)}{\sigma\sqrt{a}}$	1	-.0054	.0052	.0234	.0462	.0619	.0697
	0.5	-.0304	-.0192	-.0073	.0057	.0141	.0179
	0.25	-.0266	-.0177	-.0103	-.0032	.0012	.0030
	0.1	-.0137	-.0089	-.0054	-.0023	-.0005	.0002
$\frac{k_3(b_2)}{\sigma\sqrt{a}}$	1	-.1035	-.0958	-.0877	-.0792	-.0732	-.0697
	0.5	-.0452	-.0387	-.0320	-.0250	-.0203	-.0179
	0.25	-.0221	-.0172	-.0124	-.0076	-.0045	-.0030
	0.1	-.0106	-.0076	-.0049	-.0024	-.0008	-.0002

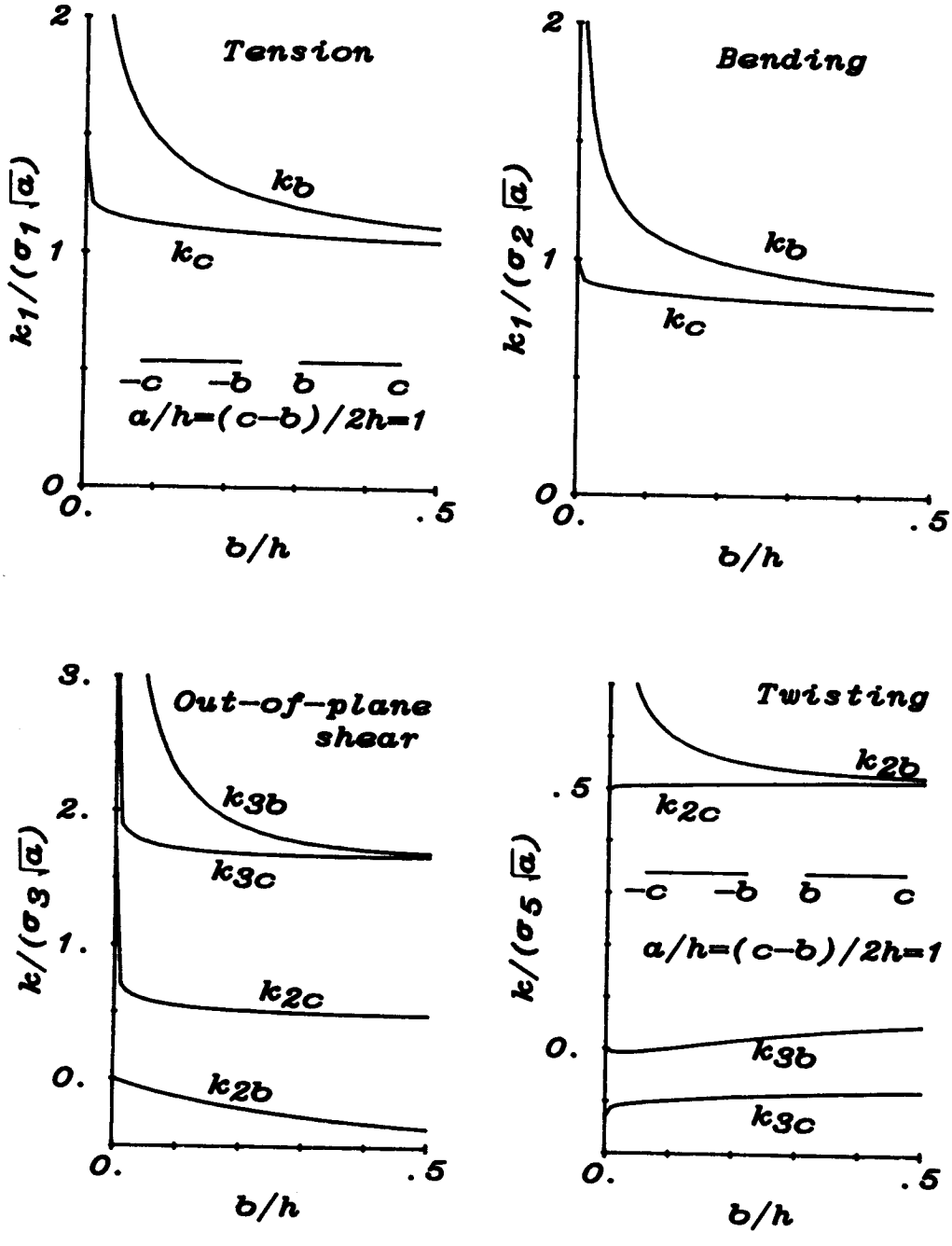

Figure 3.1a-d Normalized stress intensity factors in a plate with two identical collinear cracks of half length a/h=1 loaded in tension (a), bending (b), out-of-plane shear (c), and twisting (d). ν=.3, $\sigma_1=N_{xx}/h$, $\sigma_2=6M_{xx}/h^2$, $\sigma_3=3V_x/(2h)$, $\sigma_4=6M_{xy}/h^2$

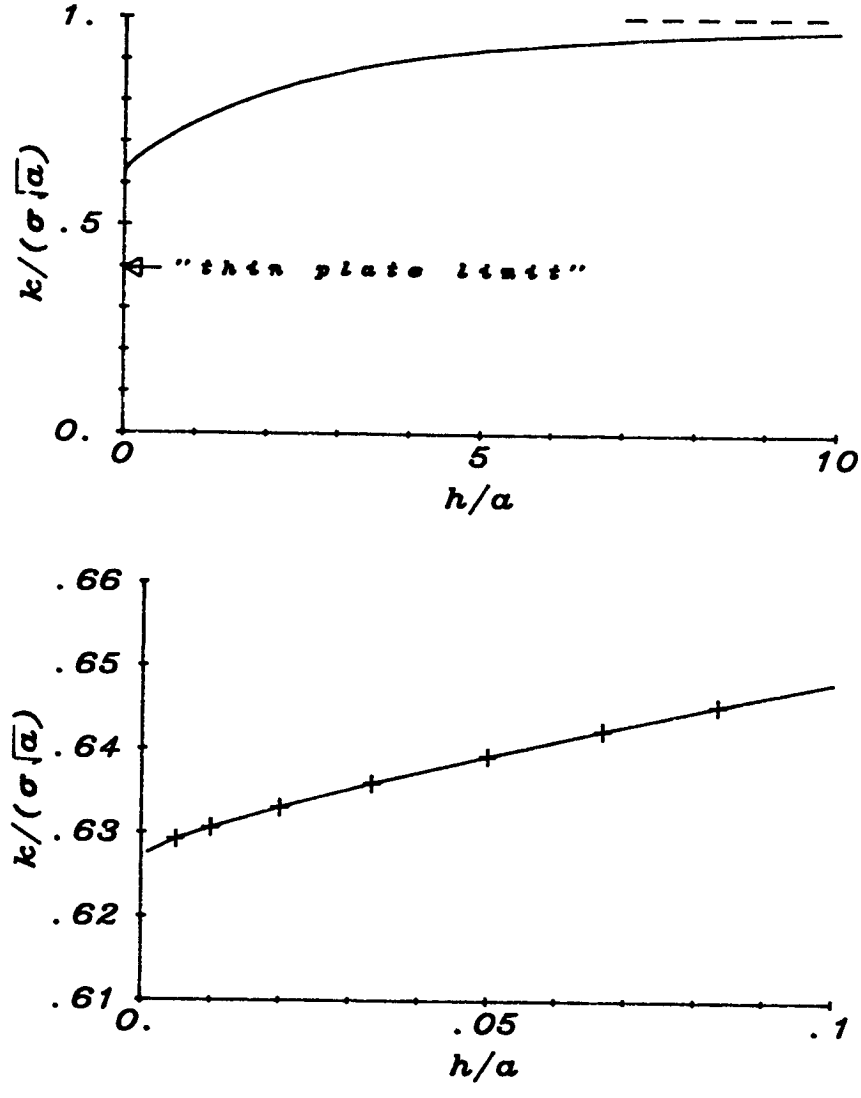

Figure 3.2 Normalized stress intensity factors in a plate for bending, ν=.3, σ=6M_{xx}/h^2.

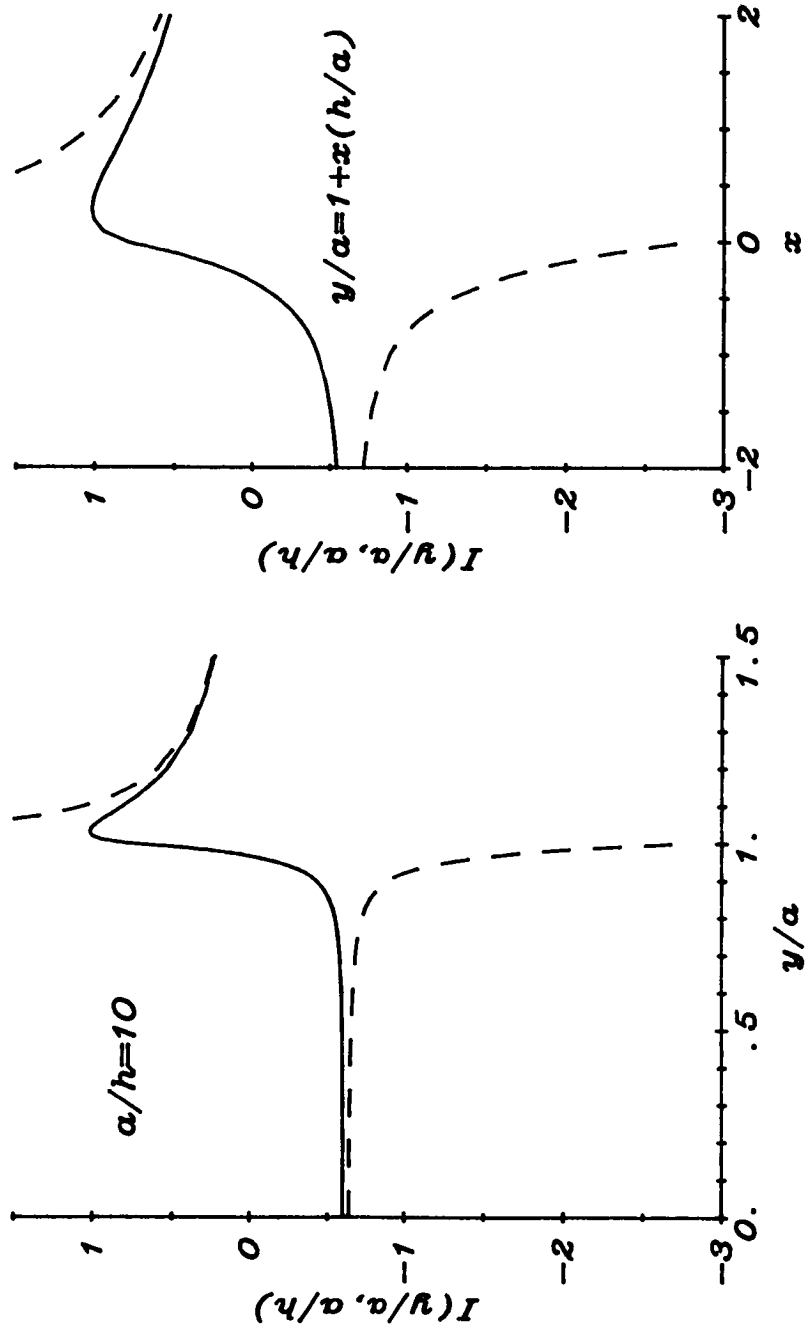

Figure 3.3a-c Plots of the Fredholm integral term from Reissner's theory of plate bending (Eqns. 3.129, 140) for a/h=10 (a), a/h=100 (b), a/h=1000 (c), (solid lines), compared to the limit from Appendix E, (dashed lines).

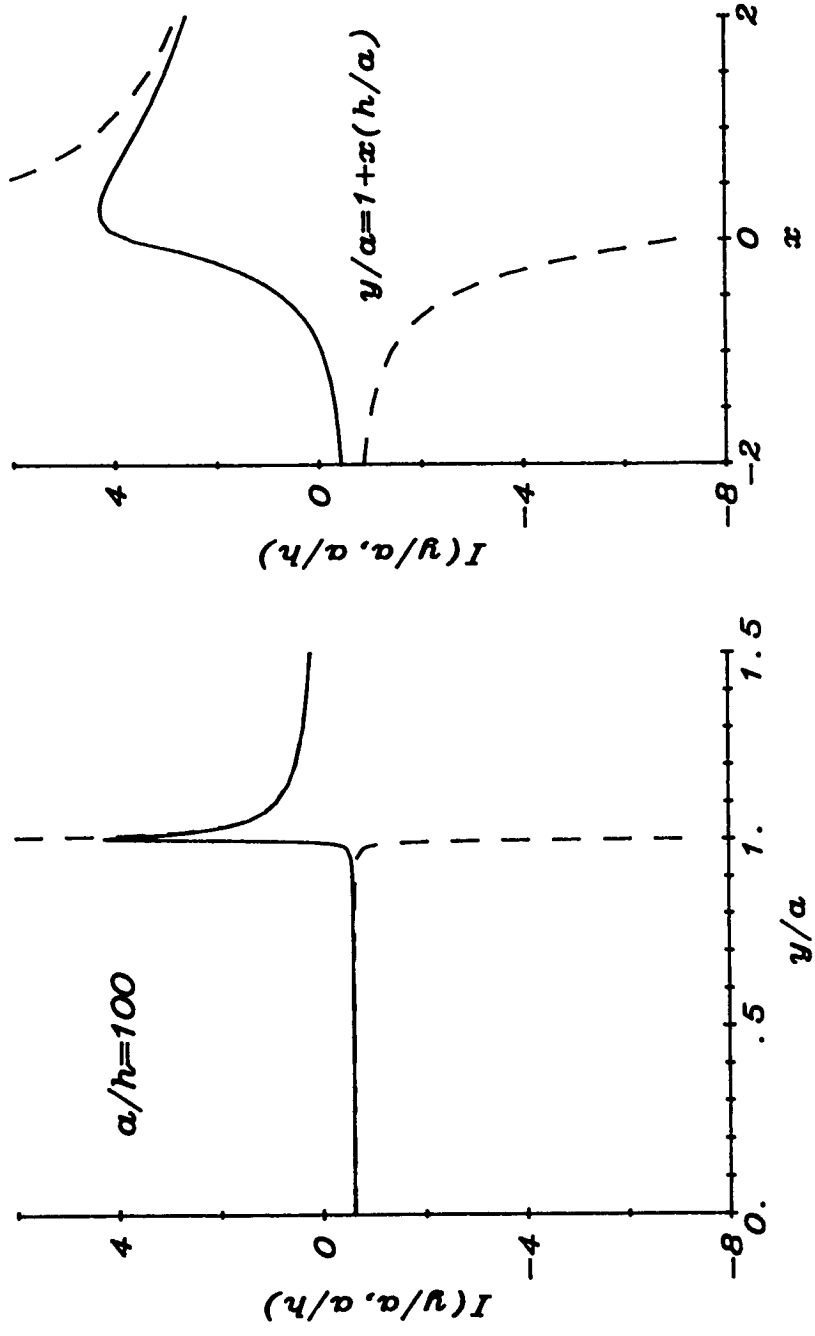

Figure 3.3 continued.

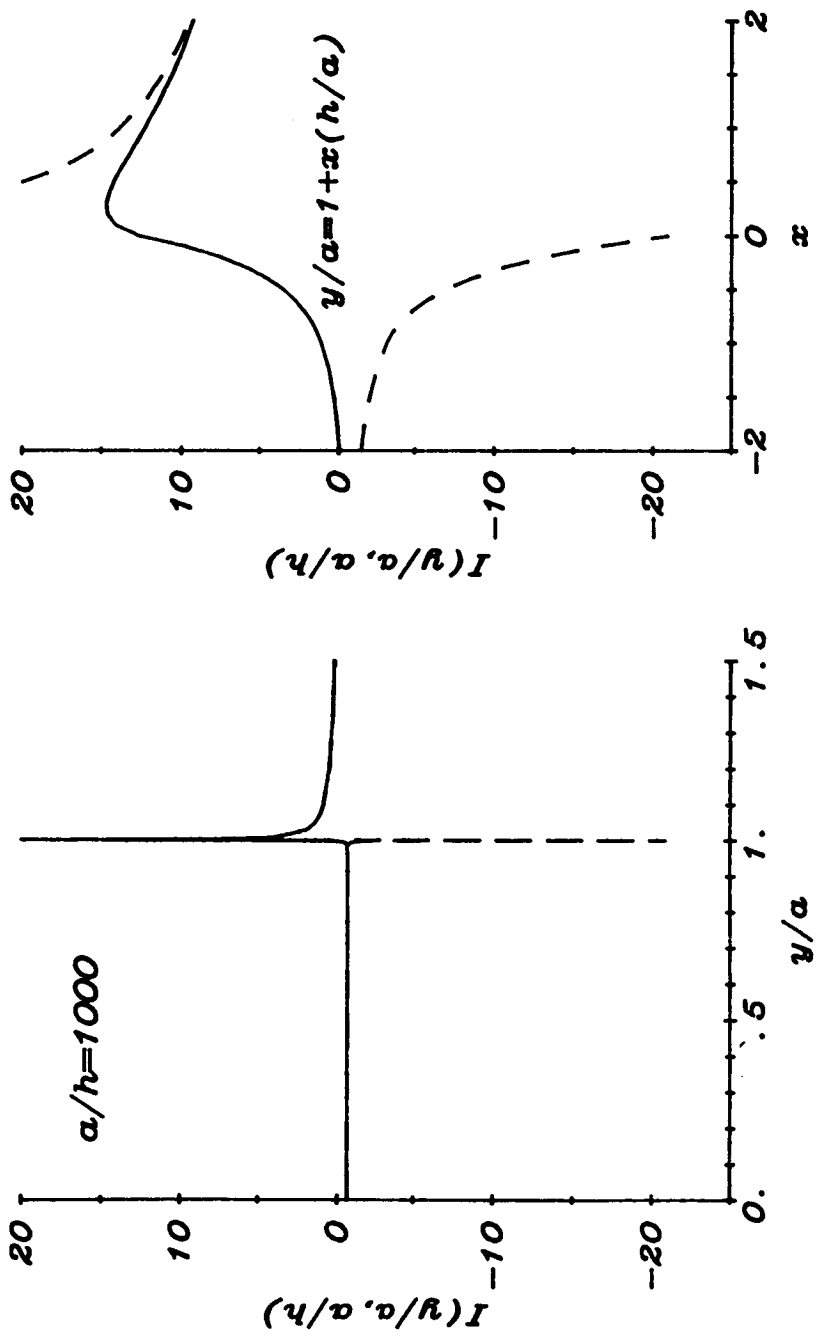

Figure 3.3 continued.

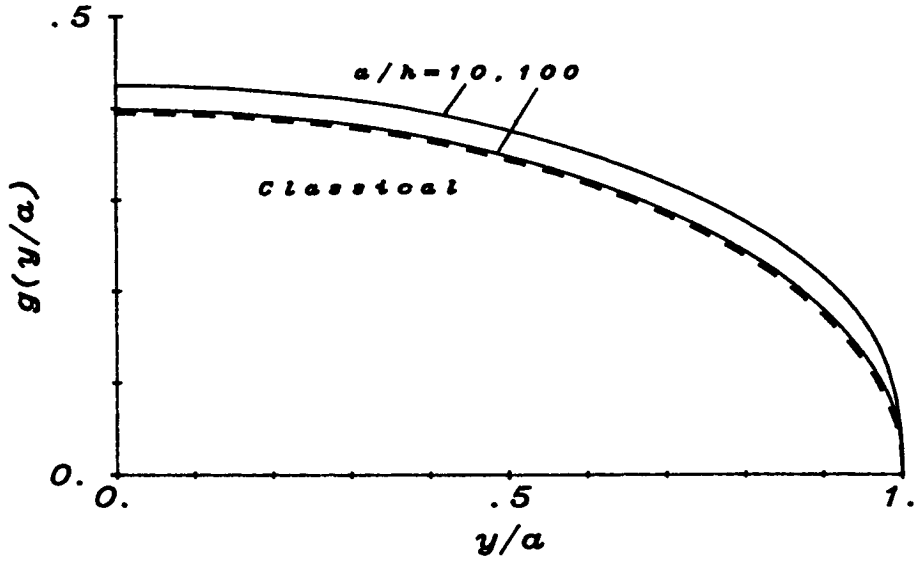

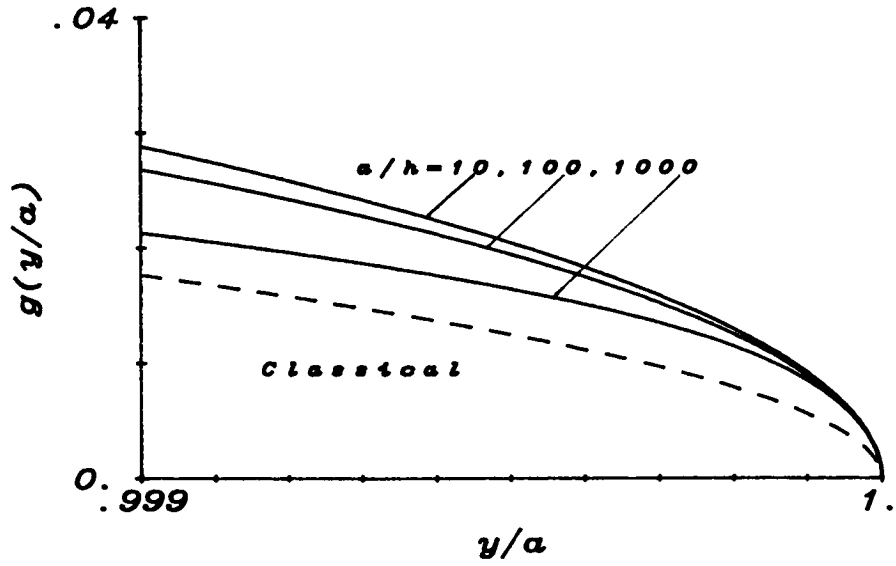

Figure 3.4 plots of the normalized rotation for plate bending for a/h=10,100,1000 from Reissner's theory compared to classical theory, ν=.3,

$\beta(y/a) = (a/h)(\overset{\infty}{\sigma}/E)\ g(y/a)$.

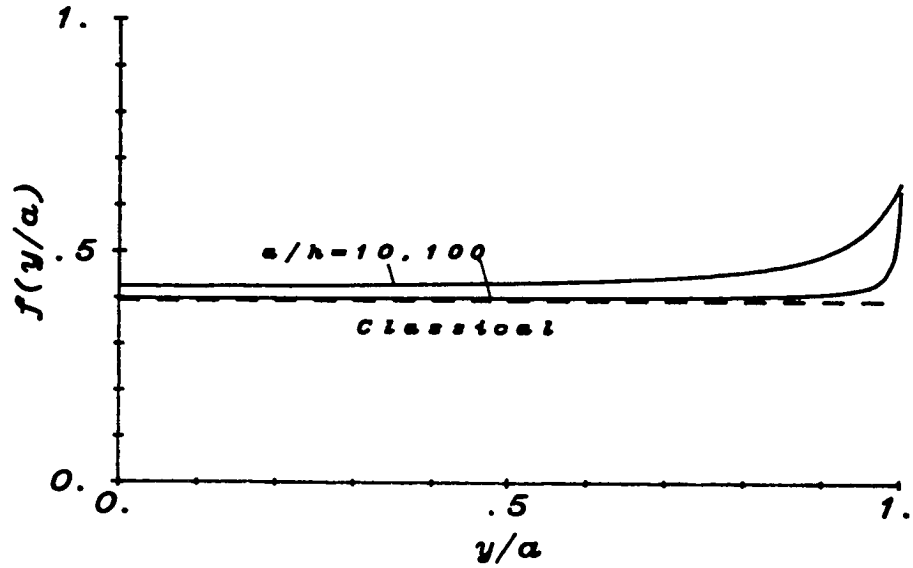

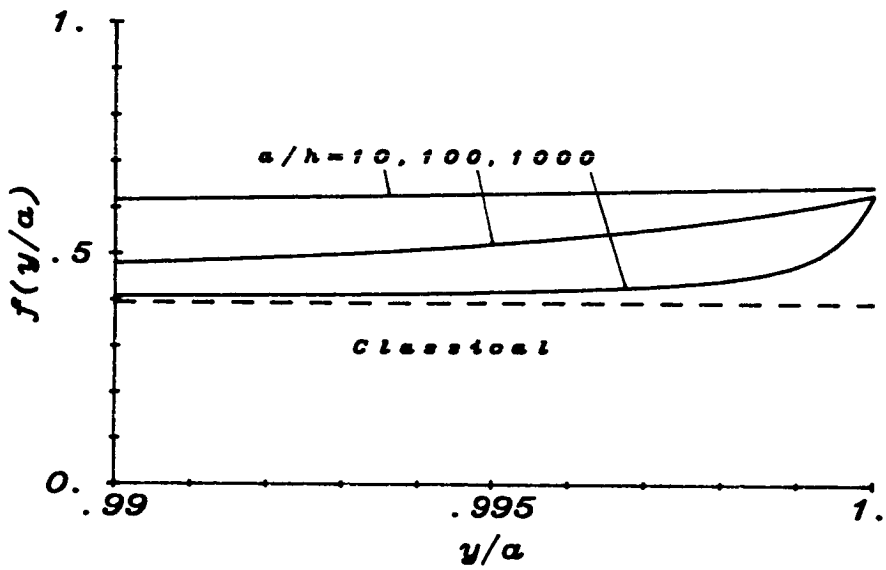

Figure 3.5 plots of the normalized rotation divided by the weight function, $[1-(y/a)^2]^{1/2}$ for plate bending for a/h=10,100,1000 from Reissner's theory compared to classical theory, ν=.3
$\beta(y/a) = (a/h)(\overset{\infty}{\sigma}/E)f(y/a)[1-(y/a)^2]^{1/2}$.

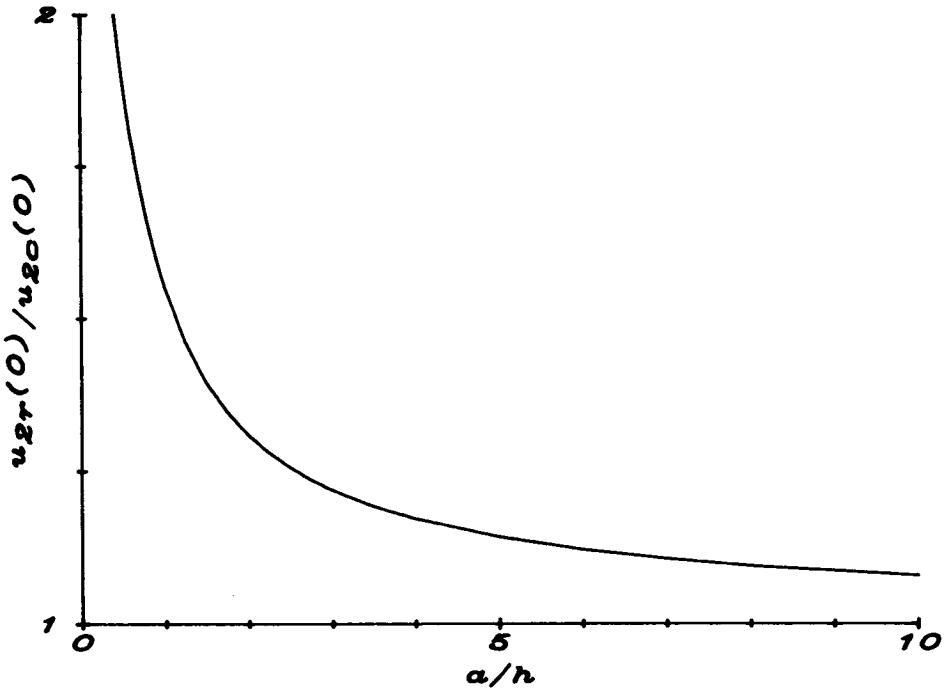

Figure 3.6 The ratio of crack surface rotation for Reissner's theory to that of the classical theory at the center of a cracked plate subjected to bending, ν=.3. See also Table 3.2.

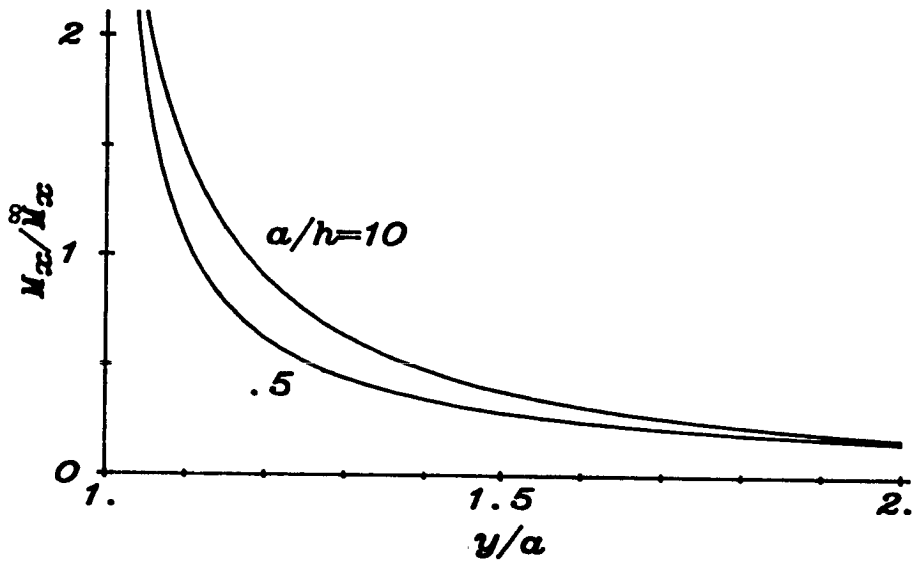

Figure 3.7 Bending stresses in front of the crack tip for a/h=.5,10. ν=.3

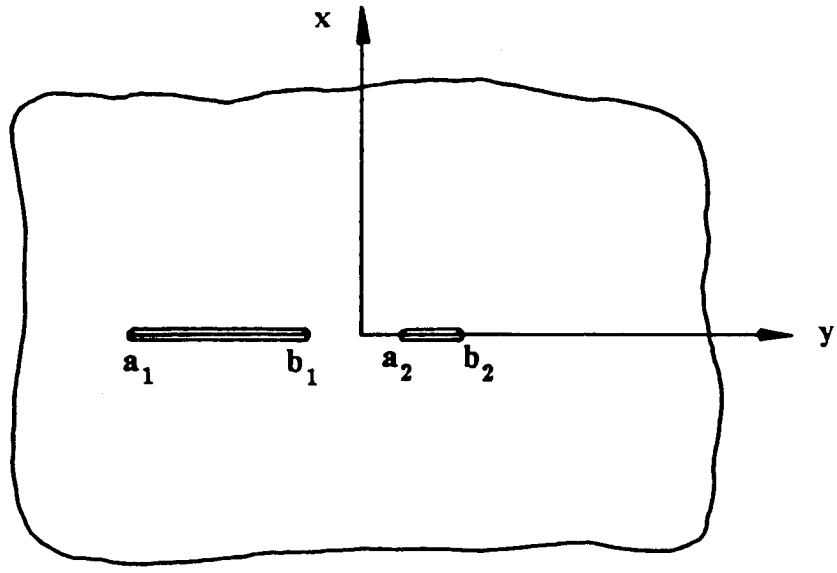

(a)

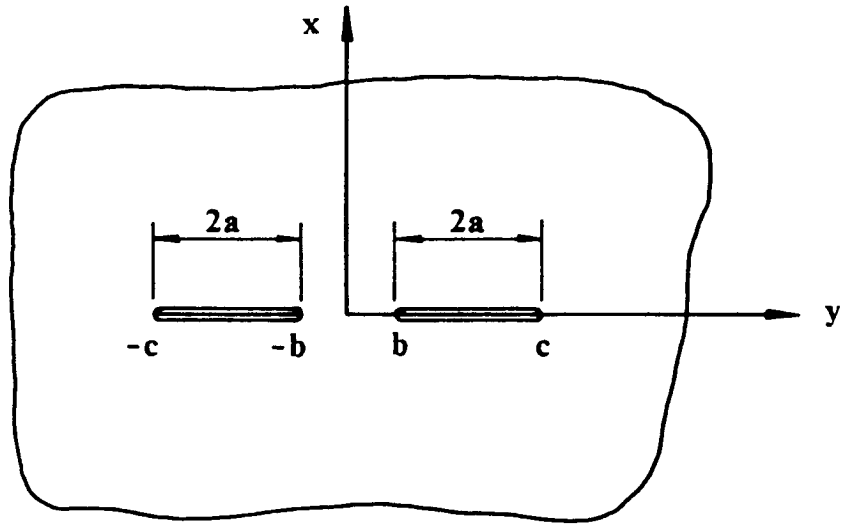

(b)

Figure 3.8a,b Geometry of the double crack for (a) unequal length and (b) equal length cracks.

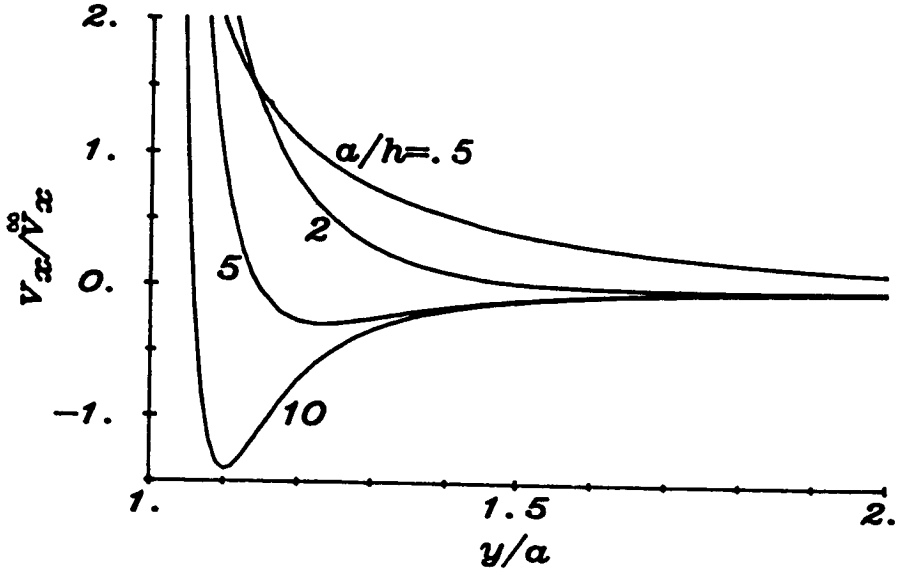

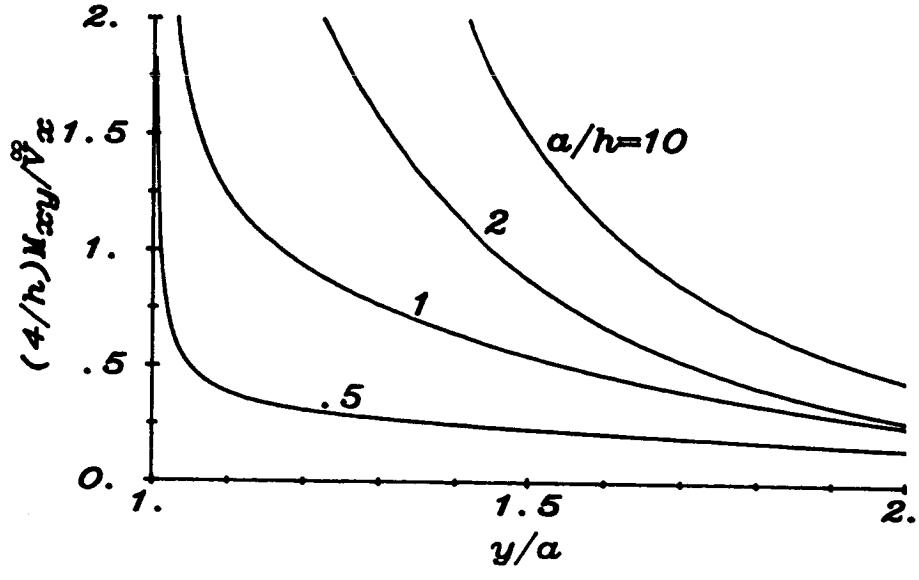

Figure 3.9a,b Stresses in front of the crack tip resulting from out-of-plane shear loading (a), and from twisting (b). ν=.3

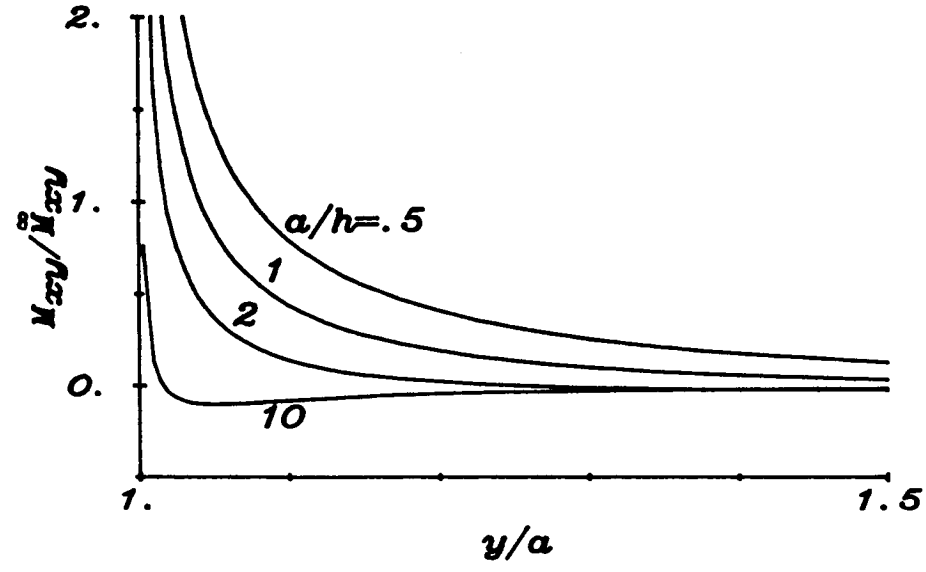

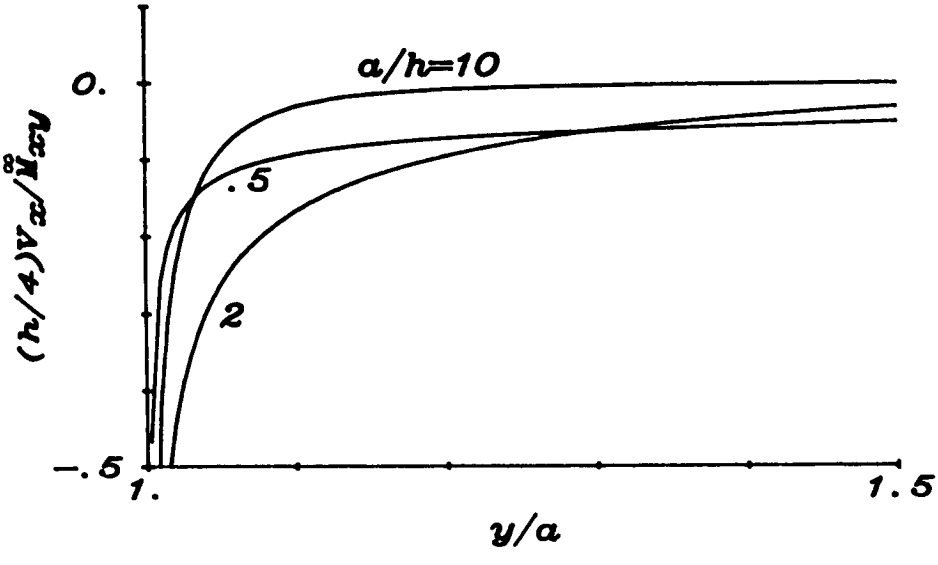

Figure 3.9a,b continued.

CHAPTER 4

Part-Through Cracks in Plates

The singular integral equations for part-through crack problems are obtained directly from the corresponding through crack equations combined with the compliance relations of Chapter 2. The edge crack SIFs needed for these relations are derived and presented in Appendix C. All line-spring model (LSM) solutions presented in this section are normalized with respect to the edge crack solution for the corresponding loading and crack depth at the center of the given part-through crack, see section C.4 of Appendix C.

4.1 Mode 1.

From Eqns. 3.102,118, 2.31, and from the superposition of Fig. 2.4, the integral equations for the symmetrically loaded part-through crack are,

$$\frac{1}{2\pi} \fint_{L_n} \frac{u_1(t)}{(t-y)^2}\, dt - \gamma_{11} u_1(y) - \gamma_{12} u_2(y) = -\overset{\infty}{N}_x = -\overset{\infty}{\sigma}_1 \ , \tag{4.1}$$

$$\frac{\gamma(1-\nu^2)}{2\pi} \fint_{L_n} \frac{u_2(t)}{(t-y)^2}\, dt + \frac{5}{12(1+\nu)} \frac{1}{2\pi} \int_{L_n} u_2(t) K(z)\, dt$$

$$-\gamma_{12} u_1(y) - \gamma_{22} u_2(y) = -\overset{\infty}{M}_x = -\overset{\infty}{\sigma}_2/6 \ , \tag{4.2}$$

where

$$z = \beta |t-y| \ , \tag{4.3}$$

$$K(z) = \left\{ \frac{-48}{z^4} + \frac{4}{z^2} - 4K_0(z) + 4K_2(z) + \frac{24}{z^2} K_2(z) \right\} . \tag{4.4}$$

This problem has already been solved for a Reissner plate [48]. The early line-spring model stress intensity factor solutions utilized the classical plate bending theory which in Chapter 3 was shown to be inadequate for through crack stress intensity factor determination. Recall that the LSM provides stress intensity factors along the crack front of a surface crack such that $-a<y<a$, while the solution to a through crack gives the SIF at $y=\pm a$. For the classical formulation, Eqn. 4.2 is replaced with,

$$\frac{3+\nu}{1+\nu}\,\frac{\gamma(1-\nu^2)}{2\pi}\,\fint_{L_n}\frac{u_2(t)}{(t-y)^2}\,dt - \gamma_{12}u_1(y) - \gamma_{22}u_2(y) = -\overset{\infty}{M}_x\ , \qquad (4.5)$$

while Eqn. 4.1 stays the same. It was also shown in Chapter 3 that for large a/h the Reissner plate bending rotation approaches that of the classical solution except at the endpoints, see Figs. 3.4-6 and table 3.2. Since the LSM does not use the solution at the endpoints, it is expected that for long cracks, the classical and Reissner theories become identical. This is shown in Figs. 4.1-4 where the LSM for both theories is compared to the 3-D Finite element solution of Newman and Raju, [33], see also [43]. In these figures K1t and K1b correspond to the edge-cracked strip SIF solution for tension and bending respectfully. For a/h smaller than about 2, which is the realistic geometry range for part-through cracks, the transverse shear theory shows significant improvement over the classical theory. For larger a/h it seems that the extra expense of integrating the Fredholm kernel, Eqn. 4.4, is unnecessary. Also as a/h gets larger, the numerical solution of 4.1,2 gets more difficult. With regard to table

3.2, it is rather surprising that the classical theory gives such good results for a/h as small as 2. Probably the reason is that tension, which is the same for both theories, dominates the behavior of the solution. Otherwise the difference would be of the order of 10% for a/h as high as 7.

In tables 4.1-10a,b the normalized SIFs along the crack front for both rectangular (a) and semi-elliptical (b) cracks are listed for tension and bending. The value of the normalized SIF at the center of a semi-elliptical crack for various crack lengths and depths is given in table 4.11 and the effect of Poisson's ratio on this quantity is shown in table 4.12. The only difference between this solution and the previous solutions which use Reissner plate theory [48] is the compliance functions, i.e. γ_{ij} of Eqns. 4.1,2. For $\xi \leq .8$ the curves used here, Eqns. C.102 with coefficients listed in table C.2, are slightly more accurate, see Eqns. C.108,109. This improved accuracy is minimized after going through the solution process because of normalization such that the results of tables 4.1-10 differ from those using Eqns. C.102 by at most .002, an insignificant amount considering the approximate nature of the model. The contribution given here is for deep cracks, i.e. $.8 < \xi \leq .95$. As noted in Appendix C, the compliance curves can actually be extrapolated to $\xi = 1$ because they match the asymptotic behavior given by Benthem and Koiter [65]. Although the values in these tables for crack depths of .9 and .95 are small, the normalization factor, which is the corresponding stress intensity factor for the edge-cracked strip, is very large. Tables 4.13,14 list the stress intensity factors at the maximum penetration

point of a semi-elliptical crack normalized with respect to the solution of the edge-cracked strip for both the corresponding depth (4.13a,14a) and for comparative purposes, with respect to a depth of .2 (4.13b,14b). The results for tension, table 4.13, show that the driving force, (dimensional SIF), does not simply increase with crack depth like the solution for the edge crack. For bending, table 4.14, the driving force is maximum for shallow cracks because of the constraining effect of the ends which actually causes interference and negative SIFs for deep cracks as discussed in the next section.

4.1.1 Contact Bending

The boundary conditions of the bending through crack problem specify the crack surface loading, $\overset{\infty}{\sigma}_2$. This can only be satisfied if tension is applied (superimposed) to open the crack to prevent interference due to bending rotation. The crack opening displacements due to tension and bending loads are such that contact will first occur at the ends of the crack, therefore the condition for no contact is satisfied if the combined stress intensity factor (tension plus bending component) at the corner on the compressive side of the plate is zero. The necessary ratio of tension to bending is

$$\frac{\overset{\infty}{\sigma}_1}{\overset{\infty}{\sigma}_2} \geq \frac{k_1(h/2)}{\overset{\infty}{\sigma}_{2D}\sqrt{a}} , \tag{4.6}$$

where the subscript D refers to dimensional.

There is a similar problem with bending of a part-through crack. As can be seen from tables 4.1-10a,b, the stress intensity factors due

to bending change sign as the crack gets deeper. Since a negative SIF has no meaning, these solutions require a superposition of a tensile solution to make $K/K_{0b} \geq 0$. The contact curve for the through crack case where $\overset{\infty}{\sigma}_1$ is zero in Eqn. 4.6, can be obtained from the line-spring model by finding the $K/K_{0b}=0$ curve. Along this curve, imagined to be a crack front, the crack opening displacement is cusp shaped. This solution is obtained by an iterative process where the "crack depth" L(y)/h, is the unknown and the condition

$$K = \sqrt{h}\left[\sigma_1 g_1(y) + \sigma_2 g_2(y)\right] = 0 \quad , \tag{4.7}$$

is used to determine it. These curves for various a/h values are given in table 4.15. A more useful problem is to determine the reduction in the stress intensity factor at the corner for bending with interference, see Fig. 4.5. The line-spring model can be used to approximate this quantity as shown in the next section.

4.1.2 Using the LSM to Calculate SIFs at the Corners

In the development of the line-spring model, the net ligament of the part-through crack is replaced with "net ligament" stresses. In solving the problem these stresses are determined. There is no difference between this problem and a through crack problem with these net ligament stresses applied as additional crack surface loads. Therefore in the same way that SIFs are calculated for a through crack, SIFs at the corners of a surface crack, i.e. $y=\pm a$, $z=h/2$ can be calculated and with no extra work. The problem with this idea is that close to the endpoints the net ligament stresses as provided by the

C-2

model are not accurate and this has a significant effect on the crack tip stress intensity factors.

As discussed in Chapter 2, section 2.3 and in Appendix C, the crack shape controls the endpoint behavior. For example the net ligament stresses are forced to zero at the ends of a rectangular crack yet have a square root singularity in the case of a semi-ellipse. In Appendix F it is shown that for the ellipse the stress intensity factor at the corner as predicted by the LSM is zero. Numerically this could not be shown but the results indicate a diminishing value as more terms are taken in solving the integral equation. The only crack profile that will make the net ligament stresses finite is the 1/4 power curve, i.e.

$$L(y)/h = \xi = \xi_0(1-s^2)^{1/4} \quad . \tag{4.8}$$

The technique of section 2.3, presented again in Eqns. 4.9,10, where this behavior is imposed at the ends of the crack profile in order to get well behaved net ligament stresses, did not work. The corner stress intensity factor was too sensitive to M, the number of terms in the series giving the crack profile:

$$\xi = \xi_0(1-s^2)^n \simeq \xi_0(1-s^2)^{1/4}h(s) \quad , \tag{4.9}$$

where

$$h(s) \simeq (1-s^2)^{n-1/4} \simeq \sum_{i=0}^{M} a_i s^{2i} \quad . \tag{4.10}$$

Probably the best geometry for approximating the corner stress intensity factor is one for which crack depth at the end is non-zero. In this case as noted previously the net ligament stresses as

predicted by the line-spring model go to zero at the endpoints. Since the net ligament stresses restrict the crack from opening, the error of the method should overestimate the correct value of the SIF. Note that the "actual" net ligament stresses (normalized with respect to the stress at "infinity") are probably between zero (for deep cracks) and one (for shallow cracks), while the normalized applied perturbation load is negative one.

The simplest problem that satisfies this geometry condition is the rectangular crack. The tension and bending cases are given in Fig. 4.6 as a function of the crack depth for a/h=1. Note that as the crack depth goes to one, the through crack value is approached in a manner similar to the case when two collinear cracks approach each other where behavior at the outer crack tip resembles that of one long crack instead of two, see Figs. 3.1a-d. In Fig. 4.7 plots similar to those of Fig. 4.6 are presented for the crack shape given in Eqn. 4.8. This figure is included only for purposes of comparison.

The contact problem of the last section also satisfies the condition of non-zero crack depths at the ends. Results for the "corrected" bending stress intensity factor are presented in Fig. 4.8. This plot shows how the interference of bending reduces the stress intensity factor from the value calculated when Eqn. 4.6 is assumed to be satisfied.

This method is of course very approximate. From the results of Fig. 4.6 it seems as though the tension case is wrong because the stress intensity factor exceeds the through crack value of one. This is due to the contribution from induced bending. It is conceivable

that at the corner opposite the constraint, crack growth is more likely than without the constraint although total failure of the plate is less likely. In Newman's finite element results, [33], there are some geometries where this occurs but only by about 2% ($k(h/2)/\sigma\sqrt{a}$ =1.023 for a/h=.4, L_0/h=.8), not the 20% that is calculated here, although it should be noted that the semi-ellipse has a constraining effect on the corner that the rectangle does not. I believe that the trend is correct, however the result should be considered only approximate.

Perhaps a method for approximating the value of the SIF at the corner of a semi-ellipse, or for any other profile, is to use the rectangular crack that has an equal amount of net ligament as the shape being considered. This simply results in a shift along the L_0/h axis of Fig. 4.6. For the semi-ellipse this shift factor which results from equating the area of an ellipse to that of a rectangle is:

$$(L_0/h)_{rectangle} = (\pi/4)(L_0/h)_{semi\text{-}ellipse} \quad . \tag{4.11}$$

In Fig. 4.9 this shifted curve is presented along with some corresponding values from Ref. [33]. These results are quite close but for some other geometries the method does not predict such good agreement. One would think that the model would predict an upper bound because the material is redistributed away from the ends and placed in the central portion. This should allow the crack to open more therefore increasing the SIF. This is observed in most, but not all cases. Especially for shorter crack lengths, say a/h≤1, does this

reasoning fail. For large a/h the approximation in some cases overestimates the finite element value by as much as 50%.

Part of the problem with this method is in the interpretation of the SIF obtained. In a plate theory the stress distribution, and therefore, the stress intensity factor distribution, through the thickness is assumed, see Appendix G. The value of the SIF that is being attributed to the corner is actually the sum of the tension component (constant through the thickness) and the bending component (linear). To expect good results for a semi-ellipse is wishful thinking. In fact, the elasticity solution of Benthem [1] indicates that at a free surface, the SIF is zero for mode 1. It is interesting to note that the values obtained from this method compare rather well to the results by Mattheck et. al. [41] where the "corner" SIF is averaged in order to get a general idea of the surface crack to grow outwards. Comparison is good for all geometries given in this reference. Perhaps the interpretation of the LSM approximation should also be regarded as an average, especially taking into account the results from Benthem. More work needs to be done to use the model to investigate this problem.

Theocaris and Wu [53,54] have devised a technique which uses the LSM and classical plate theory to obtain the SIF distribution over the entire range, including the corner. To obtain the value at the corner, they equate the SIF from the LSM (which is in a plane perpendicular to the plate surface) to the SIF from the plate with a through crack (which is in a plane parallel to the plate surface). They assume the semi-elliptical crack profile has some small, non-zero

depth at the endpoint which is measured experimentally. The shortcoming of this method, besides assuming that there is a displacement at the endpoint, is that the classical plate theory is used which is inadequate to solve for through crack SIFs that involve bending as the part-through crack problem always does. This same technique cannot be applied to the Reissner plate because of convergence problems. Theocaris and Wu have solved the integral equations in closed form so this difficulty is overcome [53].

4.1.3 Double Cracks

Crack interaction introduces more of a three-dimensional nature to the problem. For through cracks the plate theory should be accurate for crack tip separations of the order of the plate thickness. The justification for letting the cracks get closer together comes from asymptotic properties of the theory that for example are correct in terms of elasticity theory for small cracks, i.e. a/h approaching zero. The part-through crack problem is different. The model is inaccurate near the end, both along the crack front, and in terms of its influence on the solid at $|y|>a$ as shown in the last section. Note that essentially the singular stress field causes the interaction. The contribution from the Fredholm kernel is secondary, especially at small separations where the problem is most interesting.

For the semi-ellipse, the most studied geometry in the literature, it was shown in Appendix F that a singular stress field does not exist, although numerically this is nearly impossible to show

because of convergence difficulties. This means that numerically there will be a singular stress field. Therefore the crack interaction problem for this crack shape cannot be properly solved. In table 4.16 the tension solution to two symmetrically positioned surface cracks is presented. The geometry of the problem is shown in Fig. 3.8b. Results for both the semi-ellipse and the 1/4 power curve of Eqn. 4.8 are included in this table. The difference in the behavior of the solution for two nearly similar crack shapes, for $-.98 < s < 0$, shows that the line-spring model does not predict the correct trends. The semi-ellipse has a SIF that is nearly constant, whereas the other curve varies considerably. For a larger separation it should not be expected to be nearly as accurate as for a single crack. Perhaps the SIF in the center of the crack will be reasonably accurate. Results for a semi-elliptical crack under both tension and bending are given in table 4.17. These results can also be found in Ref. [59].

4.2 Modes 2 and 3

From Eqns. 3.168,179,180, 2.31, and from the superposition of Fig. C.1, the integral equations for the skew-symmetrically loaded part-through crack are:

$$\frac{1}{2\pi} \fint_a^b \frac{2u_3(t)}{(t-y)^2}\, dt + \frac{1}{2\pi} \int_a^b \left\{ u_3(t)K_{33}(z) + u_5(t)K_{35}(z) \right\} dt -$$

$$- \gamma_{33} u_3(y) = -\overset{\infty}{V}_x = -8(1+\nu)/5\ \overset{\infty}{\sigma}_3 \quad , \qquad (4.12)$$

$$\frac{1}{2\pi}\fint_a^b \frac{u_4(t)}{(t-y)^2}\,dt - \gamma_{44}u_4(y) - \gamma_{45}u_5(y) = -\overset{\infty}{N}_{xy} = -\overset{\infty}{\sigma}_4 \quad , \tag{4.13}$$

$$\gamma(1-\nu^2)\frac{1}{2\pi}\fint_a^b \frac{u_5(t)}{(t-y)^2}\,dt + \frac{1}{2\pi}\int_a^b \left\{u_5(t)K_{55}(z) + u_3(t)K_{53}(z)\right\} dt$$

$$- \gamma_{54}u_4(y) - \gamma_{55}u_5(y) = -\overset{\infty}{M}_{xy} = -\overset{\infty}{\sigma}_5/6 \quad , \tag{4.14}$$

where

$$z=\beta|t-y|, \quad a<y<b \quad , \tag{4.15}$$

$$K_{33}(z) = \beta^2\left\{-\ln(z) + \left[K_2(z) - \frac{2}{z^2}\right] + \left[K_0(z) + \ln(z)\right]\right\} \quad , \tag{4.16}$$

$$K_{35}(z) = \beta\left\{\frac{8}{z^3} - \left[z + \frac{4}{z}\right]K_2(z) + zK_0(z)\right\} \quad , \tag{4.17}$$

$$K_{55}(z) = \frac{5}{12(1+\nu)}\left\{\ln(z) + \left[\frac{48}{z^4} - \frac{4}{z^2} + 4K_0(z) - 4K_2(z) - \frac{24}{z^2}K_2(z)\right.\right.$$

$$\left.\left. + \ln(z)\right] - \left[2K_0(z) + 2\ln(z)\right]\right\} \quad , \tag{4.18}$$

$$K_{53}(z) = \frac{5\beta}{12(1+\nu)}\left\{\frac{-8}{z^3} + \left[z + \frac{4}{z}\right]K_2(z) - zK_0(z)\right\} \quad . \tag{4.19}$$

Again it is noted that in crack propagation studies this solution may be used only if the crack grows in its own plane. Results for crack lengths of $a/h = .5, 1., 2., 4.$, and crack depths of $L_0/h = .2, .4, .6, .8, .9, .95$ are given in tables 4.19-21a,b for rectangular (a) and semi-elliptical (b) cracks for out-of-plane shear, in-plane-shear and for twisting. Because there are two stress intensity factors (modes 2,3), normalization will be with respect to the primary value obtained from the edge-cracked strip at the maximum depth, see section C.4 of Appendix C. In the tables and figures this normalization factor will be denoted by K2O, K3IO, and K3TO for out-of-plane shear, in-plane

shear, and twisting, respectively. Profiles of the SIFs for a/h=1, ν=.3 are given in Figs. 4.10-15. Note that because of the symmetry of the problem the secondary stress intensity factor at the center of the crack is zero. When the primary loading is mode 3, (twisting or in-plane shear), out-of-plane crack growth which results from mode 2 contributions is minimized in the central portion of the crack front. The model also shows that the secondary value is insignificant throughout the range. For the rectangular crack this is expected, but for the semi-ellipse this should not be the case. As in the mode 1 problem for which the model works well, it can only be hoped that the inaccuracies towards the ends do not significantly affect the solution in the center. The value of the SIF at the center of a semi-elliptical crack is listed in table 4.22 for various crack lengths and depths for all loading cases. The closer the value in these tables is to one, the closer the conditions are to plane strain. For the loading case of out-of-plane shear, plane strain conditions are more easily met than in the mode 1 cases of tension and bending, which are shown in Table 4.11. The opposite is true for in-plane shear and twisting. The effect of Poisson's ratio on the solution is shown in table 4.23.

The method of approximating the value of the "corner" SIF of a semi-elliptical crack used in Sec. 4.1.2 for the mode 1 case is applied here. The results are given in table 4.24. As discussed in Appendix G, the work of Benthem [1] shows that at a free surface the stress singularity for shear (modes 2 and 3) is greater than .5. The plate theory used predicts a zero value for the mode 3 SIF at the

surface because of the assumed parabolic shear distribution, when in fact it should be infinite. Therefore as with the mode 1 prediction the numbers obtained from this method should be regarded as an average value that gives some idea of outward crack growth.

Table 4.1a,b Normalized stress intensity factors for a rectangular (a), or semi-elliptical (b), surface crack in a plate under tension or bending loads, a/h=.5, ν=.3

Rectangular crack, Tension.

L_0/h	.2	.4	.6	.8	.9	.95
y/a						
0.	.784	.428	.193	.0595	.0206	.00767
.1	.783	.427	.192	.0594	.0205	.00765
.2	.779	.423	.190	.0588	.0203	.00756
.3	.773	.417	.187	.0579	.0199	.00741
.4	.762	.407	.183	.0565	.0194	.00719
.5	.747	.393	.177	.0545	.0186	.00689
.6	.724	.374	.169	.0519	.0176	.00648
.7	.688	.348	.158	.0484	.0162	.00593
.8	.631	.311	.142	.0432	.0143	.00515
.9	.523	.253	.118	.0345	.0111	.00392
.95	.417	.205	.096	.0267	.0083	.00290
.98	.301	.157	.071	.0182	.0055	.00190

Rectangular crack, Bending.

L_0/h	.2	.4	.6	.8	.9	.95
y/a						
0.	.765	.339	.0620	-.0308	-.0236	-.0121
.1	.764	.338	.0614	-.0309	-.0236	-.0121
.2	.760	.333	.0594	-.0312	-.0235	-.0120
.3	.752	.326	.0561	-.0316	-.0234	-.0119
.4	.741	.314	.0513	-.0322	-.0232	-.0117
.5	.724	.298	.0447	-.0329	-.0229	-.0113
.6	.699	.277	.0361	-.0337	-.0223	-.0109
.7	.660	.247	.0249	-.0342	-.0214	-.0102
.8	.598	.205	.0102	-.0339	-.0196	-.0091
.9	.480	.139	-.0091	-.0308	-.0161	-.0072
.95	.366	.087	-.0201	-.0258	-.0125	-.0054
.98	.239	.038	-.0237	-.0187	-.0085	-.0036

Table 4.1b Normalized stress intensity factors for a semi-elliptical surface crack in a plate under tension or bending loads, a/h=.5, ν=.3

Semi-elliptical crack, Tension.

y/a \ L_0/h	.2	.4	.6	.8	.9	.95
0.	.729	.390	.174	.0499	.0158	.00547
.1	.728	.390	.174	.0500	.0159	.00546
.2	.724	.388	.174	.0503	.0160	.00547
.3	.717	.385	.173	.0507	.0163	.00554
.4	.708	.381	.172	.0512	.0166	.00567
.5	.695	.376	.169	.0515	.0170	.00583
.6	.677	.369	.166	.0514	.0173	.00598
.7	.654	.361	.162	.0506	.0173	.00603
.8	.622	.351	.157	.0484	.0166	.00584
.9	.571	.342	.152	.0452	.0151	.00525
.95	.526	.340	.153	.0440	.0142	.00485
.98	.474	.347	.163	.0460	.0145	.00484

Semi-elliptical crack, Bending.

y/a \ L_0/h	.2	.4	.6	.8	.9	.95
0.	.709	.306	.053	-.0281	-.0198	-.00960
.1	.709	.307	.055	-.0273	-.0194	-.00934
.2	.709	.310	.059	-.0249	-.0182	-.00867
.3	.708	.316	.066	-.0208	-.0164	-.00776
.4	.706	.324	.076	-.0151	-.0139	-.00667
.5	.704	.335	.089	-.0077	-.0107	-.00539
.6	.699	.348	.105	.0018	-.0067	-.00383
.7	.692	.364	.124	.0132	-.0017	-.00189
.8	.678	.385	.147	.0269	.0044	.00054
.9	.649	.413	.178	.0432	.0117	.00347
.95	.616	.437	.202	.0542	.0162	.00519
.98	.569	.467	.233	.0661	.0205	.00675

Table 4.2a,b Normalized stress intensity factors for a rectangular (a), or semi-elliptical (b), surface crack in a plate under tension or bending loads, a/h=1 , ν=.3

Rectangular crack, Tension.

L_0/h	.2	.4	.6	.8	.9	.95
y/a						
0.	.864	.561	.273	.0844	.0293	.0112
.1	.863	.559	.273	.0841	.0292	.0112
.2	.861	.555	.270	.0833	.0289	.0111
.3	.857	.549	.266	.0819	.0284	.0109
.4	.850	.538	.259	.0798	.0277	.0106
.5	.840	.523	.251	.0769	.0266	.0101
.6	.825	.502	.239	.0731	.0252	.0095
.7	.800	.471	.222	.0679	.0233	.0088
.8	.755	.425	.199	.0605	.0205	.0077
.9	.655	.347	.163	.0487	.0161	.0059
.95	.541	.279	.132	.0382	.0123	.0044
.98	.399	.208	.098	.0266	.0083	.0030

Rectangular crack, Bending.

L_0/h	.2	.4	.6	.8	.9	.95
y/a						
0.	.852	.492	.153	-.0101	-.0210	-.0128
.1	.851	.490	.152	-.0104	-.0210	-.0128
.2	.848	.486	.149	-.0111	-.0211	-.0128
.3	.844	.478	.145	-.0122	-.0213	-.0128
.4	.837	.466	.137	-.0140	-.0216	-.0128
.5	.826	.448	.127	-.0162	-.0218	-.0127
.6	.809	.424	.114	-.0192	-.0221	-.0125
.7	.782	.389	.096	-.0227	-.0222	-.0121
.8	.733	.336	.071	-.0267	-.0218	-.0114
.9	.624	.246	.033	-.0297	-.0195	-.0096
.95	.500	.169	.006	-.0283	-.0161	-.0076
.98	.345	.091	-.013	-.0227	-.0115	-.0052

Table 4.2b Normalized stress intensity factors for a semi-elliptical surface crack in a plate under tension or bending loads, a/h=1 , ν=.3

Semi-elliptical crack, Tension.

y/a \ L_0/h	.2	.4	.6	.8	.9	.95
0.	.817	.507	.244	.0725	.0235	.00833
.1	.816	.506	.244	.0726	.0235	.00830
.2	.810	.503	.243	.0727	.0236	.00825
.3	.800	.498	.242	.0730	.0238	.00825
.4	.786	.491	.239	.0731	.0240	.00830
.5	.766	.481	.236	.0731	.0242	.00838
.6	.740	.469	.231	.0725	.0243	.00842
.7	.706	.452	.225	.0712	.0240	.00835
.8	.657	.431	.217	.0687	.0232	.00807
.9	.581	.401	.207	.0654	.0218	.00752
.95	.513	.379	.203	.0644	.0213	.00726
.98	.438	.359	.205	.0665	.0219	.00742

Semi-elliptical crack, Bending.

y/a \ L_0/h	.2	.4	.6	.8	.9	.95
0.	.804	.441	.133	-.0114	-.0186	-.01064
.1	.804	.441	.134	-.0102	-.0180	-.01023
.2	.802	.444	.139	-.0068	-.0161	-.00914
.3	.798	.449	.147	-.0012	-.0131	-.00763
.4	.792	.455	.158	.0065	-.0093	-.00585
.5	.783	.463	.172	.0163	-.0045	-.00382
.6	.771	.472	.189	.0280	.0010	-.00152
.7	.752	.482	.208	.0415	.0073	.00107
.8	.722	.492	.231	.0568	.0145	.00398
.9	.665	.499	.259	.0747	.0225	.00719
.95	.606	.500	.280	.0867	.0275	.00911
.98	.531	.496	.302	.0996	.0325	.01096

Table 4.3a,b Normalized stress intensity factors for a rectangular (a), or semi-elliptical (b), surface crack in a plate under tension or bending loads, a/h=1 , ν=.0

Rectangular crack, Tension.

L_0/h	.2	.4	.6	.8	.9	.95
y/a						
0.	.838	.521	.254	.0815	.0290	.0112
.1	.837	.520	.253	.0813	.0289	.0111
.2	.835	.516	.251	.0804	.0286	.0110
.3	.831	.510	.247	.0791	.0281	.0108
.4	.824	.500	.241	.0771	.0273	.0105
.5	.814	.487	.233	.0743	.0262	.0100
.6	.799	.468	.222	.0705	.0247	.0094
.7	.774	.440	.208	.0654	.0228	.0086
.8	.729	.398	.186	.0582	.0200	.0075
.9	.630	.326	.153	.0467	.0156	.0057
.95	.519	.262	.124	.0365	.0119	.0043
.98	.381	.197	.092	.0253	.0080	.0028

Rectangular crack, Bending.

L_0/h	.2	.4	.6	.8	.9	.95
y/a						
0.	.824	.446	.130	-.0123	-.0198	-.0118
.1	.823	.444	.129	-.0125	-.0199	-.0118
.2	.820	.440	.127	-.0132	-.0200	-.0118
.3	.816	.433	.122	-.0143	-.0202	-.0118
.4	.809	.422	.116	-.0159	-.0204	-.0117
.5	.798	.406	.107	-.0180	-.0207	-.0117
.6	.781	.384	.095	-.0207	-.0210	-.0115
.7	.754	.352	.079	-.0239	-.0211	-.0112
.8	.705	.303	.056	-.0275	-.0207	-.0105
.9	.597	.221	.023	-.0298	-.0185	-.0089
.95	.476	.150	-.001	-.0280	-.0153	-.0070
.98	.326	.079	-.017	-.0221	-.0109	-.0048

Table 4.3b Normalized stress intensity factors for a semi-elliptical surface crack in a plate under tension or bending loads, a/h=1 , ν=.0

Semi-elliptical crack, Tension.

y/a \ L_0/h	.2	.4	.6	.8	.9	.95
0.	.791	.473	.228	.0699	.0232	.00829
.1	.790	.472	.228	.0699	.0232	.00825
.2	.785	.470	.227	.0699	.0232	.00817
.3	.776	.466	.225	.0699	.0233	.00813
.4	.764	.460	.222	.0697	.0236	.00814
.5	.747	.451	.219	.0692	.0234	.00815
.6	.724	.441	.214	.0682	.0232	.00812
.7	.693	.428	.208	.0663	.0227	.00797
.8	.649	.410	.200	.0635	.0217	.00759
.9	.578	.387	.192	.0600	.0201	.00695
.95	.515	.369	.190	.0591	.0195	.00665
.98	.442	.355	.194	.0613	.0200	.00678

Semi-elliptical crack, Bending.

y/a \ L_0/h	.2	.4	.6	.8	.9	.95
0.	.776	.401	.113	-.0129	-.0174	-.00966
.1	.776	.402	.115	-.0119	-.0168	-.00931
.2	.774	.405	.119	-.0089	-.0152	-.00838
.3	.771	.410	.126	-.0039	-.0127	-.00710
.4	.768	.417	.137	.0029	-.0094	-.00558
.5	.762	.427	.150	.0116	-.0052	-.00383
.6	.752	.438	.166	.0222	-.0003	-.00182
.7	.737	.450	.186	.0347	.0054	.00052
.8	.712	.465	.209	.0491	.0121	.00320
.9	.661	.479	.239	.0665	.0197	.00625
.95	.607	.486	.261	.0785	.0246	.00812
.98	.535	.488	.286	.0914	.0295	.00992

Table 4.4a,b Normalized stress intensity factors for a rectangular (a), or semi-elliptical (b), surface crack in a plate under tension or bending loads, a/h=1 , ν=.5

Rectangular crack, Tension.

L_0/h	.2	.4	.6	.8	.9	.95
y/a						
0.	.891	.615	.308	.0927	.0314	.0119
.1	.890	.613	.307	.0924	.0313	.0119
.2	.888	.609	.304	.0915	.0310	.0118
.3	.885	.602	.300	.0899	.0305	.0116
.4	.879	.591	.292	.0876	.0297	.0113
.5	.870	.575	.282	.0844	.0286	.0108
.6	.856	.552	.268	.0802	.0271	.0102
.7	.833	.519	.249	.0744	.0251	.0094
.8	.791	.469	.223	.0664	.0222	.0083
.9	.695	.383	.181	.0536	.0176	.0065
.95	.580	.307	.146	.0423	.0136	.0049
.98	.431	.228	.109	.0297	.0092	.0033

Rectangular crack, Bending.

L_0/h	.2	.4	.6	.8	.9	.95
y/a						
0.	.881	.554	.194	-.0024	-.0206	-.0136
.1	.881	.553	.193	-.0027	-.0207	-.0136
.2	.879	.548	.189	-.0035	-.0208	-.0136
.3	.874	.540	.184	-.0049	-.0210	-.0136
.4	.868	.527	.175	-.0070	-.0214	-.0136
.5	.858	.508	.164	-.0097	-.0219	-.0135
.6	.843	.482	.148	-.0133	-.0223	-.0134
.7	.819	.444	.127	-.0177	-.0226	-.0131
.8	.773	.387	.098	-.0229	-.0225	-.0123
.9	.667	.288	.053	-.0279	-.0206	-.0105
.95	.542	.201	.020	-.0280	-.0173	-.0084
.98	.380	.113	-.006	-.0234	-.0126	-.0058

Table 4.4b Normalized stress intensity factors for a semi-elliptical surface crack in a plate under tension or bending loads, a/h=1 , ν=.5

Semi-elliptical crack, Tension.

y/a \ L_0/h	.2	.4	.6	.8	.9	.95
0.	.848	.554	.273	.0789	.0254	.00895
.1	.845	.553	.273	.0799	.0255	.00892
.2	.839	.549	.272	.0802	.0256	.00888
.3	.828	.543	.270	.0807	.0259	.00891
.4	.811	.534	.268	.0811	.0263	.00900
.5	.789	.522	.264	.0814	.0266	.00912
.6	.759	.506	.259	.0812	.0269	.00924
.7	.720	.485	.251	.0801	.0268	.00924
.8	.666	.457	.241	.0778	.0262	.00904
.9	.582	.417	.227	.0742	.0249	.00855
.95	.509	.387	.219	.0727	.0242	.00830
.98	.429	.358	.217	.0741	.0248	.00846

Semi-elliptical crack, Bending.

y/a \ L_0/h	.2	.4	.6	.8	.9	.95
0.	.837	.496	.167	-.0052	-.0188	-.01147
.1	.836	.496	.169	-.0039	-.0180	-.01097
.2	.833	.499	.174	.0001	-.0157	-.00964
.3	.828	.502	.182	.0066	-.0122	-.00782
.4	.820	.507	.193	.0154	-.0076	-.00567
.5	.809	.512	.208	.0263	-.0022	-.00326
.6	.793	.518	.225	.0392	.0041	-.00061
.7	.769	.523	.244	.0538	.0112	.00231
.8	.733	.527	.265	.0699	.0188	.00545
.9	.667	.523	.289	.0880	.0271	.00881
.95	.602	.513	.305	.0996	.0322	.01078
.98	.521	.497	.322	.1119	.0372	.01266

Table 4.5a,b Normalized stress intensity factors for a rectangular (a), or semi-elliptical (b), surface crack in a plate under tension or bending loads, a/h=1.5 , ν=.3

Rectangular crack, Tension.

y/a \ L_0/h	.2	.4	.6	.8	.9	.95
0.	.899	.639	.333	.1037	.0357	.0137
.1	.898	.638	.332	.1034	.0355	.0136
.2	.897	.634	.329	.1024	.0352	.0135
.3	.893	.627	.324	.1006	.0346	.0132
.4	.888	.616	.317	.0981	.0337	.0129
.5	.880	.601	.307	.0946	.0324	.0124
.6	.868	.580	.292	.0898	.0307	.0117
.7	.849	.549	.272	.0832	.0283	.0107
.8	.813	.500	.244	.0739	.0250	.0094
.9	.727	.413	.198	.0592	.0196	.0073
.95	.617	.332	.159	.0465	.0151	.0055
.98	.465	.246	.118	.0327	.0103	.0037

Rectangular crack, Bending.

y/a \ L_0/h	.2	.4	.6	.8	.9	.95
0.	.890	.582	.222	.0084	-.0173	-.0126
.1	.889	.581	.221	.0081	-.0174	-.0126
.2	.887	.576	.218	.0072	-.0176	-.0126
.3	.884	.568	.212	.0056	-.0179	-.0127
.4	.878	.556	.203	.0032	-.0184	-.0127
.5	.870	.539	.192	.0000	-.0191	-.0128
.6	.857	.514	.175	-.0042	-.0199	-.0128
.7	.836	.478	.153	-.0098	-.0207	-.0127
.8	.797	.422	.121	-.0169	-.0214	-.0123
.9	.702	.322	.071	-.0251	-.0208	-.0109
.95	.582	.230	.032	-.0276	-.0182	-.0090
.98	.417	.133	-.000	-.0245	-.0136	-.0064

Table 4.5b Normalized stress intensity factors for a semi-elliptical surface crack in a plate under tension or bending loads, a/h=1.5 , ν=.3

Semi-elliptical crack, Tension.

y/a \ L_0/h	.2	.4	.6	.8	.9	.95
0.	.858	.577	.295	.0895	.0291	.0104
.1	.856	.576	.294	.0895	.0291	.0103
.2	.849	.571	.293	.0897	.0292	.0102
.3	.837	.564	.291	.0899	.0294	.0102
.4	.820	.554	.287	.0900	.0296	.0102
.5	.797	.541	.282	.0898	.0298	.0103
.6	.767	.523	.276	.0890	.0298	.0103
.7	.726	.500	.267	.0873	.0295	.0102
.8	.670	.469	.254	.0844	.0286	.0099
.9	.582	.424	.238	.0801	.0271	.0094
.95	.506	.389	.227	.0781	.0264	.0091
.98	.422	.352	.221	.0786	.0268	.0092

Semi-elliptical crack, Bending.

y/a \ L_0/h	.2	.4	.6	.8	.9	.95
0.	.848	.521	.191	.0040	-.0162	-.01078
.1	.847	.522	.193	.0054	-.0153	-.01025
.2	.844	.524	.198	.0095	-.0129	-.00884
.3	.838	.527	.206	.0161	-.0092	-.00690
.4	.830	.531	.217	.0251	-.0044	-.00463
.5	.818	.535	.231	.0362	.0013	-.00211
.6	.801	.540	.247	.0491	.0077	.00063
.7	.776	.543	.265	.0636	.0148	.00358
.8	.738	.544	.285	.0795	.0224	.00673
.9	.669	.535	.307	.0974	.0307	.01009
.95	.600	.519	.320	.1087	.0358	.01207
.98	.513	.493	.331	.1200	.0407	.01394

Table 4.6a,b Normalized stress intensity factors for a rectangular (a), or semi-elliptical (b), surface crack in a plate under tension or bending loads, a/h=2 , ν=.3

Rectangular crack, Tension.

y/a \ L_0/h	.2	.4	.6	.8	.9	.95
0.	.920	.693	.382	.120	.0408	.0155
.1	.920	.692	.381	.120	.0407	.0155
.2	.918	.688	.378	.119	.0403	.0153
.3	.915	.681	.373	.117	.0396	.0151
.4	.910	.671	.364	.114	.0386	.0147
.5	.903	.656	.353	.110	.0372	.0141
.6	.893	.635	.337	.104	.0353	.0134
.7	.877	.604	.314	.097	.0326	.0123
.8	.847	.555	.282	.086	.0287	.0108
.9	.772	.464	.228	.068	.0225	.0083
.95	.669	.375	.182	.053	.0173	.0063
.98	.515	.277	.134	.038	.0118	.0042

Rectangular crack, Bending.

y/a \ L_0/h	.2	.4	.6	.8	.9	.95
0.	.913	.645	.279	.0254	-.0136	-.0121
.1	.912	.644	.278	.0250	-.0137	-.0121
.2	.910	.639	.274	.0239	-.0140	-.0121
.3	.907	.631	.267	.0220	-.0144	-.0122
.4	.902	.619	.258	.0192	-.0151	-.0123
.5	.895	.602	.245	.0152	-.0159	-.0124
.6	.884	.577	.226	.0100	-.0171	-.0126
.7	.866	.542	.201	.0029	-.0185	-.0127
.8	.834	.485	.164	-.0066	-.0202	-.0126
.9	.752	.380	.105	-.0193	-.0210	-.0117
.95	.640	.279	.056	-.0254	-.0194	-.0100
.98	.472	.168	.013	-.0252	-.0151	-.0073

Table 4.6b Normalized stress intensity factors for a semi-elliptical surface crack in a plate under tension or bending loads, a/h=2 , ν=.3

Semi-elliptical crack, Tension.

y/a \ L_0/h	.2	.4	.6	.8	.9	.95
0.	.883	.627	.336	.104	.0336	.0120
.1	.880	.625	.335	.104	.0337	.0119
.2	.873	.620	.333	.104	.0338	.0118
.3	.860	.611	.330	.104	.0340	.0118
.4	.841	.598	.326	.104	.0343	.0118
.5	.815	.581	.319	.104	.0346	.0119
.6	.781	.558	.310	.103	.0346	.0119
.7	.737	.530	.298	.101	.0342	.0119
.8	.676	.491	.281	.097	.0332	.0115
.9	.582	.435	.258	.091	.0314	.0109
.95	.501	.390	.241	.088	.0304	.0105
.98	.413	.344	.227	.086	.0303	.0105

Semi-elliptical crack, Bending.

y/a \ L_0/h	.2	.4	.6	.8	.9	.95
0.	.875	.578	.239	.0180	-.0135	-.01066
.1	.874	.579	.241	.0196	-.0125	-.01002
.2	.870	.580	.245	.0242	-.0097	-.00834
.3	.863	.581	.253	.0316	-.0054	-.00604
.4	.852	.582	.264	.0416	.0001	-.00338
.5	.838	.584	.277	.0536	.0066	-.00481
.6	.818	.584	.291	.0672	.0136	.00259
.7	.789	.582	.307	.0822	.0212	.00580
.8	.746	.575	.323	.0981	.0291	.00911
.9	.670	.553	.338	.115	.0374	.0125
.95	.595	.525	.343	.125	.0422	.0144
.98	.503	.485	.344	.133	.0465	.0162

Table 4.7a,b Normalized stress intensity factors for a rectangular (a), or semi-elliptical (b), surface crack in a plate under tension or bending loads, a/h=3 , ν=.3

Rectangular crack, Tension.

y/a \ L_0/h	.2	.4	.6	.8	.9	.95
0.	.944	.766	.461	.150	.0495	.0184
.1	.944	.765	.460	.149	.0493	.0183
.2	.942	.761	.456	.148	.0489	.0182
.3	.940	.754	.449	.146	.0481	.0179
.4	.936	.743	.430	.142	.0470	.0175
.5	.930	.729	.426	.137	.0453	.0169
.6	.922	.708	.407	.130	.0431	.0160
.7	.909	.678	.382	.121	.0399	.0148
.8	.886	.630	.343	.107	.0351	.0130
.9	.827	.537	.279	.085	.0274	.0100
.95	.738	.440	.222	.066	.0209	.0075
.98	.588	.327	.162	.046	.0142	.0051

Rectangular crack, Bending.

y/a \ L_0/h	.2	.4	.6	.8	.9	.95
0.	.939	.729	.370	.0565	-.0065	-.0108
.1	.939	.727	.369	.0560	-.0066	-.0108
.2	.937	.723	.365	.0545	-.0069	-.0109
.3	.934	.715	.357	.0520	-.0075	-.0110
.4	.930	.703	.346	.0484	-.0084	-.0111
.5	.924	.686	.330	.0433	-.0096	-.0114
.6	.915	.662	.308	.0364	-.0112	-.0117
.7	.901	.627	.279	.0270	-.0135	-.0121
.8	.875	.572	.235	.0138	-.0165	-.0125
.9	.811	.465	.162	-.0060	-.0199	-.0125
.95	.715	.354	.099	-.0188	-.0203	-.0113
.98	.551	.224	.038	-.0245	-.0172	-.0087

Table 4.7b Normalized stress intensity factors for a semi-elliptical surface crack in a plate under tension or bending loads, a/h=3 , ν=.3

Semi-elliptical crack, Tension.

y/a \ L_0/h	.2	.4	.6	.8	.9	.95
0.	.913	.695	.400	.128	.0411	.0144
.1	.910	.693	.399	.128	.0412	.0144
.2	.901	.685	.396	.128	.0415	.0143
.3	.886	.673	.392	.129	.0419	.0144
.4	.865	.656	.384	.130	.0424	.0145
.5	.836	.633	.374	.128	.0428	.0147
.6	.798	.603	.360	.127	.0429	.0148
.7	.749	.565	.341	.123	.0424	.0147
.8	.682	.515	.316	.117	.0410	.0143
.9	.581	.444	.281	.108	.0383	.0134
.95	.495	.387	.254	.101	.0362	.0127
.98	.402	.330	.228	.095	.0348	.0123

Semi-elliptical crack, Bending.

y/a \ L_0/h	.2	.4	.6	.8	.9	.95
0.	.907	.657	.315	.0434	-.0081	-.01004
.1	.905	.657	.316	.0452	-.0069	-.00924
.2	.900	.656	.320	.0506	-.0034	-.00713
.3	.891	.654	.327	.0591	.0019	-.00424
.4	.879	.651	.226	.0703	.0086	-.00095
.5	.861	.647	.346	.0834	.0161	.00254
.6	.837	.639	.357	.0977	.0241	.00611
.7	.803	.628	.367	.113	.0323	.00966
.8	.754	.608	.374	.127	.0403	.0131
.9	.670	.569	.375	.140	.0479	.0164
.95	.589	.527	.367	.146	.0516	.0179
.98	.492	.470	.351	.149	.0542	.0192

Table 4.8a,b Normalized stress intensity factors for a rectangular (a), or semi-elliptical (b), surface crack in a plate under tension or bending loads, a/h=4 , ν=.3

Rectangular crack, Tension.

y/a \ L_0/h	.2	.4	.6	.8	.9	.95
0.	.957	.812	.523	.176	.0571	.0207
.1	.957	.811	.521	.176	.0569	.0206
.2	.956	.807	.517	.174	.0564	.0205
.3	.954	.800	.510	.171	.0555	.0202
.4	.950	.790	.499	.167	.0542	.0197
.5	.946	.776	.484	.161	.0524	.0191
.6	.938	.756	.463	.153	.0499	.0182
.7	.927	.726	.434	.142	.0463	.0169
.8	.907	.680	.392	.126	.0408	.0149
.9	.858	.588	.321	.099	.0318	.0114
.95	.782	.489	.255	.076	.0240	.0085
.98	.639	.366	.185	.053	.0162	.0057

Rectangular crack, Bending.

y/a \ L_0/h	.2	.4	.6	.8	.9	.95
0.	.954	.782	.442	.0852	.00057	-.0093
.1	.953	.781	.440	.0846	.00043	-.0093
.2	.952	.776	.435	.0828	-.00001	-.0094
.3	.950	.769	.427	.0797	-.00077	-.0096
.4	.946	.757	.414	.0752	-.00188	-.0098
.5	.941	.741	.397	.0690	-.00340	-.0101
.6	.933	.717	.373	.0607	-.00545	-.0106
.7	.920	.683	.340	.0493	-.00825	-.0111
.8	.899	.629	.291	.0332	-.0122	-.0119
.9	.846	.524	.209	.0078	-.0177	-.0126
.95	.762	.410	.136	-.0107	-.0201	-.0121
.98	.607	.268	.062	-.0223	-.0185	-.0098

Table 4.8b Normalized stress intensity factors for a semi-elliptical surface crack in a plate under tension or bending loads, a/h=4 , ν=.3

Semi-elliptical crack, Tension.

y/a \ L_0/h	.2	.4	.6	.8	.9	.95
0.	.930	.741	.450	.149	.0475	.0165
.1	.927	.738	.449	.149	.0477	.0164
.2	.918	.729	.445	.150	.0481	.0164
.3	.901	.715	.439	.150	.0487	.0165
.4	.878	.693	.429	.150	.0494	.0168
.5	.847	.665	.415	.149	.0500	.0171
.6	.807	.630	.396	.146	.0502	.0173
.7	.755	.584	.371	.141	.0495	.0172
.8	.685	.526	.338	.133	.0474	.0166
.9	.579	.445	.292	.119	.0434	.0154
.95	.491	.382	.258	.109	.0402	.0143
.98	.397	.319	.224	.099	.0375	.0135

Semi-elliptical crack, Bending.

y/a \ L_0/h	.2	.4	.6	.8	.9	.95
0.	.926	.710	.374	.0663	-.0027	-.00918
.1	.924	.709	.375	.0683	-.0013	-.00824
.2	.918	.707	.379	.0742	.0027	-.00577
.3	.908	.702	.384	.0834	.0088	-.00241
.4	.894	.696	.390	.0952	.0163	.00137
.5	.874	.687	.397	.109	.0247	.00531
.6	.847	.673	.403	.123	.0333	.00924
.7	.810	.654	.407	.137	.0417	.0130
.8	.758	.626	.406	.149	.0494	.0164
.9	.669	.575	.395	.158	.0557	.0193
.95	.585	.523	.377	.159	.0580	.0205
.98	.486	.459	.350	.157	.0588	.0211

Table 4.9a,b Normalized stress intensity factors for a rectangular (a), or semi-elliptical (b), surface crack in a plate under tension or bending loads, a/h=6 , ν=.3

Rectangular crack, Tension.

L_0/h	.2	.4	.6	.8	.9	.95
y/a						
0.	.971	.866	.613	.224	.0710	.0246
.1	.971	.865	.612	.223	.0708	.0246
.2	.970	.862	.607	.221	.0702	.0244
.3	.969	.856	.599	.217	.0690	.0240
.4	.966	.848	.586	.212	.0674	.0235
.5	.962	.835	.569	.204	.0651	.0228
.6	.957	.816	.546	.194	.0619	.0218
.7	.948	.789	.514	.180	.0575	.0203
.8	.931	.744	.466	.160	.0511	.0181
.9	.893	.657	.385	.126	.0398	.0140
.95	.834	.558	.309	.096	.0297	.0103
.98	.709	.425	.224	.066	.0196	.0067

Rectangular crack, Bending.

L_0/h	.2	.4	.6	.8	.9	.95
y/a						
0.	.969	.845	.548	.137	.0143	-.00622
.1	.968	.844	.546	.137	.0141	-.00626
.2	.968	.840	.540	.134	.0135	-.00641
.3	.966	.834	.531	.130	.0124	-.00665
.4	.963	.823	.516	.124	.0108	-.00700
.5	.959	.809	.497	.116	.0087	-.00748
.6	.953	.787	.469	.104	.0058	-.00812
.7	.943	.755	.432	.090	.0020	-.00899
.8	.925	.704	.377	.069	-.0035	-.0102
.9	.884	.603	.284	.035	-.0121	-.0120
.95	.819	.489	.196	.007	-.0179	-.0126
.98	.683	.336	.102	-.015	-.0196	-.0112

Table 4.9b Normalized stress intensity factors for a semi-elliptical surface crack in a plate under tension or bending loads, a/h=6 , ν=.3

Semi-elliptical crack, Tension.

y/a \ L_0/h	.2	.4	.6	.8	.9	.95
0.	.950	.800	.526	.186	.0588	.0199
.1	.947	.796	.524	.186	.0590	.0199
.2	.936	.785	.518	.186	.0597	.0200
.3	.919	.766	.508	.186	.0607	.0203
.4	.893	.740	.493	.186	.0619	.0209
.5	.860	.705	.472	.183	.0627	.0214
.6	.817	.661	.444	.178	.0627	.0217
.7	.761	.606	.408	.169	.0613	.0215
.8	.687	.537	.362	.155	.0576	.0205
.9	.577	.443	.300	.133	.0507	.0183
.95	.486	.373	.256	.117	.0452	.0164
.98	.390	.304	.215	.102	.0402	.0148

Semi-elliptical crack, Bending.

y/a \ L_0/h	.2	.4	.6	.8	.9	.95
0.	.947	.777	.463	.107	.0078	-.00713
.1	.945	.775	.463	.109	.0095	-.00597
.2	.938	.771	.465	.115	.0144	-.00292
.3	.927	.763	.467	.125	.0217	.00188
.4	.911	.751	.467	.138	.0305	.00574
.5	.888	.735	.469	.151	.0400	.0104
.6	.858	.713	.468	.164	.0491	.0148
.7	.818	.683	.459	.175	.0573	.0187
.8	.761	.642	.443	.181	.0636	.0218
.9	.667	.576	.412	.180	.0667	.0237
.95	.580	.515	.381	.173	.0661	.0239
.98	.478	.442	.341	.163	.0636	.0233

Table 4.10a,b Normalized stress intensity factors for a rectangular (a), or semi-elliptical (b), surface crack in a plate under tension or bending loads, a/h=10 , ν=.3

Rectangular crack, Tension.

L_0/h	.2	.4	.6	.8	.9	.95
y/a						
0.	.983	.917	.723	.305	.0966	.0315
.1	.983	.916	.721	.304	.0963	.0314
.2	.982	.914	.717	.300	.0953	.0312
.3	.981	.910	.708	.295	.0937	.0307
.4	.980	.903	.695	.287	.0912	.0300
.5	.977	.893	.677	.276	.0879	.0291
.6	.973	.880	.652	.262	.0834	.0278
.7	.967	.855	.617	.242	.0774	.0260
.8	.955	.815	.564	.215	.0688	.0233
.9	.926	.735	.472	.171	.0541	.0183
.95	.883	.642	.385	.131	.0403	.0134
.98	.788	.506	.281	.088	.0257	.0083

Rectangular crack, Bending.

L_0/h	.2	.4	.6	.8	.9	.95
y/a						
0.	.981	.904	.676	.226	.0406	.00012
.1	.981	.903	.674	.225	.0403	.00000
.2	.980	.901	.668	.222	.0393	-.00020
.3	.979	.895	.659	.216	.0376	-.00061
.4	.978	.888	.644	.207	.0351	-.00120
.5	.975	.876	.623	.195	.0317	-.00201
.6	.971	.859	.593	.179	.0273	-.00306
.7	.964	.832	.552	.158	.0214	-.00447
.8	.951	.786	.490	.129	.0133	-.00641
.9	.919	.694	.384	.082	.0003	-.00954
.95	.873	.586	.283	.041	-.0106	-.0120
.98	.769	.429	.166	.002	-.0186	-.0126

Table 4.10b Normalized stress intensity factors for a semi-elliptical surface crack in a plate under tension or bending loads, a/h=10 , ν=.3

Semi-elliptical crack, Tension.

y/a \ L_0/h	.2	.4	.6	.8	.9	.95
0.	.968	.862	.624	.245	.0780	.0255
.1	.965	.857	.621	.245	.0784	.0256
.2	.953	.843	.611	.244	.0796	.0261
.3	.935	.819	.595	.244	.0813	.0269
.4	.907	.786	.571	.241	.0830	.0279
.5	.871	.743	.538	.235	.0839	.0288
.6	.825	.689	.497	.224	.0830	.0292
.7	.766	.623	.445	.207	.0793	.0285
.8	.688	.542	.381	.181	.0716	.0262
.9	.574	.436	.300	.145	.0587	.0218
.95	.481	.360	.246	.120	.0493	.0185
.98	.383	.287	.197	.098	.0410	.0155

Semi-elliptical crack, Bending.

y/a \ L_0/h	.2	.4	.6	.8	.9	.95
0.	.966	.846	.576	.173	.0274	-.00266
.1	.964	.844	.576	.176	.0296	-.00116
.2	.957	.837	.574	.182	.0357	.00275
.3	.944	.824	.570	.192	.0445	.00797
.4	.926	.806	.564	.204	.0549	.0136
.5	.901	.781	.553	.215	.0653	.0191
.6	.868	.749	.537	.223	.0745	.0240
.7	.824	.708	.512	.225	.0810	.0277
.8	.763	.653	.475	.219	.0832	.0296
.9	.664	.572	.419	.200	.0792	.0290
.95	.575	.502	.373	.182	.0733	.0272
.98	.471	.422	.322	.161	.0661	.0248

Table 4.11 Normalized stress intensity factor at the center of a semi-elliptical crack subjected to tension and bending, ν=.3

Tension

L_0/h \ a/h	.5	1.	1.5	2.	3.	4.	5.	6.	8.	10.
.1	.910	.945	.959	.967	.976	.981	.984	.987	.990	.992
.2	.729	.817	.858	.883	.913	.930	.942	.950	.961	.968
.3	.545	.662	.724	.765	.817	.850	.873	.889	.912	.927
.4	.390	.507	.577	.627	.695	.741	.774	.800	.837	.862
.5	.268	.365	.430	.479	.552	.605	.646	.679	.728	.763
.6	.174	.244	.295	.336	.400	.450	.491	.526	.581	.624
.7	.102	.146	.179	.207	.253	.291	.324	.353	.402	.443
.8	.050	.073	.089	.104	.128	.149	.168	.186	.217	.245
.85	.031	.045	.055	.064	.079	.092	.104	.115	.135	.153
.9	.012	.024	.029	.034	.041	.048	.053	.059	.069	.078
.95	.005	.008	.010	.012	.014	.016	.018	.020	.023	.025

Bending

L_0/h \ a/h	.5	1.	1.5	2.	3.	4.	5.	6.	8.	10.
.1	.907	.943	.957	.966	.975	.981	.984	.986	.990	.992
.2	.709	.804	.848	.875	.907	.926	.938	.947	.959	.966
.3	.495	.626	.696	.741	.799	.836	.861	.879	.904	.921
.4	.306	.441	.521	.578	.657	.710	.748	.777	.818	.846
.5	.157	.271	.346	.404	.490	.552	.599	.637	.693	.734
.6	.053	.133	.191	.239	.315	.374	.422	.463	.527	.576
.7	-.007	.038	.074	.105	.157	.201	.240	.273	.331	.378
.8	-.028	-.011	.004	.018	.043	.066	.087	.107	.142	.173
.85	-.027	-.020	-.012	-.005	.009	.022	.035	.046	.068	.088
.9	-.020	-.019	-.016	-.014	-.008	-.003	.003	.078	.018	.027
.95	-.005	-.011	-.011	-.011	-.010	-.009	-.008	-.007	-.005	-.003

Table 4.12 The effect of Poisson's ratio on the normalized stress intensity factor at the center of a semi-elliptical crack subjected to tension and bending, a/h=1.

	Tension			Bending		
ν	0.	.3	.5	0.	.3	.5
L_0/h						
.1	.935	.945	.956	.933	.943	.954
.2	.791	.817	.848	.776	.804	.837
.3	.628	.662	.707	.587	.626	.676
.4	.473	.507	.554	.401	.441	.496
.5	.339	.365	.406	.239	.271	.319
.6	.228	.244	.273	.113	.133	.167
.7	.138	.146	.163	.029	.038	.056
.8	.070	.073	.080	-.013	-.011	-.005
.85	.044	.045	.049	-.019	-.020	-.017
.9	.023	.024	.025	-.017	-.019	-.019
.95	.008	.008	.009	-.010	-.011	-.011

Table 4.13a,b Normalized stress intensity factor at the center of a semi-elliptical surface crack subjected to tension. In 13a the normalization factor is for the corresponding depth edge crack given by L_0/h. The data in 13b is normalized with respect to a crack depth of .2 for all L_0/h, ν=.3

a/h \ L_0/h	.2	.4	.6	.8	.9	.95
.5	.729	.390	.174	.0499	.0158	.00547
1.	.817	.507	.244	.0725	.0235	.00833
1.5	.858	.577	.295	.0895	.0291	.0104
2.	.883	.627	.336	.104	.0336	.0120
3.	.913	.695	.400	.128	.0411	.0144
4.	.930	.741	.450	.149	.0475	.0165
5.	.942	.774	.491	.168	.0534	.0182
6.	.950	.800	.526	.186	.0588	.0199
8.	.961	.837	.581	.217	.0688	.0228
10.	.968	.862	.624	.245	.0780	.0255

Table 4.13b

a/h \ L_0/h	.2	.4	.6	.8	.9	.95
.5	.729	.852	.890	.873	.849	.864
1.	.817	1.107	1.248	1.268	1.263	1.317
1.5	.858	1.261	1.506	1.564	1.563	1.638
2.	.883	1.368	1.714	1.814	1.806	1.889
3.	.913	1.518	2.044	2.240	2.209	2.283
4.	.930	1.618	2.301	2.608	2.554	2.603
5.	.942	1.691	2.511	2.941	2.867	2.884
6.	.950	1.747	2.687	3.245	3.158	3.139
8.	.961	1.827	2.969	3.792	3.695	3.603
10.	.968	1.882	3.186	4.276	4.190	4.025

Table 4.14a,b Normalized stress intensity factor at the center of a semi-elliptical surface crack subjected to bending. In 14a the normalization factor is for the corresponding depth edge crack given by L_0/h. The data in 14b is normalized with respect to a crack depth of .2 for all L_0/h, ν=.3

a/h \ L_0/h	.2	.4	.6	.8	.9	.95
.5	.709	.306	.0532	-.0281	-.0198	-.00960
1.	.804	.441	.133	-.0114	-.0186	-.0106
1.5	.848	.521	.191	-.0400	-.0162	-.0108
2.	.875	.578	.239	-.0180	-.0135	-.0107
3.	.907	.857	.315	.0434	-.00813	-.0100
4.	.926	.710	.374	.0663	-.00273	-.00918
5.	.938	.748	.422	.0873	.00258	-.00819
6.	.947	.777	.463	.107	.00779	-.00713
8.	.959	.818	.527	.142	.0178	-.00492
10.	.966	.846	.576	.173	.0274	-.00266

Table 4.14b

a/h \ L_0/h	.2	.4	.6	.8	.9	.95
.5	.709	.516	.167	-.249	-.496	-.680
1.	.804	.774	.417	-.101	-.466	-.754
1.5	.848	.881	.601	-.0355	-.405	-.764
2.	.875	.836	.751	-.190	-.339	-.755
3.	.907	1.110	.989	.385	-.204	-.712
4.	.926	1.199	1.175	.588	-.0685	-.650
5.	.938	1.263	1.326	.774	.0647	-.580
6.	.947	1.312	1.453	.947	.195	-.505
8.	.959	1.382	1.655	1.259	.447	-.348
10.	.966	1.430	1.810	1.536	.687	-.188

Table 4.15 Contact curve for through crack bending without addition of tensile field to prevent interference as approximated by the line-spring model, ν=.3

y/a \ a/h	.5	1.0	1.5	2.0	3.0	4.0	5.0	6.0	8.0	10.0
.0	.690	.774	.818	.846	.881	.902	.916	.927	.941	.950
.1	.689	.774	.818	.846	.880	.901	.916	.926	.941	.950
.2	.687	.772	.816	.844	.879	.900	.915	.925	.940	.950
.3	.683	.768	.813	.841	.877	.898	.913	.924	.939	.949
.4	.678	.763	.808	.837	.873	.895	.911	.922	.937	.947
.51	.669	.754	.800	.830	.868	.891	.906	.918	.934	.944
.6	.659	.744	.791	.822	.861	.885	.901	.913	.930	.941
.7	.645	.729	.776	.808	.849	.875	.892	.905	.924	.936
.8	.622	.706	.753	.786	.829	.857	.877	.892	.912	.926
.9	.584	.665	.712	.745	.790	.821	.844	.861	.886	.903

Table 4.16 Normalized stress intensity factors are listed at positions along the crack front of two collinear, symmetric part-through cracks subjected to tension such that ±b defines the inner crack tip and ±c refers to the outer tip. Two different crack shapes are used for four different values of the separation distance, b. results are given for the crack from b to c.
ν=.3, (c-b)/(2h)=a/h, s=2/(c-b)[y-(c+b)/2]

	$\xi=\xi_0(1-s^2)^{1/2}$				$\xi=\xi_0(1-s^2)^{1/4}$			
s	b=.1	b=.5	b=1.	b→∞	b=.1	b=.5	b=1.	b→∞
-.98	.279	.230	.218	.205	.186	.153	.145	.138
-.95	.266	.224	.213	.203	.212	.178	.170	.163
-.90	.262	.226	.216	.207	.234	.200	.192	.185
-.80	.262	.233	.225	.217	.255	.225	.217	.210
-.70	.264	.240	.232	.225	.266	.240	.232	.225
-.60	.265	.244	.238	.231	.273	.250	.242	.236
-.51	.265	.248	.242	.236	.278	.256	.249	.243
-.40	.266	.250	.245	.239	.281	.262	.256	.249
-.30	.265	.252	.247	.242	.283	.266	.260	.253
-.20	.265	.253	.248	.243	.284	.268	.262	.256
-.10	.264	.253	.249	.244	.284	.269	.264	.258
.0	.263	.253	.249	.244	.283	.269	.264	.258
.10	.262	.252	.249	.244	.281	.268	.263	.258
.20	.261	.251	.248	.243	.278	.266	.262	.256
.30	.259	.250	.246	.242	.274	.263	.259	.253
.40	.256	.247	.244	.239	.269	.259	.254	.249
.51	.252	.244	.240	.236	.262	.252	.248	.243
.60	.248	.239	.236	.231	.254	.244	.240	.236
.70	.241	.233	.230	.225	.242	.233	.230	.225
.80	.233	.225	.221	.217	.226	.217	.214	.210
.90	.224	.216	.212	.207	.199	.192	.189	.185
.95	.221	.212	.209	.203	.176	.170	.167	.163
.98	.226	.217	.213	.205	.151	.145	.142	.138

Table 4.17 The normalized stress intensity factor at the maximum penetration point of two interacting semi-elliptical surface cracks for both tension and bending loads, ν=.3

$$\left(a = \frac{b_1-a_1}{2h} = 1,\ c = \frac{b_2-a_2}{2h},\ d = a_2-b_1,\ \frac{l_0}{h} = .5,\ A = \frac{b_1+a_1}{2},\ B=\frac{b_2+a_2}{2}\right)$$

PLATE TENSION

	c/a \ d/a	0.1	0.25	0.5	1	2	∞
$\frac{K_t(A)}{K_{t0}}$	1	.397	.392	.386	.379	.374	.366
	0.5	.382	.378	.375	.371	.368	.366
	0.25	.373	.371	.369	.368	.366	.366
	0.1	.367	.367	.366	.366	.366	.366
$\frac{K_t(B)}{K_{t0}}$	1	.397	.392	.386	.379	.374	.366
	0.5	.300	.293	.286	.279	.274	.269
	0.25	.217	.209	.203	.198	.194	.190
	0.1	.136	.130	.126	.124	.124	.123

PLATE BENDING

$\frac{K_b(A)}{K_{b0}}$	1	.313	.306	.299	.290	.283	.272
	0.5	.292	.287	.282	.278	.274	.272
	0.25	.280	.275	.275	.273	.272	.272
	0.1	.273	.273	.272	.272	.272	.272
$\frac{K_b(B)}{K_{b0}}$	1	.313	.301	.299	.290	.283	.272
	0.5	.197	.188	.179	.171	.164	.272
	0.25	.101	.091	.083	.076	.072	.069
	0.1	.012	.0045	-.0004	-.0038	-.0057	-.0058

Table 4.18a,b Normalized stress intensity factors for a rectangular (a), or semi-elliptical (b), surface crack in a plate under out-of-plane shear, in-plane shear, or twisting loads, a/h=.5 , ν=.3

Rectangular crack, Out-of-plane shear

Mode 2, K2/K20

y/a \ L_0/h	.2	.4	.6	.8	.9	.95
0.	.998	.960	.810	.568	.429	.344
.1	.997	.959	.807	.566	.427	.342
.2	.997	.956	.799	.557	.420	.336
.3	.997	.950	.786	.544	.408	.327
.4	.996	.942	.766	.524	.392	.313
.5	.995	.928	.738	.497	.370	.295
.6	.994	.909	.699	.461	.341	.271
.7	.991	.877	.645	.415	.304	.241
.8	.985	.823	.566	.352	.256	.201
.9	.968	.706	.438	.260	.186	.146
.95	.932	.575	.328	.189	.134	.104
.98	.858	.409	.217	.122	.086	.066

Mode 3, K3/K20(x100)

y/a \ L_0/h	.2	.4	.6	.8	.9	.95
0.	.000	.000	.000	.000	.000	.000
.1	.026	.057	-.027	-.204	-.234	-.209
.2	.051	.112	-.056	-.404	-.463	-.413
.3	.076	.163	-.089	-.598	-.680	-.605
.4	.099	.207	-.127	-.780	-.879	-.779
.5	.120	.241	-.173	-.946	-1.05	-.926
.6	.138	.261	-.229	-1.09	-1.18	-1.04
.7	.149	.261	-.296	-1.19	-1.26	-1.09
.8	.151	.230	-.378	-1.23	-1.26	-1.08
.9	.132	.146	-.465	-1.13	-1.09	-.914
.95	.104	.063	-.483	-.941	-.869	-.714
.98	.067	-.022	-.426	-.673	-.597	-.484

Table 4.18a continued, Normalized stress intensity factors for a rectangular surface crack in a plate under in-plane shear loading, a/h=.5 , ν=.3

Rectangular crack, In-plane shear

Mode 3, K3/K3I0

L_0/h	.2	.4	.6	.8	.9	.95
y/a						
0.	.780	.584	.513	.420	.316	.240
.1	.779	.582	.512	.418	.314	.239
.2	.776	.578	.508	.414	.311	.236
.3	.769	.571	.502	.408	.305	.231
.4	.760	.560	.492	.397	.296	.224
.5	.746	.545	.478	.383	.283	.213
.6	.725	.524	.460	.364	.266	.199
.7	.692	.495	.434	.337	.243	.181
.8	.638	.451	.396	.299	.211	.155
.9	.534	.379	.333	.235	.161	.116
.95	.430	.316	.272	.179	.119	.085
.98	.321	.251	.199	.121	.078	.055

Mode 2, K2/K3I0(x100)

L_0/h	.2	.4	.6	.8	.9	.95
y/a						
0.	.000	.000	.000	.000	.000	.000
.1	-.091	-.279	-.274	-.135	-.067	-.038
.2	-.181	-.553	-.540	-.265	-.132	-.075
.3	-.269	-.816	-.788	-.384	-.191	-.108
.4	-.354	-1.06	-1.01	-.487	-.241	-.136
.5	-.435	-1.28	-1.19	-.568	-.280	-.158
.6	-.510	-1.46	-1.32	-.619	-.304	-.171
.7	-.576	-1.58	-1.38	-.633	-.308	-.173
.8	-.629	-1.62	-1.33	-.594	-.287	-.160
.9	-.657	-1.47	-1.10	-.475	-.227	-.126
.95	-.644	-1.22	-.847	-.355	-.169	-.093
.98	-.596	-.879	-.567	-.233	-.110	-.061

Table 4.18a cont. Normalized stress intensity factors for a rectangular surface crack in a plate under twisting loads, a/h=.5 , ν=.3

Rectangular crack, Twisting

Mode 3, K3/K3TO

y/a \ L_0/h	.2	.4	.6	.8	.9	.95
0.	.754	.443	.124	-.723	-2.61	-7.45
.1	.753	.441	.122	-.725	-2.61	-7.44
.2	.749	.436	.115	-.730	-2.61	-7.41
.3	.743	.426	.105	-.740	-2.61	-7.37
.4	.732	.412	.089	-.752	-2.60	-7.29
.5	.716	.392	.068	-.767	-2.58	-7.16
.6	.693	.364	.040	-.782	-2.53	-6.95
.7	.656	.326	.002	-.791	-2.45	-6.62
.8	.596	.268	-.046	-.782	-2.28	-6.03
.9	.480	.176	-.109	-.709	-1.90	-4.89
.95	.366	.100	-.138	-.592	-1.50	-3.76
.98	.235	.027	-.136	-.426	-1.03	-2.54

Mode 2, K2/K3TO

y/a \ L_0/h	.2	.4	.6	.8	.9	.95
0.	.00000	.00000	.0000	.0000	.0000	.000
.1	-.00101	-.00381	-.0058	-.0096	-.0217	-.057
.2	-.00202	-.00755	-.0114	-.0189	-.0425	-.111
.3	-.00301	-.0111	-.0167	-.0275	-.0618	-.162
.4	-.00396	-.0145	-.0214	-.0350	-.0785	-.205
.5	-.00487	-.0175	-.0253	-.0410	-.0916	-.239
.6	-.00571	-.0199	-.0281	-.0450	-.1001	-.261
.7	-.00644	-.0217	-.0294	-.0463	-.1024	-.266
.8	-.00703	-.0222	-.0284	-.0438	-.0962	-.249
.9	-.00734	-.0202	-.0236	-.0352	-.0767	-.198
.95	-.00720	-.0168	-.0182	-.0265	-.0523	-.147
.98	-.00666	-.0121	-.0122	-.0174	-.0374	-.096

Table 4.18b Normalized stress intensity factors for a semi-elliptical surface crack in a plate under out-of-plane shear, in-plane shear, or twisting loads, a/h=.5 , ν=.3

Semi-elliptical crack, Out-of-plane shear

Mode 2, K2/K20

y/a \ L_0/h	.2	.4	.6	.8	.9	.95
0.	.988	.883	.685	.467	.350	.277
.1	.982	.880	.684	.466	.348	.273
.2	.963	.871	.683	.465	.343	.262
.3	.931	.855	.680	.464	.337	.251
.4	.884	.830	.675	.464	.332	.242
.5	.821	.795	.668	.465	.330	.237
.6	.740	.745	.657	.469	.332	.236
.7	.636	.672	.637	.476	.340	.241
.8	.501	.564	.596	.485	.355	.254
.9	.319	.387	.487	.478	.374	.275
.95	.198	.249	.354	.423	.362	.277
.98	.103	.132	.200	.295	.288	.234

Mode 3, K3/K20(×100)

y/a \ L_0/h	.2	.4	.6	.8	.9	.95
0.	.000	.000	.000	.000	.000	.000
.1	.024	.171	-.027	-.143	-.155	-.133
.2	.048	.336	-.049	-.274	-.300	-.256
.3	.070	.489	-.044	-.379	-.426	-.363
.4	.090	.623	-.015	-.443	-.520	-.447
.5	.108	.736	.048	-.449	-.568	-.499
.6	.123	.825	.151	-.376	-.546	-.500
.7	.134	.891	.295	-.203	-.423	-.420
.8	.141	.943	.482	.086	-.160	-.220
.9	.142	1.01	.722	.496	.262	.134
.95	.139	1.12	.898	.767	.540	.371
.98	.132	1.30	1.07	1.01	.765	.555

Table 4.18b cont. Normalized stress intensity factors for a semi-elliptical surface crack in a plate under in-plane shear loading, a/h=.5 , ν=.3

Semi-elliptical crack, In-plane shear

Mode 3, K3/K3I0

y/a \ L_0/h	.2	.4	.6	.8	.9	.95
0.	.738	.547	.467	.350	.249	.184
.1	.737	.546	.465	.350	.249	.183
.2	.734	.542	.462	.350	.250	.181
.3	.730	.537	.455	.349	.250	.179
.4	.723	.529	.446	.348	.252	.180
.5	.714	.518	.433	.344	.254	.182
.6	.702	.506	.415	.335	.253	.184
.7	.685	.492	.393	.319	.247	.182
.8	.661	.477	.367	.290	.228	.171
.9	.622	.465	.340	.248	.190	.142
.95	.583	.467	.336	.228	.166	.121
.98	.540	.480	.348	.226	.157	.111

Mode 2, K2/K3I0(x100)

y/a \ L_0/h	.2	.4	.6	.8	.9	.95
0.	.000	.000	.000	.000	.000	.000
.1	-.087	-.229	-.207	-.107	-.058	-.037
.2	-.168	-.450	-.412	-.213	-.116	-.071
.3	-.239	-.656	-.614	-.320	-.172	-.103
.4	-.295	-.838	-.809	-.428	-.229	-.135
.5	-.331	-.984	-.994	-.539	-.288	-.169
.6	-.341	-1.08	-1.16	-.654	-.352	-.206
.7	-.323	-1.10	-1.30	-.777	-.427	-.252
.8	-.270	-1.01	-1.36	-.904	-.515	-.309
.9	-.177	-.732	-1.22	-1.00	-.618	-.385
.95	-.110	-.477	-.924	-.937	-.638	-.415
.98	-.057	-.254	-.534	-.677	-.528	-.367

Table 4.18b cont. Normalized stress intensity factors for a semi-elliptical surface crack in a plate under twisting loads, a/h=.5 , ν=.3

Semi-elliptical crack, Twisting

Mode 3, K3/K3TO

y/a \ L_0/h	.2	.4	.6	.8	.9	.95
0.	.712	.411	.103	-.636	-2.17	-6.01
.1	.713	.413	.108	-.625	-2.15	-5.92
.2	.714	.419	.124	-.592	-2.08	-5.70
.3	.717	.431	.149	-.533	-1.97	-5.39
.4	.720	.447	.186	-.445	-1.79	-4.99
.5	.724	.468	.235	-.320	-1.53	-4.44
.6	.729	.496	.297	-.149	-1.16	-3.63
.7	.733	.531	.375	.078	-.628	-2.40
.8	.734	.577	.472	.370	.124	-.578
.9	.724	.645	.604	.741	1.13	1.98
.95	.702	.703	.713	.994	1.76	3.59
.98	.667	.765	.831	1.23	2.30	4.87

Mode 2, K2/K3TO

y/a \ L_0/h	.2	.4	.6	.8	.9	.95
0.	.00000	.00000	.0000	.0000	.0000	.000
.1	-.00097	-.00320	-.0046	-.0080	-.0179	-.045
.2	-.00189	-.00631	-.0093	-.0160	-.0351	-.087
.3	-.00269	-.00922	-.0138	-.0238	-.0516	-.124
.4	-.00333	-.0118	-.0182	-.0316	-.0674	-.159
.5	-.00373	-.0139	-.0224	-.0394	-.0831	-.193
.6	-.00386	-.0153	-.0262	-.0473	-.0994	-.229
.7	-.00366	-.0156	-.0293	-.0554	-.117	-.269
.8	-.00307	-.0144	-.0308	-.0638	-.138	-.319
.9	-.00202	-.0105	-.0277	-.0698	-.161	-.383
.95	-.00126	-.00686	-.0209	-.0650	-.164	-.405
.98	-.00065	-.00365	-.0121	-.0468	-.135	-.354

Table 4.19a,b Normalized stress intensity factors for a rectangular (a), or semi-elliptical (b), surface crack in a plate under out-of-plane shear, in-plane shear, or twisting loads, a/h=1. , ν=.3

Rectangular crack, Out-of-plane shear

Mode 2, K2/K20

y/a \ L_0/h	.2	.4	.6	.8	.9	.95
0.	1.00	.994	.957	.839	.730	.644
.1	1.00	.994	.955	.836	.727	.640
.2	1.00	.993	.949	.825	.715	.629
.3	.999	.990	.939	.807	.696	.610
.4	.999	.986	.923	.780	.668	.583
.5	.999	.979	.899	.744	.630	.547
.6	.998	.969	.864	.694	.581	.501
.7	.997	.950	.812	.628	.517	.443
.8	.994	.915	.731	.537	.434	.367
.9	.985	.826	.587	.401	.315	.263
.95	.968	.709	.452	.293	.226	.187
.98	.919	.534	.306	.190	.145	.119

Mode 3, K3/K20(×10)

y/a \ L_0/h	.2	.4	.6	.8	.9	.95
0.	.0000	.0000	.0000	.0000	.000	.000
.1	.0031	.0212	.0060	-.0298	-.052	-.056
.2	.0063	.0427	.0115	-.0599	-.103	-.112
.3	.0095	.0646	.0157	-.0905	-.153	-.165
.4	.0127	.0870	.0180	-.122	-.201	-.215
.5	.0160	.110	.0177	-.153	-.245	-.260
.6	.0192	.132	.0136	-.184	-.284	-.297
.7	.0221	.153	.0044	-.212	-.313	-.322
.8	.0240	.169	-.0119	-.234	-.325	-.326
.9	.0229	.174	-.0385	-.236	-.299	-.290
.95	.0192	.167	-.0562	-.211	-.249	-.235
.98	.0134	.151	-.0626	-.161	-.178	-.164

Table 4.19a cont. Normalized stress intensity factors for a rectangular surface crack in a plate under in-plane shear loading, a/h=1. , ν=.3

Rectangular crack, In-plane shear

Mode 3, K3/K3I0

y/a \ L_0/h	.2	.4	.6	.8	.9	.95
0.	.826	.669	.625	.570	.472	.384
.1	.826	.668	.624	.568	.470	.382
.2	.824	.665	.620	.564	.466	.378
.3	.821	.659	.613	.555	.457	.370
.4	.816	.651	.603	.543	.445	.359
.5	.809	.639	.589	.526	.428	.344
.6	.796	.621	.570	.502	.404	.323
.7	.775	.593	.541	.469	.372	.295
.8	.736	.549	.498	.421	.327	.255
.9	.646	.468	.424	.340	.254	.194
.95	.540	.392	.354	.265	.191	.144
.98	.405	.308	.268	.183	.128	.095

Mode 2, K2/K3I0(x10)

y/a \ L_0/h	.2	.4	.6	.8	.9	.95
0.	.0000	.000	.000	.000	.000	.0000
.1	-.0105	-.043	-.063	-.049	-.031	-.0200
.2	-.0211	-.086	-.125	-.096	-.060	-.0392
.3	-.0320	-.128	-.185	-.140	-.088	-.0567
.4	-.0432	-.170	-.240	-.178	-.111	-.0715
.5	-.0548	-.211	-.289	-.209	-.129	-.0827
.6	-.0665	-.248	-.327	-.229	-.140	-.0893
.7	-.0780	-.279	-.349	-.236	-.142	-.0898
.8	-.0882	-.298	-.346	-.222	-.131	-.0825
.9	-.0950	-.286	-.296	-.178	-.103	-.0639
.95	-.0951	-.249	-.232	-.133	-.076	-.0468
.98	-.0905	-.188	-.158	-.873	-.049	-.0302

Table 4.19a cont. Normalized stress intensity factors for a rectangular surface crack in a plate under twisting loads, a/h=1. , ν=.3

Rectangular crack, Twisting

Mode 3, K3/K3TO

y/a \ L_0/h	.2	.4	.6	.8	.9	.95
0.	.806	.555	.310	-.354	-2.01	-6.48
.1	.805	.554	.308	-.358	-2.02	-6.49
.2	.804	.550	.302	-.369	-2.03	-6.51
.3	.800	.543	.291	-.389	-2.06	-6.55
.4	.795	.532	.274	-.417	-2.10	-6.59
.5	.786	.515	.251	-.455	-2.15	-6.63
.6	.773	.491	.218	-.504	-2.20	-6.66
.7	.749	.455	.172	-.564	-2.24	-6.62
.8	.705	.397	.104	-.630	-2.24	-6.40
.9	.605	.291	.004	-.673	-2.07	-5.63
.95	.487	.193	-.073	-.628	-1.75	-4.60
.98	.336	.091	-.116	-.497	-1.27	-3.25

Mode 2, K2/K3TO

y/a \ L_0/h	.2	.4	.6	.8	.9	.95
0.	.00000	.0000	.0000	.0000	.000	.000
.1	-.00117	-.0058	-.0126	-.0267	-.063	-.171
.2	-.00236	-.0116	-.0250	-.0527	-.125	-.337
.3	-.00357	-.0174	-.0369	-.0770	-.182	-.491
.4	-.00483	-.0231	-.0480	-.0989	-.233	-.625
.5	-.00612	-.0286	-.0579	-.117	-.274	-.733
.6	-.00743	-.0337	-.0658	-.130	-.301	-.804
.7	-.00871	-.0380	-.0705	-.135	-.310	-.824
.8	-.00985	-.0405	-.0702	-.129	-.293	-.774
.9	-.0106	-.0390	-.0603	-.105	-.234	-.613
.95	-.0106	-.0339	-.0475	-.0791	-.175	-.454
.98	-.0101	-.0256	-.0325	-.0522	-.114	-.295

Table 4.19b Normalized stress intensity factors for a semi-elliptical surface crack in a plate under out-of-plane shear, in-plane shear, or twisting loads, a/h=1. , ν=.3

Semi-elliptical crack, Out-of-plane shear

Mode 2, K2/K20

y/a \ L_0/h	.2	.4	.6	.8	.9	.95
0.	.996	.953	.851	.693	.576	.487
.1	.989	.949	.848	.690	.571	.477
.2	.969	.935	.840	.682	.557	.453
.3	.939	.910	.826	.670	.538	.425
.4	.888	.875	.805	.655	.518	.399
.5	.823	.826	.776	.637	.498	.377
.6	.740	.760	.736	.616	.479	.360
.7	.634	.671	.680	.590	.462	.346
.8	.499	.548	.593	.551	.442	.333
.9	.318	.366	.437	.466	.398	.308
.95	.197	.232	.295	.356	.328	.263
.98	.102	.123	.161	.213	.212	.178

Mode 3, K3/K20(×10)

y/a \ L_0/h	.2	.4	.6	.8	.9	.95
0.	.0000	.0000	.0000	.0000	.0000	.000
.1	.0048	.0125	.0031	-.0283	-.0405	-.040
.2	.0094	.0250	.0080	-.0523	-.0766	-.075
.3	.0135	.0375	.0165	-.0680	-.104	-.102
.4	.0170	.0498	.0299	-.0712	-.119	-.118
.5	.0197	.0616	.0489	-.0583	-.116	-.120
.6	.0215	.0726	.0733	-.0266	-.0914	-.102
.7	.0221	.0823	.102	.0245	-.0410	-.062
.8	.0216	.0907	.135	.0924	.0351	.005
.9	.0196	.0964	.170	.173	.131	.092
.95	.0176	.0989	.193	.223	.187	.144
.98	.0153	.101	.217	.272	.239	.188

Table 4.19b cont. Normalized stress intensity factors for a semi-elliptical surface crack in a plate under in-plane shear loading, a/h=1. , ν=.3

Semi-elliptical crack, In-plane shear

Mode 3, K3/K3I0

y/a \ L_0/h	.2	.4	.6	.8	.9	.95
0.	.800	.635	.577	.489	.382	.299
.1	.799	.634	.575	.487	.381	.295
.2	.795	.629	.568	.483	.376	.288
.3	.789	.622	.557	.475	.370	.279
.4	.780	.612	.542	.463	.362	.271
.5	.767	.598	.521	.446	.352	.263
.6	.750	.582	.496	.421	.336	.253
.7	.726	.563	.466	.389	.311	.236
.8	.690	.541	.433	.346	.275	.209
.9	.627	.513	.399	.297	.227	.170
.95	.567	.496	.387	.277	.204	.149
.98	.493	.483	.393	.277	.200	.144

Mode 2, K2/K3I0(x10)

y/a \ L_0/h	.2	.4	.6	.8	.9	.95
0.	.0000	.000	.000	.000	.0000	.0000
.1	-.0133	-.043	-.050	-.031	-.0174	-.0101
.2	-.0259	-.083	-.099	-.063	-.0347	-.0199
.3	-.0368	-.121	-.145	-.094	-.0519	-.0296
.4	-.0452	-.153	-.189	-.124	-.0695	-.0396
.5	-.0503	-.176	-.227	-.155	-.0878	-.0506
.6	-.0514	-.188	-.257	-.184	-.107	-.0630
.7	-.0478	-.186	-.273	-.210	-.127	-.0769
.8	-.0390	-.162	-.265	-.228	-.146	-.0915
.9	-.0246	-.110	-.208	-.218	-.154	-.1019
.95	-.0148	-.069	-.142	-.175	-.136	-.0948
.98	-.0075	-.036	-.077	-.107	-.916	-.0675

Table 4.19b cont. Normalized stress intensity factors for a semi-elliptical surface crack in a plate under twisting loads, a/h=1. , ν=.3

Semi-elliptical crack, Twisting

Mode 3, K3/K3TO

y/a \ L_0/h	.2	.4	.6	.8	.9	.95
0.	.779	.523	.277	-.335	-1.71	-5.27
.1	.780	.525	.282	-.322	-1.68	-5.16
.2	.781	.532	.297	-.281	-1.59	-4.88
.3	.782	.543	.323	-.212	-1.43	-4.45
.4	.784	.559	.359	-.109	-1.19	-3.88
.5	.786	.581	.408	.030	-.863	-3.10
.6	.786	.608	.470	.213	-.413	-2.03
.7	.783	.642	.547	.445	.186	-.567
.8	.771	.684	.644	.734	.957	1.38
.9	.737	.739	.779	1.11	1.93	3.86
.95	.690	.774	.884	1.37	2.58	5.46
.98	.618	.800	1.00	1.65	3.23	6.99

Mode 2, K2/K3TO

y/a \ L_0/h	.2	.4	.6	.8	.9	.95
0.	.00000	.0000	.0000	.0000	.000	.000
.1	-.00147	-.0057	-.0103	-.0210	-.050	-.133
.2	-.00285	-.0112	-.0204	-.0417	-.098	-.253
.3	-.00407	-.0163	-.0302	-.0618	-.143	-.358
.4	-.00502	-.0207	-.0394	-.0810	-.184	-.449
.5	-.00561	-.0241	-.0476	-.0991	-.222	-.533
.6	-.00577	-.0260	-.0543	-.116	-.259	-.613
.7	-.00540	-.0259	-.0581	-.130	-.292	-.690
.8	-.00443	-.0229	-.0571	-.140	-.321	-.761
.9	-.00281	-.0158	-.0455	-.132	-.325	-.791
.95	-.00170	-.0100	-.0313	-.106	-.281	-.712
.98	-.00086	-.0052	-.0107	-.0644	-.187	-.497

Table 4.20a,b Normalized stress intensity factors for a rectangular (a), or semi-elliptical (b), surface crack in a plate under out-of-plane shear, in-plane shear, or twisting loads, a/h=2. , ν=.3

Rectangular crack, Out-of-plane shear

Mode 2, K2/K20

y/a \ L_0/h	.2	.4	.6	.8	.9	.95
0.	1.00	1.00	1.00	.984	.955	.921
.1	1.00	1.00	.999	.983	.952	.917
.2	1.00	1.00	.998	.976	.942	.905
.3	1.00	1.00	.995	.965	.925	.885
.4	1.00	.999	.989	.947	.899	.853
.5	1.00	.997	.979	.919	.860	.809
.6	1.00	.994	.961	.877	.806	.749
.7	.999	.987	.929	.813	.730	.668
.8	.998	.969	.867	.714	.621	.557
.9	.994	.915	.733	.548	.456	.399
.95	.977	.826	.587	.407	.329	.283
.98	.995	.670	.414	.268	.212	.180

Mode 3, K3/K20(x10)

y/a \ L_0/h	.2	.4	.6	.8	.9	.95
0.	.0000	.0000	.0000	.0000	.000	.000
.1	.0016	.0072	.0114	-.0066	-.034	-.052
.2	.0034	.0148	.0227	-.0151	-.071	-.106
.3	.0054	.0232	.0339	-.0274	-.112	-.163
.4	.0078	.0327	.0445	-.0456	-.159	-.224
.5	.0108	.0435	.0535	-.0718	-.214	-.290
.6	.0145	.0556	.0591	-.108	-.276	-.359
.7	.0191	.0678	.0579	-.155	-.341	-.424
.8	.0241	.0768	.0443	-.211	-.400	-.472
.9	.0275	.0725	.0070	-.263	-.421	-.467
.95	.0257	.0556	-.0279	-.267	-.381	-.405
.98	.0197	.0291	-.0585	-.229	-.294	-.300

Table 4.20a cont. Normalized stress intensity factors for a rectangular surface crack in a plate under in-plane shear loading, a/h=2. , ν=.3

Rectangular crack, In-plane shear

Mode 3, K3/K3I0

L_0/h	.2	.4	.6	.8	.9	.95
y/a						
0.	.841	.709	.699	.706	.641	.559
.1	.841	.709	.698	.704	.640	.558
.2	.841	.707	.695	.700	.634	.552
.3	.840	.705	.691	.692	.625	.542
.4	.838	.700	.684	.680	.611	.528
.5	.835	.693	.673	.663	.591	.508
.6	.830	.683	.657	.639	.563	.481
.7	.820	.664	.633	.604	.525	.444
.8	.799	.631	.592	.551	.468	.390
.9	.738	.556	.515	.457	.372	.303
.95	.646	.472	.437	.367	.287	.228
.98	.512	.381	.345	.263	.196	.153

Mode 2, K2/K3I0(x10)

L_0/h	.2	.4	.6	.8	.9	.95
y/a						
0.	.0000	.000	.000	.000	.000	.000
.1	-.0053	-.026	-.054	-.070	-.061	-.049
.2	-.0110	-.054	-.110	-.140	-.122	-.098
.3	-.0176	-.085	-.170	-.210	-.180	-.143
.4	-.0256	-.122	-.236	-.278	-.235	-.184
.5	-.0357	-.165	-.306	-.343	-.282	-.219
.6	-.0484	-.216	-.380	-.399	-.317	-.242
.7	-.0643	-.273	-.447	-.435	-.334	-.250
.8	-.0829	-.329	-.490	-.435	-.320	-.234
.9	-.101	-.359	-.463	-.365	-.256	-.182
.95	-.106	-.337	-.383	-.279	-.189	-.133
.98	-.109	-.274	-.272	-.185	-.123	-.085

Table 4.20a cont. Normalized stress intensity factors for a rectangular surface crack in a plate under twisting loads, a/h=2. , ν=.3

Rectangular crack, Twisting

Mode 3, K3/K3T0

y/a \ L_0/h	.2	.4	.6	.8	.9	.95
0.	.823	.608	.434	.012	-1.15	-4.53
.1	.823	.607	.433	-.008	-1.16	-4.55
.2	.822	.605	.428	-.004	-1.19	-4.61
.3	.821	.602	.421	-.025	-1.23	-4.71
.4	.819	.596	.409	-.057	-1.30	-4.85
.5	.816	.587	.391	-.101	-1.39	-5.03
.6	.810	.573	.364	-.163	-1.51	-5.26
.7	.799	.549	.323	-.250	-1.67	-5.54
.8	.776	.504	.256	-.370	-1.85	-5.81
.9	.708	.406	.132	-.532	-1.99	-5.78
.95	.607	.300	.023	-.597	-1.88	-5.18
.98	.448	.165	-.077	-.551	-1.51	-3.96

Mode 2, K2/K3T0

y/a \ L_0/h	.2	.4	.6	.8	.9	.95
0.	.00000	.0000	.0000	.000	.000	.000
.1	-.00059	-.0035	-.0103	-.031	-.086	-.251
.2	-.00123	-.0073	-.0211	-.063	-.172	-.502
.3	-.00197	-.0115	-.0326	-.095	-.258	-.748
.4	-.00287	-.0164	-.0453	-.128	-.342	-.986
.5	-.00399	-.0223	-.0592	-.160	-.421	-1.20
.6	-.00541	-.0292	-.0737	-.190	-.489	-1.38
.7	-.00718	-.0369	-.0874	-.212	-.534	-1.49
.8	-.00926	-.0446	-.0967	-.218	-.534	-1.47
.9	-.0113	-.0488	-.0923	-.189	-.448	-1.21
.95	-.0118	-.0458	-.0767	-.147	-.340	-.906
.98	-.0121	-.0373	-.0546	-.098	-.224	-.591

Table 4.20b Normalized stress intensity factors for a semi-elliptical surface crack in a plate under out-of-plane shear, in-plane shear, or twisting loads, a/h=2. , ν=.3

Semi-elliptical crack, Out-of-plane shear

Mode 2, K2/K20

y/a \ L_0/h	.2	.4	.6	.8	.9	.95
0.	.999	.986	.950	.876	.799	.723
.1	.992	.981	.946	.870	.789	.704
.2	.972	.964	.931	.852	.760	.658
.3	.938	.935	.906	.823	.718	.601
.4	.889	.893	.871	.786	.670	.544
.5	.824	.837	.823	.741	.619	.491
.6	.740	.762	.761	.687	.567	.442
.7	.634	.665	.680	.623	.512	.395
.8	.498	.536	.568	.538	.446	.344
.9	.317	.354	.395	.403	.347	.271
.95	.196	.224	.259	.281	.252	.201
.98	.102	.119	.140	.159	.147	.120

Mode 3, K3/K20(x10)

y/a \ L_0/h	.2	.4	.6	.8	.9	.95
0.	.0000	.0000	.000	.0000	.000	.000
.1	.0060	.0189	.015	-.0257	-.055	-.065
.2	.0116	.0373	.032	-.0446	-.101	-.118
.3	.0166	.0550	.052	-.0504	-.129	-.151
.4	.0206	.0712	.076	-.0383	-.131	-.160
.5	.0232	.0851	.103	-.0515	-.105	-.139
.6	.0243	.0959	.134	.0489	.046	-.087
.7	.0237	.1023	.163	.119	.039	-.006
.8	.0213	.1031	.189	.197	.142	.094
.9	.0170	.0970	.207	.271	.244	.196
.95	.0140	.0901	.214	.309	.296	.247
.98	.0113	.0828	.218	.340	.338	.284

Table 4.20b cont. Normalized stress intensity factors for a semi-elliptical surface crack in a plate under in-plane shear loading, a/h=2. , ν=.3

Semi-elliptical crack, In-plane shear

Mode 3, K3/K3I0

L_0/h	.2	.4	.6	.8	.9	.95
y/a						
0.	.829	.687	.659	.623	.532	.442
.1	.828	.686	.656	.619	.528	.434
.2	.824	.681	.647	.608	.516	.417
.3	.817	.672	.631	.590	.497	.395
.4	.807	.660	.610	.564	.474	.371
.5	.792	.644	.583	.531	.444	.346
.6	.772	.625	.550	.489	.407	.317
.7	.744	.602	.513	.440	.362	.281
.8	.701	.573	.472	.384	.309	.237
.9	.624	.530	.428	.325	.251	.188
.95	.549	.493	.403	.298	.224	.166
.98	.467	.453	.387	.287	.213	.157

Mode 2, K2/K3I0(×10)

L_0/h	.2	.4	.6	.8	.9	.95
y/a						
0.	.0000	.000	.000	.000	.0000	.0000
.1	-.0125	-.043	-.059	-.041	-.0181	-.0038
.2	-.0243	-.084	-.116	-.083	-.0384	-.0106
.3	-.0349	-.123	-.172	-.127	-.0626	-.0224
.4	-.0436	-.157	-.226	-.174	-.0919	-.0403
.5	-.0493	-.183	-.274	-.222	-.127	-.0646
.6	-.0512	-.199	-.310	-.268	-.165	-.0943
.7	-.0482	-.198	-.326	-.306	-.204	-.127
.8	-.0393	-.172	-.308	-.320	-.233	-.156
.9	-.0241	-.114	-.226	-.275	-.223	-.160
.95	-.0141	-.069	-.146	-.197	-.173	-.131
.98	-.0068	-.035	-.076	-.110	-.102	-.0806

Table 4.20b cont. Normalized stress intensity factors for a semi-elliptical surface crack in a plate under twisting loads, a/h=2. , ν=.3

Semi-elliptical crack, Twisting

Mode 3, K3/K3TO

y/a \ L_0/h	.2	.4	.6	.8	.9	.95
0.	.811	.587	.401	-.020	-1.03	-3.75
.1	.811	.589	.406	-.006	-.999	-3.65
.2	.812	.596	.421	.035	-.895	-3.34
.3	.813	.607	.445	.106	-.719	-2.87
.4	.814	.624	.481	.208	-.463	-2.23
.5	.815	.646	.528	.345	-.115	-1.37
.6	.813	.673	.588	.521	.343	-.228
.7	.806	.706	.665	.743	.927	1.24
.8	.788	.745	.763	1.02	1.66	3.11
.9	.738	.784	.893	1.39	2.60	5.48
.95	.673	.792	.980	1.65	3.25	7.07
.98	.590	.776	1.05	1.89	3.84	8.48

Mode 2, K2/K3TO

y/a \ L_0/h	.2	.4	.6	.8	.9	.95
0.	.00000	.0000	.0000	.0000	.000	.000
.1	-.00133	-.0052	-.0104	-.0245	-.065	-.187
.2	-.00261	-.0103	-.0208	-.0490	-.128	-.354
.3	-.00376	-.0153	-.0312	-.0732	-.186	-.496
.4	-.00473	-.0198	-.0416	-.0973	-.240	-.618
.5	-.00540	-.0237	-.0514	-.121	-.291	-.729
.6	-.00568	-.0264	-.0600	-.144	-.340	-.833
.7	-.00541	-.0270	-.0655	-.163	-.384	-.928
.8	-.00447	-.0242	-.0643	-.173	-.412	-.994
.9	-.00277	-.0165	-.0494	-.152	-.383	-.941
.95	-.00163	-.0102	-.0325	-.111	-.296	-.749
.98	-.00079	-.0052	-.0172	-.0624	-.176	-.458

Table 4.21a,b Normalized stress intensity factors for a rectangular (a), or semi-elliptical (b), surface crack in a plate under out-of-plane shear, in-plane shear, or twisting loads, a/h=4. , ν=.3

Rectangular crack, Out-of-plane shear

Mode 2, K2/K20

y/a \ L_0/h	.2	.4	.6	.8	.9	.95
0.	1.00	1.00	1.00	1.00	1.00	1.00
.1	1.00	1.00	1.00	1.00	1.00	1.00
.2	1.00	1.00	1.00	1.00	1.00	.999
.3	1.00	1.00	1.00	1.00	.998	.993
.4	1.00	1.00	1.00	.999	.992	.982
.5	1.00	1.00	1.00	.993	.978	.962
.6	1.00	1.00	.997	.978	.952	.925
.7	1.00	.999	.988	.947	.902	.862
.8	1.00	.994	.961	.876	.806	.752
.9	.998	.967	.866	.713	.620	.558
.95	.982	.914	.732	.547	.455	.399
.98	1.03	.799	.543	.368	.295	.254

Mode 3, K3/K20(x100)

y/a \ L_0/h	.2	.4	.6	.8	.9	.95
0.	.0000	.000	.000	.000	.000	.000
.1	.0044	.021	.047	.066	.027	-.038
.2	.0094	.044	.098	.130	.036	-.104
.3	.0157	.074	.161	.186	.004	-.234
.4	.0245	.115	.241	.221	-.106	-.473
.5	.0378	.175	.346	.207	-.348	-.879
.6	.0594	.268	.479	.085	-.803	-1.53
.7	.0960	.411	.627	-.240	-1.57	-2.47
.8	.158	.616	.720	-.910	-2.70	-3.70
.9	.250	.809	.526	-2.01	-3.97	-4.81
.95	.283	.760	.131	-2.57	-4.23	-4.77
.98	.249	.493	-.380	-2.60	-3.64	-3.88

Table 4.21a cont. Normalized stress intensity factors for a rectangular surface crack in a plate under in-plane shear loading, a/h=4. , ν=.3

Rectangular crack, In-plane shear

Mode 3, K3/K3I0

y/a \ L_0/h	.2	.4	.6	.8	.9	.95
0.	.844	.722	.735	.797	.782	.728
.1	.844	.722	.734	.796	.781	.726
.2	.844	.722	.733	.793	.776	.720
.3	.844	.721	.731	.788	.768	.711
.4	.844	.720	.727	.779	.755	.696
.5	.843	.717	.722	.766	.737	.675
.6	.842	.713	.713	.747	.711	.646
.7	.838	.704	.697	.718	.672	.604
.8	.830	.686	.668	.669	.611	.541
.9	.799	.633	.600	.573	.502	.432
.95	.737	.556	.521	.474	.398	.334
.98	.621	.458	.424	.354	.281	.229

Mode 2, K2/K3I0(×10)

y/a \ L_0/h	.2	.4	.6	.8	.9	.95
0.	.0000	.0000	.000	.000	.000	.000
.1	-.0014	-.0068	-.016	-.031	-.038	-.041
.2	-.0029	-.0146	-.034	-.064	-.080	-.083
.3	-.0049	-.0247	-.058	-.105	-.126	-.129
.4	-.0077	-.0388	-.090	-.156	-.181	-.181
.5	-.0120	-.0604	-.136	-.222	-.245	-.236
.6	-.0191	-.0946	-.205	-.306	-.317	-.293
.7	-.0313	-.150	-.303	-.404	-.388	-.343
.8	-.0526	-.237	-.429	-.493	-.435	-.364
.9	-.0860	-.345	-.526	-.499	-.399	-.316
.95	-.103	-.372	-.491	-.411	-.310	-.238
.98	-.114	-.336	-.373	-.282	-.204	-.153

Table 4.21a cont. Normalized stress intensity factors for a rectangular surface crack in a plate under twisting loads, a/h=4. , ν=.3

Rectangular crack, Twisting

Mode 3, K3/K3T0

y/a \ L_0/h	.2	.4	.6	.8	.9	.95
0.	.826	.624	.492	.259	-.405	-2.48
.1	.826	.624	.491	.257	-.413	-2.51
.2	.826	.624	.490	.248	-.438	-2.58
.3	.826	.623	.486	.233	-.483	-2.70
.4	.825	.621	.480	.210	-.551	-2.88
.5	.825	.618	.471	.175	-.648	-3.13
.6	.823	.612	.456	.123	-.785	-3.47
.7	.820	.601	.430	.044	-.979	-3.92
.8	.810	.577	.381	-.085	-1.26	-4.54
.9	.776	.507	.269	-.311	-1.67	-5.28
.95	.708	.411	.145	-.484	-1.85	-5.39
.98	.570	.261	-.006	-.570	-1.72	-4.65

Mode 2, K2/K3T0

y/a \ L_0/h	.2	.4	.6	.8	.9	.95
0.	.00000	.00000	.0000	.000	.000	.000
.1	-.00015	-.00092	-.0030	-.012	-.037	-.122
.2	-.00033	-.00197	-.0064	-.024	-.079	-.255
.3	-.00055	-.00331	-.0107	-.040	-.128	-.412
.4	-.00086	-.00522	-.0167	-.061	-.191	-.606
.5	-.00134	-.00812	-.0255	-.090	-.271	-.845
.6	-.00214	-.0127	-.0387	-.127	-.372	-1.13
.7	-.00350	-.0202	-.0578	-.175	-.488	-1.45
.8	-.00587	-.0319	-.0828	-.224	-.593	-1.70
.9	-.00961	-.0467	-.1031	-.240	-.599	-1.66
.95	-.0115	-.0505	-.0973	-.205	-.492	-1.34
.98	-.0127	-.0457	-.0745	-.144	-.335	-.895

Table 4.21b Normalized stress intensity factors for a semi-elliptical surface crack in a plate under out-of-plane shear, in-plane shear, or twisting loads, a/h=4. , ν=.3

Semi-elliptical crack, Out-of-plane shear

Mode 2, K2/K20

y/a \ L_0/h	.2	.4	.6	.8	.9	.95
0.	1.00	.997	.988	.965	.932	.889
.1	.993	.991	.982	.956	.916	.860
.2	.973	.973	.964	.930	.872	.788
.3	.939	.943	.935	.890	.809	.699
.4	.890	.899	.893	.838	.737	.612
.5	.824	.840	.838	.776	.662	.531
.6	.740	.763	.767	.703	.586	.458
.7	.633	.663	.675	.618	.507	.390
.8	.497	.532	.553	.513	.419	.319
.9	.316	.349	.376	.362	.301	.230
.95	.196	.221	.244	.244	.206	.159
.98	.102	.117	.132	.136	.117	.092

Mode 3, K3/K20(x10)

y/a \ L_0/h	.2	.4	.6	.8	.9	.95
0.	.0000	.0000	.000	.0000	.0000	.000
.1	.0049	.0170	.020	-.0077	-.0408	-.063
.2	.0095	.0336	.040	-.0097	-.0700	-.107
.3	.0135	.0492	.062	-.0144	-.0790	-.123
.4	.0167	.0632	.086	.0201	-.0638	-.109
.5	.0188	.0750	.110	.0553	-.0246	-.068
.6	.0194	.0826	.134	.102	.0344	-.007
.7	.0183	.0850	.153	.154	.105	.065
.8	.0154	.0800	.162	.201	.173	.134
.9	.0108	.0660	.156	.230	.223	.186
.95	.0097	.0585	.145	.228	.230	.196
.98	-.0030	.0244	.120	.254	.280	.244

Table 4.21b cont. Normalized stress intensity factors for a semi-elliptical surface crack in a plate under in-plane shear loading, a/h=4. , ν=.3

Semi-elliptical crack, In-plane shear

Mode 3, K3/K3I0

y/a \ L_0/h	.2	.4	.6	.8	.9	.95
0.	.840	.712	.709	.728	.672	.590
.1	.839	.710	.705	.722	.664	.577
.2	.835	.704	.693	.704	.640	.545
.3	.828	.695	.675	.675	.606	.503
.4	.817	.682	.649	.635	.562	.458
.5	.802	.666	.616	.586	.511	.411
.6	.781	.645	.579	.529	.453	.360
.7	.751	.620	.537	.466	.390	.306
.8	.705	.587	.491	.400	.323	.249
.9	.622	.535	.439	.334	.257	.193
.95	.540	.485	.403	.301	.226	.166
.98	.451	.427	.370	.279	.208	.156

Mode 2, K2/K3I0(x10)

y/a \ L_0/h	.2	.4	.6	.8	.9	.95
0.	.0000	.000	.000	.000	.0000	.0000
.1	-.0079	-.027	-.039	-.025	.0021	.0237
.2	-.0156	-.053	-.078	-.053	-.0031	.0349
.3	-.0227	-.079	-.117	-.087	-.0206	.0279
.4	-.0290	-.103	-.158	-.128	-.0524	.0283
.5	-.0338	-.125	-.197	-.176	-.0971	-.0369
.6	-.0365	-.142	-.233	-.227	-.151	-.0863
.7	-.0360	-.149	-.257	-.273	-.205	-.138
.8	-.0306	-.137	-.254	-.295	-.242	-.178
.9	-.0190	-.094	-.191	-.249	-.222	-.174
.95	-.0132	-.062	-.126	-.172	-.161	-.130
.98	.0064	.000	-.039	-.079	-.0810	-.0675

Table 4.21b cont. Normalized stress intensity factors for a semi-elliptical surface crack in a plate under twisting loads, a/h=4. , ν=.3

Semi-elliptical crack, Twisting

Mode 3, K3/K3T0

L_0/h	.2	.4	.6	.8	.9	.95
y/a						
0.	.822	.615	.470	.211	-.425	-2.21
.1	.822	.617	.475	.224	-.391	-2.11
.2	.823	.624	.489	.263	-.290	-1.82
.3	.824	.636	.513	.330	-.119	-1.37
.4	.826	.653	.548	.427	.129	-.736
.5	.826	.676	.594	.557	.464	.107
.6	.824	.704	.655	.724	.898	1.20
.7	.816	.738	.733	.936	1.45	2.59
.8	.795	.776	.832	1.21	2.15	4.34
.9	.738	.806	.960	1.58	3.08	6.65
.95	.664	.794	1.03	1.83	3.72	8.24
.98	.572	.749	1.06	2.02	4.24	9.53

Mode 2, K2/K3T0

L_0/h	.2	.4	.6	.8	.9	.95
y/a						
0.	.00000	.0000	.0000	.0000	.000	.000
.1	-.00082	-.0029	-.0052	-.0116	-.033	-.106
.2	-.00161	-.0058	-.0107	-.0238	-.066	-.199
.3	-.00237	-.0088	-.0167	-.0372	-.098	-.281
.4	-.00306	-.0119	-.0235	-.0529	-.133	-.357
.5	-.00363	-.0150	-.0313	-.0719	-.173	-.442
.6	-.00399	-.0179	-.0399	-.0949	-.223	-.547
.7	-.00401	-.0198	-.0480	-.121	-.284	-.680
.8	-.00350	-.0194	-.0522	-.144	-.344	-.822
.9	-.00222	-.0141	-.0434	-.136	-.345	-.844
.95	-.00155	-.0095	-.0297	-.100	-.265	-.664
.98	.00068	-.0004	-.0104	-.0480	-.138	-.360

Table 4.22 Normalized stress intensity factor at the center of a semi-elliptical crack subjected to out-of-plane shear, in-plane shear, and twisting loads, ν=.3

Out-of-plane shear, Mode 2, K2/K20

L_0/h \ a/h	.5	1.	1.5	2.	3.	4.	5.	6.	8.	10.
.1	.999	1.00	1.00	1.00	1.00	1.00	1.00	1.00	1.00	1.00
.2	.998	.996	.998	.999	.999	1.00	1.00	1.00	1.00	1.00
.3	.952	.982	.991	.995	.998	.999	.999	.999	1.00	1.00
.4	.883	.953	.976	.986	.994	.997	.998	.999	.999	1.00
.5	.790	.909	.952	.972	.987	.993	.996	.997	.998	.999
.6	.685	.851	.918	.950	.978	.988	.992	.995	.997	.998
.7	.576	.780	.873	.920	.963	.979	.987	.991	.995	.997
.8	.467	.693	.811	.876	.938	.965	.978	.985	.992	.995
.85	.410	.640	.769	.844	.919	.952	.969	.979	.988	.993
.9	.350	.576	.714	.799	.889	.932	.954	.968	.982	.988
.95	.277	.487	.629	.723	.832	.889	.921	.942	.965	.977

In-plane shear, Mode 3, K3/K3I0

L_0/h \ a/h	.5	1.	1.5	2.	3.	4.	5.	6.	8.	10.
.1	.899	.927	.935	.939	.942	.943	.943	.943	.944	.944
.2	.738	.800	.820	.829	.837	.840	.842	.843	.843	.844
.3	.619	.698	.727	.740	.752	.758	.760	.762	.764	.765
.4	.547	.635	.670	.688	.704	.712	.716	.719	.722	.724
.5	.503	.600	.642	.665	.688	.699	.706	.710	.716	.719
.6	.467	.577	.629	.659	.692	.709	.720	.727	.736	.741
.7	.420	.547	.613	.653	.700	.726	.743	.755	.770	.780
.8	.350	.489	.570	.623	.688	.728	.754	.773	.799	.815
.85	.304	.443	.529	.588	.664	.711	.744	.767	.800	.821
.9	.249	.382	.470	.532	.617	.672	.711	.740	.781	.809
.95	.184	.299	.380	.442	.530	.590	.635	.670	.721	.757

Twisting, Mode 3, K3/K3T0

L_0/h \ a/h	.5	1.	1.5	2.	3.	4.	5.	6.	8.	10.
.1	.895	.924	.932	.936	.939	.940	.940	.941	.941	.941
.2	.712	.779	.801	.811	.819	.822	.823	.824	.825	.826
.3	.550	.642	.674	.689	.702	.708	.710	.712	.714	.715
.4	.411	.523	.566	.587	.606	.615	.619	.622	.626	.628
.5	.273	.410	.467	.497	.526	.539	.547	.552	.559	.562
.6	.103	.277	.357	.401	.447	.470	.484	.493	.504	.511
.7	-.152	.074	.193	.263	.341	.382	.408	.425	.447	.460
.8	-.636	-.335	-.144	-.020	.128	.211	.264	.300	.347	.377
.85	-1.13	-.766	-.508	-.330	-.109	.020	.103	.162	.238	.286
.9	-2.17	-1.71	-1.32	-1.03	-.654	-.425	-.273	-.165	-.021	.071
.95	-6.01	-5.27	-4.43	-3.75	-2.81	-2.21	-1.79	-1.49	-1.09	-.823

Table 4.23 The effect of Poisson's ratio on the normalized stress intensity factor at the center of a semi-elliptical crack subjected to out-of-plane shear, in-plane shear, and twisting loads, a/h=1.

	Out-of-plane shear Mode 2, K2/K20			In-plane shear Mode 3, K3/K3I0			Twisting Mode 3, K3/K3T0		
ν	0.	.3	.5	0.	.3	.5	0.	.3	.5
L_0/h									
.1	1.00	1.00	1.00	.935	.927	.921	.932	.924	.918
.2	.994	.996	.997	.820	.800	.787	.801	.779	.766
.3	.974	.982	.987	.725	.698	.682	.673	.642	.623
.4	.936	.953	.966	.666	.635	.617	.562	.523	.500
.5	.878	.909	.932	.634	.940	.580	.457	.410	.382
.6	.806	.851	.886	.615	.577	.555	.337	.277	.242
.7	.721	.780	.827	.591	.547	.521	.155	.074	.028
.8	.624	.693	.751	.541	.489	.460	-.216	-.335	-.398
.85	.569	.640	.703	.498	.443	.414	-.613	-.766	-.844
.9	.503	.576	.643	.437	.382	.353	-1.50	-1.71	-1.82
.95	.416	.487	.554	.350	.299	.273	-4.85	-5.27	-5.44

Table 4.24 The LSM approximation to the stress intensity factor at the corner of a semi-elliptical surface crack subjected to out-of-plane shear, in-plane shear, and twisting loads, a/h=1, ν=.3.

	OUT-OF-PLANE SHEAR		IN-PLANE SHEAR		TWISTING	
	$\frac{k_2(h/2)}{\sigma_3\sqrt{a}}$	$\frac{k_3(0)}{\sigma_3\sqrt{a}}$	$\frac{k_2(h/2)}{\sigma_4\sqrt{a}}$	$\frac{k_3(0)}{\sigma_4\sqrt{a}}$	$\frac{k_2(h/2)}{\sigma_5\sqrt{a}}$	$\frac{k_3(0)}{\sigma_5\sqrt{a}}$
L_0/h						
.1	.000	.005	.124	-.000	.116	-.000
.2	.000	.033	.237	-.0005	.206	-.0005
.3	.001	.074	.336	-.002	.272	-.002
.4	.004	.125	.421	-.005	.317	-.004
.5	.009	.186	.496	-.009	.348	-.006
.6	.017	.256	.563	-.014	.368	-.009
.7	.028	.332	.625	-.020	.380	-.012
.8	.042	.416	.682	-.025	.387	-.014
.85	.050	.461	.709	-.028	.389	-.015
.9	.059	.507	.735	-.030	.390	-.016
.95	.069	.556	.761	-.032	.390	-.017

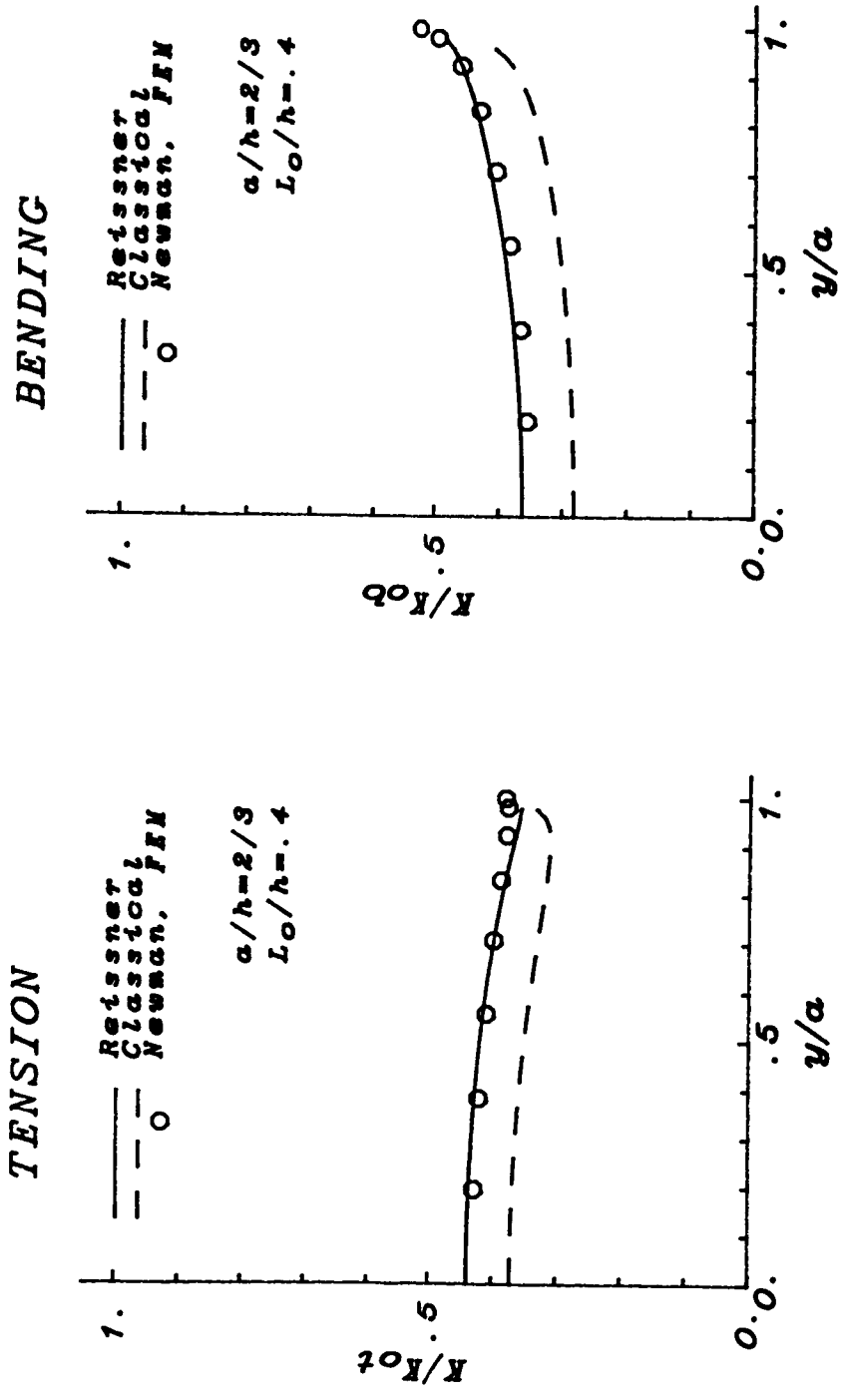

Figure 4.1 Comparison of mode 1 line-spring model with and without transverse shear deformation to Newman's and Raju's finite element solution, Ref. [33], for a/h=2/3, ν=.3

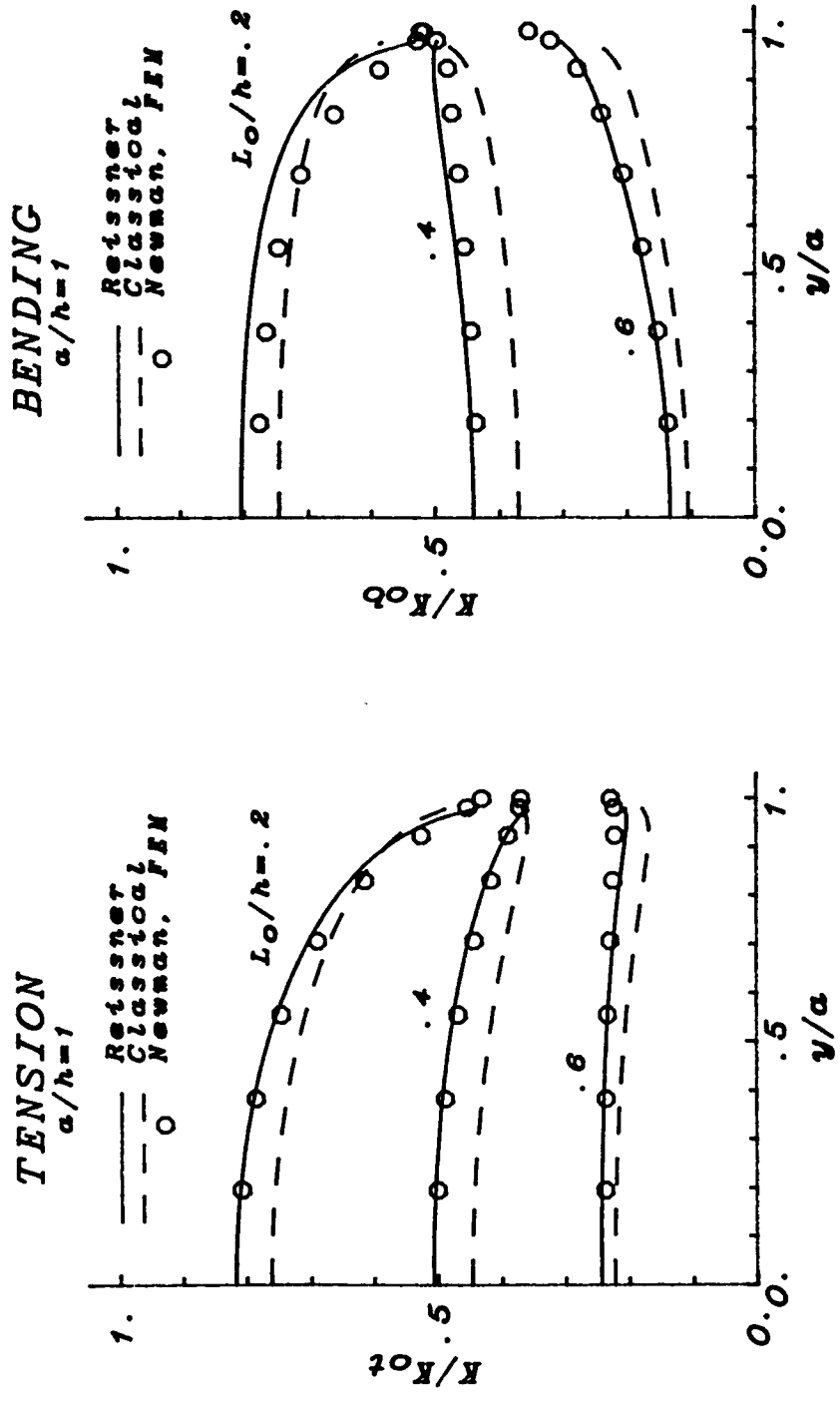

Figure 4.2 Comparison of mode 1 line-spring model with and without transverse shear deformation to Newman's and Raju's finite element solution, Ref. [33], for a/h=1., ν=.3

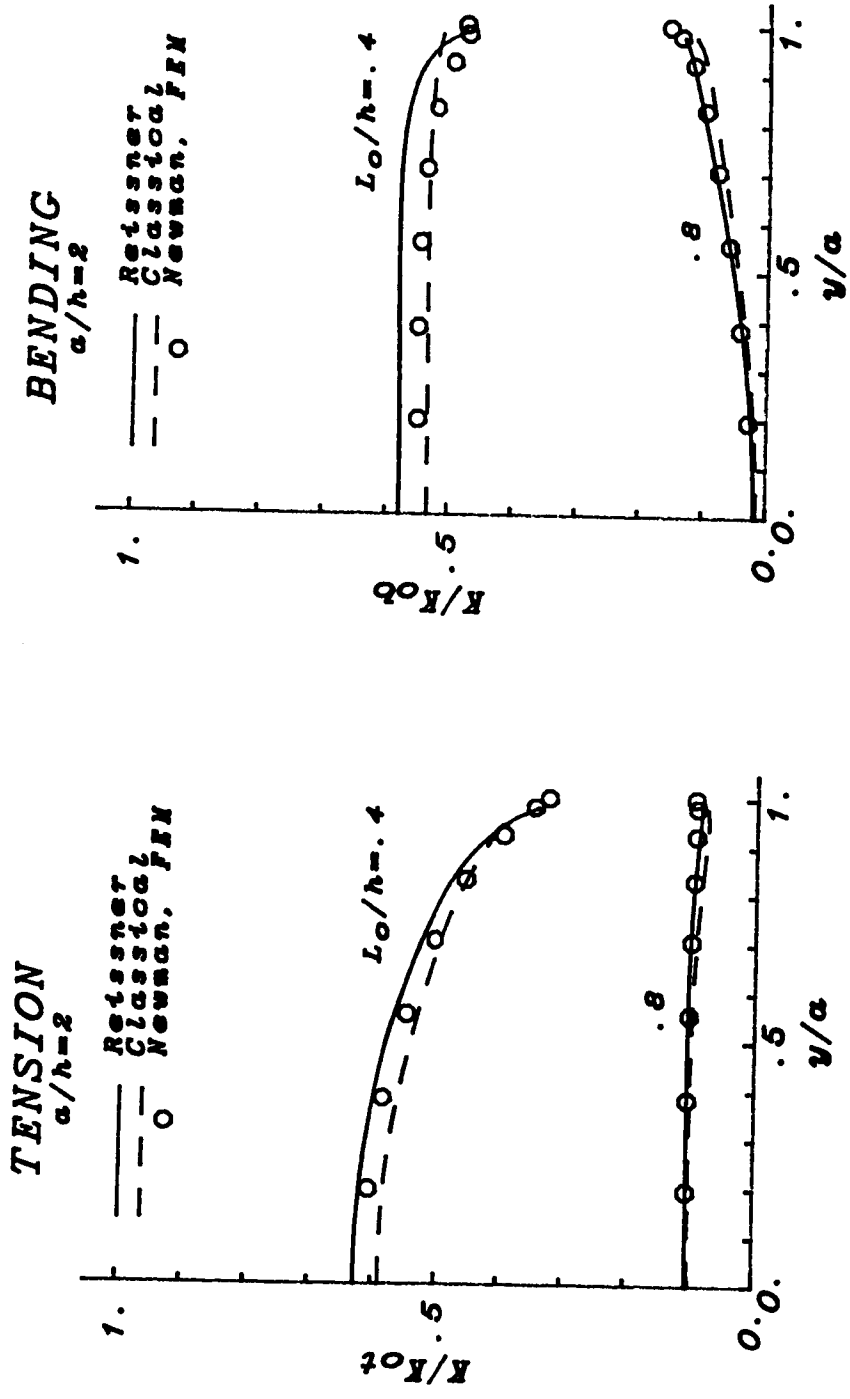

Figure 4.3 Comparison of mode 1 line-spring model with and without transverse shear deformation to Newman's and Raju's finite element solution, Ref. [33], for a/h=2., ν=.3

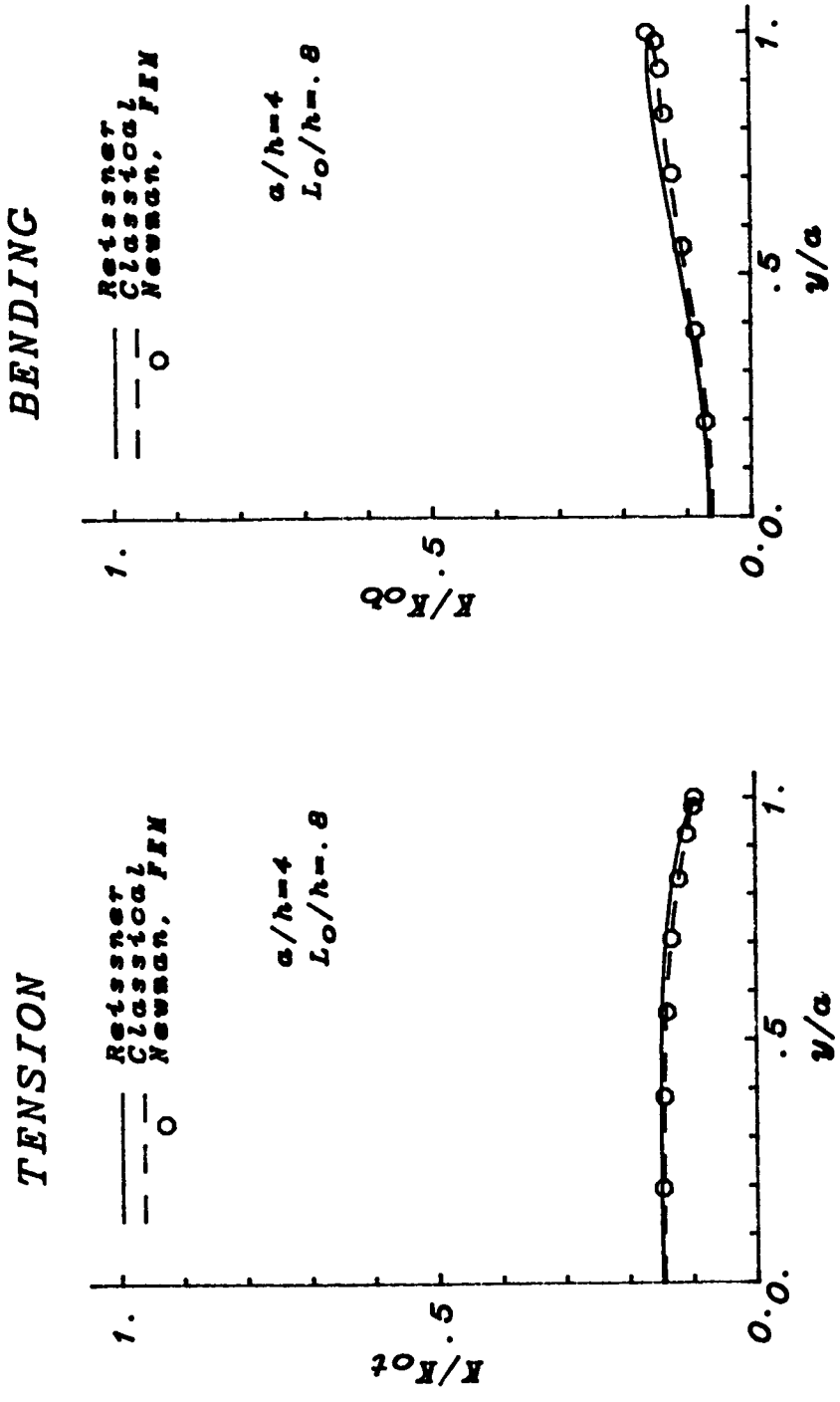

Figure 4.4 Comparison of mode 1 line-spring model with and without transverse shear deformation to Newman's and Raju's finite element solution, Ref. [33], for a/h=4., ν=.3

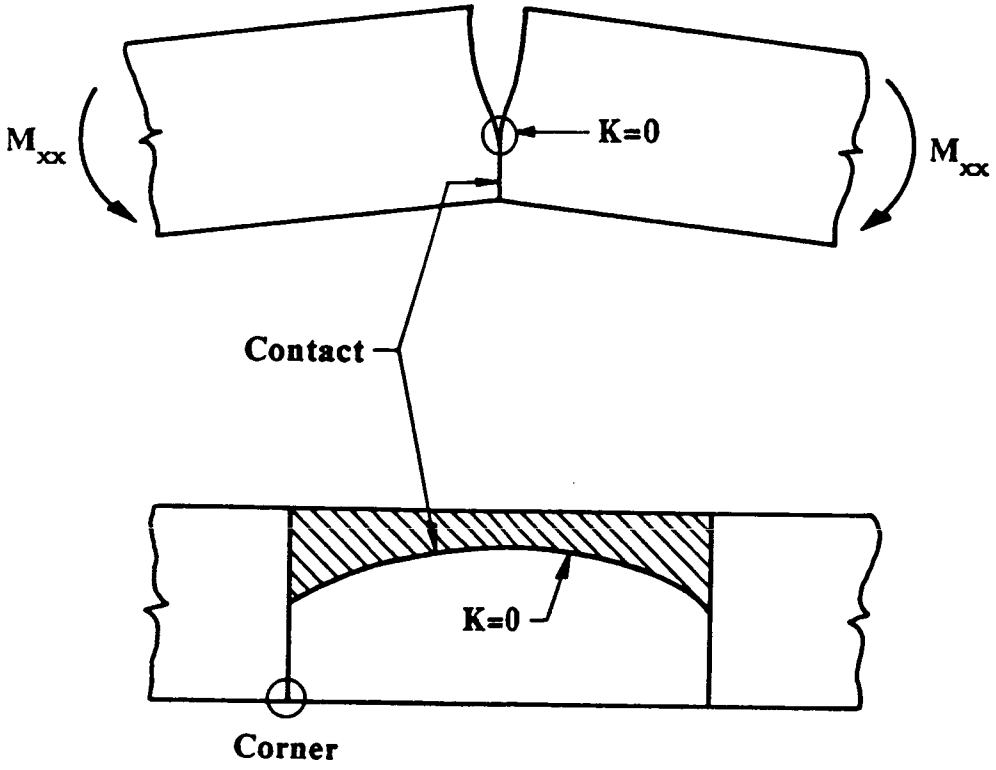

Figure 4.5 Geometry of the bending contact problem.

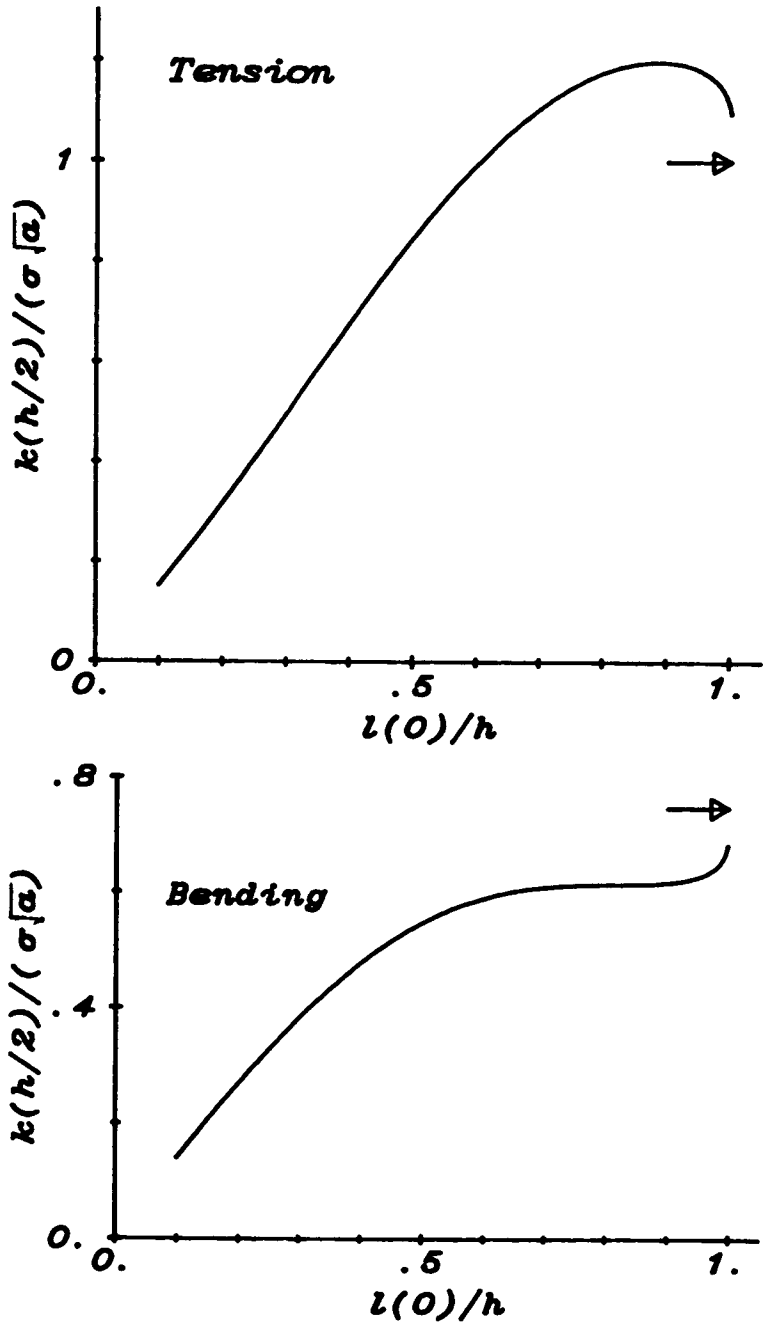

Figure 4.6 Line-spring model approximation to the stress intensity factor at the corner of rectangularly shaped surface crack, a/h=1., ν=.3. The arrow points to the through crack limit.

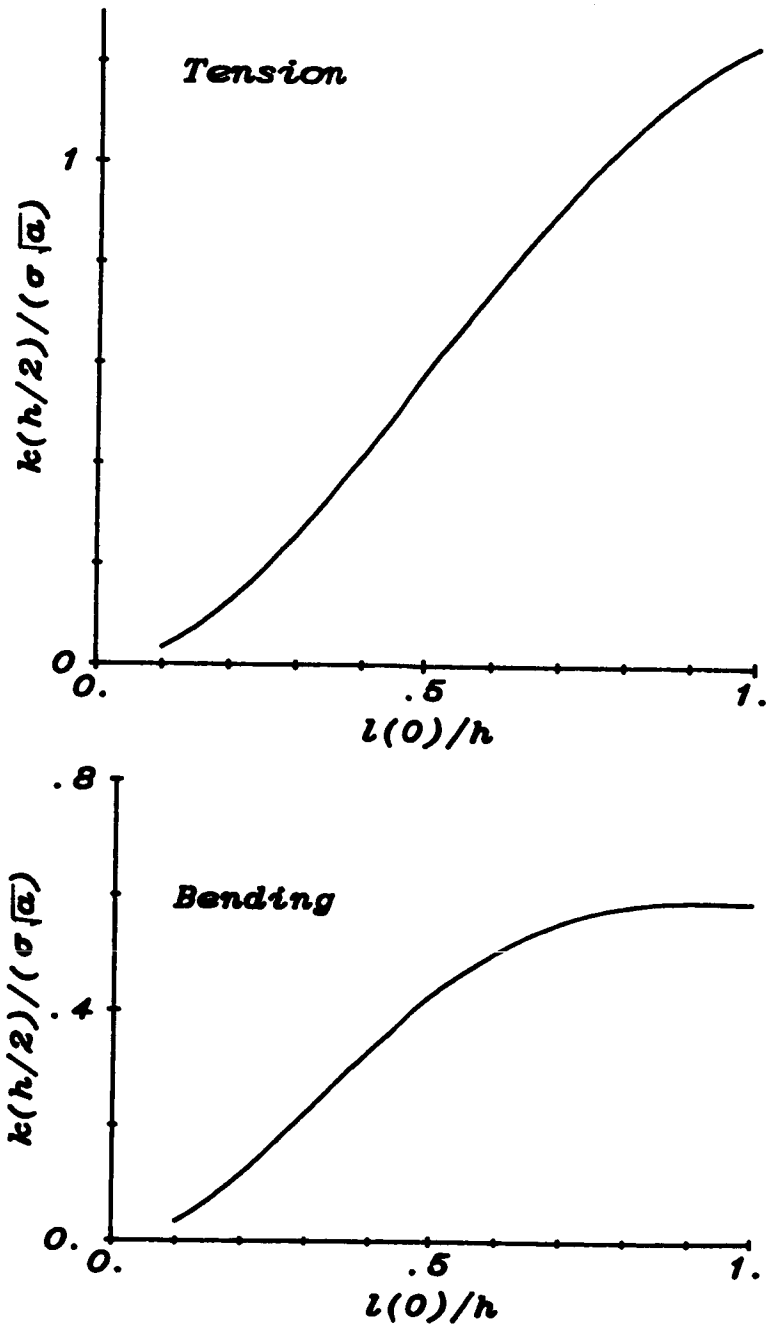

Figure 4.7 Line-spring model approximation to the stress intensity factor at the corner of 1/4 power "semi-elliptical" surface crack, a/h=1., ν=.3

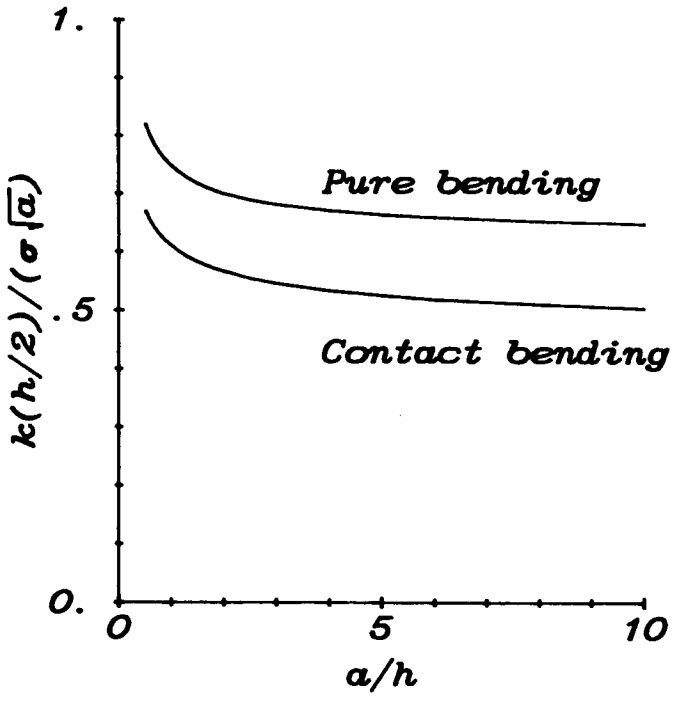

Figure 4.8 Line-spring model approximation to the stress intensity factor at the corner of a through crack subjected to bending allowing for contact stresses as compared to the value assuming no contact, a/h=1., ν=.3

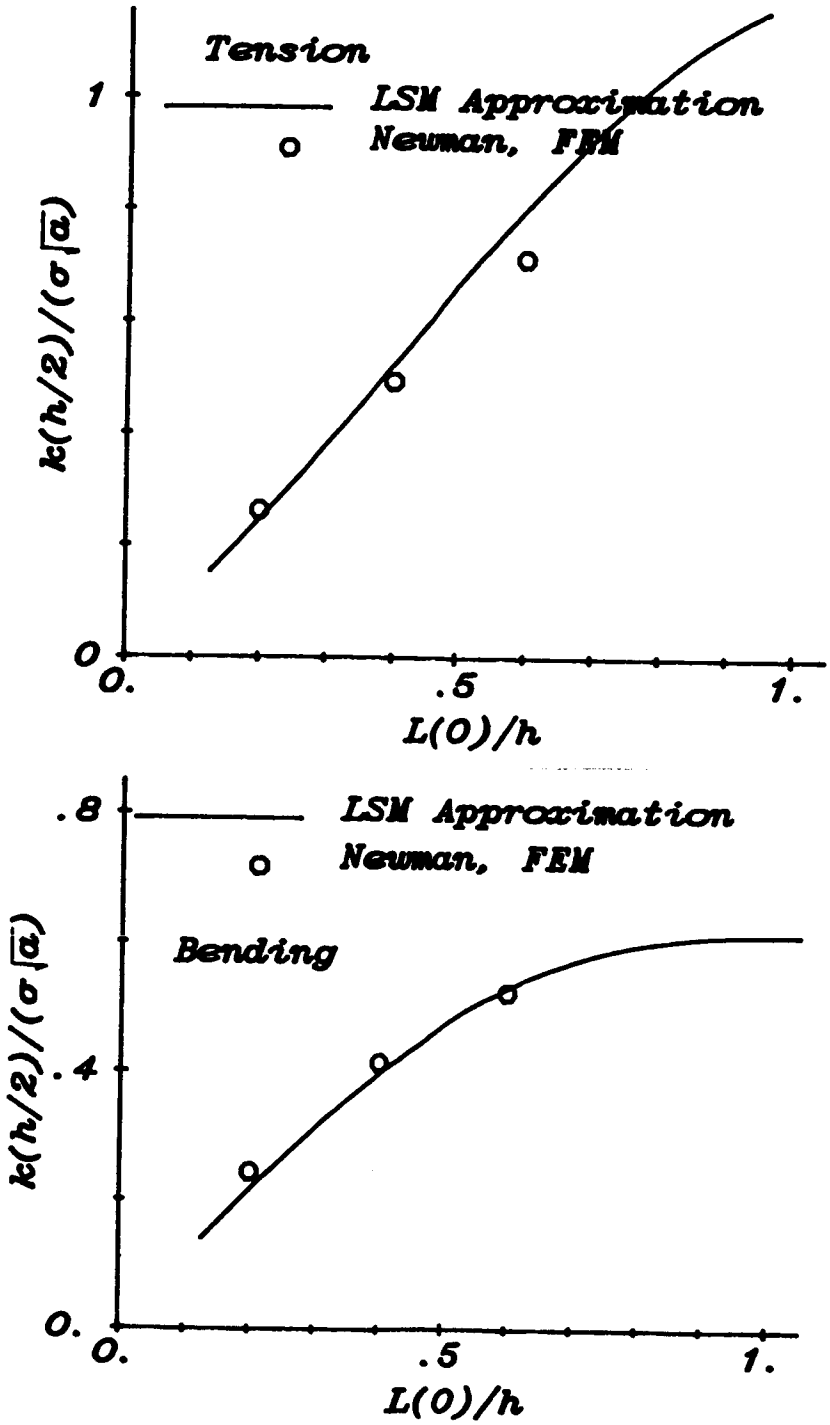

Figure 4.9 The LSM approximation to the stress intensity factor at the corner of a semi-elliptical surface crack, a/h=1., ν=.3. The finite element results are from Ref. [33].

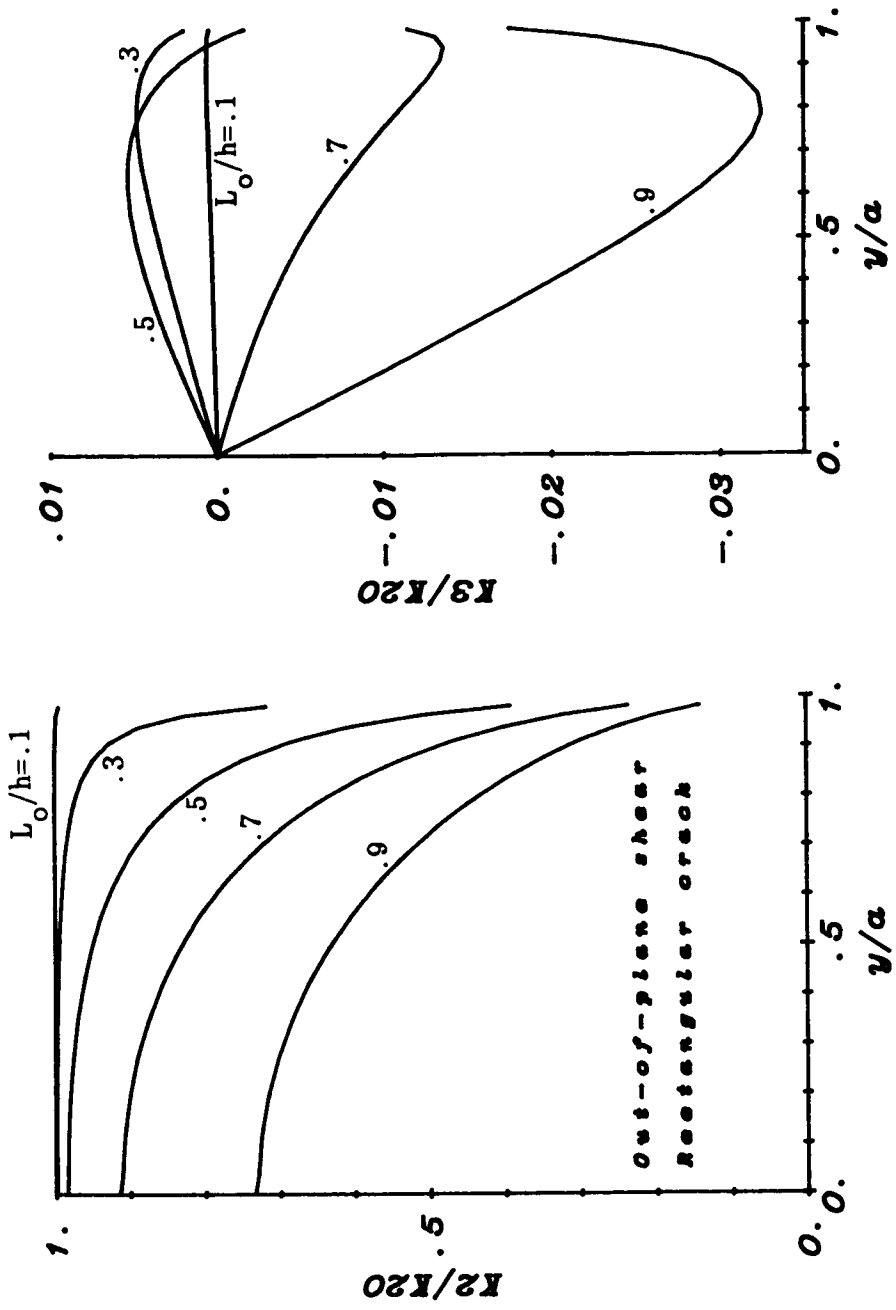

Figure 4.10 Normalized stress intensity factor profiles for the mode 2,3 line-spring model for a rectangular crack subjected to out-of-plane shear, a/h=1., ν=.3

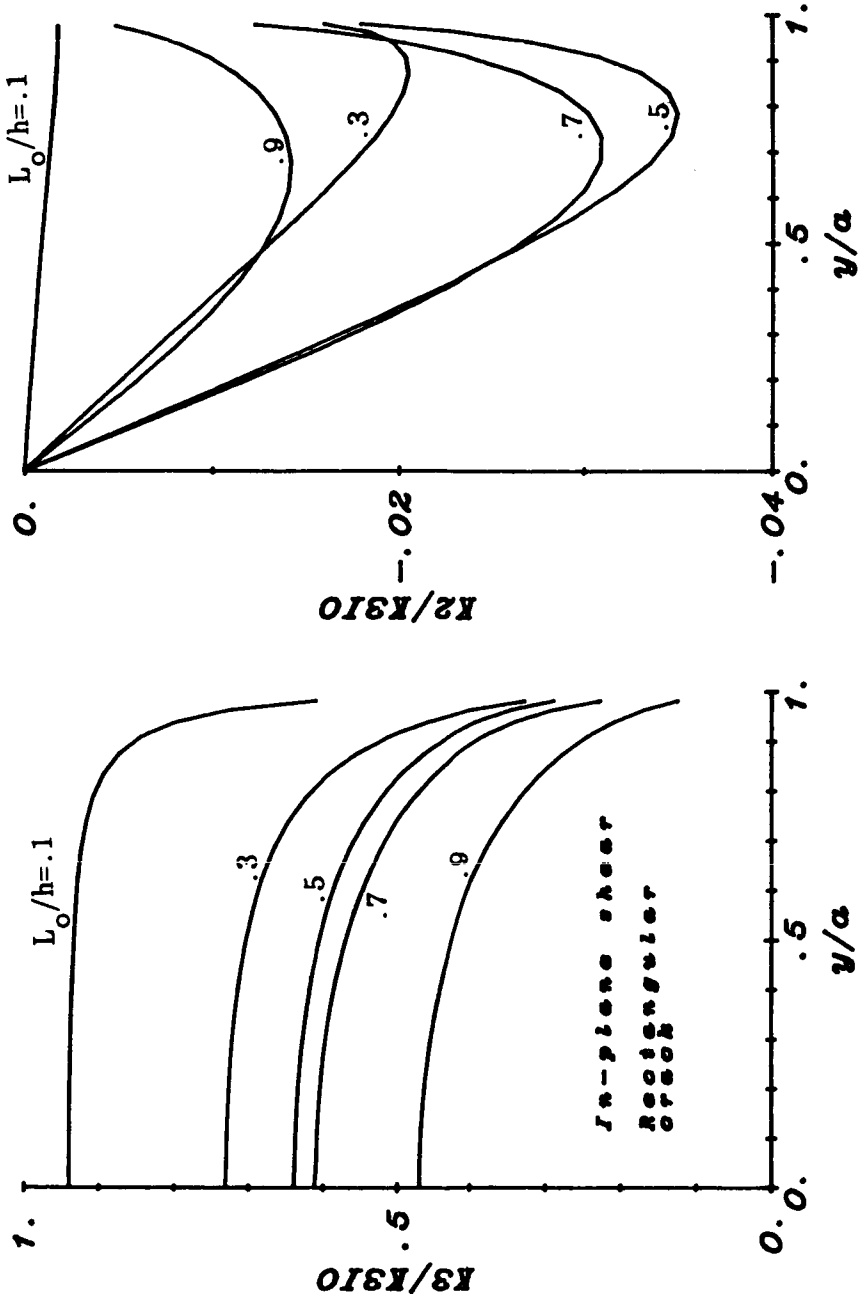

Figure 4.11 Normalized stress intensity factor profiles for the mode 2,3 line-spring model for a rectangular crack subjected to in-plane shear, a/h=1., ν=.3

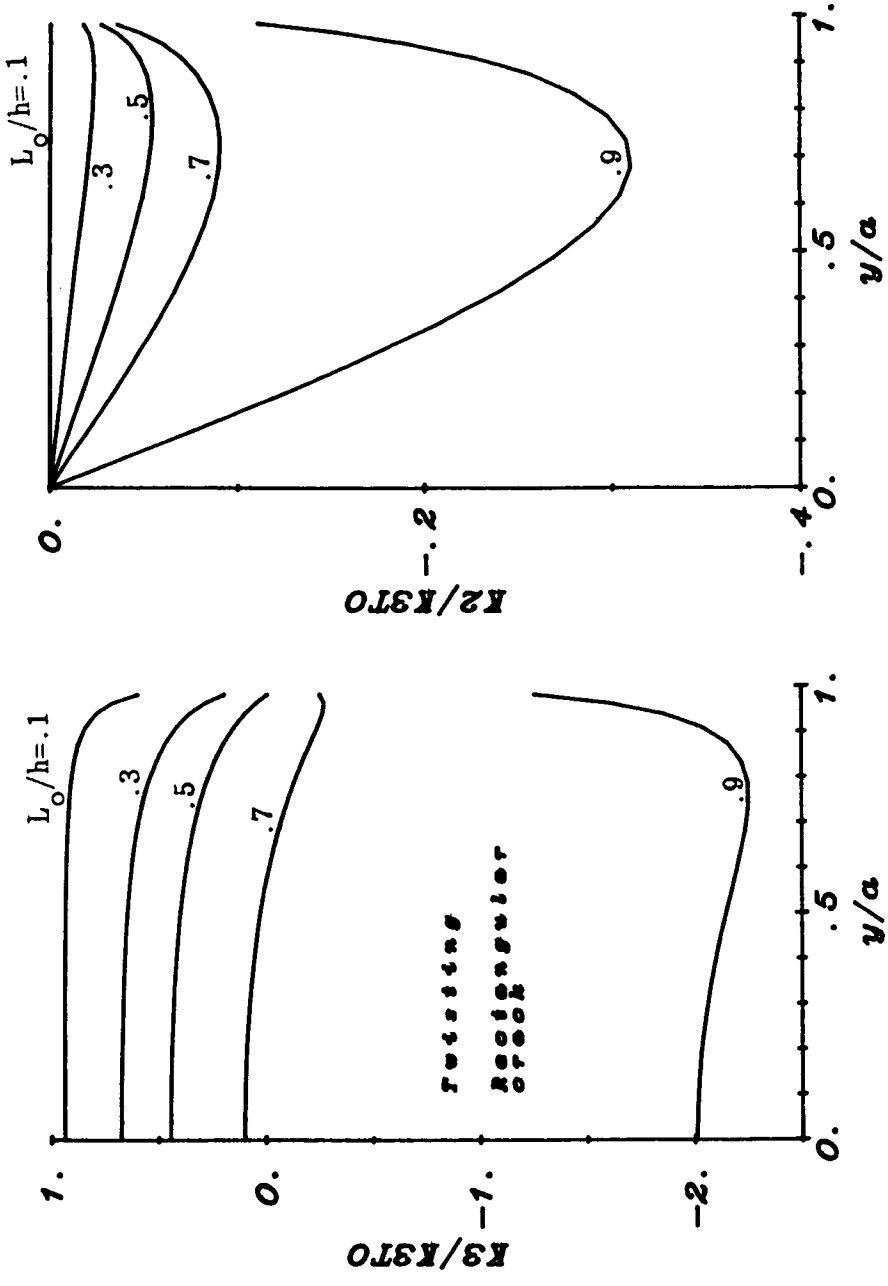

Figure 4.12 Normalized stress intensity factor profiles for the mode 2,3 line-spring model for a rectangular crack subjected to twisting, a/h=1., ν=.3

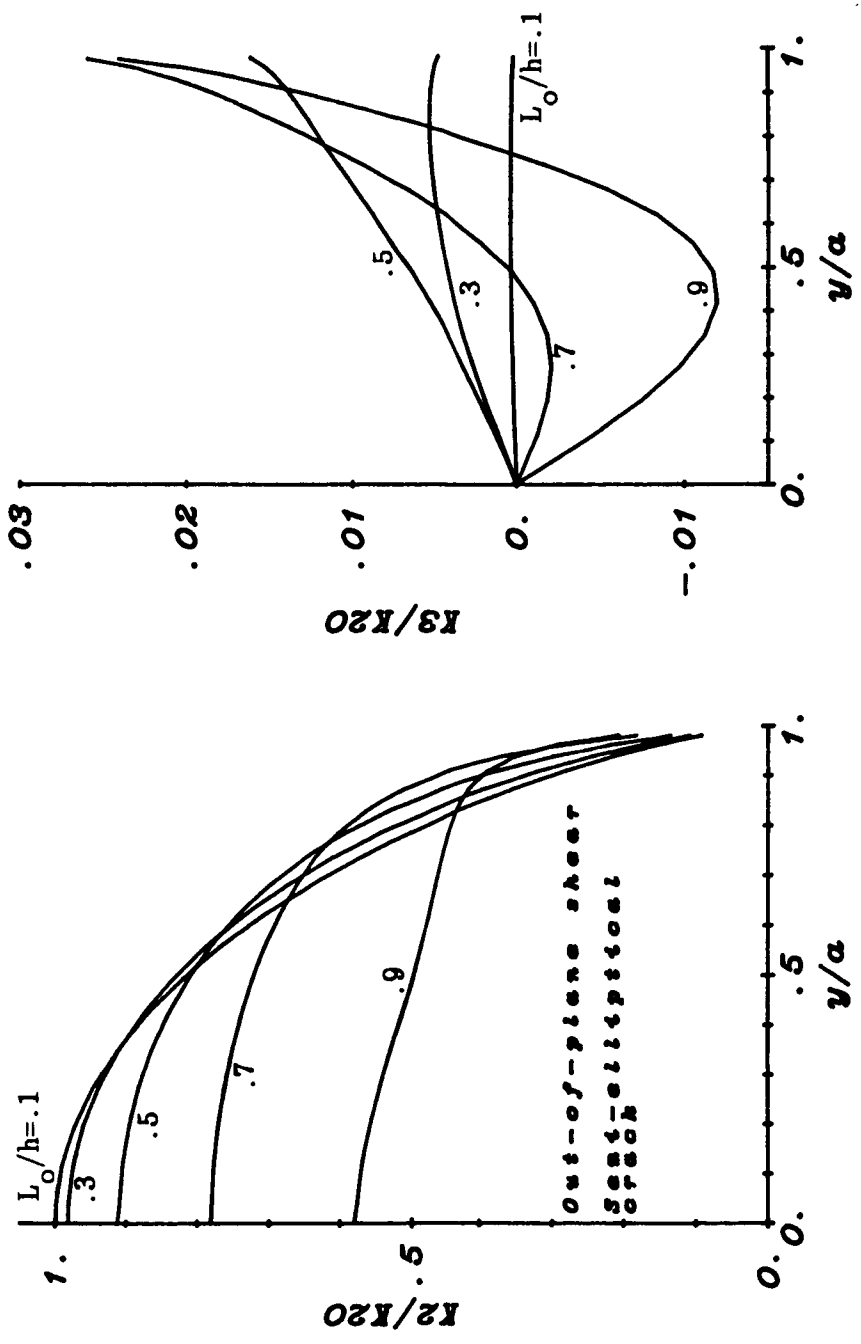

Figure 4.13 Normalized stress intensity factor profiles for the mode 2,3 line-spring model for a semi-elliptical crack subjected to out-of-plane shear, a/h=1., ν=.3

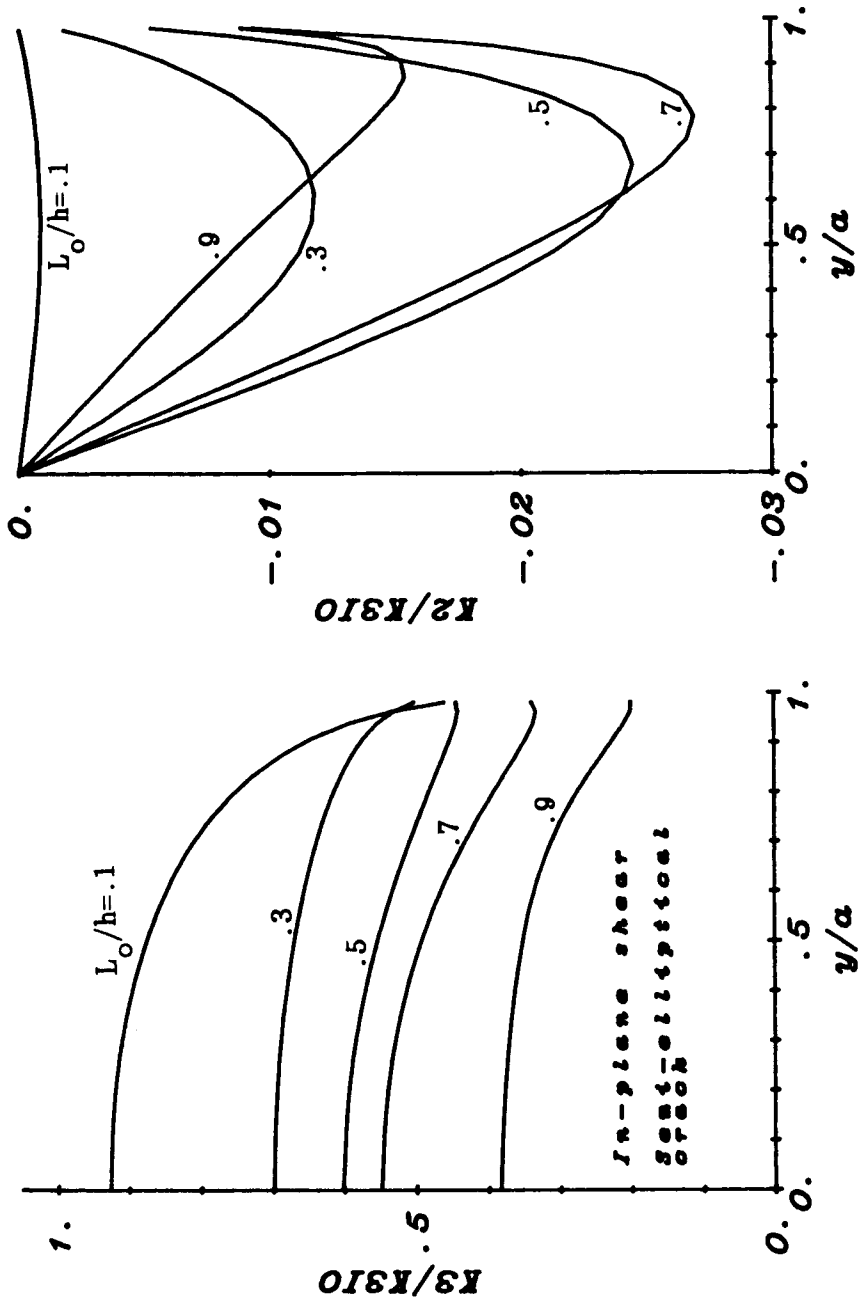

Figure 4.14 Normalized stress intensity factor profiles for the mode 2,3 line-spring model for a semi-elliptical crack subjected to in-plane shear, a/h=1., ν=.3

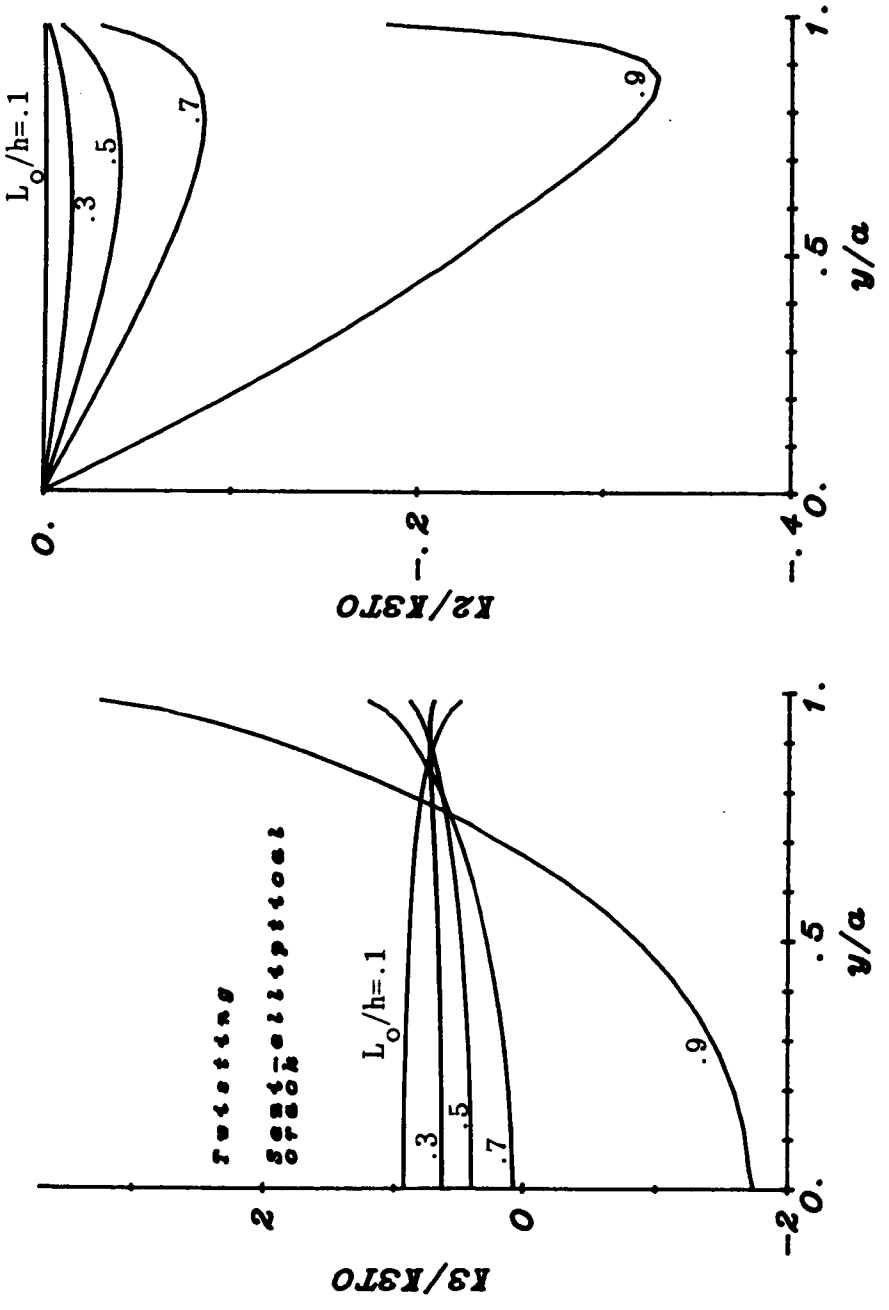

Figure 4.15 Normalized stress intensity factor profiles for the mode 2,3 line-spring model for a semi-elliptical crack subjected to twisting, a/h=1., ν=.3

CHAPTER 5

Through Cracks in Shallow Shells

In this chapter the singular integral equations for a series of collinear cracks in a shallow shell which allows for transverse shear deformations will be derived. The crack will be assumed to lie along a principal line of curvature which uncouples the symmetric (mode 1) from the skew-symmetric (modes 2,3) formulation. The emphasis will be on crack interaction for some common geometries. Also the equations are needed for the part-through crack problem of the next chapter.

5.1 Formulation

The governing equations, both dimensional (Eqns. 5.1a-16a,18a, 19a) and non-dimensional (Eqns. 5.1b-16b,18b,19b) are listed below. The dimensional relationships are defined in Appendix A. From equilibrium,

$$\frac{\partial N_{11}}{\partial x_1} + \frac{\partial N_{12}}{\partial x_2} = 0 \quad , \quad \frac{\partial N_{xx}}{\partial x} + \frac{\partial N_{xy}}{\partial y} = 0 \quad , \tag{5.1a,b}$$

$$\frac{\partial N_{12}}{\partial x_1} + \frac{\partial N_{22}}{\partial x_2} = 0 \quad , \quad \frac{\partial N_{xy}}{\partial x} + \frac{\partial N_{yy}}{\partial y} = 0 \quad , \tag{5.2a,b}$$

$$\frac{\partial V_1}{\partial x_1} + \frac{\partial V_2}{\partial x_2} + \frac{\partial}{\partial x_1}\left(\frac{\partial Z}{\partial x_1}N_{11}\right) + \frac{\partial}{\partial x_1}\left(\frac{\partial Z}{\partial x_2}N_{12}\right)$$

$$+ \frac{\partial}{\partial x_2}\left(\frac{\partial Z}{\partial x_1}N_{12}\right) + \frac{\partial}{\partial x_2}\left(\frac{\partial Z}{\partial x_2}N_{22}\right) + \bar{q}(x_1,x_2) = 0 \quad ,$$

$$\frac{\partial V_x}{\partial x} + \frac{\partial V_y}{\partial y} + \frac{12(1+\nu)}{5}\left\{ \frac{\partial}{\partial x}\left(\frac{\partial Z}{\partial x}N_{xx}\right) + \frac{\partial}{\partial x}\left(\frac{\partial Z}{\partial y}N_{xy}\right) + \right.$$

$$+ \frac{\partial}{\partial y}\left(\frac{\partial Z}{\partial x}N_{xy}\right) + \frac{\partial}{\partial y}\left(\frac{\partial Z}{\partial y}N_{yy}\right) + q(x,y) \Big\} = 0 \quad , \qquad (5.3a,b)$$

$$\frac{\partial M_{11}}{\partial x_1} + \frac{\partial M_{12}}{\partial x_2} - V_1 = 0 \quad ,$$

$$\frac{\partial M_{xx}}{\partial x} + \frac{\partial M_{xy}}{\partial y} - \frac{5}{12(1+\nu)} V_x = 0 \quad , \qquad (5.4a,b)$$

$$\frac{\partial M_{12}}{\partial x_1} + \frac{\partial M_{22}}{\partial x_2} - V_2 = 0 \quad ,$$

$$\frac{\partial M_{xy}}{\partial x} + \frac{\partial M_{yy}}{\partial y} - \frac{5}{12(1+\nu)} V_y = 0 \quad , \qquad (5.5a,b)$$

where $q(x,y)$ is normal loading to the plate surface and $Z(x,y)$ is the equation of the mid-plane of the shell. The other variables are standard shell quantities (see Figs. 2.1,2.3). From kinematical considerations,

$$\epsilon_{11} = \frac{\partial u_{1D}}{\partial x_1} + \frac{\partial Z}{\partial x_1}\frac{\partial u_{3D}}{\partial x_1} \quad , \quad \epsilon_{xx} = \frac{\partial u}{\partial x} + \frac{\partial Z}{\partial x}\frac{\partial w}{\partial x} \quad , \qquad (5.6a,b)$$

$$\epsilon_{22} = \frac{\partial u_{2D}}{\partial x_2} + \frac{\partial Z}{\partial x_2}\frac{\partial u_{3D}}{\partial x_2} \quad , \quad \epsilon_{yy} = \frac{\partial v}{\partial y} + \frac{\partial Z}{\partial y}\frac{\partial w}{\partial y} \quad , \qquad (5.7a,b)$$

$$\epsilon_{12} = \frac{1}{2}\left[\frac{\partial u_{1D}}{\partial x_2} + \frac{\partial u_{2D}}{\partial x_1} + \frac{\partial Z}{\partial x_1}\frac{\partial u_{3D}}{\partial x_2} + \frac{\partial Z}{\partial x_2}\frac{\partial u_{3D}}{\partial x_1}\right] \quad ,$$

$$\epsilon_{xy} = \frac{1}{2}\left[\frac{\partial u}{\partial y} + \frac{\partial v}{\partial x} + \frac{\partial Z}{\partial x}\frac{\partial w}{\partial y} + \frac{\partial Z}{\partial y}\frac{\partial w}{\partial x}\right] \quad , \qquad (5.8a,b)$$

$$\theta_1 = \frac{\partial u_{3D}}{\partial x_1} + \beta_1 \quad , \quad \theta_x = \frac{\partial w}{\partial x} + \beta_x \quad , \qquad (5.9a,b)$$

$$\theta_2 = \frac{\partial u_{3D}}{\partial x_2} + \beta_2 \quad , \quad \theta_y = \frac{\partial w}{\partial y} + \beta_y \quad , \qquad (5.10a,b)$$

where θ_1 and θ_2 are the total rotations of the normals. For classical theory they are zero showing that normals to the shell surface stay normal, i.e. there is no deformation transversely. The constitutive relations (Hooke's law) are,

$$h\epsilon_{11} = \frac{1}{E}\,(N_{11} - \nu N_{22}) \quad , \quad \epsilon_{xx} = N_{xx} - \nu N_{yy} \quad , \tag{5.11a,b}$$

$$h\epsilon_{22} = \frac{1}{E}\,(N_{22} - \nu N_{11}) \quad , \quad \epsilon_{yy} = N_{yy} - \nu N_{xx} \quad , \tag{5.12a,b}$$

$$h\epsilon_{12} = \frac{1}{2\mu}\,N_{12} \quad , \quad \epsilon_{xy} = (1+\nu)N_{xy} \quad , \tag{5.13a,b}$$

where E is Young's modulus and ν is Poisson's ratio. From bending,

$$M_{11} = D\left[\frac{\partial\beta_1}{\partial x_1} + \nu\frac{\partial\beta_2}{\partial x_2}\right] \quad ,$$

$$M_{xx} = \frac{1}{12(1-\nu^2)}\left[\frac{\partial\beta_x}{\partial x} + \nu\frac{\partial\beta_y}{\partial y}\right] \quad , \tag{5.14a,b}$$

$$M_{22} = D\left[\frac{\partial\beta_2}{\partial x_2} + \nu\frac{\partial\beta_1}{\partial x_1}\right] \quad ,$$

$$M_{yy} = \frac{1}{12(1-\nu^2)}\left[\nu\frac{\partial\beta_x}{\partial x} + \frac{\partial\beta_y}{\partial y}\right] \quad , \tag{5.15a,b}$$

$$M_{12} = \frac{D(1-\nu)}{2}\left[\frac{\partial\beta_1}{\partial x_2} + \frac{\partial\beta_2}{\partial x_1}\right] \quad ,$$

$$M_{xy} = \frac{1}{24(1+\nu)}\left[\frac{\partial\beta_x}{\partial y} + \frac{\partial\beta_y}{\partial x}\right] \quad , \tag{5.16a,b}$$

where

$$D = \frac{Eh^3}{12(1-\nu^2)} \quad . \tag{5.17}$$

The linear transverse shear stress-strain relationships are,

$$\theta_1 = \frac{1}{hB} V_1 \quad , \quad \theta_x = V_x \quad , \tag{5.18a,b}$$

$$\theta_2 = \frac{1}{hB} V_2 \quad , \quad \theta_y = V_y \quad , \tag{5.19a,b}$$

where

$$B = \frac{5E}{12(1+\nu)} \quad . \tag{5.20}$$

From here on only non-dimensional variables will be used. Define $\phi(x,y)$ such that

$$N_{xx} = \frac{\partial^2\phi}{\partial y^2} \quad , \quad N_{yy} = \frac{\partial^2\phi}{\partial x^2} \quad , \quad N_{xy} = -\frac{\partial^2\phi}{\partial x\partial y} \quad . \tag{5.21}$$

Introduce the new unknowns $\Omega(x,y)$ and $\psi(x,y)$ defined as follows,

$$\Omega(x,y) = \frac{\partial\beta_x}{\partial y} - \frac{\partial\beta_y}{\partial x} \quad , \tag{5.22}$$

$$\psi(x,y) = \kappa\left[\frac{\partial\beta_x}{\partial x} + \frac{\partial\beta_y}{\partial y}\right] - w(x,y) \quad , \tag{5.23}$$

where

$$\kappa = \frac{1}{5(1-\nu)} \quad . \tag{5.24}$$

Also it will be assumed that $Z(x,y)$ is limited to the following,

$$\frac{\partial^2 Z}{\partial x^2} = \frac{-1}{R_1} \quad , \quad \frac{\partial^2 Z}{\partial y^2} = \frac{-1}{R_2} \quad , \quad \frac{\partial^2 Z}{\partial x\partial y} = \frac{-1}{R_{12}} \quad , \tag{5.25}$$

thus making the curvatures constant. For convenience the following constants are introduced,

$$\lambda_1^4 = 12(1-\nu^2)(h/R_1)^2 \quad , \quad \lambda_2^4 = 12(1-\nu^2)(h/R_2)^2 \quad ,$$

$$\lambda_{12}^4 = 12(1-\nu^2)(h/R_{12})^2 \quad , \quad \lambda^2 = 12(1-\nu^2) \quad , \quad \gamma = \lambda^{-2} \quad . \tag{5.26}$$

If all but λ_1 are zero, an axially cracked cylinder results; if λ_2 is

the only non-zero quantity, then the crack will be circumferential, see Fig. 2.1. R_{12} is needed when the crack does not lie along a principal line of curvature. After some algebra Eqns. 5.1-19 are reduced to the following equations,

$$\nabla^4\phi - \frac{1}{\lambda^2}\left\{ \lambda_1^2\frac{\partial^2}{\partial y^2} - 2\lambda_{12}^2\frac{\partial^2}{\partial x\partial y} + \lambda_2^2\frac{\partial^2}{\partial x^2}\right\} w(x,y) = 0 \quad , \tag{5.27}$$

$$\nabla^4 w + \lambda^2(1-\kappa\nabla^2)\left\{ \lambda_1^2\frac{\partial^2}{\partial y^2} - 2\lambda_{12}^2\frac{\partial^2}{\partial x\partial y} + \lambda_2^2\frac{\partial^2}{\partial x^2}\right\} \phi(x,y) = \lambda^4(1-\kappa\nabla^2)q(x,y) \quad , \tag{5.28}$$

$$\kappa\nabla^2\psi - \psi - w = 0 \quad , \tag{5.29}$$

$$\frac{\kappa(1-\nu)}{2}\nabla^2\Omega - \Omega = 0 \quad . \tag{5.30}$$

Now let $q(x,y) = 0$ and also confine the crack to a principal line of curvature by setting $\lambda_{12} = 0$. This reduces Eqns. 5.27,28 to

$$\nabla^4\phi - \frac{1}{\lambda^2}\left\{ \lambda_1^2\frac{\partial^2}{\partial y^2} + \lambda_2^2\frac{\partial^2}{\partial x^2}\right\} w(x,y) = 0 \quad , \tag{5.31}$$

$$\nabla^4 w + \lambda^2(1-\kappa\nabla^2)\left\{ \lambda_1^2\frac{\partial^2}{\partial y^2} + \lambda_2^2\frac{\partial^2}{\partial x^2}\right\} \phi(x,y) = 0 \quad . \tag{5.32}$$

These last four equations will be solved by using Fourier transforms. First Eqns. 5.31,32 are reduced to one equation in $\phi(x,y)$,

$$\nabla^4\nabla^4\phi + (1-\kappa\nabla^2)\nabla_\lambda^2\nabla_\lambda^2\phi = 0 \quad , \tag{5.33}$$

where

$$\nabla_\lambda^2 = \lambda_1^2\frac{\partial^2}{\partial y^2} + \lambda_2^2\frac{\partial^2}{\partial x^2} \quad . \tag{5.34}$$

The Fourier transform is defined for any function as

$$F(x,y) = \frac{1}{2\pi}\int_{-\infty}^{+\infty}\bar{F}(x,\alpha)\ e^{-iy\alpha}\ d\alpha \quad ,$$

$$\bar{F}(x,\alpha) = \int_{-\infty}^{+\infty}F(x,y)\ e^{iy\alpha}\ dy \quad . \tag{5.35}$$

The transforms of the various operators of Eqn. 5.33 are

$$FT[\ \nabla^2 F\ ] = \frac{d^2\bar{F}}{d^2x} - \alpha^2\bar{F} \quad ,$$

$$FT[\ \nabla^4 F\ ] = \frac{d^4\bar{F}}{d^4x} - 2\alpha^2\frac{d^2\bar{F}}{d^2x} + \alpha^4\bar{F} \quad ,$$

$$FT[\ \nabla^4\nabla^4 F\ ] = \frac{d^8\bar{F}}{d^8x} - 4\alpha^2\frac{d^6\bar{F}}{d^6x} + 6\alpha^4\frac{d^4\bar{F}}{d^4x} - 4\alpha^6\frac{d^2\bar{F}}{d^2x} + \alpha^8\bar{F} \quad ,$$

$$FT[\ \nabla_\lambda^2\nabla_\lambda^2 F\ ] = \lambda_2^4\frac{d^4\bar{F}}{d^4x} - 2\lambda_1^2\lambda_2^2\alpha^2\frac{d^2\bar{F}}{d^2x} + \lambda_1^4\alpha^4\bar{F} \quad ,$$

$$FT[\ \nabla^2\nabla_\lambda^2\nabla_\lambda^2 F\ ] = \lambda_2^4\frac{d^6\bar{F}}{d^6x} - (2\lambda_1^2\lambda_2^2\alpha^2 + \alpha^2\lambda_2^4)\frac{d^4\bar{F}}{d^4x} +$$

$$(\lambda_1^4\alpha^4 + 2\lambda_1^2\lambda_2^2\alpha^4)\frac{d^2\bar{F}}{d^2x} - \alpha^6\lambda_1^4\bar{F} \quad . \tag{5.36}$$

The Fourier transform of Eqn. 5.33 is

$$\frac{d^8\bar{\phi}}{d^8x} - (4\alpha^2 + \kappa\lambda_2^4)\frac{d^6\bar{\phi}}{d^6x} + (6\alpha^4 + \lambda_2^4 + 2\kappa\lambda_1^2\lambda_2^2\alpha^2 + \kappa\lambda_2^4\alpha^2)\frac{d^4\bar{\phi}}{d^4x}$$

$$- (4\alpha^6 + 2\lambda_1^2\lambda_2^2\alpha^2 + \kappa\lambda_1^4\alpha^4 + 2\kappa\lambda_1^2\lambda_2^2\alpha^4)\frac{d^2\bar{\phi}}{d^2x} + (\alpha^8 + \lambda_1^4\alpha^4 + \kappa\alpha^6\lambda_2^4)\bar{\phi} = 0 \quad , \tag{5.37}$$

which has the solution

$$\bar{\phi}(x,\alpha) = \sum_{j=1}^{4}R_j(\alpha)e^{m_j x} \quad , \quad x > 0 \quad ,$$

$$\bar{\phi}(x,\alpha) = \sum_{j=5}^{8} R_j(\alpha) e^{m_j x} \quad , \quad x < 0 \quad , \tag{5.38}$$

where

$$m_j = -(p_j+\alpha^2)^{1/2} \quad , \quad j=1,2,3,4 \quad ,$$

$$m_j = +(p_{j-4}+\alpha^2)^{1/2} \quad , \quad j=5,6,7,8 \quad . \tag{5.39}$$

The roots p_j, $j=1,2,3,4$ are obtained from the solution of the following characteristic equation,

$$p^4 - \kappa\lambda_2^4 p^3 + (2\kappa\lambda_1^2\lambda_2^2\alpha^2 - 2\kappa\lambda_2^4\alpha^2 + \lambda_2^4)p^2 +$$

$$+ (2\kappa\lambda_1^2\lambda_2^2\alpha^2 - \kappa\lambda_2^4\alpha^2 - \kappa\lambda_1^4\alpha^2 + 2\lambda_2^4 - 2\lambda_1^2\lambda_2^2)\alpha^2 p +$$

$$+ (\lambda_2^2 - \lambda_1^2)^2\alpha^4 = 0 \quad . \tag{5.40}$$

This quartic is solved numerically. For large and small α an asymptotic expansion for the roots is given in section J.1 of Appendix J. Since the crack has been assumed to lie on a principal line of curvature, only the portion of the shell for x>0 need be considered. The transformed solutions of the other unknowns appearing in Eqns. 5.29-32 are:

$$\bar{\Omega}(x,\alpha) = A(\alpha)e^{-rx} \quad , \quad x > 0 \quad , \tag{5.41}$$

$$\bar{\psi}(x,\alpha) = \sum_{j=1}^{4} R_j(\alpha)K_j(\alpha)e^{m_j x} \quad , \quad x > 0 \quad , \tag{5.42}$$

$$\bar{w}(x,\alpha) = \sum_{j=1}^{4} R_j(\alpha)K_j(\alpha)(\kappa p_j-1)e^{m_j x} \quad , \quad x > 0 \quad , \tag{5.43}$$

where

$$r = -\left[\alpha^2 + \frac{2}{\kappa(1-\nu)} \right]^{1/2} , \tag{5.44}$$

$$K_j(\alpha) = \frac{p_j^2\lambda^2}{(\kappa p_j - 1)(m_j^2\lambda_2^2 - \lambda_1^2\alpha^2)} . \tag{5.45}$$

The next step is to express the shell quantities in terms of $A(\alpha)$ and $R_j(\alpha)$, $j=1,2,3,4$, which are unknowns in the problem to be determined by boundary conditions as yet unspecified. These expressions are

$$N_{xx} = \frac{-1}{2\pi} \int_{-\infty}^{+\infty} \alpha^2 \sum_{j=1}^{4} R_j(\alpha) e^{m_j x} e^{-i\alpha y} \, d\alpha , \tag{5.46}$$

$$N_{yy} = \frac{1}{2\pi} \int_{-\infty}^{+\infty} \sum_{j=1}^{4} m_j^2 R_j(\alpha) e^{m_j x} e^{-i\alpha y} \, d\alpha , \tag{5.47}$$

$$N_{xy} = \frac{i}{2\pi} \int_{-\infty}^{+\infty} \alpha \sum_{j=1}^{4} m_j R_j(\alpha) e^{m_j x} e^{-i\alpha y} \, d\alpha , \tag{5.48}$$

$$\beta_x = \kappa\frac{1-\nu}{2} \frac{-i}{2\pi} \int_{-\infty}^{+\infty} \alpha A(\alpha) e^{rx} e^{-i\alpha y} d\alpha +$$

$$+ \frac{1}{2\pi} \int_{-\infty}^{+\infty} \sum_{j=1}^{4} m_j K_j R_j(\alpha) e^{m_j x} e^{-i\alpha y} d\alpha , \tag{5.49}$$

$$\beta_y = \kappa\frac{1-\nu}{2} \frac{1}{2\pi} \int_{-\infty}^{+\infty} r A(\alpha) e^{rx} e^{-i\alpha y} d\alpha -$$

$$- \frac{i}{2\pi} \int_{-\infty}^{+\infty} \alpha \sum_{j=1}^{4} K_j R_j(\alpha) e^{m_j x} e^{-i\alpha y} d\alpha , \tag{5.50}$$

$$M_{xx} = \frac{1}{\lambda^4} \frac{1}{2\pi} \int_{-\infty}^{+\infty} \sum_{j=1}^{4} (m_j^2 - \nu\alpha^2) K_j R_j(\alpha) e^{m_j x} e^{-i\alpha y} d\alpha$$

$$- \frac{\kappa(1-\nu)^2}{2\lambda^4} \frac{i}{2\pi} \int_{-\infty}^{+\infty} \alpha r A(\alpha) e^{rx} e^{-i\alpha y} \, d\alpha + \tag{5.51}$$

$$M_{yy} = \frac{1}{\lambda^4}\frac{1}{2\pi}\int_{-\infty}^{+\infty}\sum_{j=1}^{4}(\nu m_j^2-\alpha^2)K_jR_j(\alpha)e^{m_jx}e^{-i\alpha y}d\alpha$$

$$+\frac{\kappa(1-\nu)^2}{2\lambda^4}\frac{i}{2\pi}\int_{-\infty}^{+\infty}\alpha rA(\alpha)e^{rx}e^{-i\alpha y}\,d\alpha + \tag{5.52}$$

$$M_{xy} = \frac{-(1-\nu)}{\lambda^4}\frac{i}{2\pi}\int_{-\infty}^{+\infty}\alpha\sum_{j=1}^{4}m_jK_jR_j(\alpha)e^{m_jx}e^{-i\alpha y}\,d\alpha$$

$$-\frac{\kappa(1-\nu)^2}{4\lambda^4}\frac{1}{2\pi}\int_{-\infty}^{+\infty}(\alpha^2+r^2)A(\alpha)e^{rx}e^{-i\alpha y}\,d\alpha\ , \tag{5.53}$$

$$V_x = \frac{\kappa(1-\nu)}{2}\frac{-i}{2\pi}\int_{-\infty}^{+\infty}\alpha A(\alpha)e^{rx}e^{-i\alpha y}\,d\alpha +$$

$$+\frac{\kappa}{2\pi}\int_{-\infty}^{+\infty}\sum_{j=1}^{4}m_jp_jK_jR_j(\alpha)e^{m_jx}e^{-i\alpha y}\,d\alpha\ , \tag{5.54}$$

$$V_y = \frac{(1-\nu)}{2\lambda^4}\frac{-1}{2\pi}\int_{-\infty}^{+\infty}rA(\alpha)e^{rx}e^{-i\alpha y}\,d\alpha +$$

$$-\frac{1}{\lambda^4}\frac{i}{2\pi}\int_{-\infty}^{+\infty}\alpha\sum_{j=1}^{4}p_jK_jR_j(\alpha)e^{m_jx}e^{-i\alpha y}\,d\alpha\ , \tag{5.55}$$

$$\left.\frac{\partial u}{\partial y}\right|_{x\to 0} = \frac{i}{2\pi}\int_{-\infty}^{+\infty}\frac{1}{\alpha}\left\{(\lambda_2^2/\lambda^2)\sum_{j=1}^{4}R_j(\alpha)[m_jK_j(\kappa p_j-1) - m_j^3]\right\}e^{-i\alpha y}d\alpha \tag{5.56}$$

$$\left.\frac{\partial v}{\partial y}\right|_{x\to 0} = \frac{1}{2\pi}\int_{-\infty}^{+\infty}\sum_{j=1}^{4}m_j^2R_j(\alpha)\ e^{-i\alpha y}\,d\alpha +$$

$$+\ y(\lambda_2/\lambda)^2\frac{-i}{2\pi}\int_{-\infty}^{+\infty}\alpha\sum_{j=1}^{4}R_j(\alpha)K_j(\kappa p_j-1)\ e^{-i\alpha y}\,d\alpha\ , \tag{5.57}$$

$$= \frac{1}{2\pi}\int_{-\infty}^{+\infty}\sum_{j=1}^{4}m_j^2R_j(\alpha)\ e^{-i\alpha y}\,d\alpha + y(\lambda_2/\lambda)^2\left.\frac{\partial w}{\partial y}\right|_{x\to 0}\ . \tag{5.58}$$

5.2 Symmetric Loading, Mode 1

There are currently five unknowns in the problem, $A(\alpha)$, and $R_j(\alpha)$ for $j=1,2,3,4$. The first step is to reduce these to two unknowns by using the symmetry conditions,

$$N_{xy}(0,y) = 0 \quad , \tag{5.59}$$

$$M_{xy}(0,y) = 0 \quad , \tag{5.60}$$

$$V_x(0,y) = 0 \quad . \tag{5.61}$$

Then replace the remaining two unknowns with the crack surface displacements,

$$u_1(y) = u(x_2)/h = u(0^+,x_2)/h \ , \tag{5.62}$$

$$u_2(y) = \beta_x(x_2) = \beta_x(0^+,x_2) \ . \tag{5.63}$$

The equations that relate $u_i(y)$ to the original unknowns are:

$$A(\alpha) = \frac{2}{i\alpha(1-\nu)} \sum_{j=1}^{4} m_j p_j K_j R_j \quad , \tag{5.64}$$

$$\sum_{j=1}^{4} m_j K_j R_j \left\{ \left[\kappa(1-\nu)\alpha^2 + 1\right] p_j - \alpha^2(1-\nu) \right\} = 0 \quad , \tag{5.65}$$

$$\sum_{j=1}^{4} m_j K_j R_j \left\{ \kappa p_j - 1 \right\} = \frac{-1}{\alpha} q_2(\alpha) \quad , \tag{5.66}$$

$$\sum_{j=1}^{4} m_j R_j = 0 \quad , \tag{5.67}$$

$$\sum_{j=1}^{4} m_j R_j \left\{ \lambda_2^2 K_j \frac{\kappa p_j - 1}{\lambda^2} - m_j^2 \right\} = -\alpha q_1(\alpha) \quad , \tag{5.68}$$

where

$$q_k(\alpha) = \alpha\int_{-\infty}^{+\infty} u_k(t)e^{i\alpha t}\,dt \quad , \quad k=1,2 \quad . \tag{5.69}$$

The solution to Eqns. 5.65-68 is

$$R_j(\alpha) = \sum_{k=1}^{2} \frac{\gamma_{kj}q_k}{m_j D(\alpha)} \quad , \quad j=1,2,3,4 \quad , \tag{5.70}$$

where

$$D(\alpha) = (K_1K_2 + K_3K_4)(p_1 - p_2)(p_4 - p_3) +$$

$$+ (K_1K_3 + K_2K_4)(p_1 - p_3)(p_2 - p_4) + (K_2K_3 + K_1K_4)(p_1 - p_4)(p_3 - p_2) \quad , \tag{5.71}$$

$$\gamma_{11} = \alpha\left[K_2K_3(p_3 - p_2) + K_2K_4(p_2 - p_4) + K_3K_4(p_4 - p_3)\right] \quad ,$$

$$\gamma_{12} = -\alpha\left[K_1K_3(p_3 - p_1) + K_1K_4(p_1 - p_4) + K_3K_4(p_4 - p_3)\right] \quad ,$$

$$\gamma_{13} = \alpha\left[K_1K_2(p_2 - p_1) + K_1K_4(p_1 - p_4) + K_2K_4(p_4 - p_2)\right] \quad ,$$

$$\gamma_{14} = -\alpha\left[K_1K_2(p_2 - p_1) + K_1K_3(p_1 - p_3) + K_2K_3(p_3 - p_2)\right] \quad ,$$

$$\gamma_{21} = \frac{-\gamma_{11}\lambda_2^2}{\alpha^2\lambda^2} - \frac{K_2}{\alpha}(p_4 - p_3)\left\{[\kappa(1-\nu)\alpha^2 + 1]p_2 - \alpha^2(1-\nu)\right\} -$$

$$- \frac{K_3}{\alpha}(p_2 - p_4)\left\{[\kappa(1-\nu)\alpha^2 + 1]p_3 - \alpha^2(1-\nu)\right\} -$$

$$- \frac{K_4}{\alpha}(p_3 - p_2)\left\{[\kappa(1-\nu)\alpha^2 + 1]p_4 - \alpha^2(1-\nu)\right\} \quad ,$$

$$\gamma_{22} = \frac{-\gamma_{12}\lambda_2^2}{\alpha^2\lambda^2} + \frac{K_1}{\alpha}(p_4 - p_3)\left\{[\kappa(1-\nu)\alpha^2 + 1]p_1 - \alpha^2(1-\nu)\right\} +$$

$$+ \frac{K_3}{\alpha}(p_1 - p_4)\left\{[\kappa(1-\nu)\alpha^2 + 1]p_3 - \alpha^2(1-\nu)\right\} +$$

$$+ \frac{K_4}{\alpha}(p_3 - p_1)\left\{[\kappa(1-\nu)\alpha^2 + 1]p_4 - \alpha^2(1-\nu)\right\} \quad ,$$

$$\gamma_{23} = \frac{-\gamma_{13}\lambda_2^2}{\alpha^2\lambda^2} - \frac{K_1}{\alpha}(p_4 - p_2)\left\{[\kappa(1-\nu)\alpha^2 + 1]p_1 - \alpha^2(1-\nu)\right\} -$$

$$- \frac{K_2}{\alpha}(p_1 - p_4)\left\{[\kappa(1-\nu)\alpha^2 + 1]p_2 - \alpha^2(1-\nu)\right\} -$$

$$- \frac{K_4}{\alpha}(p_2 - p_1)\left\{[\kappa(1-\nu)\alpha^2 + 1]p_4 - \alpha^2(1-\nu)\right\} \quad ,$$

$$\gamma_{24} = \frac{-\gamma_{14}\lambda_2^2}{\alpha^2\lambda^2} + \frac{K_1}{\alpha}(p_3 - p_2)\left\{[\kappa(1-\nu)\alpha^2 + 1]p_1 - \alpha^2(1-\nu)\right\} +$$

$$+ \frac{K_2}{\alpha}(p_1 - p_3)\left\{[\kappa(1-\nu)\alpha^2 + 1]p_2 - \alpha^2(1-\nu)\right\} +$$

$$+ \frac{K_3}{\alpha}(p_2 - p_1)\left\{[\kappa(1-\nu)\alpha^2 + 1]p_3 - \alpha^2(1-\nu)\right\} \quad . \tag{5.72}$$

The following two mixed boundary conditions will produce two singular integral equations for the determination of the crack opening displacements:

$$N_{xx}(0^+,y) = -f_1(y) \quad , \quad y \text{ in } L_n \quad , \tag{5.73}$$

$$u_1(y) = u(0^+,x_2)/h = 0 \quad , \quad y \text{ outside of } L_n \quad , \tag{5.74}$$

$$M_{xx}(0^+,y) = -f_2(y) \quad , \quad y \text{ in } L_n \quad , \tag{5.75}$$

$$u_2(y) = \beta_x(0^+,x_2) = 0 \quad , \quad y \text{ outside of } L_n \quad , \tag{5.76}$$

where

$$L_n = (a_1,b_1),\ (a_2,b_2),\ \ldots\ ,\ (a_n,b_n) \quad , \tag{5.77}$$

each section (a_i, b_i), defining a crack on x=0. Eqns. 5.73,75 with 46,51,64 for y in L_n become,

$$-f_1(y) = \frac{-1}{2\pi} \lim_{x\to 0} \int_{-\infty}^{+\infty} \alpha^2 \sum_{j=1}^{4} R_j e^{m_j x} e^{-i\alpha y} \, d\alpha \quad , \tag{5.78}$$

$$\frac{-\lambda^4}{1-\nu} f_2(y) = \frac{1+\nu}{2\pi} \lim_{x\to 0} \int_{-\infty}^{+\infty} \Big\{ -\kappa r e^{rx} \sum_{j=1}^{4} m_j p_j K_j R_j +$$

$$+ \frac{1}{1-\nu} \sum_{j=1}^{4} p_j K_j R_j e^{m_j x} + \alpha^2 \sum_{j=1}^{4} K_j R_j e^{m_j x} \Big\} e^{-i\alpha y} \, d\alpha \quad . \tag{5.79}$$

After making use of the odd/even nature of the infinite integrals, Eqns. 5.78,79 may be written as follows,

$$-f_1(y) = -\frac{1}{\pi} \lim_{x\to 0} \int_{0}^{+\infty} \alpha^2 \sum_{j=1}^{4} R_j e^{m_j x} \cos\alpha(t-y) \, d\alpha \quad , \tag{5.80}$$

$$\frac{-\lambda^4}{1-\nu} f_2(y) = \frac{1+\nu}{\pi} \lim_{x\to 0} \int_{0}^{+\infty} \Big\{ -\kappa r e^{rx} \sum_{j=1}^{4} m_j p_j K_j R_j +$$

$$+ \frac{1}{1-\nu} \sum_{j=1}^{4} p_j K_j R_j e^{m_j x} + \alpha^2 \sum_{j=1}^{4} K_j R_j e^{m_j x} \Big\} \cos\alpha(t-y) \, d\alpha \quad . \tag{5.81}$$

Next Eqns. 5.69,70,74,76 are substituted into Eqns. 5.80,81 to obtain

$$-f_1(y) = -\frac{1}{\pi} \lim_{x\to 0} \int_{L_n} \sum_{k=1}^{2} u_k(t) \int_{0}^{+\infty} \frac{\alpha^3}{D(\alpha)} \sum_{j=1}^{4} \frac{\gamma_{kj}}{m_j} e^{m_j x} \cos\alpha(t-y) \, d\alpha \, dt + \tag{5.82}$$

$$\frac{-\lambda^4}{1-\nu} f_2(y) = \frac{1+\nu}{\pi} \lim_{x\to 0} \int_{L_n} \sum_{k=1}^{2} u_k(t) \int_{0}^{+\infty} \frac{\alpha}{D(\alpha)} \sum_{j=1}^{4} \frac{\gamma_{kj}}{m_j} K_j \Big\{ -\kappa r m_j p_j e^{rx} +$$

$$+ \frac{1}{1-\nu} (m_j^2 - \nu\alpha^2) e^{m_j x} \Big\} \cos\alpha(t-y) \, d\alpha \, dt \quad . \tag{5.83}$$

The infinite integrals must now be analyzed. These integrals may not exist without the exponential decay in x. In the limit as x gets

small, the leading order term at α approaching infinity provides the integral that must be interpreted in the finite-part sense or perhaps in the Cauchy principal value sense, see Appendix B. Also the large α behavior must be determined so that the infinite integrals will numerically converge. The more terms that are known, the more accurate/less expensive the numerical integration. This analysis is presented in section J.2 of Appendix J. The form of the equations after using these results is,

$$
\begin{aligned}
-f_1(y) = {} & \frac{1}{2\pi} \oint_{L_n} \frac{u_1(t)}{(t-y)^2}\, dt + \\
& + \beta_1^{11} \frac{1}{\pi} \int_{L_n} \ln|t-y| u_1(t) dt + \beta_1^{12} \frac{1}{\pi} \int_{L_n} \ln|t-y| u_2(t) dt + \\
& - \frac{1}{\pi} \int_{L_n} u_1(t) \int_0^A \left\{ \frac{\alpha^3}{D(\alpha)} \sum_{j=1}^{4} \frac{\gamma_{1j}}{m_j} - \frac{\alpha}{2} \right\} \cos\alpha(t-y)\, d\alpha\, dt + \\
& - \frac{1}{\pi} \int_{L_n} u_2(t) \int_0^A \frac{\alpha^3}{D(\alpha)} \sum_{j=1}^{4} \frac{\gamma_{2j}}{m_j} \cos\alpha(t-y)\, d\alpha\, dt + \\
& - \frac{1}{\pi} \int_{L_n} u_1(t)\, \bar{I}_{11}(t,y)\, dt - \frac{1}{\pi} \int_{L_n} u_2(t)\, \bar{I}_{12}(t,y)\, dt \quad , \qquad (5.84)
\end{aligned}
$$

$$
\begin{aligned}
\frac{-\lambda^4}{1-\nu} f_2(y) = {} & \frac{1+\nu}{2\pi} \oint_{L_n} \frac{u_2(t)}{(t-y)^2}\, dt + \\
& - \beta_1^{21} \frac{1}{\pi} \int_{L_n} \ln|t-y| u_1(t) dt - \beta_1^{22} \frac{1}{\pi} \int_{L_n} \ln|t-y| u_2(t) dt + \\
& + \frac{1}{\pi} \int_{L_n} u_1(t) \int_0^A \frac{\alpha}{D(\alpha)} \sum_{j=1}^{4} \frac{\gamma_{1j}}{m_j} K_j \left\{ -\kappa r m_j p_j + \right.
\end{aligned}
$$

$$+ \frac{1}{1-\nu} (m_j^2 - \nu\alpha^2) \Big\} \cos\alpha(t-y) \, d\alpha \, dt +$$

$$+ \frac{1}{\pi} \int_{L_n} u_2(t) \int_0^A \Big[\frac{\alpha}{D(\alpha)} \sum_{j=1}^{4} \frac{\gamma_{2j}}{m_j} K_j \Big\{ -\kappa r m_j p_j +$$

$$+ \frac{1}{1-\nu} (m_j^2 - \nu\alpha^2) \Big\} + \frac{(1+\nu)\alpha}{2} \Big] \cos\alpha(t-y) \, d\alpha \, dt +$$

$$+ \frac{1}{\pi} \int_{L_n} u_1(t) \, \bar{I}_{21}(t,y) \, dt + \frac{1}{\pi} \int_{L_n} u_2(t) \, \bar{I}_{22}(t,y) \, dt \quad . \qquad (5.85)$$

All quantities not defined in this chapter are given in Appendix J.

5.3 Symmetric Loading, Mode 1, results.

As mentioned at the start of this chapter, the primary motivation for this analysis is to study the effect of shell curvature on crack interaction as seen through the SIFs. This problem has been considered by Erdogan and Ratwani [73], by using the classical shell theory. As with the single crack solution, the theory used here that includes transverse shear deformations is better suited for this problem.

The results presented in Figs. 5.1-4, show the effect of cylinder radius on the stresses ahead of a single crack (both axial, Figs. 5.1,2, and circumferential, Figs. 5.3,4) of length a/h=1 subjected to crack surface tension and bending loads. It is observed that although the primary stresses are not considerably different from those of the plate solution ($R/h \to \infty$), the secondary values are now non-zero and increase with decreasing radius. These effects would be magnified for larger a/h. The results for axial cracks seem to be more sensitive to

curvature in tension than for the circumferential crack and the reverse is true for bending.

The out-of-plane displacement $w(0^+,y)$, or bulging of a single crack has been examined in [28], and has been used as an interpretation for the trends observed in the crack interaction problem [73]. In Fig. 5.5 the tension and bending results for an axially cracked cylinder with radius R/h=10 are presented for various crack lengths. Fig. 5.6 gives the results for a circumferential crack. In these plots the zero is fixed at y/a=0 in the deformed state. Again it is observed that the axial crack has more complicated behavior in tension, while the circumferential orientation shows a similar trend in bending. For these loadings the w displacement in the region ahead of the crack tip has more of a tendency to become negative.

The symmetric double crack SIF solutions are presented in tables 5.1-8. The geometries are again the axially cracked cylinder, a/h=1 in 5.1 (tension) and 5.2 (bending), a/h=2 in 5.3 (tension) and 5.4 (bending), and the circumferentially cracked cylinder where these four cases are repeated in tables 5.5-8. For both geometries the primary stress intensity factor increases for decreasing radius in tension, and decreases for decreasing radius in bending. Again the axial crack is more sensitive to curvature than the circumferential crack in tension and the circumferential crack is similarly more sensitive to curvature in bending. The secondary SIFs decrease with increasing cylinder radius except for the outer crack tip of the circumferential crack, a/h=2 loaded in tension presented in Fig. 5.7. Also the

secondary values have fluctuations for increasing separation. This type of behavior was not observed with the primary SIFs as it was by Erdogan and Ratwani [73]. It is possible that for larger a/h the curvature effect is strong enough that there can be regions of increase of the SIFs as the cracks get farther apart. The shortest crack for which this trend was observed in Ref. [73] was a/h=2.5 for R/h=5. Because of convergence difficulties and the shallow shell assumption, longer cracks were not investigated.

5.4 Skew-Symmetric Loading, Modes 2,3

There are currently five unknowns in the problem, $A(\alpha)$, and $R_j(\alpha)$ for j=1,2,3,4. The first step is to reduce this to three unknowns by using the symmetry conditions,

$$N_{xx}(0,y) = 0 \quad , \tag{5.86}$$

$$M_{xx}(0,y) = 0 \quad . \tag{5.87}$$

Then replace the remaining unknowns with the crack surface displacements,

$$g_3(y) = u_3(y) = w(x_2)/h = w(0^+,x_2)/h \ , \tag{5.88}$$

$$g_4(y) = u_4(y)-(\lambda_2/\lambda)^2 y u_3(y) = v(x_2)/h-(\lambda_2/\lambda)^2 x_2 w(x_2)/h^2 \ ,$$

$$= v(0^+,x_2)/h-(\lambda_2/\lambda)^2 x_2 w(0^+,x_2)/h^2, \tag{5.89}$$

$$u_4(y) = v(x_2) = g_4(y) + (\lambda_2/\lambda)^2 y g_3(y) \quad , \tag{5.90}$$

$$g_5(y) = u_5(y) = \beta_y(x_2) = \beta_y(0^+,x_2) \ , \tag{5.91}$$

where $u_i(y)$ are the crack opening displacements and $g_i(y)$ are the

unknowns to be used. The in-plane displacement component, i=4, determines this, see Eqns. 5.57,58. If u_4 were used as an unknown the resulting matrix would not be diagonally dominant and there may be numerical problems. The equations that relate $g_i(y)$ to the original unknowns are:

$$A(\alpha) = \frac{2}{i\alpha\kappa(1-\nu)^2 r} \sum_{j=1}^{4} (m_j^2-\nu\alpha^2)K_jR_j \quad , \tag{5.92}$$

$$\frac{1}{1-\nu}\sum_{j=1}^{4} p_jK_jR_j = q_5(\alpha) \quad , \tag{5.93}$$

$$\sum_{j=1}^{4} R_j = 0 \quad , \tag{5.94}$$

$$\sum_{j=1}^{4} m_j^2R_j = q_4(\alpha) \quad , \tag{5.95}$$

$$\sum_{j=1}^{4} R_jK_j(\kappa p_j-1) = \frac{i}{\alpha}q_3(\alpha) \quad , \tag{5.96}$$

where

$$q_k(\alpha) = -i\alpha\int_{-\infty}^{+\infty} g_k(t)\alpha e^{i\alpha t}\, dt \quad , \quad k=3,4,5 \quad . \tag{5.97}$$

The solution to Eqns. 5.93-96 is

$$R_j(\alpha) = \sum_{k=3}^{5} \frac{\gamma_{kj}q_k}{D(\alpha)} \quad , \quad j=1,2,3,4 \quad , \tag{5.98}$$

where $D(\alpha)$ is the same as Eqn. 5.71 and γ_{kj} are as follows:

$$\gamma_{31} = \frac{-i}{\alpha}\left\{K_3p_3(p_4-p_2) + K_4p_4(p_2-p_3) + K_2p_2(p_3-p_4)\right\} \quad ,$$

$$\gamma_{32} = \frac{i}{\alpha}\left\{K_3p_3(p_4-p_1) + K_4p_4(p_1-p_3) + K_1p_1(p_3-p_4)\right\} \quad ,$$

$$\gamma_{33} = \frac{-i}{\alpha}\left\{K_2p_2(p_4-p_1) + K_4p_4(p_1-p_2) + K_1p_1(p_2-p_4)\right\} ,$$

$$\gamma_{34} = \frac{i}{\alpha}\left\{K_2p_2(p_3-p_1) + K_3p_3(p_1-p_2) + K_1p_1(p_2-p_3)\right\} ,$$

$$\gamma_{41} = \left\{K_3K_4(p_4-p_3) + K_2K_4(p_2-p_4) + K_2K_3(p_3-p_2)\right\} ,$$

$$\gamma_{42} = -\left\{K_3K_4(p_4-p_3) + K_1K_4(p_1-p_4) + K_1K_3(p_3-p_1)\right\} ,$$

$$\gamma_{43} = \left\{K_4K_2(p_4-p_2) + K_1K_4(p_1-p_4) + K_2K_1(p_2-p_1)\right\} ,$$

$$\gamma_{44} = -\left\{K_3K_2(p_3-p_2) + K_1K_3(p_1-p_3) + K_2K_1(p_2-p_1)\right\} ,$$

$$\gamma_{51} = -(1-\nu)\left\{K_4(\kappa p_4-1)(p_3-p_2)+K_3(\kappa p_3-1)(p_2-p_4)+K_2(\kappa p_2-1)(p_4-p_3)\right\},$$

$$\gamma_{52} = (1-\nu)\left\{K_4(\kappa p_4-1)(p_3-p_1)+K_3(\kappa p_3-1)(p_1-p_4)+K_1(\kappa p_1-1)(p_4-p_3)\right\},$$

$$\gamma_{53} = -(1-\nu)\left\{K_4(\kappa p_4-1)(p_2-p_1)+K_2(\kappa p_2-1)(p_1-p_4)+K_1(\kappa p_1-1)(p_4-p_2)\right\},$$

$$\gamma_{54} = (1-\nu)\left\{K_3(\kappa p_3-1)(p_2-p_1)+K_2(\kappa p_2-1)(p_1-p_3)+K_1(\kappa p_1-1)(p_3-p_2)\right\} .$$

(5.99)

The following mixed boundary conditions will produce three singular integral equations for the determination of the crack opening displacements:

$$V_x(0^+,y) = -f_3(y) \quad , \quad y \text{ in } L_n \quad , \tag{5.100}$$

$$g_3(y) = w(0^+,y) = 0 \quad , \quad y \text{ outside of } L_n \quad , \tag{5.101}$$

$$N_{xx}(0^+,y) = -f_4(y) \quad , \quad y \text{ in } L_n \quad , \tag{5.102}$$

$$g_4(y)=v(0^+,y)-(\lambda_2^2/\lambda)^2 yw(0^+,y) = 0 \quad , \quad y \text{ outside of } L_n \quad , \tag{5.103}$$

C-3

$$M_{xy}(0^+,y) = -f_5(y) \quad , \quad y \text{ in } L_n \quad , \tag{5.104}$$

$$g_5(y) = \beta_y(0^+,y) = 0 \quad , \quad y \text{ outside of } L_n \quad . \tag{5.105}$$

See Eqn. 5.77 for the definition of L_n. Eqns. 5.100,102,104 with 5.48,53,54,92 become:

$$-f_3(y) = \frac{1}{2\pi} \lim_{x\to 0} \int_{-\infty}^{+\infty} \left\{ \frac{-1}{r(1-\nu)} \sum_{j=1}^{4} (m_j^2 - \nu\alpha^2) K_j R_j e^{rx} + \right.$$

$$\left. + \kappa \sum_{j=1}^{4} m_j p_j K_j R_j(\alpha) e^{m_j x} \right\} e^{-i\alpha y} \, d\alpha \quad , \tag{5.106}$$

$$-f_4(y) = \frac{i}{2\pi} \lim_{x\to 0} \int_{-\infty}^{+\infty} \alpha \sum_{j=1}^{4} m_j R_j(\alpha) e^{m_j x} e^{-i\alpha y} \, d\alpha \quad , \tag{5.107}$$

$$-\frac{2\lambda^4}{1-\nu} f_5(y) = \frac{1+\nu}{2\pi} \lim_{x\to 0} \int_{-\infty}^{+\infty} \left\{ \sum_{j=1}^{4} K_j R_j \left[\frac{-e^{rx}(\alpha^2+r^2)}{i\alpha r(1-\nu)} (m_j^2 - \nu\alpha^2) - \right.\right.$$

$$\left.\left. - 2i\alpha m_j e^{\bar{m}_j x} \right] \right\} e^{-i\alpha y} \, d\alpha \quad . \tag{5.108}$$

After asymptotic analysis, see section J.3 of Appendix J, these three equations may be expressed as,

$$-f_3(y) = \frac{1}{\pi} \fint_{L_n} \frac{g_3(t)}{(t-y)^2} \, dt + \kappa\lambda^2 \left[\frac{1}{8}(\lambda_2^2 - \lambda_1^2) - \frac{1}{2}\lambda_2^2 \right] \frac{1}{\pi} \fint_{L_n} \frac{g_4(t)}{t-y} \, dt +$$

$$- \left(\beta_1^{33} + (\lambda_2/\lambda)^2 \beta_0^{34} \right) \frac{1}{\pi} \int_{L_n} \ln|t-y| g_3(t) dt +$$

$$+ \frac{1}{\pi} \int_{L_n} g_3(t) \int_0^A \left\{ \frac{-1}{D(\alpha)} \sum_{j=1}^{4} K_j \left[i\alpha\gamma_{3j} - (\lambda_2/\lambda)^2 \gamma_{4j} \right] \times \right.$$

$$\left. \times \left[\frac{-(m_j^2 - \nu\alpha^2)}{r(1-\nu)} + \kappa m_j p_j \right] + \alpha \right\} \cos\alpha(t-y) \, d\alpha \, dt +$$

$$+ \frac{1}{\pi} \int_{L_n} g_4(t) \int_0^A \left\{ \frac{\alpha}{D(\alpha)} \sum_{j=1}^{4} K_j \gamma_{4j} \left[\frac{-(m_j^2 - \nu\alpha^2)}{r(1-\nu)} + \kappa m_j p_j \right] - \right.$$

$$\left. - \kappa\lambda^2 \left[\frac{1}{8}(\lambda_2^2 - \lambda_1^2) - \frac{1}{2}\lambda_2^2 \right] \right\} \sin\alpha(t-y)\, d\alpha\, dt +$$

$$+ \frac{1}{\pi} \int_{L_n} g_5(t) \int_0^A \frac{\alpha}{D(\alpha)} \sum_{j=1}^{4} K_j \gamma_{5j} \left[\frac{-(m_j^2 - \nu\alpha^2)}{r(1-\nu)} + \kappa m_j p_j \right] \sin\alpha(t-y)\, d\alpha\, dt +$$

$$+ \frac{1}{\pi} \int_{L_n} g_3(t)\, \bar{I}_{33}(t,y)\, dt + \frac{1}{\pi} \int_{L_n} g_4(t)\, \bar{I}_{34}(t,y)\, dt +$$

$$+ \frac{1}{\pi} \int_{L_n} g_5(t)\, \bar{I}_{35}(t,y)\, dt \quad , \tag{5.109}$$

$$-f_4(y) = \frac{1}{2\pi} \fint_{L_n} \frac{g_4(t)}{(t-y)^2}\, dt + \left[\frac{3\lambda_2^2 + \lambda_1^2}{8\lambda^2} \right] \frac{1}{\pi} \fint_{L_n} \frac{g_3(t)}{t-y}\, dt +$$

$$- \beta_1^{44} \frac{1}{\pi} \int_{L_n} \ln|t-y| g_4(t) dt - \beta_1^{45} \frac{1}{\pi} \int_{L_n} \ln|t-y| g_5(t) dt +$$

$$+ \frac{1}{\pi} \int_{L_n} g_3(t) \int_0^A \left\{ \frac{\alpha}{D} \sum_{j=1}^{4} m_j \left[i\alpha\gamma_{3j} - (\lambda_2/\lambda)^2 \gamma_{4j} \right] - \left[\frac{3\lambda_2^2 + \lambda_1^2}{8\lambda^2} \right] \right\} \sin\alpha(t-y)\, d\alpha\, dt +$$

$$+ \frac{1}{\pi} \int_{L_n} g_4(t) \int_0^A \left\{ \frac{\alpha^2}{D(\alpha)} \sum_{j=1}^{4} m_j \gamma_{4j} + \frac{\alpha}{2} \right\} \cos\alpha(t-y)\, d\alpha\, dt +$$

$$+ \frac{1}{\pi} \int_{L_n} g_5(t) \int_0^A \frac{\alpha^2}{D(\alpha)} \sum_{j=1}^{4} m_j \gamma_{5j} \cos\alpha(t-y)\, d\alpha\, dt +$$

$$+ \frac{1}{\pi} \int_{L_n} g_3(t)\, \bar{I}_{43}(t,y)\, dt + \frac{1}{\pi} \int_{L_n} g_4(t)\, \bar{I}_{44}(t,y)\, dt +$$

$$+ \frac{1}{\pi} \int_{L_n} g_5(t)\, \bar{I}_{45}(t,y)\, dt \quad , \tag{5.110}$$

$$
\begin{aligned}
-\frac{2\lambda^4}{1-\nu}f_5(y) &= \frac{1+\nu}{\pi}\fint_{L_n}\frac{g_5(t)}{(t-y)^2}\,dt + \\
&- \beta_1^{54}\frac{1}{\pi}\int_{L_n}\ln|t-y|g_4(t)dt - \beta_1^{55}\frac{1}{\pi}\int_{L_n}\ln|t-y|g_5(t)dt + \\
&+ \frac{1}{\pi}\int_{L_n} g_3(t)\int_0^A\Big\{\frac{1}{D}\sum_{j=1}^{4}K_j\Big[i\alpha\gamma_{3j}-(\lambda_2/\lambda)^2\gamma_{4j}\Big]\times \\
&\qquad \times\Big[\frac{\alpha^2+r^2}{\alpha r(1-\nu)}(m_j^2-\nu\alpha^2)-2\alpha m_j\Big]\Big\}\sin\alpha(t-y)\,d\alpha\,dt + \\
&+ \frac{1}{\pi}\int_{L_n} g_4(t)\int_0^A\frac{\alpha}{D}\sum_{j=1}^{4}K_j\gamma_{4j}\Big[\frac{\alpha^2+r^2}{\alpha r(1-\nu)}(m_j^2-\nu\alpha^2)-2\alpha m_j\Big]\cos\alpha(t-y)\,d\alpha\,dt + \\
&+ \frac{1}{\pi}\int_{L_n} g_5(t)\int_0^A\Big\{\frac{\alpha}{D(\alpha)}\sum_{j=1}^{4}K_j\gamma_{5j}\Big[\frac{\alpha^2+r^2}{\alpha r(1-\nu)}(m_j^2-\nu\alpha^2)-2\alpha m_j\Big] + \\
&\qquad + \alpha(1+\nu)\Big\}\cos\alpha(t-y)\,d\alpha\,dt + \\
&+ \frac{1}{\pi}\int_{L_n} g_3(t)\,\bar{I}_{53}(t,y)\,dt + \frac{1}{\pi}\int_{L_n} g_4(t)\,\bar{I}_{54}(t,y)\,dt + \\
&+ \frac{1}{\pi}\int_{L_n} g_5(t)\,\bar{I}_{55}(t,y)\,dt \quad , \qquad (5.111)
\end{aligned}
$$

5.5 Skew-Symmetric Loading, Mode 2 and 3, results.

The results for the interaction of two equal length (a/h=1) cracks in a cylinder are presented in tables 5.9-11 (axial) and 5.12-14 (circumferential). The three possible loadings, in-plane shear, twisting, and out-of-plane shear are included. The effect of curvature is not as strong as for the symmetric problem of Sec. 5.3.

Also the difference between the axial and the circumferential crack is minimal, especially for twisting, see tables 5.10,13. Both primary and secondary values of the SIFs change very little. The only trends that can be observed with respect to curvature are the mode 3 component of the SIF for in-plane shear loading is greater for the circumferential crack, see tables 5.9,12, and for out-of-plane shear there is a notable difference in the in-plane shear component of the SIF, again greater for the circumferential crack, 5.11,14.

Table 5.1 Mode 1 normalized stress intensity factors for symmetric collinear axial cracks in a cylinder of radius R/h subjected to membrane loading. The inner and outer crack tips are located at $y/a=\pm b$, $\pm c$ respectively where $a/h=(c-b)/(2h)=1$, $\sigma_1=N_x/h$, $\nu=.3$, $M\to N_x$, $B\to M_x$.

MEMBRANE LOADING

	R/h \ b/a	0.05	0.125	0.25	0.5	1	$\to\infty$
$\frac{k_M(b)}{\sigma_1\sqrt{a}}$	5	2.074	1.634	1.431	1.318	1.265	1.158
	10	1.889	1.489	1.299	1.188	1.139	1.081
	20	1.825	1.439	1.252	1.139	1.082	1.041
	50	1.802	1.420	1.234	1.118	1.056	1.016
	$\to\infty$	1.795	1.414	1.229	1.112	1.048	1.000
$\frac{k_M(c)}{\sigma_1\sqrt{a}}$	5	1.392	1.341	1.304	1.274	1.244	1.158
	10	1.241	1.199	1.169	1.144	1.128	1.081
	20	1.182	1.143	1.113	1.087	1.069	1.041
	50	1.158	1.119	1.089	1.060	1.039	1.016
	$\to\infty$	1.115	1.112	1.081	1.052	1.028	1.000
$\frac{k_B(b)}{\sigma_1\sqrt{a}}$	5	.248	.169	.124	.093	.084	.103
	10	.192	.136	.103	.076	.060	.071
	20	.139	.100	.077	.058	.045	.046
	50	.081	.060	.047	.037	.028	.025
	$\to\infty$	.000	.000	.000	.000	.000	.000
$\frac{k_B(c)}{\sigma_1\sqrt{a}}$	5	.106	.096	.089	.087	.093	.103
	10	.087	.076	.068	.061	.059	.071
	20	.068	.059	.052	.045	.040	.046
	50	.043	.038	.033	.029	.025	.025
	$\to\infty$	.000	.000	.000	.000	.000	.000

Table 5.2 Mode 1 normalized stress intensity factors for symmetric collinear axial cracks in a cylinder of radius R/h subjected to bending. The inner and outer crack tips are located at $y/a=\pm b$, $\pm c$ respectively where $a/h=(c-b)/(2h)=1$, $\sigma_2=6M_x/h^2$, $\nu=.3$, $M\to N_x$, $B\to M_x$.

BENDING

	R/h \ b/a	0.05	0.125	0.25	0.5	1	$\to\infty$
$\frac{k_B(b)}{\sigma_2\sqrt{a}}$	5	1.205	1.006	.902	.824	.771	.725
	10	1.240	1.033	.924	.841	.783	.735
	20	1.262	1.051	.939	.853	.791	.740
	50	1.279	1.064	.950	.862	.798	.745
	$\to\infty$	1.294	1.076	.960	.870	.805	.747
$\frac{k_B(c)}{\sigma_2\sqrt{a}}$	5	.828	.809	.790	.770	.751	.725
	10	.847	.825	.804	.781	.761	.735
	20	.860	.837	.815	.790	.768	.740
	50	.870	.846	.823	.797	.774	.747
	$\to\infty$	.880	.855	.831	.805	.780	.747
$\frac{k_M(b)}{\sigma_2\sqrt{a}}$	5	.089	.069	.060	.055	.049	.033
	10	.048	.038	.033	.031	.030	.022
	20	.025	.020	.018	.017	.018	.014
	50	.011	.008	.008	.007	.008	.007
	$\to\infty$	.000	.000	.000	.000	.000	.000
$\frac{k_M(c)}{\sigma_2\sqrt{a}}$	5	.063	.059	.055	.051	.045	.033
	10	.036	.034	.033	.031	.030	.022
	20	.020	.019	.018	.018	.018	.014
	50	.009	.008	.008	.008	.008	.007
	$\to\infty$	.000	.000	.000	.000	.000	.000

Table 5.3 Mode 1 normalized stress intensity factors for symmetric collinear axial cracks in a cylinder of radius R/h subjected to membrane loading. The inner and outer crack tips are located at $y/a=\pm b$, $\pm c$ respectively where $a/h=(c-b)/(2h)=2$, $\sigma_1=N_x/h$, $\nu=.3$, $M\to N_x$, $B\to M_x$.

MEMBRANE LOADING

	b/a R/h	0.05	0.125	0.25	0.5	1	$\to\infty$
$\frac{k_M(b)}{\sigma_1\sqrt{a}}$	5	3.904	2.924	2.464	2.117	1.779	1.480
	10	2.442	1.917	1.683	1.553	1.456	1.267
	20	2.019	1.593	1.397	1.290	1.245	1.144
	50	1.850	1.459	1.272	1.161	1.109	1.033
	$\to\infty$	1.795	1.414	1.229	1.112	1.048	1.000
$\frac{k_M(c)}{\sigma_1\sqrt{a}}$	5	2.553	2.305	2.109	1.889	1.668	1.480
	10	1.674	1.596	1.539	1.480	1.401	1.267
	20	1.359	1.311	1.278	1.251	1.227	1.144
	50	1.208	1.168	1.139	1.114	1.099	1.033
	$\to\infty$	1.115	1.112	1.081	1.052	1.028	1.000
$\frac{k_B(b)}{\sigma_1\sqrt{a}}$	5	.371	.206	.140	.140	.175	.166
	10	.305	.196	.136	.107	.119	.135
	20	.251	.170	.122	.088	.080	.099
	50	.176	.124	.092	.067	.051	.059
	$\to\infty$	.000	.000	.000	.000	.000	.000
$\frac{k_B(c)}{\sigma_1\sqrt{a}}$	5	.197	.189	.189	.193	.188	.166
	10	.130	.122	.121	.127	.139	.135
	20	.103	.092	.085	.082	.089	.099
	50	.078	.068	.060	.052	.049	.059
	$\to\infty$	.000	.000	.000	.000	.000	.000

Table 5.4 Mode 1 normalized stress intensity factors for symmetric collinear axial cracks in a cylinder of radius R/h subjected to bending. The inner and outer crack tips are located at $y/a=\pm b$, $\pm c$ respectively where $a/h=(c-b)/(2h)=2$, $\sigma_2=6M_x/h^2$, $\nu=.3$, $M\to N_x$, $B\to M_x$.

BENDING

	R/h \ b/a	0.05	0.125	0.25	0.5	1	$\to\infty$
$\frac{k_B(b)}{\sigma_2\sqrt{a}}$	5	1.111	.922	.812	.735	.690	.648
	10	1.167	.966	.846	.757	.708	.668
	20	1.211	1.000	.872	.776	.721	.681
	50	1.250	1.030	.896	.793	.733	.691
	$\to\infty$	1.291	1.060	.920	.813	.748	.700
$\frac{k_B(c)}{\sigma_2\sqrt{a}}$	5	.745	.726	.709	.690	.673	.648
	10	.768	.747	.727	.708	.692	.668
	20	.789	.765	.743	.721	.704	.681
	50	.809	.782	.758	.733	.713	.691
	$\to\infty$	.833	.803	.776	.749	.726	.700
$\frac{k_M(b)}{\sigma_2\sqrt{a}}$	5	.321	.224	.173	.128	.086	.059
	10	.148	.111	.093	.079	.063	.042
	20	.079	.060	.052	.047	.042	.029
	50	.035	.027	.024	.022	.022	.016
	$\to\infty$	.000	.000	.000	.000	.000	.000
$\frac{k_M(c)}{\sigma_2\sqrt{a}}$	5	.190	.158	.130	.100	.075	.059
	10	.098	.088	.079	.068	.055	.042
	20	.056	.052	.048	.044	.039	.029
	50	.026	.025	.024	.023	.022	.016
	$\to\infty$	.000	.000	.000	.000	.000	.000

Table 5.5 Mode 1 normalized stress intensity factors for symmetric collinear circumferential cracks in a cylinder of radius R/h subjected to membrane loading. The inner and outer crack tips are located at $y/a=\pm b$, $\pm c$ respectively where $a/h=(c-b)/(2h)=1$, $\sigma_1=N_x/h$, $\nu=.3$, $M\to N_x$, $B\to M_x$.

MEMBRANE LOADING

	b/a R/h	0.05	0.125	0.25	0.5	1	$\to\infty$
$\frac{k_M(b)}{\sigma_1\sqrt{a}}$	5	1.827	1.440	1.252	1.138	1.079	1.036
	10	1.806	1.423	1.237	1.121	1.059	1.018
	20	1.798	1.417	1.231	1.115	1.052	1.009
	50	1.796	1.415	1.229	1.113	1.049	1.003
	$\to\infty$	1.795	1.414	1.229	1.112	1.048	1.000
$\frac{k_M(c)}{\sigma_1\sqrt{a}}$	5	1.182	1.142	1.111	1.083	1.064	1.036
	10	1.162	1.122	1.091	1.063	1.041	1.018
	20	1.154	1.115	1.084	1.055	1.033	1.009
	50	1.152	1.113	1.082	1.052	1.029	1.003
	$\to\infty$	1.115	1.112	1.081	1.052	1.028	1.000
$\frac{k_B(b)}{\sigma_1\sqrt{a}}$	5	.200	.143	.110	.081	.062	.076
	10	.154	.113	.088	.068	.051	.052
	20	.107	.079	.063	.050	.038	.033
	50	.058	.044	.035	.028	.022	.018
	$\to\infty$	.000	.000	.000	.000	.000	.000
$\frac{k_B(c)}{\sigma_1\sqrt{a}}$	5	.086	.077	.069	.061	.057	.076
	10	.076	.067	.059	.051	.044	.052
	20	.056	.050	.044	.038	.033	.033
	50	.033	.029	.026	.023	.020	.018
	$\to\infty$	.000	.000	.000	.000	.000	.000

Table 5.6 Mode 1 normalized stress intensity factors for symmetric collinear circumferential cracks in a cylinder of radius R/h subjected to bending. The inner and outer crack tips are located at $y/a=\pm b$, $\pm c$ respectively where $a/h=(c-b)/(2h)=1$, $\sigma_2=6M_x/h^2$, $\nu=.3$, $M\to N_x$, $B\to M_x$.

		BENDING					
	b/a R/h	0.05	0.125	0.25	0.5	1	$\to\infty$
$\frac{k_B(b)}{\sigma_2\sqrt{a}}$	5	1.013	.854	.773	.713	.676	.675
	10	1.125	.942	.847	.775	.725	.707
	20	1.199	1.001	.897	.816	.759	.725
	50	1.253	1.043	.932	.846	.785	.740
	$\to\infty$	1.294	1.076	.960	.870	.805	.747
$\frac{k_B(c)}{\sigma_2\sqrt{a}}$	5	.704	.693	.683	.673	.667	.675
	10	.770	.755	.739	.722	.708	.707
	20	.817	.798	.778	.757	.738	.725
	50	.852	.830	.808	.783	.761	.740
	$\to\infty$	.880	.855	.831	.805	.780	.747
$\frac{k_M(b)}{\sigma_2\sqrt{a}}$	5	.042	.033	.030	.029	.030	.024
	10	.024	.019	.017	.017	.018	.016
	20	.013	.010	.009	.009	.010	.010
	50	.006	.004	.004	.004	.004	.005
	$\to\infty$	.000	.000	.000	.000	.000	.000
$\frac{k_M(c)}{\sigma_2\sqrt{a}}$	5	.032	.031	.030	.030	.030	.024
	10	.019	.018	.018	.018	.018	.016
	20	.011	.010	.010	.010	.011	.010
	50	.005	.004	.004	.004	.005	.005
	$\to\infty$	.000	.000	.000	.000	.000	.000

Table 5.7 Mode 1 normalized stress intensity factors for symmetric collinear circumferential cracks in a cylinder of radius R/h subjected to membrane loading. The inner and outer crack tips are located at $y/a=\pm b$, $\pm c$ respectively where $a/h=(c-b)/(2h)=2$, $\sigma_1=N_x/h$, $\nu=.3$, $M\to N_x$, $B\to M_x$.

MEMBRANE LOADING

	R/h \ b/a	0.05	0.125	0.25	0.5	1	$\to\infty$
$\frac{k_M(b)}{\sigma_1\sqrt{a}}$	5	1.992	1.569	1.372	1.261	1.211	1.124
	10	1.868	1.472	1.283	1.171	1.118	1.066
	20	1.821	1.435	1.248	1.134	1.075	1.034
	50	1.801	1.419	1.234	1.118	1.055	1.014
	$\to\infty$	1.795	1.414	1.229	1.112	1.048	1.000
$\frac{k_M(c)}{\sigma_1\sqrt{a}}$	5	1.325	1.278	1.244	1.216	1.193	1.124
	10	1.221	1.180	1.149	1.123	1.106	1.066
	20	1.177	1.138	1.107	1.080	1.061	1.034
	50	1.157	1.118	1.087	1.059	1.037	1.014
	$\to\infty$	1.115	1.112	1.081	1.052	1.028	1.000
$\frac{k_B(b)}{\sigma_1\sqrt{a}}$	5	.212	.133	.084	.055	.061	.112
	10	.236	.163	.117	.081	.065	.099
	20	.207	.148	.110	.080	.060	.073
	50	.140	.102	.078	.059	.045	.043
	$\to\infty$	.000	.000	.000	.000	.000	.000
$\frac{k_B(c)}{\sigma_1\sqrt{a}}$	5	.056	.058	.062	.073	.093	.112
	10	.082	.075	.070	.067	.072	.099
	20	.087	.077	.068	.060	.056	.073
	50	.068	.060	.053	.045	.039	.043
	$\to\infty$	.000	.000	.000	.000	.000	.000

Table 5.8 Mode 1 normalized stress intensity factors for symmetric collinear circumferential cracks in a cylinder of radius R/h subjected to bending. The inner and outer crack tips are located at $y/a=\pm b$, $\pm c$ respectively where $a/h=(c-b)/(2h)=2$, $\sigma_2=6M_x/h^2$, $\nu=.3$, $M\to N_x$, $B\to M_x$.

BENDING

	R/h \ b/a	0.05	0.125	0.25	0.5	1	$\to\infty$
$\frac{k_B(b)}{\sigma_2\sqrt{a}}$	5	.714	.612	.555	.520	.516	.530
	10	.884	.746	.665	.607	.583	.593
	20	1.030	.860	.758	.681	.641	.637
	50	1.163	.963	.841	.748	.694	.673
	$\to\infty$	1.291	1.060	.920	.813	.748	.747
$\frac{k_B(c)}{\sigma_2\sqrt{a}}$	5	.517	.516	.517	.519	.525	.530
	10	.599	.592	.587	.583	.584	.593
	20	.677	.664	.651	.639	.632	.637
	50	.754	.733	.713	.693	.677	.673
	$\to\infty$	.833	.803	.776	.749	.726	.747
$\frac{k_M(b)}{\sigma_2\sqrt{a}}$	5	.091	.072	.063	.059	.053	.038
	10	.061	.048	.043	.041	.040	.029
	20	.038	.030	.026	.025	.026	.021
	50	.018	.014	.012	.012	.013	.012
	$\to\infty$	.000	.000	.000	.000	.000	.000
$\frac{k_M(c)}{\sigma_2\sqrt{a}}$	5	.063	.060	.057	.053	.048	.038
	10	.045	.043	.041	.040	.038	.029
	20	.029	.028	.027	.026	.026	.021
	50	.014	.013	.013	.013	.013	.012
	$\to\infty$	.000	.000	.000	.000	.000	.000

Table 5.9 Modes 2&3 normalized stress intensity factors for symmetric collinear axial cracks in a cylinder of radius R/h subjected to in-plane shear. The inner and outer crack tips are located at $y/a=\pm b$, $\pm c$ respectively where $a/h=(c-b)/(2h)=1$, $\sigma_4=N_{xy}/h$, $\nu=.3$, $I\to N_{xy}$, $M\to M_{xy}$, $0\to V_x$.

IN-PLANE SHEAR

	b/a R/h	0.05	0.125	0.25	0.5	1	$\to\infty$
$\frac{k_{2I}(b)}{\sigma_4\sqrt{a}}$	5	1.912	1.495	1.290	1.159	1.082	1.031
	10	1.860	1.460	1.265	1.141	1.069	1.016
	20	1.829	1.439	1.249	1.128	1.061	1.008
	50	1.809	1.425	1.237	1.120	1.054	1.003
	$\to\infty$	1.795	1.414	1.229	1.112	1.048	1.000
$\frac{k_{2I}(c)}{\sigma_4\sqrt{a}}$	5	1.208	1.161	1.123	1.087	1.058	1.031
	10	1.186	1.142	1.107	1.074	1.046	1.016
	20	1.171	1.129	1.096	1.065	1.039	1.008
	50	1.160	1.120	1.088	1.058	1.033	1.003
	$\to\infty$	1.115	1.112	1.081	1.052	1.028	1.000
$\frac{k_{2T}(b)}{\sigma_4\sqrt{a}}$	5	-.068	-.044	-.030	-.019	-.014	-.020
	10	-.049	-.034	-.025	-.018	-.013	-.014
	20	-.032	-.023	-.018	-.013	-.010	-.009
	50	-.017	-.013	-.010	-.008	-.006	-.005
	$\to\infty$	.000	.000	.000	.000	.000	.000
$\frac{k_{2T}(c)}{\sigma_4\sqrt{a}}$	5	-.006	-.008	-.009	-.012	-.014	-.020
	10	-.008	-.009	-.009	-.009	-.010	-.014
	20	-.008	-.008	-.008	-.008	-.007	-.009
	50	-.006	-.006	-.005	-.005	-.005	-.005
	$\to\infty$	.000	.000	.000	.000	.000	.000
$\frac{k_{30}(b)}{\sigma_4\sqrt{a}}$	5	-.008	-.017	-.028	-.039	-.047	-.050
	10	-.002	-.007	-.012	-.018	-.022	-.026
	20	-.001	-.003	-.005	-.008	-.011	-.014
	50	-.000	-.001	-.002	-.003	-.004	-.006
	$\to\infty$	.000	.000	.000	.000	.000	.000
$\frac{k_{30}(c)}{\sigma_4\sqrt{a}}$	5	.090	.078	.068	.059	.052	.050
	10	.051	.045	.039	.034	.029	.026
	20	.028	.024	.022	.019	.016	.014
	50	.012	.011	.009	.008	.007	.006
	$\to\infty$	.000	.000	.000	.000	.000	.000

Table 5.10 Modes 2&3 normalized stress intensity factors for symmetric collinear axial cracks in a cylinder of radius R/h subjected to twisting. The inner and outer crack tips are located at $y/a=\pm b$, $\pm c$ respectively where $a/h=(c-b)/(2h)=1$, $\sigma_5=6M_{xy}/h^2$, $\nu=.3$, $I\rightarrow N_{xy}$, $T\rightarrow M_{xy}$, $O\rightarrow V_x$.

TWISTING

	R/h \ b/a	0.05	0.125	0.25	0.5	1	$\rightarrow\infty$
$\frac{k_{2T}(b)}{\sigma_5\sqrt{a}}$	5	.666	.576	.537	.519	.516	.519
	10	.670	.579	.540	.521	.517	.520
	20	.672	.581	.541	.522	.518	.521
	50	.674	.582	.542	.523	.519	.521
	$\rightarrow\infty$	.675	.583	.543	.524	.519	.522
$\frac{k_{2T}(c)}{\sigma_5\sqrt{a}}$	5	.503	.505	.509	.512	.516	.519
	10	.504	.506	.509	.513	.517	.520
	20	.504	.507	.510	.514	.517	.521
	50	.505	.507	.510	.514	.518	.521
	$\rightarrow\infty$	.506	.508	.511	.515	.518	.522
$\frac{k_{2I}(b)}{\sigma_5\sqrt{a}}$	5	-.019	-.013	-.010	-.007	-.006	-.007
	10	-.014	-.010	-.007	-.005	-.004	-.005
	20	-.009	-.006	-.005	-.004	-.003	-.003
	50	-.005	-.004	-.003	-.002	-.002	-.002
	$\rightarrow\infty$	.000	.000	.000	.000	.000	.000
$\frac{k_{2I}(c)}{\sigma_5\sqrt{a}}$	5	-.006	-.006	-.006	-.006	-.006	-.007
	10	-.005	-.005	-.004	-.004	-.004	-.005
	20	-.004	-.004	-.003	-.003	-.003	-.003
	50	-.002	-.002	-.002	-.002	-.002	-.002
	$\rightarrow\infty$	.000	.000	.000	.000	.000	.000
$\frac{k_{30}(b)}{\sigma_5\sqrt{a}}$	5	-.004	.007	.025	.047	.062	.069
	10	-.005	.006	.024	.047	.062	.069
	20	-.005	.005	.024	.046	.062	.070
	50	-.005	.005	.023	.046	.062	.070
	$\rightarrow\infty$	-.005	.005	.023	.046	.062	.070
$\frac{k_{30}(c)}{\sigma_5\sqrt{a}}$	5	-.100	-.092	-.085	-.077	-.071	-.069
	10	-.102	-.094	-.086	-.078	-.072	-.069
	20	-.103	-.095	-.087	-.079	-.073	-.070
	50	-.103	-.096	-.088	-.079	-.073	-.070
	$\rightarrow\infty$	-.104	-.096	-.088	-.079	-.073	-.070

Table 5.11 Modes 2&3 normalized stress intensity factors for symmetric collinear axial cracks in a cylinder of radius R/h subjected to out-of-plane shear. The inner and outer crack tips are located at $y/a=\pm b$, $\pm c$ respectively where $a/h=(c-b)/(2h)=1$, $\sigma_3=3V_x/(2h)$, $\nu=.3$, $I\to N_{xy}$, $T\to M_{xy}$, $O\to V_x$.

OUT-OF-PLANE SHEAR

	R/h \ b/a	0.05	0.125	0.25	0.5	1	→∞
$\frac{k_{30}(b)}{\sigma_3\sqrt{a}}$	5	2.876	2.103	1.797	1.682	1.665	1.661
	10	2.897	2.116	1.806	1.689	1.672	1.671
	20	2.905	2.121	1.810	1.692	1.675	1.674
	50	2.908	2.123	1.812	1.694	1.676	1.676
	→∞	2.909	2.124	1.812	1.694	1.677	1.676
$\frac{k_{30}(c)}{\sigma_3\sqrt{a}}$	5	1.748	1.689	1.664	1.658	1.661	1.661
	10	1.757	1.697	1.671	1.665	1.669	1.671
	20	1.761	1.701	1.674	1.667	1.671	1.674
	50	1.762	1.702	1.675	1.668	1.672	1.676
	→∞	1.763	1.702	1.675	1.669	1.673	1.676
$\frac{k_{2I}(b)}{\sigma_3\sqrt{a}}$	5	.016	.024	.031	.040	.049	.053
	10	.008	.011	.014	.019	.024	.028
	20	.004	.005	.007	.009	.011	.014
	50	.001	.002	.003	.003	.004	.006
	→∞	.000	.000	.000	.000	.000	.000
$\frac{k_{2I}(c)}{\sigma_3\sqrt{a}}$	5	-.075	-.067	-.062	-.057	-.054	-.053
	10	-.042	-.038	-.034	-.032	-.029	-.028
	20	-.023	-.020	-.019	-.017	-.016	-.014
	50	-.009	-.008	-.008	-.007	-.007	-.006
	→∞	.000	.000	.000	.000	.000	.000
$\frac{k_{2T}(b)}{\sigma_3\sqrt{a}}$	5	-.074	-.155	-.251	-.358	-.429	-.455
	10	-.074	-.155	-.251	-.359	-.433	-.462
	20	-.074	-.155	-.251	-.360	-.433	-.465
	50	-.074	-.155	-.251	-.360	-.433	-.465
	→∞	-.074	-.155	-.251	-.360	-.433	-.466
$\frac{k_{2T}(c)}{\sigma_3\sqrt{a}}$	5	.568	.518	.489	.471	.462	.455
	10	.580	.528	.498	.479	.469	.462
	20	.585	.532	.502	.482	.472	.465
	50	.587	.534	.503	.484	.473	.465
	→∞	.588	.535	.504	.484	.474	.466

Table 5.12 Modes 2&3 normalized stress intensity factors for symmetric collinear circumferential cracks in a cylinder of radius R/h subjected to in-plane shear. The inner and outer crack tips are located at $y/a=\pm b$, $\pm c$ respectively where $a/h=(c-b)/(2h)=1$, $\sigma_4=N_{xy}/h$, $\nu=.3$, $I\rightarrow N_{xy}$, $T\rightarrow M_{xy}$, $O\rightarrow V_x$.

IN-PLANE SHEAR

	b/a R/h	0.05	0.125	0.25	0.5	1	$\rightarrow\infty$
$\frac{k_{2I}(b)}{\sigma_4\sqrt{a}}$	5	1.979	1.539	1.322	1.182	1.098	1.036
	10	1.880	1.474	1.275	1.149	1.077	1.018
	20	1.835	1.443	1.252	1.131	1.064	1.009
	50	1.810	1.425	1.238	1.120	1.055	1.003
	$\rightarrow\infty$	1.795	1.414	1.229	1.112	1.048	1.000
$\frac{k_{2I}(c)}{\sigma_4\sqrt{a}}$	5	1.223	1.174	1.135	1.098	1.066	1.036
	10	1.192	1.148	1.113	1.079	1.051	1.018
	20	1.173	1.132	1.099	1.067	1.042	1.009
	50	1.160	1.120	1.089	1.058	1.034	1.003
	$\rightarrow\infty$	1.115	1.112	1.081	1.052	1.028	1.000
$\frac{k_{2T}(b)}{\sigma_4\sqrt{a}}$	5	-.142	-.093	-.063	-.040	-.025	-.025
	10	-.089	-.061	-.044	-.031	-.021	-.017
	20	-.053	-.037	-.028	-.021	-.015	-.011
	50	-.025	-.018	-.014	-.011	-.009	-.006
	$\rightarrow\infty$	.000	.000	.000	.000	.000	.000
$\frac{k_{2T}(c)}{\sigma_4\sqrt{a}}$	5	.013	.007	.001	-.004	-.011	-.025
	10	-.001	-.003	-.005	-.007	-.009	-.017
	20	-.005	-.006	-.007	-.007	-.007	-.011
	50	-.005	-.005	-.005	-.005	-.005	-.006
	$\rightarrow\infty$	.000	.000	.000	.000	.000	.000
$\frac{k_{30}(b)}{\sigma_4\sqrt{a}}$	5	-.018	-.041	-.067	-.098	-.125	-.150
	10	-.005	-.015	-.028	-.043	-.057	-.075
	20	-.002	-.006	-.013	-.020	-.027	-.038
	50	-.000	-.002	-.005	-.008	-.011	-.015
	$\rightarrow\infty$	.000	.000	.000	.000	.000	.000
$\frac{k_{30}(c)}{\sigma_4\sqrt{a}}$	5	.296	.260	.230	.199	.173	.150
	10	.156	.138	.122	.107	.093	.075
	20	.080	.071	.063	.056	.049	.038
	50	.033	.029	.026	.023	.020	.015
	$\rightarrow\infty$	.000	.000	.000	.000	.000	.000

Table 5.13 Modes 2&3 normalized stress intensity factors for symmetric collinear circumferential cracks in a cylinder of radius R/h subjected to twisting. The inner and outer crack tips are located at $y/a=\pm b, \pm c$ respectively where $a/h=(c-b)/(2h)=1$, $\sigma_5=6M_{xy}/h^2$, $\nu=.3$, $I\to N_{xy}$, $T\to M_{xy}$, $O\to V_x$.

TWISTING

	R/h \ b/a	0.05	0.125	0.25	0.5	1	$\to\infty$
$\frac{k_{2T}(b)}{\sigma_5\sqrt{a}}$	5	.665	.574	.535	.517	.514	.519
	10	.670	.578	.539	.520	.516	.520
	20	.672	.580	.541	.522	.518	.521
	50	.674	.582	.542	.523	.518	.521
	$\to\infty$	.675	.583	.543	.524	.519	.522
$\frac{k_{2T}(c)}{\sigma_5\sqrt{a}}$	5	.502	.505	.508	.512	.516	.519
	10	.503	.506	.509	.513	.516	.520
	20	.504	.507	.510	.513	.517	.521
	50	.505	.507	.510	.514	.517	.521
	$\to\infty$	.506	.508	.511	.515	.518	.522
$\frac{k_{2I}(b)}{\sigma_5\sqrt{a}}$	5	-.035	-.023	-.017	-.011	-.008	-.010
	10	-.022	-.015	-.011	-.008	-.006	-.006
	20	-.014	-.010	-.007	-.005	-.004	-.004
	50	-.007	-.005	-.004	-.003	-.002	-.002
	$\to\infty$	.000	.000	.000	.000	.000	.000
$\frac{k_{2I}(c)}{\sigma_5\sqrt{a}}$	5	-.009	-.008	-.008	-.007	-.007	-.010
	10	-.007	-.006	-.006	-.005	-.005	-.006
	20	-.005	-.004	-.004	-.004	-.004	-.004
	50	-.003	-.002	-.002	-.002	-.002	-.002
	$\to\infty$	.000	.000	.000	.000	.000	.000
$\frac{k_{30}(b)}{\sigma_5\sqrt{a}}$	5	-.003	.009	.028	.050	.065	.069
	10	-.004	.006	.025	.047	.063	.070
	20	-.005	.006	.024	.047	.062	.070
	50	-.005	.005	.023	.046	.062	.070
	$\to\infty$	-.005	.005	.023	.046	.062	.070
$\frac{k_{30}(c)}{\sigma_5\sqrt{a}}$	5	-.098	-.090	-.083	-.075	-.070	-.069
	10	-.102	-.094	-.086	-.077	-.072	-.070
	20	-.103	-.095	-.087	-.078	-.073	-.070
	50	-.103	-.096	-.088	-.079	-.073	-.070
	$\to\infty$	-.104	-.096	-.088	-.079	-.073	-.070

Table 5.14 Modes 2&3 normalized stress intensity factors for symmetric collinear circumferential cracks in a cylinder of radius R/h subjected to out-of-plane shear. The inner and outer crack tips are located at $y/a=\pm b$, $\pm c$ respectively where $a/h=(c-b)/(2h)=1$, $\sigma_3=3V_x/(2h)$, $\nu=.3$, $I\rightarrow N_{xy}$, $T\rightarrow M_{xy}$, $O\rightarrow V_x$.

OUT-OF-PLANE SHEAR

	R/h \ b/a	0.05	0.125	0.25	0.5	1	$\rightarrow\infty$
$\frac{k_{30}(b)}{\sigma_3\sqrt{a}}$	5	2.565	1.897	1.632	1.537	1.532	1.547
	10	2.793	2.047	1.751	1.641	1.628	1.635
	20	2.873	2.100	1.793	1.678	1.661	1.664
	50	2.902	2.119	1.809	1.691	1.673	1.674
	$\rightarrow\infty$	2.909	2.124	1.182	1.694	1.677	1.676
$\frac{k_{30}(c)}{\sigma_3\sqrt{a}}$	5	1.561	1.526	1.514	1.518	1.532	1.547
	10	1.694	1.643	1.621	1.618	1.626	1.635
	20	1.742	1.684	1.659	1.653	1.658	1.664
	50	1.759	1.699	1.672	1.666	1.670	1.674
	$\rightarrow\infty$	1.763	1.702	1.675	1.669	1.673	1.676
$\frac{k_{2I}(b)}{\sigma_3\sqrt{a}}$	5	.040	.058	.076	.099	.124	.152
	10	.021	.030	.039	.050	.063	.081
	20	.010	.015	.019	.025	.031	.042
	50	.004	.006	.008	.010	.012	.017
	$\rightarrow\infty$	.000	.000	.000	.000	.000	.000
$\frac{k_{2I}(c)}{\sigma_3\sqrt{a}}$	5	-.222	-.201	-.187	-.176	-.164	-.152
	10	-.127	-.114	-.106	-.099	-.093	-.081
	20	-.067	-.060	-.056	-.052	-.049	-.042
	50	-.027	-.025	-.023	-.022	-.020	-.017
	$\rightarrow\infty$	.000	.000	.000	.000	.000	.000
$\frac{k_{2T}(b)}{\sigma_3\sqrt{a}}$	5	-.067	-.141	-.230	-.331	-.400	-.422
	10	-.071	-.151	-.244	-.350	-.423	-.452
	20	-.073	-.154	-.249	-.357	-.430	-.462
	50	-.074	-.155	-.251	-.359	-.433	-.465
	$\rightarrow\infty$	-.074	-.155	-.251	-.360	-.433	-.466
$\frac{k_{2T}(c)}{\sigma_3\sqrt{a}}$	5	.500	.460	.437	.424	.418	.422
	10	.557	.509	.480	.463	.454	.452
	20	.578	.526	.496	.477	.467	.462
	50	.586	.533	.502	.483	.472	.465
	$\rightarrow\infty$	.588	.535	.504	.484	.474	.466

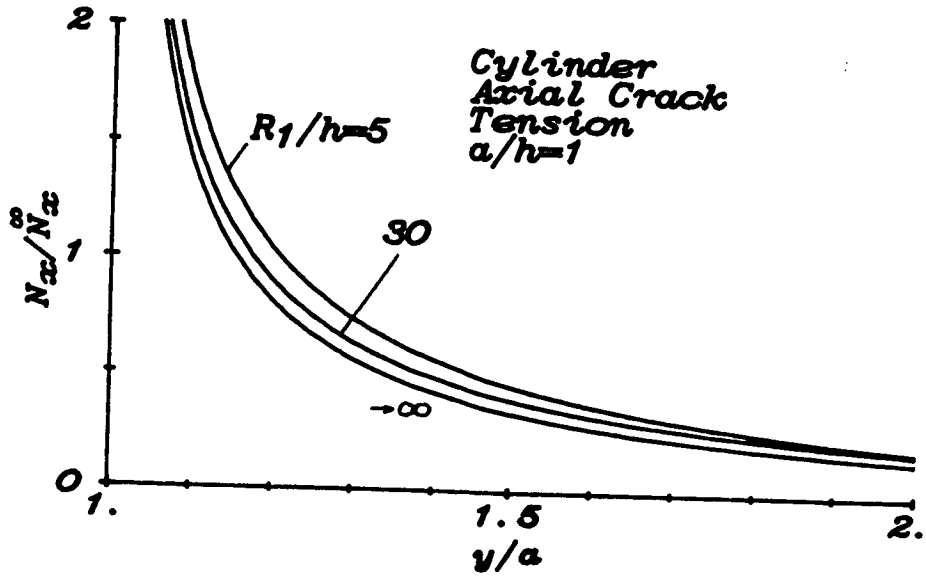

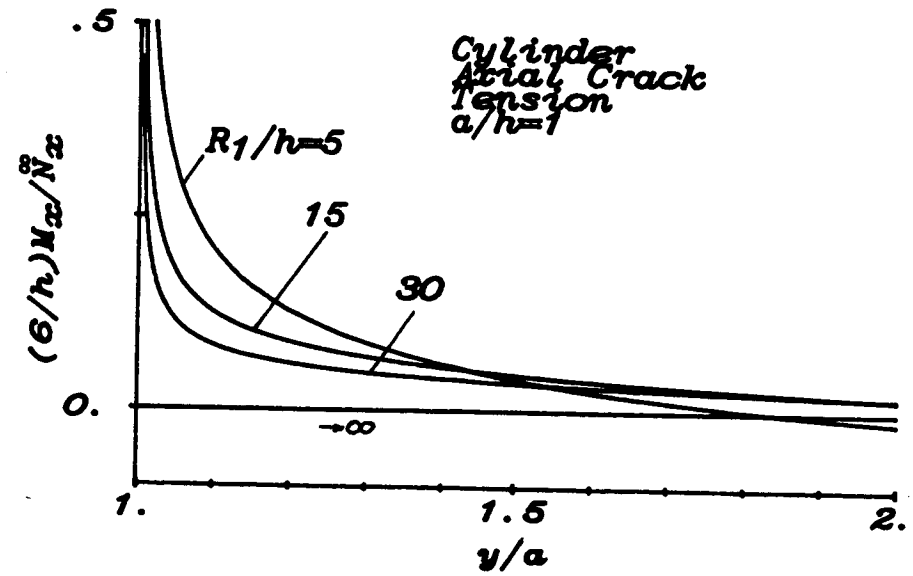

Figure 5.1 Stresses ahead of an axial crack (a/h=1) in a cylinder subjected to membrane loading, ν=.3.

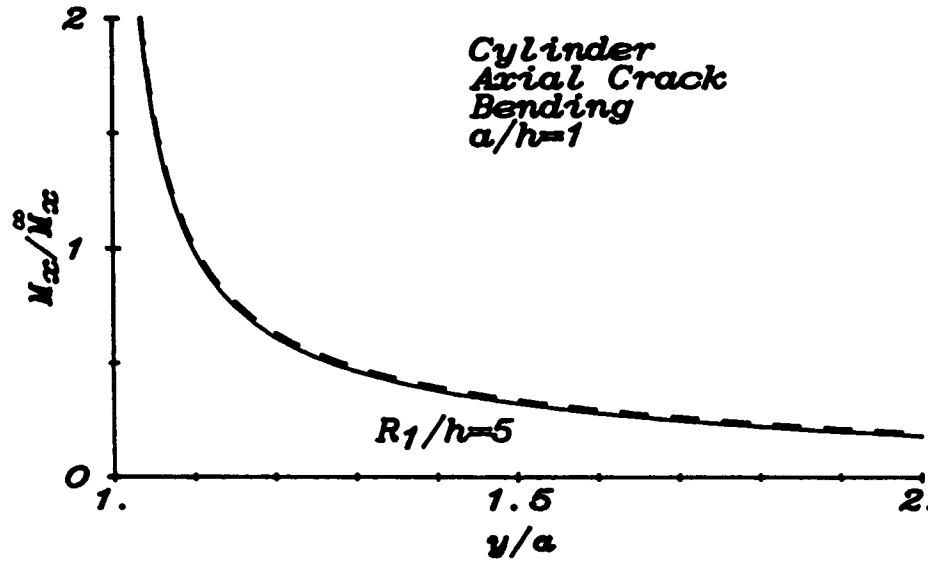

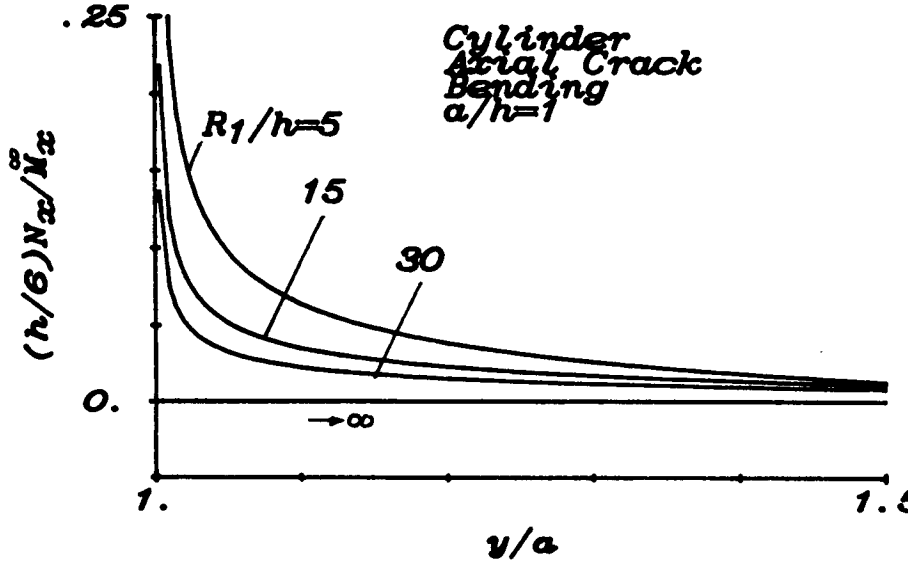

Figure 5.2 Stresses ahead of an axial crack (a/h=1) in a cylinder subjected to bending. The dashed line corresponds to $R/h \to \infty$, ν=.3.

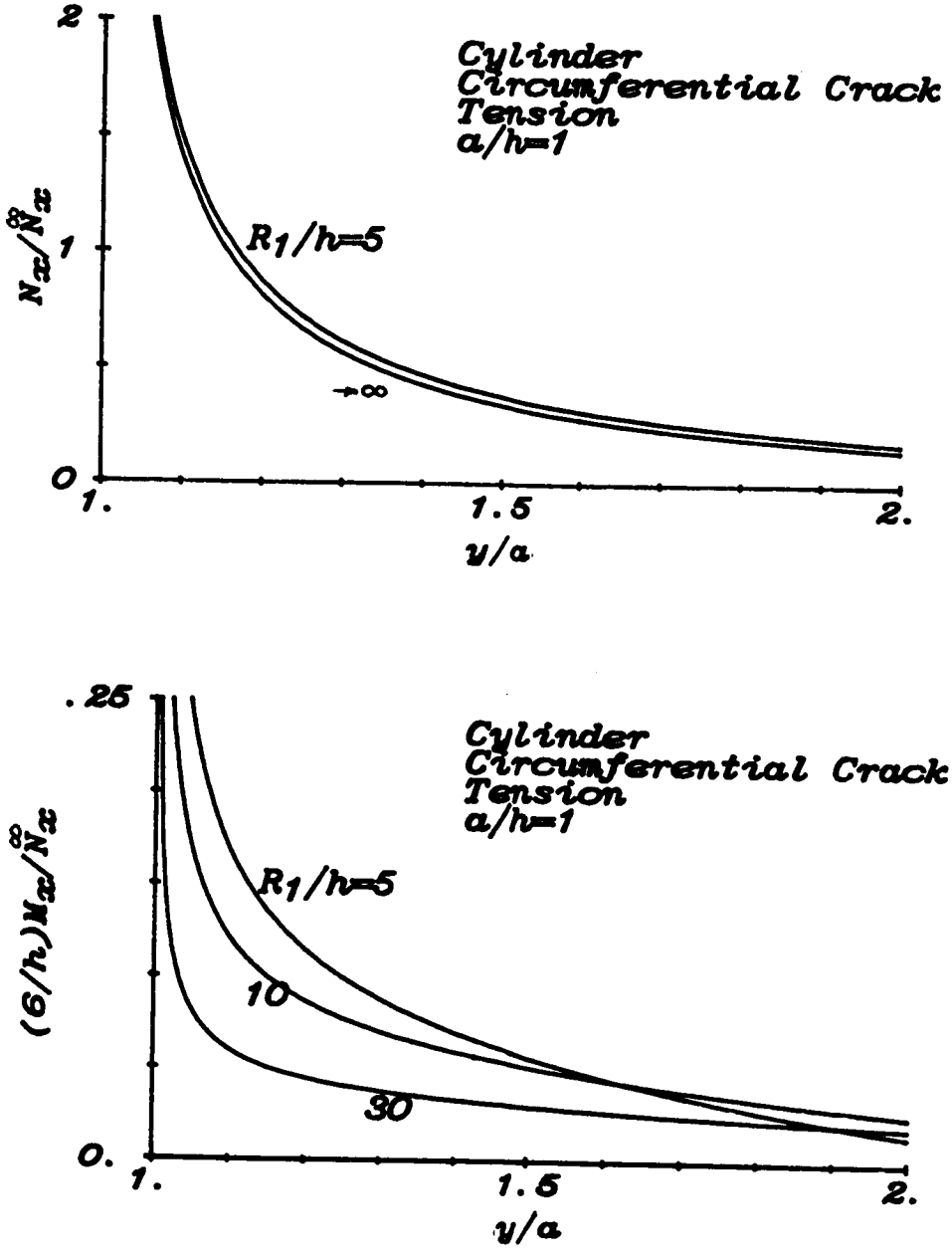

Figure 5.3 Stresses ahead of a circumferential crack (a/h=1) in a cylinder subjected to membrane loading, ν=.3.

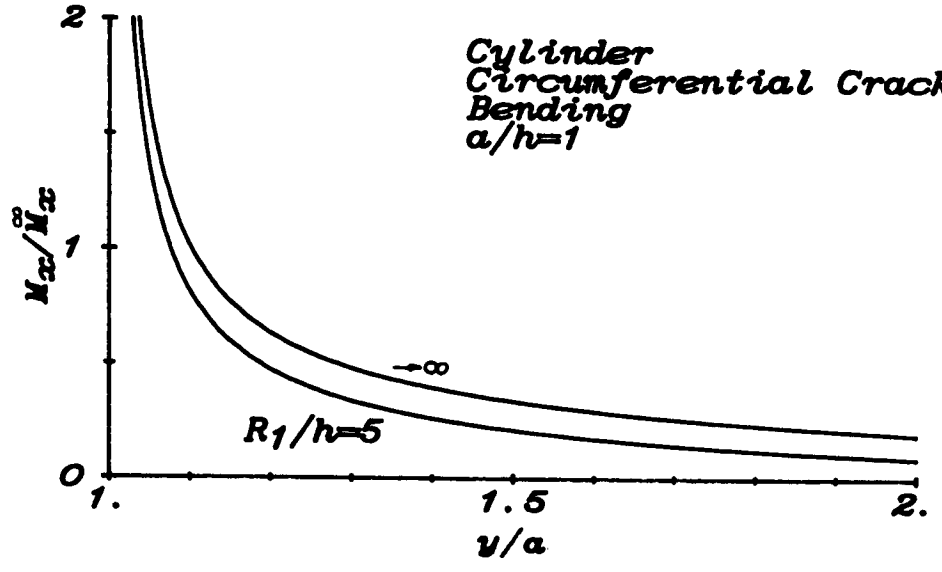

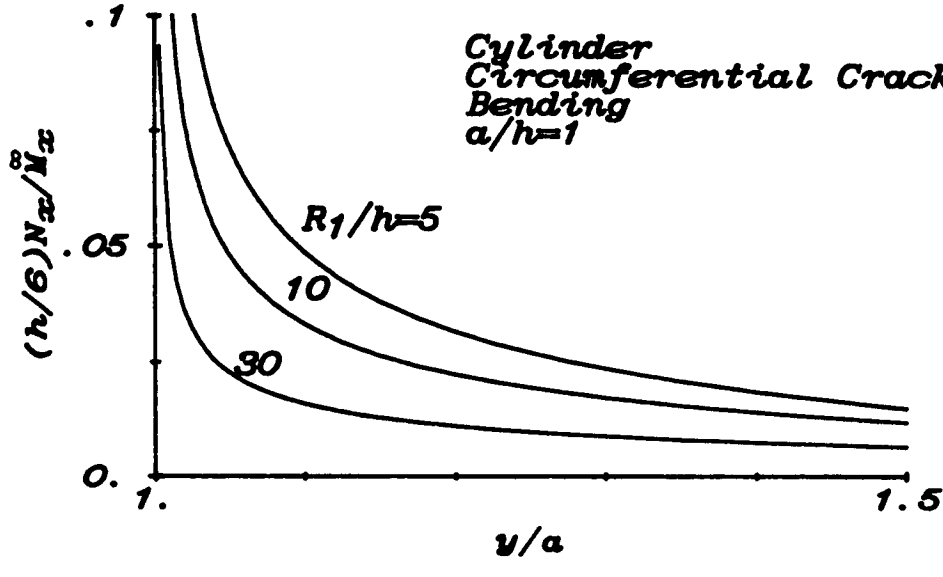

Figure 5.4 Stresses ahead of a circumferential crack (a/h=1) in a cylinder subjected to bending, ν=.3.

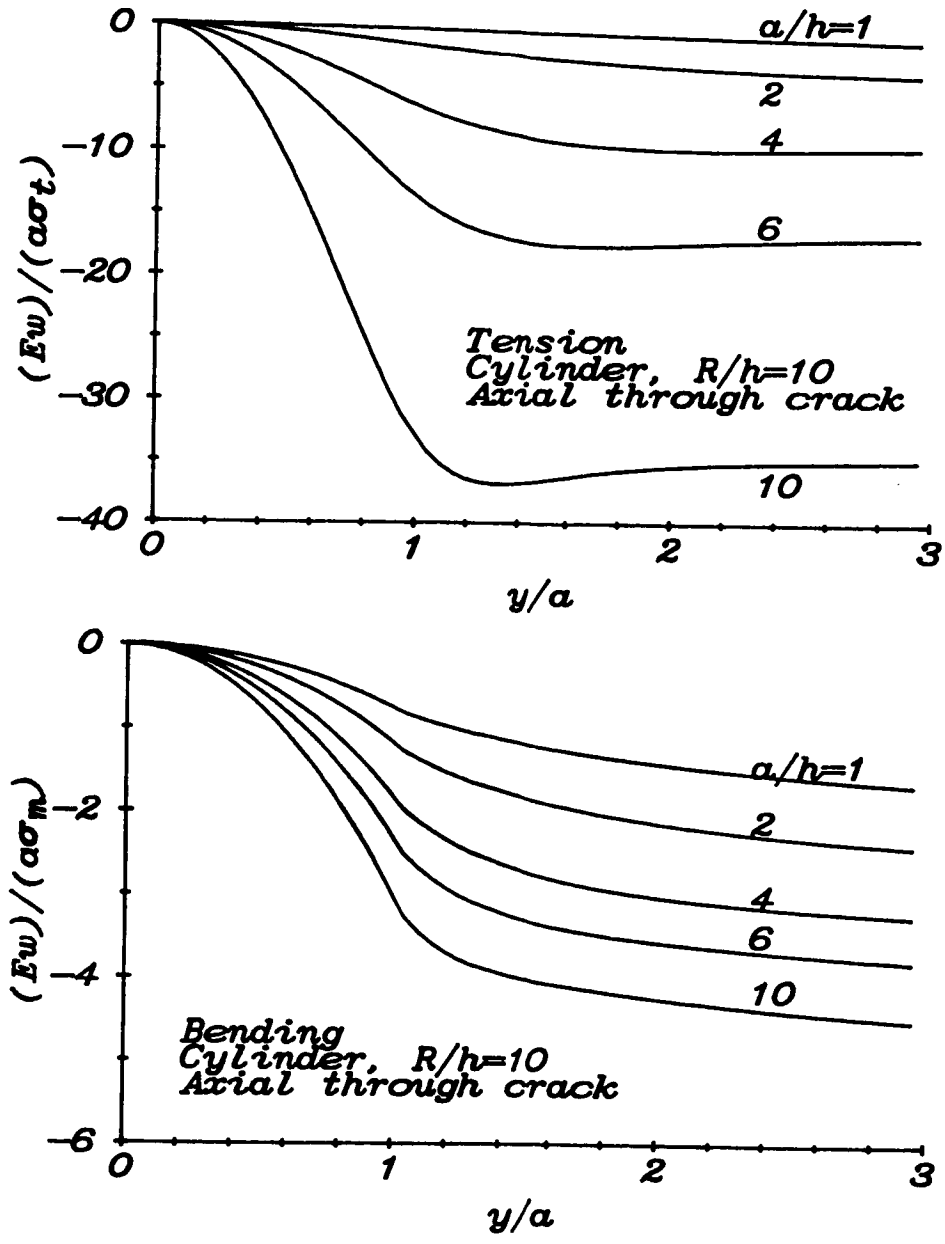

Figure 5.5 Out-of-plane displacement $w(0^+,y)$ as measured from y=0 in the deformed position for a cylinder with an axial crack subjected to either membrane loading ($\sigma_m=\overset{\infty}{N}_x/h$) or bending ($\sigma_b=6\overset{\infty}{M}_x/h^2$), ν=.3.

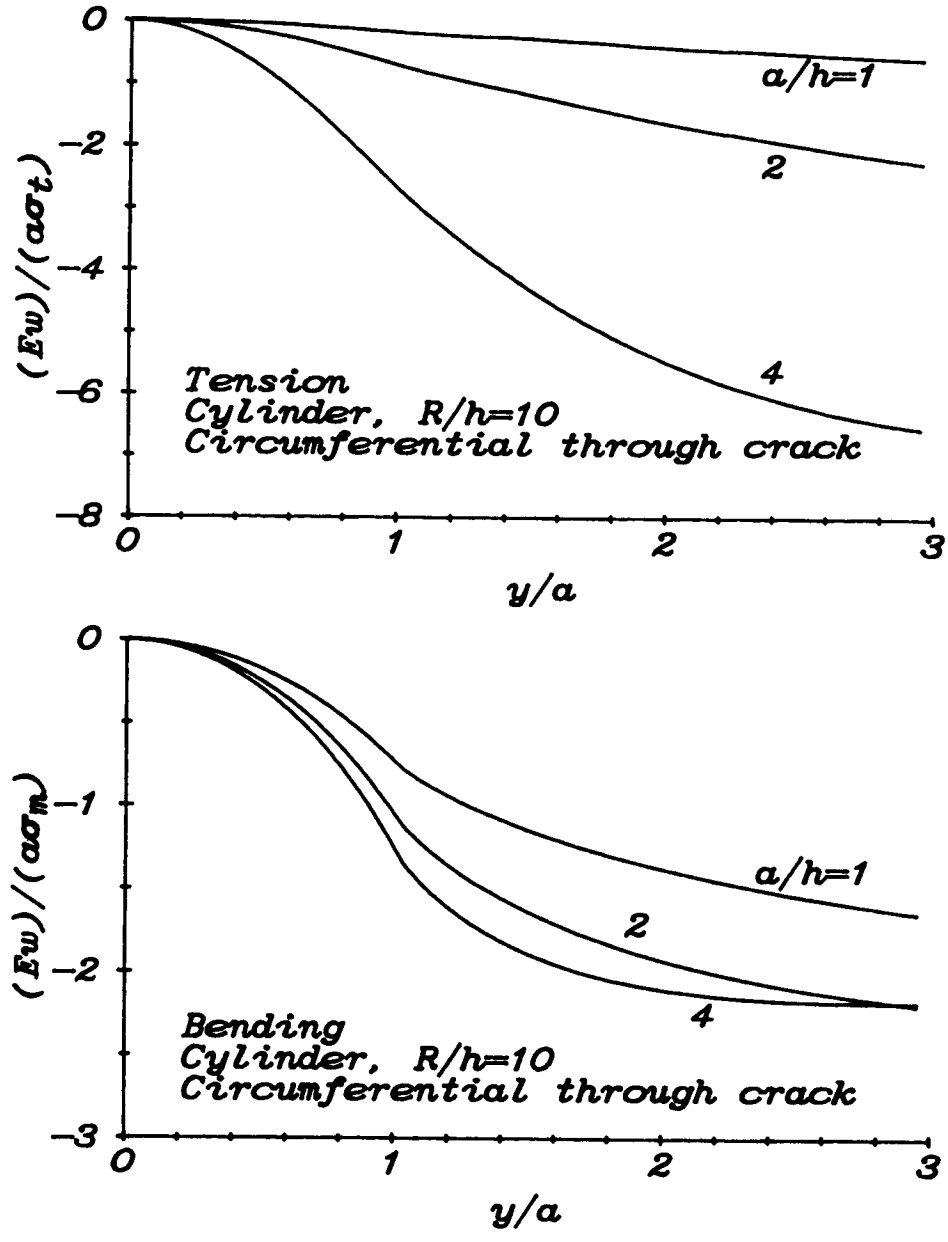

Figure 5.6 Out-of-plane displacement $w(0^+,y)$ as measured from y=0 in the deformed position for a cylinder with a circumferential crack subjected to either membrane loading ($\sigma_m=\overset{\infty}{N}_x/h$) or bending ($\sigma_b=6\overset{\infty}{M}/h^2$), ν=.3.

CHAPTER 6

Part-Through Cracks in Shells

The singular integral equations for part-through crack problems are obtained directly from the corresponding through crack equations given in Chapter 5. The compliance relations of Chapter 2 and Appendix C are used even though they correspond to the strip solution which does not take into account shell curvature. The plane strain problem for an edge cracked cylinder [74], and the axisymmetric case of a circumferentially cracked cylinder [75], could be used to obtain these coefficients, but there are convergence problems for shell-like geometries, and also a different set of constants would be required for each curvature. Since the assumption of shallowness has already been applied, neglect of this curvature effect should not be too significant, see [60]. The line-spring model solutions are normalized with respect to the edge crack solution as explained in section C.4 of Appendix C. Perhaps if the solution is considered to be normalized with respect to the actual "long crack" shell solution instead of the plane strain strip value, the accuracy of the result will improve. This idea is similar to what happens when a compliance curve that is not too accurate is used. The resulting ratio is more accurate than the actual value of the SIF.

There are some basic differences between plate and shell problems besides the mathematical complication that shell curvature introduces. In a plate, loading at "infinity" for any of the five loads of tension

(N_{xx}), bending (M_{xx}), out-of-plane shear (V_x), in-plane shear (N_{xy}), and twisting (M_{xy}), results in an "uncracked" solution that is constant throughout the plate. Therefore, in the perturbation problem, the solution to the various loading cases is obtained by simply applying the negative of these loads to the crack surfaces. The process of determining the perturbation loads in shells for a given external loading is not as easy. In a cylinder, for example, any loading at infinity can result only in membrane or in-plane shear at the crack region, (excluding minor secondary contributions). The loading cases of bending, out-of-plane shear and twisting become important when an external force is applied near the crack region. To make use of the various shell solutions, the solution to the shell without a crack must first be obtained. This will in general require numerical techniques.

With the present formulation the surface crack can lie along any principal line of constant curvature of a shell. This uncouples the symmetric mode 1 loading, from the skew-symmetric loading that couples modes 2 and 3. If the crack were positioned at an arbitrary angle, then all three fracture modes interact, see [30]. The most practical problem represented here would be a mode 1 contribution resulting from torsion of a cylinder.

The different geometries that are considered include the sphere, cylinder and circular pipe elbow, which is represented by a toroidal shell. Also the crack may lie on the outside or inside of the shell by imposing positive or negative curvature, respectively. The

emphasis in the results will be the effect of curvature on the SIF at the maximum penetration point of a semi-elliptical surface crack.

6.1 Mode 1.

From Eqns. 5.84,85, 2.31, and from the superposition of Fig. C.1, the integral equations for the symmetrically loaded part-through crack are found to be:

$$\frac{1}{2\pi} \fint_a^b \frac{u_1(t)}{(t-y)^2}\, dt + \frac{1}{\pi}\sum_{i=1}^{2}\int_a^b u_i(t)K_{i1}(z)\, dt$$

$$- \gamma_{11}u_1(y) - \gamma_{12}u_2(y) = -\overset{\infty}{N}_x = -\overset{\infty}{\sigma}_1 \ , \qquad (6.1)$$

$$\frac{(1-\nu^2)}{\lambda^4 2\pi} \fint_a^b \frac{u_2(t)}{(t-y)^2}\, dt + \frac{1}{\pi}\sum_{i=1}^{2}\int_a^b u_i(t)K_{i2}(z)\, dt$$

$$- \gamma_{12}u_1(y) - \gamma_{22}u_2(y) = -\overset{\infty}{M}_x = -\overset{\infty}{\sigma}_2/6 \ , \qquad (6.2)$$

where the kernels may be obtained from Eqns. 5.84,85 and Appendix J. The LSM for inner surface cracks in a pressurized cylinder is compared to solutions from Raju and Newman [34] in Fig. 6.1, and to solutions from O'Donoghue et. al. [40] in Fig. 6.2. The only case where agreement is poor is for the semi-circular crack with $a/h=L_0/h=.2$, which is a rather severe geometry for the model. Outward bulging of the shell surface along the line of the crack is presented in Fig. 6.3 for an outer circumferential crack in a cylinder. Fig. 6.4 shows the inner crack case where the bulging is inward. The tension case of 6.4 shows that the depression does not always increase as the crack gets deeper (i.e. increasing L_0/h) because of the tendency of the crack to

bulge outward when there is no net ligament. The net ligament causes a bending component that forces the surface inward and these two effects oppose each other. Therefore it would be difficult to predict crack depth by a measurement from the back surface.

To date, as far as I know, the LSM has only been applied to cracked cylinders, see for example [49,60]. In tables 6.1-5 the solution to the spherical shell is presented for both inner and outer cracks of varying depths and lengths. It is noted that the results are sensitive to curvature. Also for a given geometry the SIFs are higher for the external crack than for the internal crack. In table 6.6 the SIF distribution along the contour of a semi-elliptical crack located at different positions in a toroidal shell is presented. The four locations, denoted A through D, are shown in Fig. 6.5. Also the crack may be internal or external, making a total of eight cases that are given in this table, and in the tables that follow. It is noted that the functional behavior of the SIF does not vary much from position to position. This supports giving only the value of the SIF at the center of the crack. Therefore, the plate results may be used to get an idea about this distribution given the crack size and maximum penetration value. These results are given in Chapter 4 for a wide range of crack lengths and depths. The toroidal shell results for mode 1 loading are presented in tables 6.7-22. In these tables the cylinder radius to shell thickness ratio is held constant at R/h=10. The main parameter study is the elbow curvature given by R_i/R, see Fig. 6.5. Values of crack length to shell thickness (a/h),

of .5, 1., 2., 4., are used. As expected, the longer the crack, the more the influence of elbow curvature. The results given in the tables are for constant crack surface membrane and bending loads. It should be noted that in order to obtain the solution to the practical case of an internally pressurized toroidal shell, or to any other external loading, the uncracked shell solution must first be obtained. In general this solution will not be constant over the length of the crack. This is not a concern with either the sphere or cylinder because the uncracked solution is constant due to symmetry. However, it is most likely the case that the variation is not considerable and that the results in the tables may be directly applied once the actual crack surface loading is determined.

6.2 Modes 2 and 3

From Eqns. 5.109-111, 2.31, and from the superposition of Fig. C.1, the integral equations for the skew-symmetrically loaded part-through crack may be expressed as:

$$\frac{1}{\pi}\fint_a^b \frac{g_3(t)}{(t-y)^2}\,dt + \kappa\lambda^2\left[\frac{1}{8}(\lambda_2^2-\lambda_1^2)-\frac{1}{2}\lambda_2^2\right]\frac{1}{\pi}\int_{L_n}\frac{g_4(t)}{t-y}\,dt$$

$$+\frac{1}{\pi}\sum_{i=3}^{5}\int_a^b g_i(t)K_{i3}(z)\,dt - \gamma_{33}u_3(y) = -\overset{\infty}{V}_x = -8(1+\nu)/5\overset{\infty}{\sigma}_3 \;, \quad (6.3)$$

$$\frac{1}{2\pi}\fint_a^b \frac{g_4(t)}{(t-y)^2}\,dt + \frac{1}{\pi}\sum_{i=3}^{5}\int_a^b g_i(t)K_{i4}(z)\,dt$$

$$- \gamma_{44}u_4(y) - \gamma_{45}u_5(y) = -\overset{\infty}{N}_{xy} = -\overset{\infty}{\sigma}_4 \;, \quad (6.4)$$

$$\frac{(1-\nu^2)}{\lambda^4 2\pi} \fint_a^b \frac{g_5(t)}{(t-y)^2}\, dt + \left[\frac{3\lambda_2^2+\lambda_1^2}{8\lambda^2}\right] \frac{1}{\pi} \fint_{L_n} \frac{g_3(t)}{t-y}\, dt$$

$$+ \frac{1}{\pi}\sum_{i=3}^{3}\int_a^b g_i(t)K_{i5}(z)\, dt - \gamma_{54}u_4(y) - \gamma_{55}u_5(y) = -\overset{\infty}{M}_{xy} = -\overset{\infty}{\sigma}_5/6 \ , \tag{6.5}$$

where,

$$g_3(y) = w(0^+,y) = u_3(y) \ , \tag{6.6}$$

$$g_4(y)=v(0^+,y)-(\lambda_2^2/\lambda)^2 y w(0^+,y) = u_4(y)-(\lambda_2^2/\lambda)^2 y u_3(y) \ , \tag{6.7}$$

$$u_4(y) = g_4(y) + (\lambda_2^2/\lambda)^2 y g_3(y) \ , \tag{6.8}$$

$$g_5(y) = \beta_y(0^+,y) = u_5(y) \ . \tag{6.9}$$

The Fredholm kernels may be obtained from Chapter 5 and Appendix J.

Because of the assumption made in Eqn. 2.12 (see Eqn. 6.10) concerning self-similar crack growth under mode 2 loading, solutions to these equations apply only to cases where crack growth is coplanar. There are no solutions to compare with as in the mode 1 problem. If the results can be verified, then the mixed-mode solution involving all three modes should give good results. However the solution is not expected to be as accurate as for mode 1, since it was observed in Chapter 4 that there is very little difference in the value of the secondary SIF between the rectangular and the semi-elliptical profiles. In the latter case the secondary value should become of primary importance as the ends are approached because of changing crack front curvature. Physically the problem with the model is that everything is calculated in a plane perpendicular to the plate

surfaces, while the SIF is defined in a plane normal to the crack front. Considering this it is remarkable that the comparisons with the finite element solutions are so close for mode 1, see Figs. 4.1-4, 6.1,2. Perhaps the mechanism of the model is such that the energy release rate, the expression for which is repeated below,

$$\frac{d}{dL}(U-V) = G = \frac{1-\nu^2}{E}\left\{ K_1^2 + K_2^2 + \frac{1}{1-\nu} K_3^2 \right\} , \tag{6.10}$$

is more accurate than the individual values of the SIFs. If this is true, then it may explain why the secondary value of the line-spring SIF does not behave as expected, i.e. the above combination of K_2 and K_3 is more accurate. In the mode 1 case, it doesn't matter because there is only one non-zero value. Since the secondary value is zero in the center of the crack due to symmetry, the primary SIF may not be too affected by the rest of the curve. This of course is the most dependable value calculated by the LSM.

The results in tables 6.23-34 are for axial and circumferential semi-elliptical cracks in a cylinder of varying radius. Crack lengths and depths are also varied. The value at the center of the crack is reported. In the case of twisting, as can be seen from the plate results of Chapter 4, the maximum is typically at the ends. This is because of the strip results from Appendix C, table C.1 (σ_5), where the SIF decreases as the crack goes deeper into the plate. As with the mode 1 results, the plate solutions may be used to get an idea of the character of the distribution. The results for out-of-plane shear are nearly insensitive to radius, except for long and deep cracks. The in-plane shear, the most important loading case, behaves in a more

reasonable way. More results for the toroidal shell are presented in tables 6.35-46 for a/h=1,2, and R/h=10. As with the mode 1 tables, the elbow curvature is the parameter that is of most interest. Again these results are not very sensitive to curvature. This should be expected from the results of the cylinder.

Table 6.1 Mode 1 normalized stress intensity factors at the center of a semi-elliptical surface crack in a spherical shell, a/h=.5, ν=.3.

MEMBRANE LOADING

External crack

	R/h \ L_0/h	.2	.4	.6	.8	.95
$\frac{K_1(0)}{K_{1m}}$	5	.735	.400	.182	.0525	.00566
	10	.733	.396	.179	.0512	.00554
	20	.731	.394	.177	.0506	.00549
	50	.730	.392	.175	.0502	.00547
	$\to\infty$	.729	.390	.174	.0499	.00547

Internal crack

$\frac{K_1(0)}{K_{1m}}$	5	.718	.380	.172	.0514	.00594
	10	.723	.384	.173	.0506	.00571
	20	.725	.386	.173	.0502	.00559
	50	.727	.388	.174	.0500	.00552
	$\to\infty$	.792	.390	.174	.0499	.00547

BENDING

External crack

	R/h \ L_0/h	.2	.4	.6	.8	.95
$\frac{K_1(0)}{K_{1b}}$	5	.716	.318	.0630	-.0244	-.00910
	10	.713	.313	.0586	-.0262	-.00935
	20	.712	.310	.0562	-.0271	-.00947
	50	.710	.308	.0546	-.0276	-.00955
	$\to\infty$	.709	.306	.0532	-.0281	-.00960

Internal crack

$\frac{K_1(0)}{K_{1b}}$	5	.698	.294	.0501	-.0270	-.00925
	10	.702	.298	.0508	-.0277	-.00943
	20	.705	.301	.0516	-.0280	-.00951
	50	.707	.303	.0524	-.0281	-.00957
	$\to\infty$	.709	.306	.0532	-.0281	-.00960

Table 6.2 Mode 1 normalized stress intensity factors at the center of a semi-elliptical surface crack in a spherical shell, a/h=1, ν=.3.

MEMBRANE LOADING

	R/h \ L_0/h	.2	.4	.6	.8	.95
	External crack					
$\frac{K_1(0)}{K_{1m}}$	5	.824	.527	.267	.0834	.00967
	10	.822	.520	.258	.0784	.00895
	20	.821	.515	.252	.0756	.00862
	50	.819	.511	.248	.0739	.00844
	$\to\infty$	.817	.507	.244	.0725	.00833
	Internal crack					
$\frac{K_1(0)}{K_{1m}}$	5	.798	.481	.236	.0762	.00999
	10	.805	.490	.237	.0739	.00921
	20	.810	.496	.239	.0729	.00879
	50	.814	.501	.242	.0725	.00852
	$\to\infty$	.817	.507	.244	.0725	.00833

BENDING

	R/h \ L_0/h	.2	.4	.6	.8	.95
	External crack					
$\frac{K_1(0)}{K_{1b}}$	5	.812	.464	.160	-.0022	-.0086
	10	.810	.456	.150	-.0039	-.0096
	20	.808	.450	.143	-.0073	-.0101
	50	.807	.447	.138	-.0096	-.0104
	$\to\infty$	.804	.441	.133	-.0114	-.0106
	Internal crack					
$\frac{K_1(0)}{K_{1b}}$	5	.782	.409	.121	-.0087	-.0093
	10	.791	.419	.123	-.0107	-.0100
	20	.796	.427	.126	-.0114	-.0103
	50	.801	.434	.129	-.0116	-.0105
	$\to\infty$	.804	.441	.133	-.0114	-.0106

Table 6.3 Mode 1 normalized stress intensity factors at the center of a semi-elliptical surface crack in a spherical shell, a/h=2, ν=.3.

MEMBRANE LOADING

External crack

	L_0/h	.2	.4	.6	.8	.95
	R/h					
$\frac{K_1(0)}{K_{1m}}$	5	.882	.643	.375	.136	.0180
	10	.886	.644	.366	.124	.0152
	20	.886	.641	.356	.116	.0136
	50	.885	.635	.347	.109	.0126
	$\to\infty$	.883	.627	.336	.104	.0120

Internal crack

$\frac{K_1(0)}{K_{1m}}$	5	.851	.572	.310	.111	.0169
	10	.862	.589	.315	.106	.0147
	20	.870	.602	.320	.104	.0134
	50	.876	.613	.326	.103	.0126
	$\to\infty$	.883	.627	.336	.104	.0120

BENDING

External crack

	L_0/h	.2	.4	.6	.8	.95
	R/h					
$\frac{K_1(0)}{K_{1b}}$	5	.873	.595	.284	.0545	-.0034
	10	.878	.598	.275	.0421	-.0065
	20	.879	.595	.264	.0326	-.0084
	50	.878	.589	.253	.0251	-.0097
	$\to\infty$	.875	.578	.239	.0180	-.0107

Internal crack

$\frac{K_1(0)}{K_{1b}}$	5	.839	.513	.204	.0231	-.0064
	10	.852	.533	.212	.0188	-.0083
	20	.861	.549	.219	.0170	-.0094
	50	.868	.563	.227	.0166	-.0102
	$\to\infty$	.875	.578	.239	.0180	-.0107

Table 6.4 Mode 1 normalized stress intensity factors at the center of a semi-elliptical surface crack in a spherical shell, a/h=4, ν=.3.

MEMBRANE LOADING

	R/h \ L_0/h	.2	.4	.6	.8	.95
	External crack					
$\frac{K_1(0)}{K_{1m}}$	5	.907	.708	.458	.193	.0316
	10	.922	.739	.480	.191	.0273
	20	.929	.751	.484	.182	.0232
	50	.932	.753	.475	.168	.0196
	$\to\infty$	.930	.741	.450	.149	.0165
	Internal crack					
$\frac{K_1(0)}{K_{1m}}$	5	.884	.645	.384	.154	.0274
	10	.900	.674	.400	.151	.0237
	20	.911	.695	.413	.147	.0208
	50	.920	.715	.426	.146	.0184
	$\to\infty$	.930	.741	.450	.149	.0165

BENDING

	R/h \ L_0/h	.2	.4	.6	.8	.95
	External crack					
$\frac{K_1(0)}{K_{1b}}$	5	.899	.665	.372	.109	-.00620
	10	.916	.704	.404	.119	-.00281
	20	.925	.720	.412	.104	-.00130
	50	.928	.723	.403	.0888	-.00533
	$\to\infty$	.926	.710	.374	.0663	-.00918
	Internal crack					
$\frac{K_1(0)}{K_{1b}}$	5	.875	.595	.287	.0646	-.00005
	10	.892	.629	.309	.0634	-.00274
	20	.904	.655	.326	.0614	-.00528
	50	.914	.678	.343	.0608	-.00747
	$\to\infty$	.926	.710	.374	.0663	-.00918

Table 6.5 Mode 1 normalized stress intensity factors at the center of a semi-elliptical surface crack in a spherical shell, a/h=10, ν=.3.

MEMBRANE LOADING

External crack

	R/h \ L_0/h	.2	.4	.6	.8	.95
$\frac{K_1(0)}{K_{1m}}$	5	-	-	-	-	-
	10	.932	.771	.537	.243	.0429
	20	.950	.820	.598	.272	.0429
	50	.963	.856	.642	.288	.0391
	$\to\infty$	.968	.862	.624	.245	.0255

Internal crack

$\frac{K_1(0)}{K_{1m}}$	5	-	-	-	-	-
	10	.923	.741	.487	.207	.0373
	20	.939	.779	.526	.219	.0355
	50	.952	.813	.562	.227	.0318
	$\to\infty$	.968	.862	.624	.245	.0255

BENDING

External crack

	R/h \ L_0/h	.2	.4	.6	.8	.95
$\frac{K_1(0)}{K_{1b}}$	5	-	-	-	-	-
	10	.926	.735	.455	.154	.0122
	20	.945	.793	.533	.194	.0144
	50	.960	.838	.592	.219	.0120
	$\to\infty$	.966	.846	.576	.173	-.00266

Internal crack

$\frac{K_1(0)}{K_{1b}}$	5	-	-	-	-	-
	10	.917	.702	.403	.119	.00664
	20	.934	.748	.453	.136	.00605
	50	.948	.788	.499	.149	.00319
	$\to\infty$	.966	.846	.576	.173	-.00266

Table 6.6 Distribution of the mode 1 normalized stress intensity factor along a semi-elliptical surface crack in a toroidal shell located at different positions, see Fig. 6.5, a/h=1, R/h=10, $R_i/R=3$, $L_0/h=.4$, $\nu=.3$.

MEMBRANE LOADING

	Internal				External			
Position→ y/a	A	B	C	D	A	B	C	D
0.	.493	.497	.499	.501	.512	.521	.505	.517
.1	.492	.496	.498	.500	.511	.519	.504	.516
.2	.489	.493	.495	.497	.507	.516	.501	.513
.3	.484	.489	.490	.492	.502	.511	.496	.508
.4	.477	.482	.483	.485	.495	.503	.489	.500
.5	.468	.472	.473	.476	.484	.493	.479	.490
.6	.455	.460	.461	.463	.471	.479	.466	.477
.7	.439	.444	.445	.447	.454	.462	.450	.460
.8	.418	.423	.423	.426	.432	.439	.428	.437
.9	.389	.394	.393	.397	.401	.408	.398	.406
.95	.367	.373	.371	.375	.379	.385	.376	.384
.98	.348	.353	.352	.355	.358	.364	.355	.363

BENDING

	Internal				External			
Position→ y/a	A	B	C	D	A	B	C	D
0.	.423	.429	.431	.433	.446	.457	.439	.453
.1	.424	.430	.432	.434	.447	.458	.439	.454
.2	.427	.433	.435	.437	.449	.460	.442	.456
.3	.432	.437	.439	.442	.454	.464	.447	.461
.4	.438	.444	.446	.448	.459	.470	.453	.466
.5	.446	.452	.453	.456	.467	.477	.460	.473
.6	.456	.461	.462	.466	.475	.485	.469	.482
.7	.466	.472	.472	.476	.484	.493	.478	.490
.8	.476	.482	.482	.486	.493	.502	.488	.499
.9	.484	.491	.490	.494	.499	.507	.495	.505
.95	.485	.492	.490	.495	.499	.507	.495	.505
.98	.481	.488	.486	.491	.494	.502	.491	.500

Table 6.7 Mode 1 normalized stress intensity factors at the center of a semi-elliptical surface crack in a toroidal shell. The crack is located at position A of Fig. 6.5, a/h=.5, R/h=10, ν=.3.

MEMBRANE LOADING

External crack

	R_i/R \ L_0/h	.2	.4	.6	.8	.95
$\frac{K_1(0)}{K_{1m}}$	1	.731	.393	.177	.0506	.00550
	3	.730	.393	.176	.0505	.00549
	5	.730	.392	.176	.0505	.00549
	$\to\infty$	.729	.391	.175	.0503	.00549

Internal crack

$\frac{K_1(0)}{K_{1m}}$	1	.724	.385	.173	.0502	.00561
	3	.724	.385	.173	.0502	.00559
	5	.725	.386	.173	.0501	.00559
	$\to\infty$	.725	.386	.173	.0501	.00556

BENDING

External crack

	R_i/R \ L_0/h	.2	.4	.6	.8	.95
$\frac{K_1(0)}{K_{1b}}$	1	.711	.309	.0561	-.0270	-.00943
	3	.711	.308	.0556	-.0271	-.00945
	5	.710	.308	.0554	-.0272	-.00945
	$\to\infty$	.710	.307	.0548	-.0274	-.00947

Internal crack

$\frac{K_1(0)}{K_{1b}}$	1	.704	.299	.0510	-.0280	-.00948
	3	.704	.300	.0511	-.0280	-.00949
	5	.704	.300	.0512	-.0280	-.00950
	$\to\infty$	.705	.301	.0514	-.0280	-.00950

Table 6.8 Mode 1 normalized stress intensity factors at the center of a semi-elliptical surface crack in a toroidal shell. The crack is located at position B of Fig. 6.5, a/h=.5, R/h=10, ν=.3.

MEMBRANE LOADING

External crack

	R_i/R \ L_0/h	.2	.4	.6	.8	.95
$\frac{K_1(0)}{K_{1m}}$	1	.733	.396	.178	.0509	.00551
	3	.733	.396	.178	.0509	.00551
	5	.733	.396	.178	.0509	.00551
	$\to\infty$	.732	.395	.178	.0508	.00550

Internal crack

$\frac{K_1(0)}{K_{1m}}$	1	.725	.386	.173	.0504	.00565
	3	.725	.386	.173	.0504	.00564
	5	.725	.387	.173	.0504	.00564
	$\to\infty$	.726	.387	.174	.0504	.00562

BENDING

External crack

	R_i/R \ L_0/h	.2	.4	.6	.8	.95
$\frac{K_1(0)}{K_{1b}}$	1	.713	.312	.0578	-.0266	-.00943
	3	.713	.312	.0576	-.0267	-.00945
	5	.713	.312	.0576	-.0267	-.00945
	$\to\infty$	.713	.312	.0574	-.0268	-.00947

Internal crack

$\frac{K_1(0)}{K_{1b}}$	1	.705	.300	.0516	-.0278	-.00949
	3	.705	.301	.0518	-.0278	-.00950
	5	.705	.301	.0519	-.0278	-.00951
	$\to\infty$	.706	.302	.0521	-.0279	-.00952

Table 6.9 Mode 1 normalized stress intensity factors at the center of a semi-elliptical surface crack in a toroidal shell. The crack is located at position C of Fig. 6.5, a/h=.5, R/h=10, ν=.3.

MEMBRANE LOADING

	R_i/R \ L_0/h	.2	.4	.6	.8	.95
External crack						
$\frac{K_1(0)}{K_{1m}}$	1	.727	.388	.174	.0505	.00560
	3	.728	.390	.175	.0503	.00551
	5	.729	.391	.175	.0503	.00550
	$\to\infty$	.729	.391	.175	.0503	.00549
Internal crack						
$\frac{K_1(0)}{K_{1m}}$	1	.729	.392	.176	.0506	.00555
	3	.726	.388	.174	.0502	.00554
	5	.726	.387	.173	.0501	.00555
	$\to\infty$	.725	.386	.173	.0501	.00556

BENDING

	R_i/R \ L_0/h	.2	.4	.6	.8	.95
External crack						
$\frac{K_1(0)}{K_{1b}}$	1	.707	.303	.0532	-.0275	-.00946
	3	.708	.305	.0539	-.0275	-.00948
	5	.709	.306	.0542	-.0275	-.00948
	$\to\infty$	.710	.307	.0548	-.0274	-.00947
Internal crack						
$\frac{K_1(0)}{K_{1b}}$	1	.710	.307	.0551	-.0271	-.00944
	3	.707	.303	.0525	-.0278	-.00950
	5	.706	.302	.0520	-.0279	-.00950
	$\to\infty$	.705	.301	.0514	-.0280	-.00950

Table 6.10 Mode 1 normalized stress intensity factors at the center of a semi-elliptical surface crack in a toroidal shell. The crack is located at position D of Fig. 6.5, a/h=.5, R/h=10, ν=.3.

MEMBRANE LOADING

External crack

	L_0/h	.2	.4	.6	.8	.95
	R_i/R					
$\frac{K_1(0)}{K_{1m}}$	1	.729	.392	.176	.0506	.00555
	3	.732	.394	.177	.0507	.00551
	5	.732	.395	.177	.0507	.00551
	$\to\infty$	.732	.395	.178	.0508	.00550

Internal crack

$\frac{K_1(0)}{K_{1m}}$	1	.727	.388	.174	.0505	.00560
	3	.726	.388	.174	.0504	.00561
	5	.726	.388	.174	.0504	.00561
	$\to\infty$	.726	.387	.174	.0504	.00562

BENDING

External crack

	L_0/h	.2	.4	.6	.8	.95
	R_i/R					
$\frac{K_1(0)}{K_{1b}}$	1	.710	.307	.0551	-.0271	-.00944
	3	.712	.311	.0567	-.0270	-.00948
	5	.713	.311	.0570	-.0269	-.00948
	$\to\infty$	.713	.312	.0574	-.0268	-.00947

Internal crack

$\frac{K_1(0)}{K_{1b}}$	1	.707	.303	.0532	-.0275	-.00946
	3	.706	.303	.0525	-.0278	-.00952
	5	.706	.302	.0523	-.0278	-.00952
	$\to\infty$	.706	.302	.0521	-.0279	-.00952

Table 6.11 Mode 1 normalized stress intensity factors at the center of a semi-elliptical surface crack in a toroidal shell. The crack is located at position A of Fig. 6.5, a/h=1, R/h=10, ν=.3.

MEMBRANE LOADING

	R_i/R \ L_0/h	.2	.4	.6	.8	.95
	External crack					
$\frac{K_1(0)}{K_{1m}}$	1	.819	.513	.252	.0757	.00866
	3	.819	.512	.250	.0752	.00861
	5	.818	.511	.250	.0749	.00859
	$\to\infty$	.817	.509	.248	.0743	.00854
	Internal crack					
$\frac{K_1(0)}{K_{1m}}$	1	.807	.492	.237	.0727	.00885
	3	.808	.493	.237	.0725	.00878
	5	.808	.493	.238	.0724	.00875
	$\to\infty$	.810	.494	.238	.0723	.00867

BENDING

	R_i/R \ L_0/h	.2	.4	.6	.8	.95
	External crack					
$\frac{K_1(0)}{K_{1b}}$	1	.807	.448	.142	-.0071	-.0100
	3	.806	.446	.140	-.0078	-.0100
	5	.805	.445	.139	-.0081	-.0101
	$\to\infty$	.804	.443	.137	-.0089	-.0102
	Internal crack					
$\frac{K_1(0)}{K_{1b}}$	1	.793	.422	.123	-.0117	-.0102
	3	.794	.423	.124	-.0119	-.0103
	5	.794	.424	.124	-.0119	-.0103
	$\to\infty$	.795	.425	.124	-.0120	-.0103

Table 6.12 Mode 1 normalized stress intensity factors at the center of a semi-elliptical surface crack in a toroidal shell. The crack is located at position B of Fig. 6.5, a/h=1, R/h=10, ν=.3.

MEMBRANE LOADING

External crack

	R_i/R \ L_0/h	.2	.4	.6	.8	.95
$\frac{K_1(0)}{K_{1m}}$	1	.823	.520	.257	.0773	.00879
	3	.824	.521	.257	.0771	.00875
	5	.884	.520	.256	.0770	.00874
	$\to\infty$	.824	.520	.256	.0768	.00871

Internal crack

$\frac{K_1(0)}{K_{1m}}$	1	.809	.496	.240	.0738	.00901
	3	.810	.497	.241	.0738	.00897
	5	.811	.498	.241	.0738	.00895
	$\to\infty$	.812	.499	.242	.0738	.00890

BENDING

External crack

	R_i/R \ L_0/h	.2	.4	.6	.8	.95
$\frac{K_1(0)}{K_{1b}}$	1	.811	.457	.148	-.0052	-.0099
	3	.811	.457	.148	-.0055	-.0099
	5	.811	.457	.148	-.0056	-.0100
	$\to\infty$	.811	.457	.147	-.0060	-.0100

Internal crack

$\frac{K_1(0)}{K_{1b}}$	1	.796	.427	.127	-.0107	-.0102
	3	.797	.429	.128	-.0107	-.0102
	5	.797	.429	.128	-.0107	-.0102
	$\to\infty$	.798	.431	.129	-.0106	-.0103

Table 6.13 Mode 1 normalized stress intensity factors at the center of a semi-elliptical surface crack in a toroidal shell. The crack is located at position C of Fig. 6.5, a/h=1, R/h=10, ν=.3.

MEMBRANE LOADING

	R_i/R \ L_0/h	.2	.4	.6	.8	.95
External crack						
$\frac{K_1(0)}{K_{1m}}$	1	.813	.502	.244	.0744	.00888
	3	.815	.505	.245	.0739	.00859
	5	.816	.506	.246	.0739	.00855
	$\to\infty$	.817	.509	.248	.0743	.00854
Internal crack						
$\frac{K_1(0)}{K_{1m}}$	1	.817	.509	.249	.0753	.00880
	3	.812	.499	.241	.0730	.00865
	5	.811	.497	.240	.0726	.00864
	$\to\infty$	.810	.494	.238	.0723	.00867

BENDING

	R_i/R \ L_0/h	.2	.4	.6	.8	.95
External crack						
$\frac{K_1(0)}{K_{1b}}$	1	.799	.434	.132	-.0094	-.0101
	3	.802	.439	.134	-.0096	-.0102
	5	.803	.440	.135	-.0094	-.0102
	$\to\infty$	.804	.443	.137	-.0089	-.0102
Internal crack						
$\frac{K_1(0)}{K_{1b}}$	1	.804	.442	.138	-.0080	-.0100
	3	.798	.431	.129	-.0109	-.0103
	5	.797	.429	.127	-.0115	-.0103
	$\to\infty$	.795	.425	.124	-.0120	-.0103

Table 6.14 Mode 1 normalized stress intensity factors at the center of a semi-elliptical surface crack in a toroidal shell. The crack is located at position D of Fig. 6.5, a/h=1, R/h=10, ν=.3.

MEMBRANE LOADING

	R_i/R \ L_0/h	.2	.4	.6	.8	.95
External crack						
$\frac{K_1(0)}{K_{1m}}$	1	.817	.509	.249	.0753	.00880
	3	.822	.517	.254	.0762	.00871
	5	.823	.519	.255	.0764	.00870
	$\to\infty$	.824	.520	.256	.0768	.00871
Internal crack						
$\frac{K_1(0)}{K_{1m}}$	1	.813	.502	.244	.0744	.00888
	3	.813	.501	.243	.0739	.00886
	5	.813	.501	.242	.0739	.00887
	$\to\infty$	.812	.499	.242	.0738	.00890

BENDING

	R_i/R \ L_0/h	.2	.4	.6	.8	.95
External crack						
$\frac{K_1(0)}{K_{1b}}$	1	.804	.442	.138	-.0080	-.0100
	3	.810	.453	.145	-.0067	-.0101
	5	.811	.455	.146	-.0064	-.0101
	$\to\infty$	.811	.457	.147	-.0060	-.0100
Internal crack						
$\frac{K_1(0)}{K_{1b}}$	1	.799	.434	.132	-.0094	-.0101
	3	.799	.433	.131	-.0103	-.0103
	5	.799	.433	.130	-.0104	-.0103
	$\to\infty$	.798	.431	.129	-.0106	-.0103

Table 6.15 Mode 1 normalized stress intensity factors at the center of a semi-elliptical surface crack in a toroidal shell. The crack is located at position A of Fig. 6.5, a/h=2, R/h=10, ν=.3.

MEMBRANE LOADING

	R_i/R \ L_0/h	.2	.4	.6	.8	.95
External crack						
$\frac{K_1(0)}{K_{1m}}$	1	.883	.633	.351	.115	.0138
	3	.882	.630	.348	.113	.0135
	5	.881	.629	.346	.112	.0133
	$\to\infty$	.880	.625	.341	.109	.0130
Internal crack						
$\frac{K_1(0)}{K_{1m}}$	1	.864	.591	.313	.1024	.0136
	3	.865	.592	.312	.1017	.0133
	5	.865	.592	.313	.1014	.0132
	$\to\infty$	.867	.594	.313	.1008	.0129

BENDING

	R_i/R \ L_0/h	.2	.4	.6	.8	.95
External crack						
$\frac{K_1(0)}{K_{1b}}$	1	.874	.586	.258	.0318	-.00803
	3	.873	.582	.253	.0293	-.00838
	5	.873	.581	.251	.0282	-.00853
	$\to\infty$	.871	.576	.245	.0251	-.00893
Internal crack						
$\frac{K_1(0)}{K_{1b}}$	1	.854	.535	.209	.0151	-.00920
	3	.855	.537	.209	.0144	-.00939
	5	.855	.537	.209	.0141	-.00948
	$\to\infty$	.857	.539	.210	.0136	-.00968

Table 6.16 Mode 1 normalized stress intensity factors at the center of a semi-elliptical surface crack in a toroidal shell. The crack is located at position B of Fig. 6.5, a/h=2, R/h=10, ν=.3.

MEMBRANE LOADING

External crack

	R_i/R \ L_0/h	.2	.4	.6	.8	.95
$\frac{K_1(0)}{K_{1m}}$	1	.890	.650	.368	.122	.0145
	3	.891	.652	.369	.122	.0143
	5	.891	.652	.369	.121	.0142
	$\to\infty$	.892	.653	.369	.121	.0141

Internal crack

$\frac{K_1(0)}{K_{1m}}$	1	.870	.604	.324	.107	.0142
	3	.872	.607	.326	.107	.0141
	5	.873	.609	.327	.107	.0140
	$\to\infty$	.875	.613	.330	.108	.0139

BENDING

External crack

	R_i/R \ L_0/h	.2	.4	.6	.8	.95
$\frac{K_1(0)}{K_{1b}}$	1	.882	.606	.279	.0400	-.00745
	3	.883	.608	.279	.0394	-.00767
	5	.884	.608	.279	.0391	-.00777
	$\to\infty$	.884	.610	.279	.0384	-.00803

Internal crack

$\frac{K_1(0)}{K_{1b}}$	1	.861	.551	.224	.0202	-.00884
	3	.863	.555	.227	.0206	-.00896
	5	.864	.557	.228	.0208	-.00901
	$\to\infty$	.866	.562	.232	.0214	-.00914

Table 6.17 Mode 1 normalized stress intensity factors at the center of a semi-elliptical surface crack in a toroidal shell. The crack is located at position C of Fig. 6.5, a/h=2, R/h=10, ν=.3.

MEMBRANE LOADING

	R_i/R \ L_0/h	.2	.4	.6	.8	.95
External crack						
$\frac{K_1(0)}{K_{1m}}$	1	.875	.614	.333	.110	.0140
	3	.877	.618	.335	.108	.0131
	5	.878	.620	.336	.108	.0130
	$\to\infty$	.880	.625	.341	.109	.0130
Internal crack						
$\frac{K_1(0)}{K_{1m}}$	1	.879	.623	.342	.1122	.0140
	3	.871	.605	.322	.1037	.0130
	5	.869	.600	.318	.1022	.0129
	$\to\infty$	.867	.594	.313	.1008	.0129

BENDING

	R_i/R \ L_0/h	.2	.4	.6	.8	.95
External crack						
$\frac{K_1(0)}{K_{1b}}$	1	.866	.563	.235	.0243	-.00849
	3	.868	.568	.237	.0228	-.00905
	5	.869	.570	.239	.0231	-.00909
	$\to\infty$	.871	.576	.245	.0251	-.00893
Internal crack						
$\frac{K_1(0)}{K_{1b}}$	1	.870	.574	.245	.0275	-.00829
	3	.862	.552	.222	.0174	-.00941
	5	.860	.547	.217	.0155	-.00958
	$\to\infty$	.857	.539	.210	.0136	-.00968

Table 6.18 Mode 1 normalized stress intensity factors at the center of a semi-elliptical surface crack in a toroidal shell. The crack is located at position D of Fig. 6.5, a/h=2, R/h=10, ν=.3.

MEMBRANE LOADING

	R_i/R \ L_0/h	.2	.4	.6	.8	.95
External crack						
$\frac{K_1(0)}{K_{1m}}$	1	.879	.623	.342	.112	.0140
	3	.889	.645	.361	.118	.0139
	5	.890	.650	.365	.119	.0139
	$\to\infty$	.892	.653	.369	.121	.0141
Internal crack						
$\frac{K_1(0)}{K_{1m}}$	1	.875	.614	.333	.110	.0140
	3	.876	.616	.333	.108	.0138
	5	.876	.615	.332	.108	.0138
	$\to\infty$	.875	.613	.330	.108	.0139

BENDING

	R_i/R \ L_0/h	.2	.4	.6	.8	.95
External crack						
$\frac{K_1(0)}{K_{1b}}$	1	.870	.574	.245	.0275	-.00829
	3	.881	.601	.270	.0346	-.00827
	5	.883	.605	.274	.0363	-.00822
	$\to\infty$	.884	.610	.279	.0384	-.00803
Internal crack						
$\frac{K_1(0)}{K_{1b}}$	1	.866	.563	.235	.0243	-.00849
	3	.867	.565	.235	.0224	-.00906
	5	.867	.565	.234	.0220	-.00913
	$\to\infty$	.866	.562	.232	.0214	-.00914

Table 6.19 Mode 1 normalized stress intensity factors at the center of a semi-elliptical surface crack in a toroidal shell. The crack is located at position A of Fig. 6.5, a/h=4, R/h=10, ν=.3.

MEMBRANE LOADING

	R_i/R \ L_0/h	.2	.4	.6	.8	.95
External crack						
$\frac{K_1(0)}{K_{1m}}$	1	.921	.732	.463	.174	.0232
	4	.920	.727	.455	.168	.0219
	7	.920	.725	.452	.165	.0214
	$\to\infty$	.919	.720	.443	.159	.0203
Internal crack						
$\frac{K_1(0)}{K_{1m}}$	1	.900	.672	.392	.141	.0208
	4	.901	.672	.390	.138	.0199
	7	.901	.672	.389	.137	.0196
	$\to\infty$	.902	.674	.389	.135	.0189

BENDING

	R_i/R \ L_0/h	.2	.4	.6	.8	.95
External crack						
$\frac{K_1(0)}{K_{1b}}$	1	.916	.696	.385	.0943	-.00107
	4	.915	.692	.376	.0870	-.00245
	7	.914	.689	.372	.0841	-.00297
	$\to\infty$	.913	.684	.362	.0770	-.00416
Internal crack						
$\frac{K_1(0)}{K_{1b}}$	1	.893	.627	.300	.0538	-.00509
	4	.893	.627	.297	.0507	-.00587
	7	.894	.627	.296	.0496	-.00615
	$\to\infty$	.895	.628	.296	.0477	-.00673

Table 6.20 Mode 1 normalized stress intensity factors at the center of a semi-elliptical surface crack in a toroidal shell. The crack is located at position B of Fig. 6.5, a/h=4, R/h=10, ν=.3.

MEMBRANE LOADING

External crack

	L_0/h	.2	.4	.6	.8	.95
R_i/R						
$\frac{K_1(0)}{K_{1m}}$	1	.933	.763	.503	.197	.0260
	4	.935	.769	.509	.198	.0255
	7	.936	.771	.511	.198	.0253
	$\to\infty$	.938	.775	.515	.199	.0249

Internal crack

$\frac{K_1(0)}{K_{1m}}$	1	.913	.703	.425	.156	.0227
	4	.917	.713	.434	.159	.0224
	7	.918	.716	.437	.159	.0223
	$\to\infty$	.921	.723	.444	.162	.0222

BENDING

External crack

	L_0/h	.2	.4	.6	.8	.95
R_i/R						
$\frac{K_1(0)}{K_{1b}}$	1	.928	.734	.435	.120	.00142
	4	.931	.742	.443	.122	.00088
	7	.932	.744	.445	.123	.00068
	$\to\infty$	.934	.749	.451	.124	.00021

Internal crack

$\frac{K_1(0)}{K_{1b}}$	1	.907	.665	.341	.0713	-.00363
	4	.911	.676	.352	.0744	-.00387
	7	.913	.680	.356	.0756	-.00395
	$\to\infty$	.916	.689	.365	.0783	-.00410

Table 6.21 Mode 1 normalized stress intensity factors at the center of a semi-elliptical surface crack in a toroidal shell. The crack is located at position C of Fig. 6.5, a/h=4, R/h=10, ν=.3.

MEMBRANE LOADING

External crack

	R_i/R \ L_0/h	.2	.4	.6	.8	.95
$\frac{K_1(0)}{K_{1m}}$	1	.915	.712	.437	.162	.0228
	4	.917	.714	.435	.155	.0202
	7	.917	.715	.437	.156	.0200
	$\to\infty$	.919	.720	.443	.159	.0203

Internal crack

$\frac{K_1(0)}{K_{1m}}$	1	.916	.715	.439	.162	.0225
	4	.907	.686	.402	.141	.0193
	7	.905	.680	.395	.138	.0190
	$\to\infty$	.902	.674	.389	.135	.0189

BENDING

External crack

	R_i/R \ L_0/h	.2	.4	.6	.8	.95
$\frac{K_1(0)}{K_{1b}}$	1	.909	.674	.355	.0789	-.00259
	4	.910	.676	.352	.0724	-.00453
	7	.911	.678	.354	.0728	-.00462
	$\to\infty$	.913	.684	.362	.0770	-.00416

Internal crack

$\frac{K_1(0)}{K_{1b}}$	1	.910	.676	.356	.0784	-.00283
	4	.900	.643	.312	.0542	-.00615
	7	.897	.636	.304	.0507	-.00655
	$\to\infty$	.895	.628	.296	.0477	-.00673

Table 6.22 Mode 1 normalized stress intensity factors at the center of a semi-elliptical surface crack in a toroidal shell. The crack is located at position D of Fig. 6.5, a/h=4, R/h=10, ν=.3.

MEMBRANE LOADING

	R_i/R \ L_0/h	.2	.4	.6	.8	.95
External crack						
$\frac{K_1(0)}{K_{1m}}$	1	.916	.715	.439	.162	.0225
	4	.935	.766	.500	.190	.0239
	7	.937	.772	.509	.195	.0243
	$\to\infty$	.938	.775	.515	.199	.0249
Internal crack						
$\frac{K_1(0)}{K_{1m}}$	1	.915	.712	.437	.162	.0228
	4	.922	.726	.448	.163	.0221
	7	.923	.726	.448	.163	.0221
	$\to\infty$	.921	.723	.444	.162	.0222

BENDING

	R_i/R \ L_0/h	.2	.4	.6	.8	.95
External crack						
$\frac{K_1(0)}{K_{1b}}$	1	.910	.676	.356	.078	-.00283
	4	.931	.738	.432	.112	-.00103
	7	.933	.745	.443	.118	-.00051
	$\to\infty$	.934	.749	.451	.124	.00021
Internal crack						
$\frac{K_1(0)}{K_{1b}}$	1	.909	.674	.355	.0789	-.00259
	4	.917	.692	.370	.0803	-.00394
	7	.917	.692	.369	.0800	-.00407
	$\to\infty$	.916	.689	.365	.0783	-.00410

Table 6.23 Mode 3 normalized stress intensity factor at the center of a semi-elliptical surface crack in a cylindrical shell subjected to in-plane shear, a/h=.5, ν=.3.

IN-PLANE SHEAR

		Outer axial crack				
	L_0/h	.2	.4	.6	.8	.95
	R/h					
$\frac{K_3(0)}{K_{3I}}$	5	.736	.545	.466	.351	.186
	10	.737	.546	.466	.350	.185
	20	.737	.546	.466	.350	.185
	50	.738	.547	.466	.350	.184
	$\to\infty$	.738	.547	.467	.350	.184
		Inner axial crack				
$\frac{K_3(0)}{K_{3I}}$	5	.740	.550	.470	.352	.185
	10	.739	.549	.468	.351	.184
	20	.739	.548	.467	.350	.184
	50	.738	.547	.467	.350	.184
	$\to\infty$	.738	.547	.467	.350	.184

		Outer circumferential crack				
	L_0/h	.2	.4	.6	.8	.95
	R/h					
$\frac{K_3(0)}{K_{3I}}$	5	.736	.545	.466	.351	.186
	10	.737	.546	.466	.350	.185
	20	.737	.546	.466	.350	.185
	50	.738	.547	.466	.350	.184
	$\to\infty$	.738	.547	.467	.350	.184
		Inner circumferential crack				
$\frac{K_3(0)}{K_{3I}}$	5	.740	.550	.470	.352	.185
	10	.739	.549	.468	.351	.185
	20	.739	.548	.468	.350	.184
	50	.738	.548	.467	.350	.184
	$\to\infty$	.738	.547	.467	.350	.184

Table 6.24 Mode 2 normalized stress intensity factor at the center of a semi-elliptical surface crack in a cylindrical shell subjected to out-of-plane shear, a/h=.5, ν=.3.

OUT-OF-PLANE SHEAR

Outer axial crack

	R/h \ L_0/h	.2	.4	.6	.8	.95
$\frac{K_2(0)}{K_{20}}$	5	.988	.883	.684	.466	.277
	10	.988	.883	.685	.467	.277
	20	.988	.883	.685	.467	.277
	50	.988	.883	.685	.467	.277
	$\to\infty$	.988	.883	.685	.467	.277

Inner axial crack

$\frac{K_2(0)}{K_{20}}$	5	.988	.883	.685	.467	.277
	10	.988	.883	.685	.467	.277
	20	.988	.883	.685	.467	.277
	50	.988	.883	.685	.467	.277
	$\to\infty$	.988	.883	.685	.467	.277

Outer circumferential crack

	R/h \ L_0/h	.2	.4	.6	.8	.95
$\frac{K_2(0)}{K_{20}}$	5	.988	.882	.682	.463	.274
	10	.988	.883	.684	.466	.276
	20	.988	.883	.685	.467	.277
	50	.988	.883	.685	.467	.277
	$\to\infty$	.988	.883	.685	.467	.277

Inner circumferential crack

$\frac{K_2(0)}{K_{20}}$	5	.988	.882	.683	.464	.275
	10	.988	.883	.684	.466	.277
	20	.988	.883	.685	.467	.277
	50	.988	.883	.685	.467	.277
	$\to\infty$	.988	.883	.685	.467	.277

Table 6.25 Mode 3 normalized stress intensity factor at the center of a semi-elliptical surface crack in a cylindrical shell subjected to twisting, a/h=.5, ν=.3.

TWISTING

Outer axial crack

	R/h \ L_0/h	.2	.4	.6	.8	.95
$\frac{K_3(0)}{K_{3T}}$	5	.710	.408	.102	-.637	-6.01
	10	.711	.409	.102	-.637	-6.01
	20	.711	.410	.103	-.637	-6.01
	50	.712	.410	.103	-.637	-6.01
	$\to\infty$	.712	.411	.103	-.636	-6.01

Inner axial crack

$\frac{K_3(0)}{K_{3T}}$	5	.714	.415	.110	-.624	-5.94
	10	.713	.413	.107	-.630	-5.97
	20	.713	.412	.105	-.633	-5.99
	50	.712	.411	.104	-.635	-6.00
	$\to\infty$	.712	.411	.103	-.636	-6.01

Outer circumferential crack

	R/h \ L_0/h	.2	.4	.6	.8	.95
$\frac{K_3(0)}{K_{3T}}$	5	.710	.408	.101	-.637	-6.01
	10	.711	.409	.102	-.638	-6.01
	20	.711	.410	.102	-.637	-6.01
	50	.712	.410	.103	-.637	-6.01
	$\to\infty$	.712	.411	.103	-.636	-6.01

Inner circumferential crack

$\frac{K_3(0)}{K_{3T}}$	5	.714	.415	.111	-.622	-5.93
	10	.713	.413	.107	-.629	-5.97
	20	.713	.412	.106	-.632	-5.98
	50	.712	.411	.104	-.634	-6.00
	$\to\infty$	.712	.411	.103	-.636	-6.01

Table 6.26 Mode 3 normalized stress intensity factor at the center of a semi-elliptical surface crack in a cylindrical shell subjected to in-plane shear, a/h=1., ν=.3.

IN-PLANE SHEAR

	R/h \ L_0/h	.2	.4	.6	.8	.95
	Outer axial crack					
$\frac{K_3(0)}{K_{3I}}$	5	.797	.632	.576	.492	.304
	10	.798	.633	.576	.490	.301
	20	.799	.634	.576	.489	.300
	50	.799	.635	.576	.489	.299
	→∞	.800	.635	.577	.489	.299
	Inner axial crack					
$\frac{K_3(0)}{K_{3I}}$	5	.803	.641	.585	.496	.303
	10	.802	.639	.581	.493	.301
	20	.801	.637	.579	.491	.300
	50	.800	.636	.578	.490	.299
	→∞	.800	.635	.577	.489	.299

	R/h \ L_0/h	.2	.4	.6	.8	.95
	Outer circumferential crack					
$\frac{K_3(0)}{K_{3I}}$	5	.797	.631	.575	.492	.305
	10	.798	.633	.575	.490	.302
	20	.799	.634	.576	.489	.300
	50	.799	.634	.576	.489	.299
	→∞	.800	.635	.577	.489	.299
	Inner circumferential crack					
$\frac{K_3(0)}{K_{3I}}$	5	.803	.642	.586	.498	.304
	10	.802	.639	.582	.494	.301
	20	.801	.638	.580	.491	.300
	50	.800	.636	.578	.490	.299
	→∞	.800	.635	.577	.489	.299

Table 6.27 Mode 2 normalized stress intensity factor at the center of a semi-elliptical surface crack in a cylindrical shell subjected to out-of-plane shear, a/h=1., ν=.3.

OUT-OF-PLANE SHEAR

	R/h \ L_0/h	.2	.4	.6	.8	.95
	Outer axial crack					
$\frac{K_2(0)}{K_{20}}$	5	.996	.953	.850	.691	.485
	10	.996	.953	.851	.692	.486
	20	.996	.953	.851	.693	.487
	50	.996	.953	.851	.693	.487
	$\to\infty$	.996	.953	.851	.693	.487
	Inner axial crack					
$\frac{K_2(0)}{K_{20}}$	5	.996	.953	.851	.693	.486
	10	.996	.953	.851	.693	.487
	20	.996	.953	.851	.693	.487
	50	.996	.953	.851	.693	.487
	$\to\infty$	.996	.953	.851	.693	.487

	R/h \ L_0/h	.2	.4	.6	.8	.95
	Outer circumferential crack					
$\frac{K_2(0)}{K_{20}}$	5	.995	.951	.844	.679	.472
	10	.996	.953	.849	.688	.482
	20	.996	.953	.850	.691	.485
	50	.996	.953	.851	.693	.487
	$\to\infty$	.996	.953	.851	.693	.487
	Inner circumferential crack					
$\frac{K_2(0)}{K_{20}}$	5	.995	.952	.846	.685	.477
	10	.996	.953	.850	.691	.485
	20	.996	.953	.851	.693	.487
	50	.996	.953	.851	.693	.487
	$\to\infty$	.996	.953	.851	.693	.487

Table 6.28 Mode 3 normalized stress intensity factor at the center of a semi-elliptical surface crack in a cylindrical shell subjected to twisting, a/h=1., ν=.3.

TWISTING

	R/h \ L_0/h	.2	.4	.6	.8	.95
	Outer axial crack					
$\frac{K_3(0)}{K_{3T}}$	5	.776	.519	.273	-.334	-5.25
	10	.777	.520	.274	-.337	-5.27
	20	.778	.521	.275	-.337	-5.27
	50	.779	.522	.276	-.336	-5.27
	$\to\infty$	.779	.523	.277	-.335	-5.27
	Inner axial crack					
$\frac{K_3(0)}{K_{3T}}$	5	.783	.531	.292	-.298	-5.05
	10	.781	.528	.286	-.314	-5.15
	20	.780	.526	.282	-.324	-5.20
	50	.780	.525	.279	-.330	-5.24
	$\to\infty$	.779	.523	.277	-.335	-5.27

	R/h \ L_0/h	.2	.4	.6	.8	.95
	Outer circumferential crack					
$\frac{K_3(0)}{K_{3T}}$	5	.776	.517	.271	-.336	-5.27
	10	.777	.519	.273	-.339	-5.28
	20	.778	.521	.274	-.338	-5.28
	50	.779	.522	.275	-.337	-5.28
	$\to\infty$	.779	.523	.277	-.335	-5.27
	inner circumferential crack					
$\frac{K_3(0)}{K_{3T}}$	5	.783	.533	.296	-.289	-4.99
	10	.782	.529	.287	-.310	-5.12
	20	.781	.526	.283	-.322	-5.19
	50	.780	.525	.280	-.329	-5.23
	$\to\infty$	.779	.523	.277	-.335	-5.27

Table 6.29 Mode 3 normalized stress intensity factor at the center of a semi-elliptical surface crack in a cylindrical shell subjected to in-plane shear, a/h=2., ν=.3.

IN-PLANE SHEAR

	R/h \ L_0/h	.2	.4	.6	.8	.95
	Outer axial crack					
$\frac{K_3(0)}{K_{3I}}$	5	.826	.684	.659	.631	.457
	10	.827	.684	.658	.626	.449
	20	.828	.685	.658	.624	.445
	50	.829	.686	.658	.623	.443
	$\to\infty$	.829	.687	.659	.623	.442
	Inner axial crack					
$\frac{K_3(0)}{K_{3I}}$	5	.833	.696	.673	.641	.458
	10	.832	.693	.668	.633	.451
	20	.831	.691	.664	.629	.447
	50	.830	.689	.662	.625	.444
	$\to\infty$	.829	.687	.659	.623	.442

	R/h \ L_0/h	.2	.4	.6	.8	.95
	Outer circumferential crack					
$\frac{K_3(0)}{K_{3I}}$	5	.825	.682	.657	.632	.463
	10	.827	.683	.657	.626	.451
	20	.828	.685	.657	.623	.446
	50	.828	.686	.658	.623	.443
	$\to\infty$	.829	.687	.659	.623	.442
	Inner circumferential crack					
$\frac{K_3(0)}{K_{3I}}$	5	.834	.699	.677	.647	.463
	10	.832	.694	.670	.636	.452
	20	.831	.692	.665	.630	.447
	50	.830	.689	.662	.626	.444
	$\to\infty$	.829	.687	.659	.623	.442

Table 6.30 Mode 2 normalized stress intensity factor at the center of a semi-elliptical surface crack in a cylindrical shell subjected to out-of-plane shear, a/h=2., ν=.3.

OUT-OF-PLANE SHEAR

Outer axial crack

	R/h \ L_0/h	.2	.4	.6	.8	.95
$\frac{K_2(0)}{K_{20}}$	5	.999	.986	.948	.871	.716
	10	.999	.986	.950	.874	.720
	20	.999	.986	.950	.875	.722
	50	.999	.986	.950	.875	.723
	$\to\infty$	.999	.986	.950	.876	.723

Inner axial crack

$\frac{K_2(0)}{K_{20}}$	5	.999	.986	.950	.876	.722
	10	.999	.986	.950	.876	.723
	20	.999	.986	.950	.876	.723
	50	.999	.986	.950	.876	.723
	$\to\infty$	.999	.986	.950	.876	.723

Outer circumferential crack

	R/h \ L_0/h	.2	.4	.6	.8	.95
$\frac{K_2(0)}{K_{20}}$	5	.998	.982	.936	.845	.678
	10	.999	.985	.946	.865	.707
	20	.999	.986	.949	.872	.717
	50	.999	.986	.950	.875	.721
	$\to\infty$	.999	.986	.950	.876	.723

Inner circumferential crack

$\frac{K_2(0)}{K_{20}}$	5	.998	.983	.942	.857	.695
	10	.999	.985	.948	.872	.716
	20	.999	.986	.950	.876	.722
	50	.999	.986	.950	.876	.723
	$\to\infty$	.999	.986	.950	.876	.723

Table 6.31 Mode 3 normalized stress intensity factor at the center of a semi-elliptical surface crack in a cylindrical shell subjected to twisting, a/h=2., ν=.3.

TWISTING

Outer axial crack

	R/h \ L_0/h	.2	.4	.6	.8	.95
$\frac{K_3(0)}{K_{3T}}$	5	.807	.581	.398	-.007	-3.63
	10	.808	.583	.397	-.018	-3.72
	20	.809	.584	.398	-.022	-3.75
	50	.810	.585	.399	-.022	-3.76
	$\to\infty$	.811	.587	.401	-.020	-3.75

Inner axial crack

$\frac{K_3(0)}{K_{3T}}$	5	.815	.598	.427	.057	-3.21
	10	.813	.594	.417	.027	-3.43
	20	.812	.591	.411	.008	-3.56
	50	.812	.589	.406	-.007	-3.66
	$\to\infty$	.811	.587	.401	-.020	-3.75

Outer circumferential crack

	R/h \ L_0/h	.2	.4	.6	.8	.95
$\frac{K_3(0)}{K_{3T}}$	5	.806	.579	.395	-.009	-3.63
	10	.807	.581	.395	-.022	-3.74
	20	.809	.583	.396	-.025	-3.77
	50	.810	.585	.398	-.024	-3.78
	$\to\infty$	.811	.587	.401	-.020	-3.75

Inner circumferential crack

$\frac{K_3(0)}{K_{3T}}$	5	.816	.602	.436	.084	-3.00
	10	.814	.596	.422	.039	-3.34
	20	.813	.592	.413	.013	-3.52
	50	.812	.590	.407	-.005	-3.65
	$\to\infty$	.811	.587	.401	-.020	-3.75

Table 6.32 Mode 3 normalized stress intensity factor at the center of a semi-elliptical surface crack in a cylindrical shell subjected to in-plane shear, a/h=4., ν=.3.

IN-PLANE SHEAR

	R/h \ L_0/h	.2	.4	.6	.8	.95
		Outer axial crack				
$\frac{K_3(0)}{K_{3I}}$	5	.837	.709	.712	.745	.625
	10	.838	.709	.709	.737	.610
	20	.838	.709	.708	.732	.601
	50	.839	.710	.708	.729	.594
	$\to\infty$	.840	.712	.709	.728	.590
		Inner axial crack				
$\frac{K_3(0)}{K_{3I}}$	5	.843	.720	.726	.757	.627
	10	.843	.718	.721	.747	.613
	20	.842	.716	.717	.740	.604
	50	.841	.714	.713	.734	.597
	$\to\infty$	.840	.712	.709	.728	.590

	R/h \ L_0/h	.2	.4	.6	.8	.95
		Outer circumferential crack				
$\frac{K_3(0)}{K_{3I}}$	5	.836	.707	.711	.750	.643
	10	.837	.707	.708	.737	.616
	20	.838	.708	.707	.731	.602
	50	.839	.710	.707	.728	.594
	$\to\infty$	.840	.712	.709	.728	.590
		Inner circumferential crack				
$\frac{K_3(0)}{K_{3I}}$	5	.845	.725	.733	.771	.645
	10	.844	.721	.725	.754	.620
	20	.843	.718	.719	.743	.606
	50	.841	.715	.714	.735	.597
	$\to\infty$	.840	.712	.709	.728	.590

Table 6.33 Mode 2 normalized stress intensity factor at the center of a semi-elliptical surface crack in a cylindrical shell subjected to out-of-plane shear, a/h=4., ν=.3.

OUT-OF-PLANE SHEAR

Outer axial crack

	R/h \ L_0/h	.2	.4	.6	.8	.95
$\frac{K_2(0)}{K_{20}}$	5	1.00	.996	.986	.959	.879
	10	1.00	.996	.987	.962	.884
	20	1.00	.997	.987	.963	.886
	50	1.00	.997	.988	.964	.888
	$\to\infty$	1.00	.997	.988	.965	.889

Inner axial crack

$\frac{K_2(0)}{K_{20}}$	5	1.00	.996	.987	.963	.886
	10	1.00	.997	.988	.965	.888
	20	1.00	.997	.988	.965	.889
	50	1.00	.997	.988	.965	.889
	$\to\infty$	1.00	.997	.988	.965	.889

Outer circumferential crack

	R/h \ L_0/h	.2	.4	.6	.8	.95
$\frac{K_2(0)}{K_{20}}$	5	.999	.992	.968	.916	.805
	10	1.00	.995	.981	.947	.858
	20	1.00	.996	.985	.958	.877
	50	1.00	.997	.987	.963	.885
	$\to\infty$	1.00	.997	.988	.965	.889

Inner circumferential crack

$\frac{K_2(0)}{K_{20}}$	5	.999	.993	.973	.929	.828
	10	1.00	.995	.984	.955	.872
	20	1.00	.996	.987	.963	.885
	50	1.00	.997	.988	.965	.889
	$\to\infty$	1.00	.997	.988	.965	.889

Table 6.34 Mode 3 normalized stress intensity factor at the center of a semi-elliptical surface crack in a cylindrical shell subjected to twisting, a/h=4., ν=.3.

TWISTING

	R/h \ L_0/h	.2	.4	.6	.8	.95
	Outer axial crack					
$\frac{K_3(0)}{K_{3T}}$	5	.819	.611	.473	.251	-1.80
	10	.819	.611	.469	.229	-2.00
	20	.820	.611	.467	.216	-2.12
	50	.821	.612	.467	.210	-2.19
	$\to\infty$	.822	.615	.470	.211	-2.21
	Inner axial crack					
$\frac{K_3(0)}{K_{3T}}$	5	.825	.626	.499	.314	-1.33
	10	.825	.623	.491	.284	-1.60
	20	.824	.621	.484	.259	-1.81
	50	.823	.618	.478	.236	-2.00
	$\to\infty$	.822	.615	.470	.211	-2.21

	R/h \ L_0/h	.2	.4	.6	.8	.95
	Outer circumferential crack					
$\frac{K_3(0)}{K_{3T}}$	5	.817	.609	.472	.261	-1.64
	10	.818	.609	.466	.227	-1.98
	20	.819	.610	.465	.212	-2.14
	50	.820	.612	.466	.207	-2.21
	$\to\infty$	.822	.615	.470	.211	-2.21
	Inner circumferential crack					
$\frac{K_3(0)}{K_{3T}}$	5	.827	.631	.513	.367	-.854
	10	.826	.627	.499	.311	-1.36
	20	.825	.622	.489	.272	-1.70
	50	.823	.619	.479	.241	-1.96
	$\to\infty$	.822	.615	.470	.211	-2.21

Table 6.35 Mode 3 normalized stress intensity factor at the center of a semi-elliptical surface crack in a toroidal shell subjected to in-plane shear. Crack is at position A of Fig. 6.5, R/h=10, ν=.3.

IN-PLANE SHEAR

	R_i/h \ L_0/h	.2	.4	.6	.8	.95
		a/h=1, External				
$\frac{K_3(0)}{K_{3I}}$	1	.798	.632	.575	.490	.303
	3	.798	.632	.575	.490	.302
	5	.798	.632	.575	.490	.302
	$\to\infty$	.798	.633	.575	.490	.302
		a/h=1, Internal				
$\frac{K_3(0)}{K_{3I}}$	1	.802	.640	.583	.495	.302
	3	.802	.640	.583	.494	.302
	5	.802	.640	.583	.494	.302
	$\to\infty$	.802	.639	.582	.494	.301

	R_i/h \ L_0/h	.2	.4	.6	.8	.95
		a/h=2, External				
$\frac{K_3(0)}{K_{3I}}$	1	.826	.683	.657	.627	.454
	4	.826	.683	.656	.626	.453
	7	.826	.683	.656	.626	.452
	$\to\infty$	.827	.683	.657	.626	.451
		a/h=2, Internal				
$\frac{K_3(0)}{K_{3I}}$	1	.833	.696	.672	.639	.455
	4	.833	.695	.671	.638	.454
	7	.833	.695	.670	.637	.453
	$\to\infty$	.832	.694	.670	.636	.452

Table 6.36 Mode 2 normalized stress intensity factor at the center of a semi-elliptical surface crack in a toroidal shell subjected to out-of-plane shear. Crack is at position A of Fig. 6.5, R/h=10, ν=.3.

OUT-OF-PLANE SHEAR

	R_i/h \ L_0/h	.2	.4	.6	.8	.95
		a/h=1, External				
$\frac{K_2(0)}{K_{20}}$	1	.996	.953	.848	.688	.482
	3	.996	.953	.848	.688	.482
	5	.996	.953	.849	.688	.482
	$\to\infty$	.996	.953	.849	.688	.482
		a/h=1, Internal				
$\frac{K_2(0)}{K_{20}}$	1	.996	.953	.850	.691	.485
	3	.996	.953	.850	.691	.485
	5	.996	.953	.850	.691	.485
	$\to\infty$	.996	.953	.850	.691	.485

	R_i/h \ L_0/h	.2	.4	.6	.8	.95
		a/h=2, External				
$\frac{K_2(0)}{K_{20}}$	1	.999	.985	.945	.864	.706
	4	.999	.985	.945	.865	.706
	7	.999	.985	.945	.865	.707
	$\to\infty$	.999	.985	.946	.865	.707
		a/h=2, Internal				
$\frac{K_2(0)}{K_{20}}$	1	.999	.985	.948	.872	.716
	4	.999	.985	.948	.872	.716
	7	.999	.985	.948	.872	.716
	$\to\infty$	.999	.985	.948	.872	.716

Table 6.37 Mode 3 normalized stress intensity factor at the center of a semi-elliptical surface crack in a toroidal shell subjected to twisting. Crack is at position A of Fig. 6.5, R/h=10, ν=.3.

TWISTING

	R_i/h \ L_0/h	.2	.4	.6	.8	.95
		a/h=1, External				
$\frac{K_3(0)}{K_{3T}}$	1	.777	.519	.272	-.339	-5.28
	3	.777	.519	.272	-.339	-5.28
	5	.777	.519	.272	-.339	-5.28
	$\to\infty$	.777	.519	.273	-.339	-5.28
		a/h=1, Internal				
$\frac{K_3(0)}{K_{3T}}$	1	.782	.530	.290	-.304	-5.08
	3	.782	.530	.289	-.306	-5.10
	5	.782	.529	.289	-.308	-5.10
	$\to\infty$	.782	.529	.287	-.310	-5.12

	R_i/h \ L_0/h	.2	.4	.6	.8	.95
		a/h=2, External				
$\frac{K_3(0)}{K_{3T}}$	1	.807	.580	.395	-.019	-3.71
	4	.807	.581	.395	-.021	-3.73
	7	.807	.581	.395	-.021	-3.73
	$\to\infty$	.807	.581	.395	-.022	-3.74
		a/h=2, Internal				
$\frac{K_3(0)}{K_{3T}}$	1	.815	.598	.426	.052	-3.24
	4	.814	.597	.424	.046	-3.29
	7	.814	.597	.423	.044	-3.30
	$\to\infty$	.814	.596	.422	.039	-3.34

Table 6.38 Mode 3 normalized stress intensity factor at the center of a semi-elliptical surface crack in a toroidal shell subjected to in-plane shear. Crack is at position B of Fig. 6.5, R/h=10, ν=.3.

IN-PLANE SHEAR

	R_i/h \ L_0/h	.2	.4	.6	.8	.95
		a/h=1, External				
$\frac{K_3(0)}{K_{3I}}$	1	.798	.632	.575	.490	.302
	3	.798	.633	.575	.490	.302
	5	.798	.633	.575	.490	.302
	$\to\infty$	.798	.633	.576	.490	.301
		a/h=1, Internal				
$\frac{K_3(0)}{K_{3I}}$	1	.802	.640	.583	.494	.302
	3	.802	.639	.582	.494	.301
	5	.802	.639	.582	.494	.301
	$\to\infty$	.802	.639	.581	.493	.301

	R_i/h \ L_0/h	.2	.4	.6	.8	.95
		a/h=2, External				
$\frac{K_3(0)}{K_{3I}}$	1	.826	.683	.657	.627	.453
	4	.827	.684	.657	.626	.451
	7	.827	.684	.657	.626	.450
	$\to\infty$	.827	.684	.658	.626	.449
		a/h=2, Internal				
$\frac{K_3(0)}{K_{3I}}$	1	.833	.695	.671	.637	.454
	4	.832	.694	.669	.635	.452
	7	.832	.694	.669	.635	.452
	$\to\infty$	.832	.693	.668	.633	.451

Table 6.39 Mode 2 normalized stress intensity factor at the center of a semi-elliptical surface crack in a toroidal shell subjected to out-of-plane shear. Crack is at position B of Fig. 6.5, R/h=10, ν=.3.

OUT-OF-PLANE SHEAR

a/h=1, External

	R_i/h \ L_0/h	.2	.4	.6	.8	.95
$\frac{K_2(0)}{K_{20}}$	1	.996	.953	.850	.691	.485
	3	.996	.953	.850	.692	.486
	5	.996	.953	.850	.692	.486
	$\to\infty$	.996	.953	.851	.692	.486

a/h=1, Internal

$\frac{K_2(0)}{K_{20}}$	1	.996	.953	.851	.693	.487
	3	.996	.953	.851	.693	.487
	5	.996	.953	.851	.693	.487
	$\to\infty$	.996	.953	.851	.693	.487

a/h=2, External

	R_i/h \ L_0/h	.2	.4	.6	.8	.95
$\frac{K_2(0)}{K_{20}}$	1	.999	.986	.948	.871	.716
	4	.999	.986	.949	.873	.719
	7	.999	.986	.949	.873	.719
	$\to\infty$	.999	.986	.950	.874	.720

a/h=2, Internal

$\frac{K_2(0)}{K_{20}}$	1	.999	.986	.950	.876	.722
	4	.999	.986	.950	.876	.723
	7	.999	.986	.951	.876	.723
	$\to\infty$	.999	.986	.950	.876	.723

Table 6.40 Mode 3 normalized stress intensity factor at the center of a semi-elliptical surface crack in a toroidal shell subjected to twisting. Crack is at position B of Fig. 6.5, R/h=10, ν=.3.

TWISTING

	R_i/h \ L_0/h	.2	.4	.6	.8	.95
		a/h=1, External				
$\frac{K_3(0)}{K_{3T}}$	1	.777	.519	.273	-.337	-5.27
	3	.777	.520	.273	-.337	-5.27
	5	.777	.520	.273	-.337	-5.27
	$\to\infty$	.777	.520	.274	-.337	-5.27
		a/h=1, Internal				
$\frac{K_3(0)}{K_{3T}}$	1	.782	.529	.289	-.307	-5.10
	3	.782	.529	.288	-.310	-5.12
	5	.782	.529	.287	-.311	-5.13
	$\to\infty$	.781	.528	.286	-.314	-5.15

	R_i/h \ L_0/h	.2	.4	.6	.8	.95
		a/h=2, External				
$\frac{K_3(0)}{K_{3T}}$	1	.807	.581	.396	-.017	-3.70
	4	.808	.582	.397	-.018	-3.71
	7	.808	.582	.397	-.018	-3.71
	$\to\infty$	.808	.583	.397	-.018	-3.72
		a/h=2, Internal				
$\frac{K_3(0)}{K_{3T}}$	1	.814	.597	.423	.044	-3.31
	4	.814	.596	.420	.036	-3.37
	7	.814	.595	.419	.033	-3.39
	$\to\infty$	.813	.594	.417	.027	-3.43

Table 6.41 Mode 3 normalized stress intensity factor at the center of a semi-elliptical surface crack in a toroidal shell subjected to in-plane shear. Crack is at position C of Fig. 6.5, R/h=10, ν=.3.

IN-PLANE SHEAR

	R_i/h \ L_0/h	.2	.4	.6	.8	.95
		a/h=1, External				
$\frac{K_3(0)}{K_{3I}}$	1	.800	.635	.578	.491	.301
	3	.799	.633	.576	.490	.301
	5	.798	.633	.575	.490	.301
	$\to\infty$	.798	.633	.575	.490	.302
		a/h=1, Internal				
$\frac{K_3(0)}{K_{3I}}$	1	.800	.636	.579	.492	.301
	3	.801	.638	.581	.492	.301
	5	.802	.639	.581	.493	.301
	$\to\infty$	.802	.639	.582	.494	.301

	R_i/h \ L_0/h	.2	.4	.6	.8	.95
		a/h=2, External				
$\frac{K_3(0)}{K_{3I}}$	1	.829	.687	.661	.628	.450
	4	.827	.684	.657	.625	.449
	7	.827	.684	.657	.625	.450
	$\to\infty$	.827	.683	.657	.626	.451
		a/h=2, Internal				
$\frac{K_3(0)}{K_{3I}}$	1	.830	.690	.664	.630	.449
	4	.832	.693	.668	.633	.450
	7	.832	.694	.669	.634	.451
	$\to\infty$	.832	.694	.670	.636	.452

Table 6.42 Mode 2 normalized stress intensity factor at the center of a semi-elliptical surface crack in a toroidal shell subjected to out-of-plane shear. Crack is at position C of Fig. 6.5, R/h=10, ν=.3.

OUT-OF-PLANE SHEAR

a/h=1, External

	R_i/h \ L_0/h	.2	.4	.6	.8	.95
$\frac{K_2(0)}{K_{20}}$	1	.996	.953	.849	.689	.483
	3	.996	.953	.849	.689	.483
	5	.996	.953	.849	.689	.482
	$\to\infty$	.996	.953	.849	.688	.482

a/h=1, Internal

$\frac{K_2(0)}{K_{20}}$	1	.996	.953	.850	.691	.485
	3	.996	.953	.850	.691	.485
	5	.996	.953	.850	.691	.485
	$\to\infty$	.996	.953	.850	.691	.485

a/h=2, External

	R_i/h \ L_0/h	.2	.4	.6	.8	.95
$\frac{K_2(0)}{K_{20}}$	1	.999	.985	.946	.867	.710
	4	.999	.985	.946	.866	.708
	7	.999	.985	.946	.865	.708
	$\to\infty$	.999	.985	.946	.865	.707

a/h=2, Internal

$\frac{K_2(0)}{K_{20}}$	1	.999	.985	.948	.871	.716
	4	.999	.985	.948	.872	.716
	7	.999	.985	.948	.872	.716
	$\to\infty$	.999	.985	.948	.872	.716

Table 6.43 Mode 3 normalized stress intensity factor at the center of a semi-elliptical surface crack in a toroidal shell subjected to twisting. Crack is at position C of Fig. 6.5, R/h=10, ν=.3.

TWISTING

	R_i/h \ L_0/h	.2	.4	.6	.8	.95
		a/h=1, External				
$\frac{K_3(0)}{K_{3T}}$	1	.779	.523	.278	-.330	-5.23
	3	.778	.521	.274	-.337	-5.28
	5	.777	.520	.273	-.337	-5.27
	$\to\infty$	.777	.519	.273	-.339	-5.28
		a/h=1, Internal				
$\frac{K_3(0)}{K_{3T}}$	1	.780	.525	.281	-.323	-5.19
	3	.781	.527	.285	-.316	-5.16
	5	.781	.528	.286	-.314	-5.14
	$\to\infty$	.782	.529	.287	-.310	-5.12

	R_i/h \ L_0/h	.2	.4	.6	.8	.95
		a/h=2, External				
$\frac{K_3(0)}{K_{3T}}$	1	.810	.586	.403	-.006	-3.64
	4	.808	.582	.396	-.022	-3.75
	7	.808	.582	.395	-.023	-3.75
	$\to\infty$	.807	.581	.395	-.022	-3.74
		a/h=2, Internal				
$\frac{K_3(0)}{K_{3T}}$	1	.811	.590	.410	.011	-3.53
	4	.813	.594	.418	.028	-3.41
	7	.814	.595	.419	.033	-3.38
	$\to\infty$	.814	.596	.422	.039	-3.34

Table 6.44 Mode 3 normalized stress intensity factor at the center of a semi-elliptical surface crack in a toroidal shell subjected to in-plane shear. Crack is at position D of Fig. 6.5, R/h=10, ν=.3.

IN-PLANE SHEAR

	R_i/h \ L_0/h	.2	.4	.6	.8	.95
		a/h=1, External				
$\frac{K_3(0)}{K_{3I}}$	1	.800	.636	.579	.492	.301
	3	.799	.634	.576	.490	.301
	5	.799	.634	.576	.490	.301
	$\to\infty$	.798	.633	.576	.490	.301
		a/h=1, Internal				
$\frac{K_3(0)}{K_{3I}}$	1	.800	.635	.578	.491	.301
	3	.801	.637	.580	.492	.300
	5	.801	.638	.580	.492	.301
	$\to\infty$	.802	.639	.581	.493	.301

	R_i/h \ L_0/h	.2	.4	.6	.8	.95
		a/h=2, External				
$\frac{K_3(0)}{K_{3I}}$	1	.830	.690	.664	.630	.449
	4	.828	.686	.659	.626	.448
	7	.828	.685	.658	.626	.448
	$\to\infty$	.827	.684	.658	.626	.449
		a/h=2, Internal				
$\frac{K_3(0)}{K_{3I}}$	1	.829	.687	.661	.628	.450
	4	.831	.691	.665	.631	.449
	7	.831	.692	.666	.632	.449
	$\to\infty$	.832	.693	.668	.633	.451

Table 6.45 Mode 2 normalized stress intensity factor at the center of a semi-elliptical surface crack in a toroidal shell subjected to out-of-plane shear. Crack is at position D of Fig. 6.5, R/h=10, ν=.3.

OUT-OF-PLANE SHEAR

	R_i/h \ L_0/h	.2	.4	.6	.8	.95
		a/h=1, External				
$\frac{K_2(0)}{K_{20}}$	1	.996	.953	.850	.691	.485
	3	.996	.953	.851	.692	.486
	5	.996	.953	.851	.692	.486
	$\to\infty$	.996	.953	.851	.692	.486
		a/h=1, Internal				
$\frac{K_2(0)}{K_{20}}$	1	.996	.953	.849	.689	.483
	3	.996	.953	.851	.692	.486
	5	.996	.953	.851	.693	.487
	$\to\infty$	.996	.953	.851	.693	.487

	R_i/h \ L_0/h	.2	.4	.6	.8	.95
		a/h=2, External				
$\frac{K_2(0)}{K_{20}}$	1	.999	.985	.948	.871	.716
	4	.999	.986	.950	.875	.721
	7	.999	.986	.950	.875	.721
	$\to\infty$	.999	.986	.950	.874	.720
		a/h=2, Internal				
$\frac{K_2(0)}{K_{20}}$	1	.999	.985	.946	.867	.710
	4	.999	.986	.950	.875	.722
	7	.999	.986	.950	.876	.723
	$\to\infty$	.999	.986	.950	.876	.723

Table 6.46 Mode 3 normalized stress intensity factor at the center of a semi-elliptical surface crack in a toroidal shell subjected to twisting. Crack is at position D of Fig. 6.5, R/h=10, ν=.3.

TWISTING

	R_i/h \ L_0/h	.2	.4	.6	.8	.95
		a/h=1, External				
$\frac{K_3(0)}{K_{3T}}$	1	.780	.525	.281	-.323	-5.19
	3	.778	.522	.276	-.334	-5.26
	5	.778	.521	.275	-.336	-5.26
	$\to\infty$	.777	.520	.274	-.337	-5.27
		a/h=1, Internal				
$\frac{K_3(0)}{K_{3T}}$	1	.779	.523	.278	-.330	-5.23
	3	.780	.526	.282	-.322	-5.19
	5	.781	.527	.284	-.319	-5.17
	$\to\infty$	.781	.528	.286	-.314	-5.15

	R_i/h \ L_0/h	.2	.4	.6	.8	.95
		a/h=2, External				
$\frac{K_3(0)}{K_{3T}}$	1	.811	.590	.410	.011	-3.53
	4	.809	.584	.400	-.015	-3.70
	7	.809	.583	.398	-.017	-3.71
	$\to\infty$	.808	.583	.397	-.018	-3.72
		a/h=2, Internal				
$\frac{K_3(0)}{K_{3T}}$	1	.810	.586	.403	-.006	-3.64
	4	.813	.592	.413	.014	-3.52
	7	.813	.592	.415	.019	-3.48
	$\to\infty$	.813	.594	.417	.027	-3.43

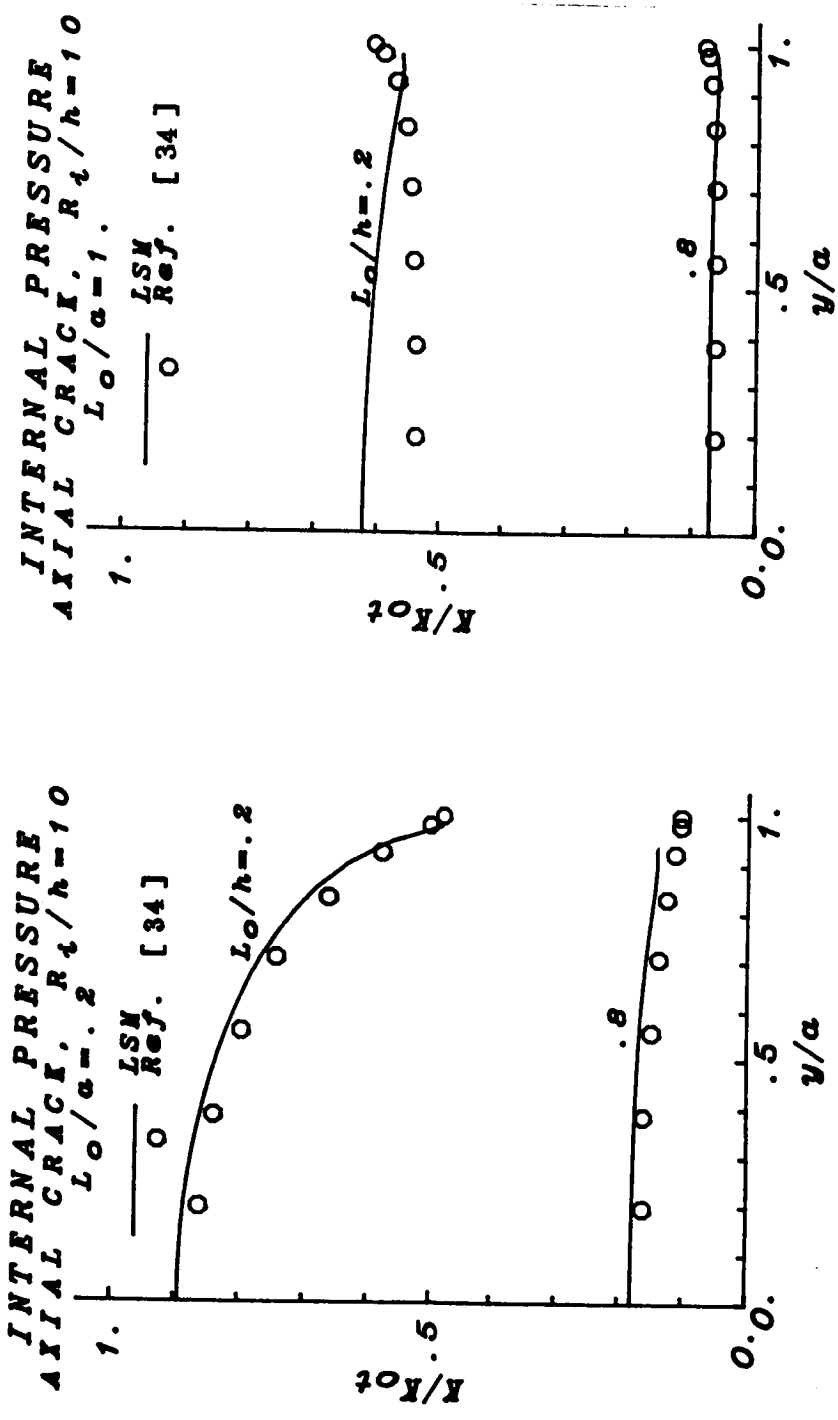

Figure 6.1 Comparison of the mode 1 LSM with results from Ref. [34] for the normalized SIF along an axial, internal, semi-elliptical surface crack in a pressurized cylinder. Crack surface pressure is taken into account, ν=.3.

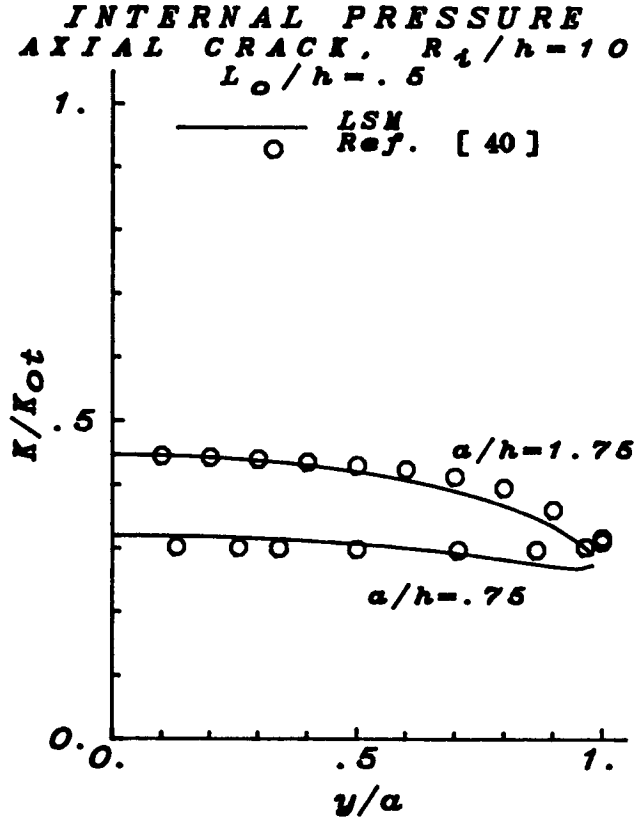

Figure 6.2 Comparison of the mode 1 LSM with results from Ref. [40] for the normalized SIF along an axial, internal, semi-elliptical surface crack in a pressurized cylinder. Crack surface pressure is not taken into account, ν=.3.

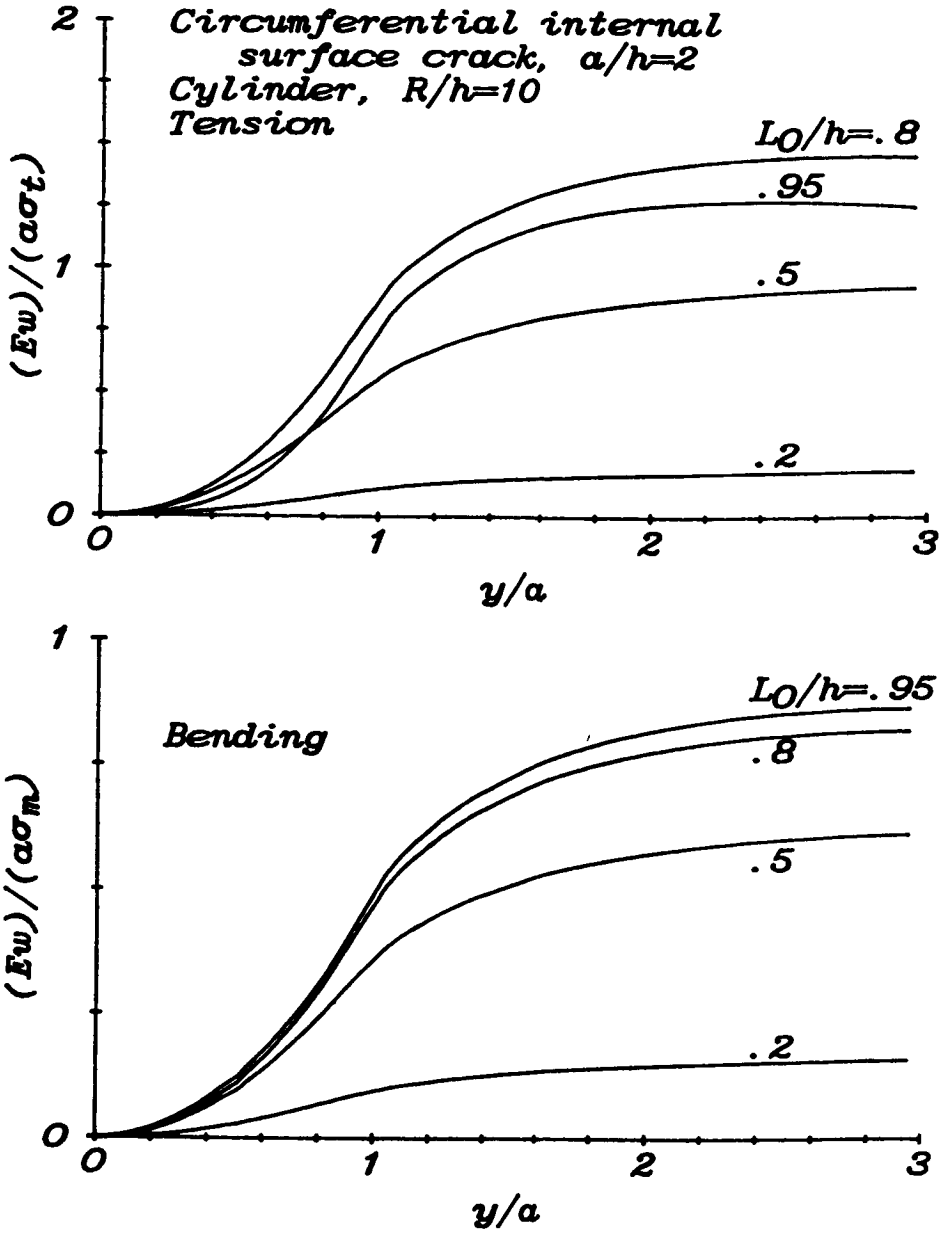

Figure 6.3 Out-of-plane displacement $w(0^+,y)$ as measured from y=0 in the deformed position for a cylinder with a circumferential, external, semi-elliptical surface crack subjected to either membrane loading ($\sigma_m=\overset{\infty}{N}_x/h$) or bending ($\sigma_b=6\overset{\infty}{M}/h^2$), ν=.3.

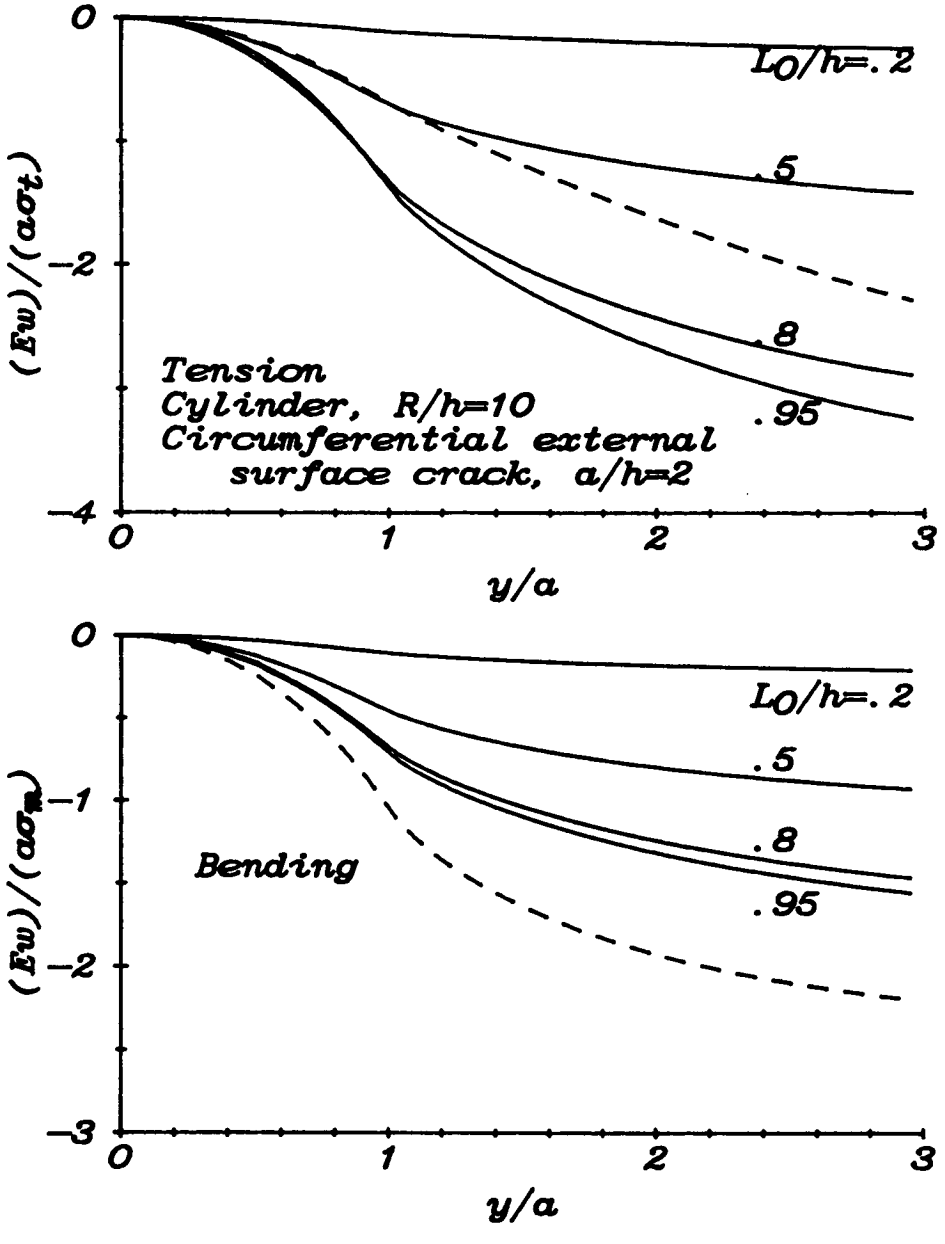

Figure 6.4 Out-of-plane displacement $w(0^+,y)$ as measured from y=0 in the deformed position for a cylinder with a circumferential, internal, semi-elliptical surface crack subjected to either membrane loading ($\sigma_m=\overset{\infty}{N}_x/h$) or bending ($\sigma_b=6\overset{\infty}{M}/h^2$), ν=.3.

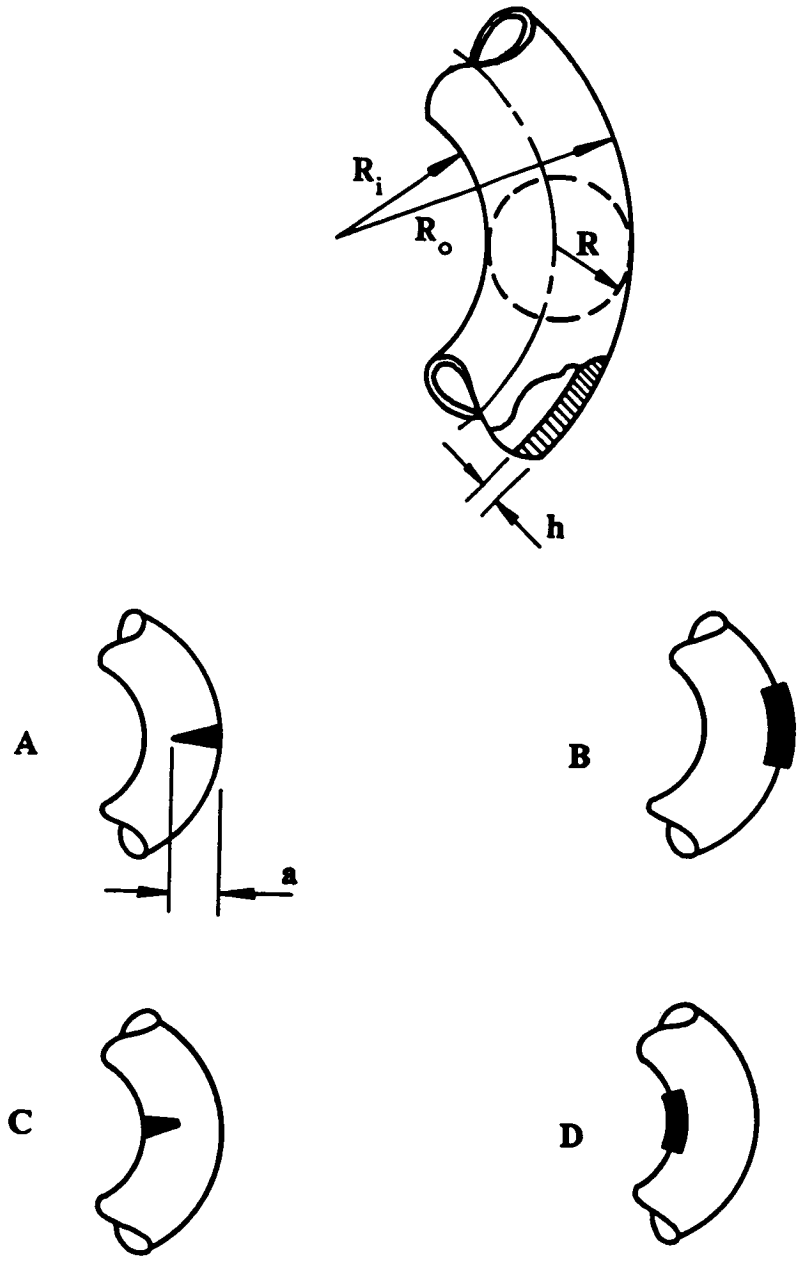

Figure 6.5 Geometry of the toroidal shell.

CHAPTER 7

Conclusions and Future Work

The severity of the underlying assumptions of the line-spring model are such that verification with three-dimensional solutions is necessary. Such comparisons, in this study as well as in others, show that the model is quite accurate, and therefore, its use in extensive parameter studies is justified. It was shown in Chapter 4 that for practical crack length to plate thickness ratios of about a/h=1, a plate theory that includes transverse shear deformation gives better results than the classical theory. The higher order plate theory does not seem to be necessary for a/h greater than about 2. When using the LSM with shallow shell theory it is more important to include transverse shear effects, because this theory is asymptotically correct for short cracks. The validity of the shallow shell theory for long cracks is not fully known, however, for surface cracks of practical dimensions it is expected to be accurate. Comparison of LSM solutions obtained in this study with three-dimensional solutions for semi-elliptical internal cracks in cylinders are also quite accurate.

It is still not understood why the model works as well as it does close to the crack ends. This is a rather curious problem. Since the stress intensity factors are defined by the model to be in a plane perpendicular to the plate surfaces, and not perpendicular to the crack front as they should be defined, the results at the ends of a semi-elliptical crack should be poor, but they are not. Several factors apparently act to cancel each other out. If these factors are

understood, and separately accounted for, the extension of the model to other crack problems will be better achieved.

This has special importance in the proposed skew-symmetric or mixed-mode line-spring model investigated in this study. Unfortunately, there are no three-dimensional solutions for verification; only the success of the symmetric case can give confidence that the results will be of some use. There are additional assumptions involved that do not have to be made in the mode 1 case. The first restricts the model to coplanar crack growth. The results may be considered as upper bounds for materials which have a weak cleavage plane. Of course, cracks along these planes would be of concern. The next assumption relates to the previously discussed problem in mode 1 which involves the crack front curvature and the plane in which the SIF is defined. Although in the mode 1 case this problem is somehow overcome, this effect is more critical in the skew-symmetric case because there are two stress intensity factors as opposed to one for the symmetric case. To illustrate this problem, consider that for a semi-elliptical crack in which a primary mode 3 loading in the center will become a primary mode 2 loading towards the ends, and vice versa. This is not observed in the results. There is no built in mechanism in the model that accounts for this, (but there isn't for the mode 1 case either). Perhaps the combination of K_2 and K_3 in the following generalized energy release rate equation is more accurate than the individual K values.

$$\frac{d}{dL}(U-V) = G = \frac{1-\nu^2}{E}\left\{ K_1^2 + K_2^2 + \frac{1}{1-\nu} K_3^2 \right\} . \qquad (7.1)$$

If the model can be verified, and improved, the shell with a crack at an arbitrary angle with respect to a principal line of curvature would be an important problem for future research.

Investigations into the endpoint behavior of the line-spring model have led to important conclusions about the ability of the model to predict stresses in front of the "crack tip". This also has applications to the crack interaction problem, and to possible uses of the model to study crack propagation in the length direction, in addition to the depth direction. It was found that only when the crack profile behaves like

$$\xi = \xi_0(1-t^2)^{1/4} \tag{7.2}$$

near the endpoints, does the numerical procedure easily converge. However, for rectangular profiles, convergence is acceptable. For the semi-ellipse, it is not.

An important application of the LSM was to solve the contact plate bending problem. Here the flexibility of the model to allow for any crack shape is exploited. Future work in this area includes predicting crack shapes for mode 1 crack growth assuming a constant K condition. Solution of this problem would involve the same iterative procedure that was used for the contact case.

It should be emphasized that all solutions presented in this study correspond to the perturbation problem, where constant loading along the length of the crack has been assumed. To make use of the results, the solution to the uncracked shell must first be obtained along the plane of the crack. Then superposition principles apply.

There may be cases where the solution to this problem varies considerably along the crack length, and studies into this effect may be necessary. This may be done in a straightforward manner.

The use of displacement quantities as unknowns in the formulation of the problem leads to strongly singular integral equations, rather than singular integral equations which result from using displacement derivatives. Although it is more convenient to deal directly with the displacement quantities, this formulation introduces log singularities into the equations which require more asymptotic analysis in order to have acceptable numerical convergence. In this study it was necessary to evaluate these log integrals in closed form. Sometimes log terms of the form $(t-y)^n \ln|t-y|$ can be extracted from the Fredholm kernel and calculated in closed form to slightly improve convergence, but in general it is not worth the extra effort. The collocation method of solving the integral equations was found to be better and more convenient than the quadrature technique. It has been my experience that orthogonal polynomials should be used as fitting functions when using the LSM as opposed to simpler functions such as power series.

LIST OF REFERENCES

1. Benthem, J. P., "The Quarter-Infinite Crack in a Half Space; Alternative and Additional Solutions", International Journal of Solids and Structures, Vol. 16, 1980, pp. 119-130.

2. Rice, J. R. and Levy, N., "The Part-Through Surface Crack in an Elastic Plate", ASME Journal of Applied Mechanics, Vol. 39, 1972, pp. 185-194.

3. Rice, J. R., "The Line Spring Model for Surface Flaws", The Surface Crack: Physical Problems and Computational Solutions, Swedlow, J. L., ed., ASME New York, 1972, pp. 171-186.

4. Williams, M. L., "On the Stress Distribution at the Base of a Stationary Crack", ASME Journal of Applied Mechanics, Vol. 24, 1957, pp. 109-114.

5. Williams, M. L., "The Bending Stress Distribution at the Base of a Stationary Crack", ASME Journal of Applied Mechanics, Vol. 28, 1961, pp. 78-82.

6. Knowles, J. K. and Wang, N. M., "On the Bending of an Elastic Plate Containing a Crack", Journal of Mathematics and Physics, Vol. 39, 1960, pp. 223-236.

7. Reissner, E., "The Effect of Transverse Shear Deformation on the Bending of Elastic Plates", ASME Journal of Applied Mechanics, Vol. 12, 1945, pp. A69-A77.

8. Reissner, E., " On Bending of Elastic Plates", Quarterly of Applied Mathematics, Vol. 5, 1947-1948, pp. 55-68.

9. Hartranft, R. J. and Sih, G. C., "Effect of Plate Thickness on the Bending Stress Distribution Around Through Cracks, " Journal of Mathematics and Physics, Vol. 47, 1968, pp. 276-291.

10. Wang, N. M., "Effects of Plate Thickness on the Bending of an Elastic Plate Containing a Crack", Journal of Mathematics and Physics, Vol. 47, 1968, pp. 371-390.

11. Civelek, M. B. and Erdogan, F., "Elastic-Plastic Problem for a Plate with a Part-Through Crack Under Extension and Bending", International Journal of Fracture Mechanics, Vol. 20, 1982, pp. 33-46.

12. Hartranft, R. J., "Improved Approximate Theories of the Bending and Extension of Flat Plates", Plates and Shells With Cracks", Sih, G. C., ed., Noordhoff International Publishing, Leyden, The Netherlands, 1977, pp. 45-83.

13. Sih, G. C., "A review of the Three-Dimensional Stress Problem for a Cracked Plate", International Journal of Fracture Mechanics, Vol. 7, 1971, pp. 39-61.

14. Wang, N. M., "Twisting of an Elastic Plate Containing a Crack", International Journal of Fracture Mechanics, Vol. 6, 1970, pp. 367-378.

15. Delale, F. and Erdogan, F., "The Effect of Transverse Shear in a Cracked Plate Under Skew-Symmetric Loading", ASME Journal of Applied Mechanics, Vol. 46, 1979, pp. 618-624.

16. Folias, E. S., "The Stresses in a Cracked Spherical Shell", Journal of Mathematics and Physics, Vol. 44, 1965, pp. 165-176.

17. Folias, E. S., "A Finite Line Crack in a Pressurized Spherical Shell", International Journal of Fracture Mechanics, Vol. 1, 1965, pp. 20-46.

18. Folias, E. S., "An Axial Crack in a Pressurized Cylindrical Shell", International Journal of Fracture Mechanics, Vol. 1, 1965, pp. 104-113.

19. Folias, E. S., "A Circumferential Crack in a Pressurized Cylindrical Shell", International Journal of Fracture Mechanics, Vol. 3, 1967, pp. 1-11.

20. Sanders, J. L., Jr., "Circumferential Through-Cracks in Cylindrical Shells Under Tension", ASME Journal of Applied Mechanics, Vol. 49, 1982, pp. 103-221.

21. Sanders, J. L., Jr., "Circumferential Through-Cracks in a Cylindrical Shell Under Combined Bending and Tension", ASME Journal of Applied Mechanics, Vol. 50, 1983, pp. 221.

22. Erdogan, F. and Kibler, J. J., "Cylindrical and Spherical Shells With Cracks", International Journal of Fracture Mechanics, Vol. 5, 1969, pp. 229-237.

23. Copley, L. G. and Sanders, J. L. Jr., "Longitudinal Crack in a Cylindrical Shell Under Internal Pressure", International Journal of Fracture Mechanics, Vol. 5, 1969, pp. 117-131.

24. Sih, G. C. and Hagendorf, H. C., "A New Theory of Spherical Shells With Cracks", Thin-Shell Structures: Theory, Experiment and Design, Fung, Y. C. and Sechler, E. E., eds., Prentice Hall, 1974.

25. Sih, G. C. and Hagendorf, H. C., "On Cracks in Shells With Shear Deformation", Plates and Shells With Cracks", Sih, G. C., ed., Noordhoff International Publishing, Leyden, The Netherlands, 1977, pp. 201-229.

26. Naghdi, P. M., "Note on the Equations of Shallow Elastic Shells", Quarterly of Applied Mathematics, Vol. 14, 1956, pp. 331-333.

27. Krenk, S., "Influence of Transverse Shear on an Axial Crack in a Cylindrical Shell", International Journal of Fracture Mechanics, Vol. 14, 1978, pp. 123-143.

28. Delale, F. and Erdogan, F., "Transverse Shear Effect in a Circumferentially Cracked Cylindrical Shell", Quarterly of Applied Mathematics, Vol. 37, 1979, pp. 239-257.

29. Delale, F. "Cracked Shells Under Skew-Symmetric Loading", NASA Project Report, Lehigh University, NGR 39-007-011, July 1981.

30. Yahsi, O. S. and Erdogan, F. E., "A Cylindrical Shell With an Arbitrarily Oriented Crack", International Journal of Solids and Structures, Vol. 19, 1983, pp.955-972.

31. Barsoum, R. S., Loomis, R. W. and Stewart, B. D., "Analysis of Through Cracks in Cylindrical Shells by the Quarter-Point Elements", International Journal of Fracture Mechanics, Vol. 15, 1979, pp. 259-280.

32. Ehlers, R., "Stress Intensity Factors and Crack Opening Areas For Axial Through Cracks in Hollow Cylinders Under Internal Pressure Loading", Engineering Fracture Mechanics, Vol. 25, 1986, pp. 63-77.

33. Newman, J. C., Jr. and Raju, I. S., "Analysis of Surface Cracks in Finite Plates Under Tension or Bending Loads", NASA Technical Paper 1578, 1979.

34. Raju, I. S. and Newman, J. C., Jr., "Stress-Intensity Factors for Internal and External Surface Cracks in Cylindrical Vessels", Journal of Pressure Vessel Technology, Vol. 104, 1982, pp. 293-298.

35. Shah, R. C. and Kobayashi, A. S., "On the Surface Flaw Problem" , The Surface Crack: Physical Problems and Computational Solutions, Swedlow, J. L., ed., ASME New York, 1972, pp.79-124.

36. Smith, F. W. and Sorensen, D. R., "The Semi-Elliptical Surface Crack - A Solution by the Alternating Method", International Journal of Fracture Mechanics, Vol. 12, 1976, pp. 47-57.

37. Heliot, J., Labbens, R. C. and Pellisier-Tanon, A., "Semi Elliptical Cracks in a Cylinder Subjected to Stress Gradients", Fracture Mechanics, ASTM, STP 677, 1979, pp. 341-364.

38. Nishioka, T. and Atluri, S. N., "Analysis of Surface Flaw in Pressure Vessels by a New 3-Dimensional Alternating Method",

Journal of Pressure Vessel Technology, Vol. 104, 1982, pp. 299-307.

39. Nishioka, T. and Atluri, S. N., "Analytical Solution for Embedded Elliptical Cracks, and Finite Element Alternating Method for Elliptical Surface Cracks, Subjected to Arbitrary Loadings", Engineering Fracture Mechanics, Vol. 17, 1982, pp. 247-268.

40. O'Donoghue, P. E., Nishioka, T. and Atluri, S. N., "Analysis of Interaction Behavior of Surface Flaws in Pressure Vessels", Journal of Pressure Vessel Technology, Vol. 108, 1986, pp. 24-32.

41. Mattheck, C., Morawietz, P. and Munz, D., "Stress Intensity Factor at the Surface and at the Deepest Point of a Semi-Elliptical Surface Crack in Plates Under Stress Gradients", International Journal of Fracture Mechanics, Vol. 23, 1983, pp. 201-212.

42. Grebner, H. and Strathmeier, U., "Stress Intensity Factors for Circumferential Semi-elliptical Surface Cracks in a Pipe Under Thermal Loading", Engineering Fracture Mechanics, Vol. 22, 1985, pp. 1-7.

43. Isida, M., Noguchi, H. and Yoshida, T, "Tension and Bending of Finite Thickness Plates With a Semi-Elliptical Surface Crack", International Journal of Fracture Mechanics, Vol. 26, 1984, pp. 157-188.

44. Swedlow, J. L., ed., The Surface Crack: Physical Problems and Computational Solutions, ASME New York, 1972.

45. Newman, J. C., Jr., "A Review and Assessment of the Stress-Intensity Factors for Surface Cracks", NASA Technical Memorandum 78805, 1978.

46. Scott, P. M. and Thorpe, T. W., "A Critical Review of Crack Tip Stress Intensity Factors For Semi-elliptic Cracks", Fatigue of Engineering Materials and Structures, Vol. 4, 1981, pp. 291-309.

47. Murakami, Y., "Analysis of Stress Intensity Factors of Modes I,II and III for Inclined Surface Cracks of Arbitrary Shape", Engineering Fracture Mechanics, Vol. 22, 1985, pp. 101-114.

48. Delale, F. and Erdogan, F., "Line-Spring Model for Surface Cracks in a Reissner Plate", International Journal of Engineering Science, Vol. 19, 1981, pp. 1331-1340.

49. Nakamura, H., Okamoto, A. and Kamichika, R., "Analysis of Surface Cracks in Weld Pipe - An Application of Line Spring Model", Transactions of the 7th International Conference on SMIRT, Vol. G, F7/5, 1983.

50. Parks, D. M., "The Inelastic Line-Spring: Estimates of Elastic-Plastic Fracture Mechanics Parameters for Surface-Cracked Plates and Shells", Journal of Pressure Vessel Technology, Vol. 103, 1981, pp. 246-254.

51. Miyoshi, T., Shiratori, M. and Yoshida, Y., "Analysis of J-Integral and Crack Growth for Surface Cracks by Line Spring Method", Journal of Pressure Vessel Technology, Vol. 108, 1986, pp. 305-311.

52. Miyazaki, N. and Kaneko, H., "On the Combination of the Boundary Element Method and the Line-Spring Model", International Journal of Fracture Mechanics, Vol. 31, 1986, pp. R3-R10.

53. Yang, C. Y., "Line Spring Method of Stress Intensity Factor Determination for Surface Cracks in Plates Under Arbitrary In-Plane Stresses", Presented at ASTM 19th National Symposium on Fracture Mechanics, San Antonio, Texas, June 30- July 2, 1986.

54. Theocaris, P. S. and Wu, D. L., "A Closed-Form Solution to the Equivalent Through-Crack Model for Surface Cracks", Acta Mechanica, Vol. 58, 1985, pp. 153-173.

55. Theocaris, P. S. and Wu, D. L., "The Equivalent Through-Crack Model for the Surface Part-Through Crack", Acta Mechanica, Vol. 59, 1986, pp. 157-181.

56. Boduroglu, H. and Erdogan, F., "Internal and Edge Cracks in a Plate of Finite Width Under Bending", ASME Journal of Applied Mechanics, Vol. 50, 1983, pp. 621-629.

57. Erdogan, F. and Boduroglu, H., "Surface Cracks in a Plate of Finite Width Under Extension or Bending", Theoretical and Applied Fracture Mechanics, Vol. 2, 1984, pp. 197-216.

58. Erdogan, F. and Axsel, B., "Line-Spring Model and its Applications to Part-Through Crack Problems in Plates and Shells", NASA Project Report, Lehigh University, NGR 39-007-011, June 1986.

59. Wu, B. H. and Erdogan, F., "The Surface Crack Problem in an Orthotropic Plate Under Bending and Tension", NASA Project Report, Lehigh University, NGR 39-007-011, November 1986.

60. Delale, F. and Erdogan F., "Application of the Line-Spring Model to a Cylindrical Shell Containing a Circumferential or Axial Part-Through Crack", ASME Journal of Applied Mechanics, Vol. 49, 1982, pp. 97-102.

61. Gross, B. and Srawley, J. E., "Stress Intensity Factors for Single Edge Notch Specimens in Bending or Combined Bending and

Tension by Boundary Collocation of a Stress Function", NASA Technical Note D-2603, 1965.

62. Tada, H., Paris, P. C. and Irwin, G. R., The Stress Analysis of Cracks Handbook, Del Research Corporation, Hellertown, Pa., 1973.

63. Kaya, A. C. and Erdogan, F., "Stress Intensity Factors and COD in an Orthotropic Strip", International Journal of Fracture Mechanics, Vol. 16, 1980, pp. 171-190.

64. Kaya, A. C. and Erdogan, F., "On the Solution of Integral Equations with Strongly Singular Kernels," (to appear in the Quarterly of Applied Mathematics).

65. Benthem, J. P. and Koiter, W. T., "Asymptotic Approximations to Crack Problems", Methods of Analysis and Solutions of Crack Problems, Sih, G. C., ed., Noordhoff International Publishing, Leyden, The Netherlands, 1973.

66. Hadamard, J., "Lectures on Cauchy's Problem in Linear Partial Differential Equations", Yale University Press, 1923.

67. Kaya, A. C., "Applications of Integral Equations with Strong Singularities in Fracture Mechanics", Ph.D. Dissertation, Lehigh University, 1984.

68. Irwin, G. R., "Analysis of Stresses and Strains Near the End of a Crack Traversing a Plate", ASME Journal of Applied Mechanics, Vol. 24, 1957, pp. 361-364.

69. Irwin, G. R., "Fracture Mechanics", Structural Mechanics, Goodier, J. N. and Hoff, N. J., eds., Pergamon Press, New York, 1960, pp. 557-591.

70. Erdogan, F., "Stress Intensity Factors", ASME Journal of Applied Mechanics, Vol. 50, 1983, pp. 992-1002.

71. Ezzat, H. A., "Experimental Verification of the Simplified Line-Spring Model", International Journal of Fracture Mechanics, Vol. 28, 1985, pp. 139-150.

72. Sih, G. C., Handbook of Stress Intensity Factors, Institute of Fracture and Solid Mechanics, Lehigh University, 1973, sec. 1.2.1-5,7.

73. Erdogan, F. and Ratwani, M., "A Note on the Interference of Two Collinear Cracks in a Cylindrical Shell", International Journal of Fracture Mechanics, Vol. 10, 1974, pp. 463-465.

74. Delale, F. and Erdogan F., "Stress Intensity Factors in a Hollow Cylinder Containing A Radial Crack", International Journal of Fracture Mechanics, Vol. 20, 1982, pp. 251-265.

75. Nied, H. F. and Erdogan, F., "The Elasticity Problem for a Thick-Walled Cylinder Containing a Circumferential Crack", International Journal of Fracture Mechanics, Vol. 22, 1983, pp. 277-301.

76. Erdogan, F., "Approximate Solutions of Systems of Singular Integral Equations", Journal of Applied Mathematics, Vol. 17, 1969, pp. 1041-1059.

77. Erdogan, F., "Mixed Boundary-Value Problems in Mechanics", Mechanics Today, Nemat-Nasser, S., ed., Vol. 4, Pergamon Press, Oxford, 1978, pp.1-86.

78. Muskhelishvili, I. N., Singular Integral Equations, Noordhoff International Publishing, Leyden, The Netherlands, 1953.

79. Kaya, A. C., "On the Solution of Integral Equations with a Generalized Cauchy Kernel", (to appear in the Quarterly of Applied Mathematics).

80. Sih, G. C., "Stress Distribution Near Internal Crack Tips for Longitudinal Shear Problems", ASME Journal of Applied Mechanics, Vol. 32, 1965, pp. 51-58.

81. Sneddon, I. N., "The Distribution of Stress in the Neighborhood of a Crack in an Elastic Solid", Proceedings of the Royal Society of London, Series A, 187, 1946, pp. 229-260.

82. Kassir, M. K. and Sih, G. C., "Three-Dimensional Stress Distribution Around an Elliptical Crack Under Arbitrary Loadings", ASME Journal of Applied Mechanics, Vol. 33, 1966, pp. 601-611.

83. Hartranft, R. J. and Sih, G. C., "Stress Singularity for a Crack With an Arbitrarily Curved Front", Engineering Fracture Mechanics, Vol. 9, 1977, pp. 705-719.

84. Timoshenko, S. and Woinowsky-Krieger, S., Theory of Plates and Shells, Mcgraw-Hill Book Company, New York, 1959, pp. 165-171.

85. Benthem, J. P., "State of Stress at the Vertex of a Quarter-Infinite Crack in a Half-Space", Vol. 13, 1977, pp. 479-492.

86. Abramowitz, M. and Stegun, I. A., Handbook of Mathematical Functions, Dover Publications, 1965.

87. Gradshteyn, I. S. and Ryzhik, I. M., Table of Integrals, Series, and Products, Academic Press, 1965.

APPENDIX A

Non-Dimensional Variables and Useful Formulae

A.1 Non-Dimensional Plate and Shell Quantities

$$x = x_1/h \ , \quad y = x_2/h \ , \quad z = x_3/h \ , \tag{A.1}$$

$$u = u_x = u_1 = u_{1D}/h \ , \ \beta_x = u_2 = \beta_1 \ , \ w = u_z = u_3 = u_{3D}/h$$

$$v = u_y = u_4 = u_{2D}/h \ , \ \beta_y = u_5 = \beta_2 \ , \tag{A.2}$$

$$\sigma_i = \sigma_{iD}/E \ , \quad q = \bar{q}/E \ , \tag{A.3}$$

$$N_{xx} = N_{11}/(hE) \ , \quad N_{yy} = N_{22}/(hE) \ , \quad N_{xy} = N_{12}/(hE) \ ,$$

$$M_{xx} = M_{11}/(h^2E) \ , \quad M_{xy} = M_{12}/(h^2E) \ , \ M_{yy} = M_{22}/(h^2E) \ ,$$

$$V_x = 12(1+\nu)V_1/(5hE) \ , \quad V_y = 12(1+\nu)V_2/(5hE) \ , \tag{A.4}$$

$$\lambda^4 = \gamma^{-1} = 12(1-\nu^2) \ , \quad \kappa = \frac{1}{5(1-\nu)} \ ,$$

$$\lambda_1^4 = \lambda^4(h/R_1)^2 \ , \quad \lambda_2^4 = \lambda^4(h/R_2)^2 \ , \quad \lambda_{12}^4 = \lambda^4(h/R_{12})^2 \ . \tag{A.5}$$

A.2 Some Useful Properties of Modified Bessel Functions

$$K_1(z) = \frac{z}{2}\left[K_2(z) - K_0(z)\right] \ , \tag{A.6}$$

$$\frac{d}{dz} K_0(z) = -K_1(z) = \frac{-z}{2}\left[K_2(z) - K_0(z)\right] \ , \tag{A.7}$$

$$\frac{d}{dz} K_2(z) = -K_1(z) - \frac{2}{z} K_2(z) = \frac{-z}{2}\left[K_2(z) - K_0(z)\right] - \frac{2}{z} K_2(z) \ . \tag{A.8}$$

If $z = \beta|t-y|$,

$$\frac{d}{dt} = \frac{dz}{dt}\frac{d}{dz} = \beta \mathrm{sign}(t-y)\frac{d}{dz} \ . \tag{A.9}$$

For small z,

$$K_0(z) \sim -\ln(z/2) - \gamma_e - (z/2)^2\ln(z/2) + O(z^2) \ , \tag{A.10}$$

$$K_2(z) \sim 2/z^2 - 1/2 - 1/2(z/2)^2\ln(z/2) - 1/2(z/2)^2(\gamma_e+5/4)$$

$$- 1/6(z/2)^4\ln(z/2) + O(z^4) \ , \tag{A.11}$$

where Euler's constant, γ_e = .57721566490153....

A.3 Chebychev Polynomials

Of the first kind: $T_n(x) = \cos n\theta \ , \ \theta = \cos^{-1}x \ ,$ (A.12)

Of the second kind: $U_n(x) = \dfrac{\sin(n+1)\theta}{\sin\theta} \ , \ \theta = \cos^{-1}x \ .$ (A.13)

Some expressions needed to integrate

$$\int_{-1}^{+1}(r-s)^i U_j(r)\sqrt{1-r^2}\ \ln|r-s|\ dr \ , \ i=1,2,3 \ , \tag{A.14}$$

are,

$$rU_j(r) = \frac{1}{2}\left[U_{j+1}(r) + U_{j-1}(r)\right] \ ,$$

$$r^2U_j(r) = \frac{1}{4}\left[U_{j+2}(r) + 2U_j(r) + U_{j-2}(r)\right] \ ,$$

$$r^3U_j(r) = \frac{1}{8}\left[U_{j+3}(r) + 3U_{j+1}(r) + 3U_{j-1}(r) + U_{j-3}(r)\right] \ . \tag{A.15}$$

An important relation between Chebychev Polynomials of the first and second kinds when using the line-spring model with displacement derivatives as the unknowns is,

$$\int \frac{T_n(x)dx}{(1-x^2)^{1/2}} = \frac{1}{n}\ (1-x^2)^{1/2}U_{n-1}(x) + \text{constant} \ . \tag{A.16}$$

The following integrals are useful for calculating stresses ahead of the crack tip,

$$\int_{-1}^{+1} \frac{U_n(t)(1-t^2)^{1/2}}{x-t}\,dt = -\left[x-(x^2-1)^{1/2}\right]^{n+1} \quad , \quad |x| > 1 \quad , \tag{A.17}$$

$$\int_{-1}^{+1} \frac{T_n(t)}{(1-t^2)^{1/2}(t-x)}\,dt = -\frac{\left[x-(x^2-1)^{1/2}\right]^n}{(x^2-1)^{1/2}} \quad , \quad |x| > 1 \quad , \tag{A.18}$$

$$\int_{-1}^{+1} \frac{U_n(t)(1-t^2)^{1/2}}{(x-t)^2}\,dt = -(n+1)\left[x-(x^2-1)^{1/2}\right]^n\left[1-\frac{x}{(x^2-1)^{1/2}}\right] \quad , \quad |x| > 1 \quad . \tag{A.19}$$

A.4 Finite-Part, Cauchy Principal Value, and Log Integrals

Except for the log integrals, these expressions are copied from [67].

$$\fint_{-1}^{+1} \frac{(1-t)^{\alpha}(1+t)^{\beta}P_n^{(\alpha,\beta)}(t)}{t-x}\,dt = \pi\cot(\alpha\pi)(1-x)^{\alpha}(1+x)^{\beta}P_n^{(\alpha,\beta)}(x) - \frac{2^{\alpha+\beta}\Gamma(\alpha)\Gamma(n+\beta+1)}{\Gamma(n+\alpha+\beta+1)}\,F(n+1,-n-\alpha-\beta;\ 1-\alpha,\ \frac{1-x}{2}),$$

$$(\alpha > -1,\ \beta > -1,\ \alpha \neq 0,1,2\ldots) \quad , \tag{A.20}$$

$$\fint_{-1}^{+1} \frac{P_n(t)}{t-x}\,dt = -2Q_n(x) \quad , \tag{A.21}$$

$$\fint_{-1}^{+1} \frac{T_n(t)}{(1-t^2)^{1/2}(t-x)}\,dt = \pi U_{n-1}(x) \quad , \tag{A.22}$$

$$\fint_{-1}^{+1} \frac{U_n(t)(1-t^2)^{1/2}}{t-x}\,dt = -\pi T_{n+1}(x) \quad , \tag{A.23}$$

$$\fint_{-1}^{+1} \frac{P_n(t)}{(t-x)^2}\,dt = \frac{-2(n+1)}{1-x^2}\left[\,xQ_n(x) - Q_{n+1}(x)\,\right] \quad , \tag{A.24}$$

C-4

$$\fint_{-1}^{+1} \frac{T_n(t)}{(1-t^2)^{1/2}(t-x)^2}\, dt = \frac{\pi}{1-x^2}\left[\frac{-n+1}{2}\, U_n(x) + \frac{n+1}{2}\, U_{n-2}(x)\right] , \tag{A.25}$$

$$\fint_{-1}^{+1} \frac{U_n(t)(1-t^2)^{1/2}}{(t-x)^2}\, dt = -\pi(n+1)U_n(x) , \tag{A.26}$$

where $P_n^{(\alpha,\beta)}(t)$ are Jacobi Polynomials, $F(a,b;c;z)$ are Hypergeometric functions, $P_n(t)$ are Lagendre Polynomials, $Q_n(t)$ are Lagendre Polynomials of the second kind, and $\Gamma(\alpha)$ is the gamma function.

Some integrals that can be used with Eqn. B.27 are:

$$\fint_{-1}^{+1} \frac{1}{t-x}\, dt = \ln\left[\frac{1-x}{1+x}\right] , \tag{A.27}$$

$$\fint_{-1}^{+1} \frac{1}{(t-x)^2}\, dt = \frac{-1}{1-x} - \frac{1}{1+x} , \tag{A.28}$$

$$\fint_{-1}^{+1} \frac{1}{(1-t^2)^{1/2}(t-x)}\, dt = 0 , \tag{A.29}$$

$$\fint_{-1}^{+1} \frac{1}{(1-t^2)^{1/2}(t-x)^2}\, dt = 0 , \tag{A.30}$$

$$\fint_{-1}^{+1} \frac{(1-t^2)^{1/2}}{t-x}\, dt = -\pi x , \tag{A.31}$$

$$\fint_{-1}^{+1} \frac{(1-t^2)^{1/2}}{(t-x)^2}\, dt = -\pi , \tag{A.32}$$

$$\fint_{-1}^{+1} \frac{(1-t)^{1/2}}{t-x}\, dt = -2\sqrt{2}\left[1 - \frac{1}{2}\sqrt{\frac{1-x}{2}}\ln(B)\right] , \tag{A.33}$$

$$\fint_{-1}^{+1} \frac{(1-t)^{1/2}}{(t-x)^2}\, dt = -\sqrt{2}\left[\frac{1}{1+x} + \frac{1}{4}\sqrt{\frac{2}{1-x}}\ln(B)\right] , \tag{A.34}$$

$$\fint_{-1}^{+1} \frac{1}{(1-t)^{1/2}(t-x)}\, dt = \frac{\ln(B)}{\sqrt{1-x}} \quad , \tag{A.35}$$

$$\fint_{-1}^{+1} \frac{1}{(1-t)^{1/2}(t-x)^2}\, dt = \frac{\sqrt{2}}{1-x}\left[\frac{-1}{1+x} + \frac{1}{4}\sqrt{\frac{2}{1-x}}\ln(B) \right] \quad , \tag{A.36}$$

where

$$B = \frac{1 + \sqrt{\frac{1-x}{2}}}{1 - \sqrt{\frac{1-x}{2}}} \quad . \tag{A.37}$$

There are similar formulas for power series.

$$\frac{1}{\pi}\int_{-1}^{+1} t^{j-1}(1-t^2)^{1/2}\ln|t-y|\, dt = \sum_{k=1}^{j+2} a_k y^{k-1} \quad , \tag{A.38}$$

$$\frac{1}{\pi}\fint_{-1}^{+1} \frac{t^{j-1}(1-t^2)^{1/2}}{t-y}\, dt = \sum_{k=1}^{j+1} b_k y^{k-1} \quad , \tag{A.39}$$

$$\frac{1}{\pi}\fint_{-1}^{+1} \frac{t^{j-1}(1-t^2)^{1/2}}{(t-y)^2}\, dt = \sum_{k=1}^{j} c_k y^{k-1} \quad , \tag{A.40}$$

where

$$b_k = \frac{1}{2\sqrt{\pi}}\,\frac{\Gamma\left(\frac{j-k}{2}\right)}{\Gamma\left(\frac{j-k+3}{2}\right)} \quad , \quad k = 1,2,\ldots,j+1, \text{ for } j = 1,2,3,\ldots \text{ and } j-k \text{ odd,} \quad ,$$

$$b_k = 0 \quad , \quad j-k \text{ even} \quad , \tag{A.41}$$

$$c_k = k b_{k+1} \quad , \quad k = 1,2,3,\ldots,j \quad , \tag{A.42}$$

$$a_k = \frac{-b_{k-1}}{k-1} \quad , \quad k = 2,3,4,\ldots,j+2 \quad ,$$

$$a_1 = 0 \quad , \quad j = 2,4,6,\ldots \quad ,$$

$$a_1 = \frac{(j-2)!}{2^{j-1}\left(\frac{j-3}{2}\right)!\ \left(\frac{j+1}{2}\right)!} \left\{ \sum_{k=1}^{j-1} \frac{(-1)^{k-1}}{k} - \frac{1}{j+1} - \ln(2) \right\} \qquad j = 3,5,7,..$$

$$a_1 = -(1/4 + 1/2 \ln(2)) \quad , \quad j=1 \quad . \tag{A.43}$$

And for the weight in the denominator,

$$\int_{-1}^{+1} \frac{t^n}{(1-t^2)^{1/2}(t-x)}\, dt = \sum_{k=0}^{n-1} d_k x^k \quad , \tag{A.44}$$

$$d_k = 0 \quad , \quad n-k \text{ even},$$

$$d_k = \sqrt{\pi}\, \frac{\Gamma\left(\frac{n-k}{2}\right)}{\Gamma\left(\frac{n-k+1}{2}\right)} \quad , \quad n-k \text{ odd} \quad , \tag{A.45}$$

$$\frac{1}{\pi} \fint_{-1}^{+1} \frac{t^n}{(1-t^2)^{1/2}(t-x)^2}\, dt = \sum_{k=0}^{n-2} e_k x^k \quad , \tag{A.46}$$

$$e_k = 0 \quad , \quad n-k \text{ odd} \quad ,$$

$$e_k = \sqrt{\pi}\, \frac{\Gamma\left(\frac{n-k-1}{2}\right)}{\Gamma\left(\frac{n-k}{2}\right)} (k+1) \quad , \quad n-k \text{ even} \quad . \tag{A.47}$$

For integration of logs with Chebychev Polynomials [76] (with corrections) of the second kind that are typical when using the strongly singular formulation,

$$\int_{-1}^{+1} U_j(r)\sqrt{1-r^2}\, \ln|r-s|\, dr = V_j(s) \quad , \quad -1 \le s \le 1 \quad , \tag{A.48}$$

where

$$V_j(s) = \frac{-\pi}{2}\left[\frac{T_j(s)}{j} - \frac{T_{J+2}(s)}{j+2}\right] \quad , \quad j > 0$$

$$= \frac{-\pi}{2}\left[-s^2 + 1/2 + \ln 2\right] \quad , \quad j = 0 \quad . \tag{A.49}$$

APPENDIX B

Finite-part Integrals

Singular integral equations result naturally from the formulation of two-dimensional crack problems in mechanics when the crack opening displacement derivative is used as the unknown. The theory is well established due principally to the work of Muskhelishvili [78]. If the displacement is used as the unknown, the resulting singular integral equation takes on a new form and is referred to as strongly singular. To illustrate the differences consider the two-dimensional, half-space crack problem of Fig. B.1 with boundary conditions given by Eqns. B.1-4. This simple geometry produces all of the important mathematical features of the geometries studied in this dissertation.

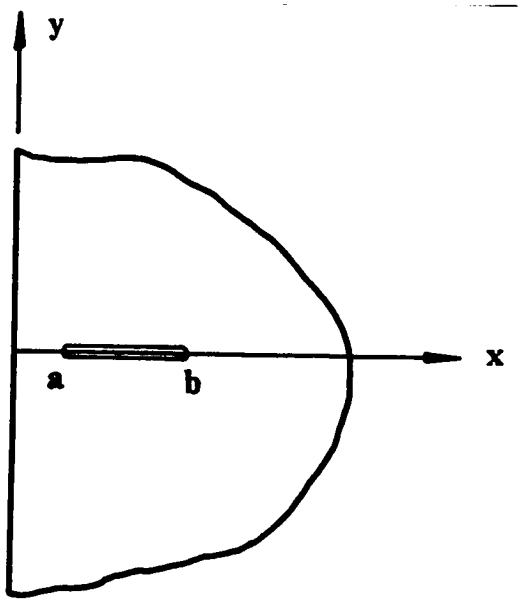

$$\sigma_{xy}(0,y) = 0 \qquad \text{(B.1)}$$

$$\sigma_{xx}(0,y) = 0 \qquad \text{(B.2)}$$

σ_{ij} is bounded at infinity. (B.3)

$$v(x,y) = v(y) = 0 \ , \ x \le a \ , \ x \ge b$$

$$\sigma_y(x,0) = -p(x) \ , \ a<x<b. \qquad \text{(B.4)}$$

Figure B.1

The resulting integral equation is

$$\int_a^b \frac{\phi(t)}{t-x}\,dt + \int_a^b \phi(t)K(x,t)\,dt = -\frac{\pi(1+\kappa)}{2\mu}\,p(x)\ ,\quad a<x<b\ , \tag{B.5}$$

where the non-singular Fredholm kernel,

$$K(x,t) = \frac{-1}{t+x} + \frac{6x}{(t+x)^2} - \frac{4x^2}{(t+x)^3}\ , \tag{B.6}$$

and $\phi(t)$ is the unknown derivative of the crack opening displacement $v(t)$, μ is the shear modulus of the material, and κ is defined in terms of Poisson's ratio ν for both

plane stress: $\kappa = \frac{3-\nu}{1+\nu}$,

and for plane strain: $\kappa = 3-4\nu$. (B.7)

The first integral in Eqn. B.5 is singular and is interpreted in the Cauchy principal value sense, specified as such by a line through the integral sign. One way to define a Cauchy principal value integral is as follows,

$$\int_a^b \frac{\phi(t)}{t-x}\,dt = \lim_{\epsilon\to 0}\left\{\int_a^{x-\epsilon} \frac{\phi(t)}{t-x}\,dt + \int_{x+\epsilon}^b \frac{\phi(t)}{t-x}\,dt\right\}\ . \tag{B.8}$$

By using the standard interpretation of an integral as the area under a curve, note that individually the integrals on the right hand side of Eqn. B.8 do not exist in the limit, but when added together the "infinite areas" will be of opposite sign and will cancel giving a finite result. When the problem in Fig. B.1 is formulated by using the displacement $v(t)$ as the unknown instead of the derivative $\phi(t)$, the resulting integral equation is found to be,

$$\oint_a^b \frac{v(t)}{(t-x)^2}\,dt + \int_a^b v(t)\left[\frac{-\partial K(t,x)}{\partial t}\right] dt = -\frac{\pi(1+\kappa)}{2\mu}\,p(x)\ ,$$

$$a<x<b\ , \qquad \text{(B.9)}$$

where the first integral no longer exists in the Cauchy principal value sense and requires a special interpretation. Throughout the dissertation these integrals are identified by a double dash through the integral sign.

Consider a direct integration by parts of the integrals in Eqn. B.5.

$$\int_a^b \phi(t)K(x,t)\,dt = v(t)K(x,t)\Big|_a^b - \int_a^b v(t)\left[\frac{\partial K(t,x)}{\partial t}\right] dt\ , \qquad \text{(B.10)}$$

$$\int_a^b \frac{\phi(t)}{t-x}\,dt \neq \frac{v(t)}{t-x}\Big|_a^b + \int_a^b \frac{v(t)}{(t-x)^2}\,dt\ . \qquad \text{(B.11)}$$

Here again the same "strongly singular" integral appears. For Eqn. B.11 to be an equality, this integral must be finite just as it must be in Eqn. B.9, so we write,

$$\int_a^b \frac{\phi(t)}{t-x}\,dt = \frac{v(t)}{t-x}\Big|_a^b + \oint_a^b \frac{v(t)}{(t-x)^2}\,dt\ . \qquad \text{(B.12)}$$

Note that Eqn. B.9 is obtained if Eqns. B.10,12 are substituted into Eqn. B.5. The integrated terms cancel for either an internal crack ($0<a<b$) where

$$v(a) = v(b) = 0\ , \qquad \text{(B.13)}$$

or for an edge crack ($0=a$, $0<b$) where

$$v(0)\left[\frac{1}{-x}+K(x,0)\right]=0\ ,\quad v(b)=0\ . \tag{B.14}$$

The fact that a special interpretation of the strongly singular integral in Eqns. B.9,12 is necessary apparently reveals that a "mistake" has been made in the derivation of each equation. This mistake in Eqn. B.11 is corrected when Eqn. B.8 is used when integrating by parts as follows,

$$\fint_a^b \frac{\phi(t)}{t-x}\,dt = \lim_{\epsilon\to 0}\left\{\left[\frac{v(t)}{t-x}\Big|_a^{x-\epsilon}+\int_a^{x-\epsilon}\frac{v(t)}{(t-x)^2}\,dt\right]\right.$$

$$\left.+\left[\frac{v(t)}{t-x}\Big|_{x+\epsilon}^{b}+\int_{x+\epsilon}^{b}\frac{v(t)}{(t-x)^2}\,dt\right]\right\}\ ,$$

$$=\lim_{\epsilon\to 0}\left\{\frac{v(t)}{t-x}\Big|_a^b+\left[\frac{v(x-\epsilon)}{-\epsilon}+\int_a^{x-\epsilon}\frac{v(t)}{(t-x)^2}\,dt\right]\right.$$

$$\left.+\left[\frac{-v(x+\epsilon)}{\epsilon}+\int_{x+\epsilon}^{b}\frac{v(t)}{(t-x)^2}\,dt\right]\right\}\ . \tag{B.15}$$

From Eqns. B.12 and B.15 we obtain a result similar to Eqn. B.8 but for strongly singular integrals:

$$\fint_a^b \frac{v(t)}{(t-x)^2}\,dt = \lim_{\epsilon\to 0}\left\{\left[\frac{v(x-\epsilon)}{-\epsilon}+\int_a^{x-\epsilon}\frac{v(t)}{(t-x)^2}\,dt\right]\right.$$

$$\left.+\left[\frac{-v(x+\epsilon)}{\epsilon}+\int_{x+\epsilon}^{b}\frac{v(t)}{(t-x)^2}\,dt\right]\right\}\ . \tag{B.16}$$

With this definition Eqns. B.9,12 are correct. Consider for example $v(t)=1$.

$$\oint_a^b \frac{1}{(t-x)^2}\,dt = \lim_{\epsilon\to 0}\left\{\left[\frac{-1}{\epsilon} + \frac{-1}{t-x}\Big|_a^{x-\epsilon}\right] + \left[\frac{-1}{\epsilon} + \frac{-1}{t-x}\Big|_{x+\epsilon}^{b}\right]\right\}, \tag{B.17}$$

$$= \lim_{\epsilon\to 0}\left\{\left[\frac{-1}{\epsilon} + \frac{1}{\epsilon} + \frac{1}{a-x}\right] + \left[\frac{-1}{\epsilon} - \frac{1}{b-x} + \frac{1}{\epsilon}\right]\right\}, \tag{B.18}$$

$$= \frac{1}{a-x} - \frac{1}{b-x}\,. \tag{B.19}$$

Note that this would be the result obtained if Eqn. B.17 is integrated directly as though the singularity were not present.

Integrals of this type were studied by Hadamard in 1923 [66] and were referred to as finite-part integrals, a name which describes Eqn. B.16 where the infinite part is subtracted out. For more information on finite-part integrals and their use for problems of the type studied in this dissertation see Kaya [67].

To derive a property that is more useful than eqn B.16 for evaluating finite-part integrals, differentiate Eqn. B.8 with respect to x as follows.

$$\frac{\partial}{\partial x}\oint_a^b \frac{v(t)}{t-x}\,dt = \frac{\partial}{\partial x}\lim_{\epsilon\to 0}\left\{\int_a^{x-\epsilon}\frac{v(t)}{t-x}\,dt + \int_{x+\epsilon}^{b}\frac{v(t)}{t-x}\,dt\right\}. \tag{B.20}$$

Next differentiate on the right before the limit is taken and before integration,

$$\frac{\partial}{\partial x}\oint_a^b \frac{v(t)}{t-x}\,dt = \lim_{\epsilon\to 0}\left\{\left[\frac{v(x-\epsilon)}{-\epsilon} + \int_a^{x-\epsilon}\frac{v(t)}{(t-x)^2}\,dt\right]\right.$$

$$\left. + \left[\frac{-v(x+\epsilon)}{\epsilon} + \int_{x+\epsilon}^{b}\frac{v(t)}{(t-x)^2}\,dt\right]\right\}. \tag{B.21}$$

From Eqn. B.16 we conclude,

$$\oint_a^b \frac{v(t)}{(t-x)^2}\,dt = \frac{\partial}{\partial x}\int_a^b \frac{v(t)}{t-x}\,dt\ . \tag{B.22}$$

By expanding v(t) near the point t=x, another method for the evaluation of finite-part integrals is obtained,

$$\oint_a^b \frac{v(t)}{(t-x)^2}\,dt = \oint_a^b \frac{v(t)-(v(x)+(t-x)v'(x))+(v(x)+(t-x)v'(x))}{(t-x)^2}\,dt \tag{B.23}$$

$$= \int_a^b \frac{v(t)-v(x)-(t-x)v'(x)}{(t-x)^2}\,dt + v(x)\oint_a^b \frac{1}{(t-x)^2}\,dt$$

$$+ v'(x)\oint_a^b \frac{1}{t-x}\,dt\ , \tag{B.24}$$

where

$$v'(x) = \frac{dv}{dx}\ . \tag{B.25}$$

If

$$v(t) = f(t)w(t)\ , \tag{B.26}$$

$$\oint_a^b \frac{f(t)w(t)}{(t-x)^2}\,dt = \int_a^b \frac{f(t)-f(x)-(t-x)f'(x)}{(t-x)^2}w(t)dt + f(x)\oint_a^b \frac{w(t)}{(t-x)^2}\,dt$$

$$+ f'(x)\oint_a^b \frac{w(t)}{t-x}\,dt\ . \tag{B.27}$$

See Appendix A for finite-part and Cauchy principal value integrals with various weight functions and with some commonly used forms of f(t).

APPENDIX C

The Compliance Functions

As indicated in chapter two, the mixed-mode line-spring model requires stress intensity factor solutions of the edge cracked strip for each of the five loadings shown in Fig. 2.3. Three separate two-dimensional problems must be solved to obtain these results. The tension and bending solutions come from symmetric (mode 1) loading, out-of-plane shear results come from skew-symmetric (mode 2) loading, and the anti-plane (mode 3) results are obtained from twisting and from in-plane shear loading. Note that in-plane for a plate corresponds to out-of-plane for plane strain and vice versa.

C.1 Governing equations for in-plane loading.

The governing equations for the mode 1 and 2 cases are from plane elasticity where all field quantities are independent of z. Equilibrium of the solid requires,

$$\frac{\partial \sigma_{xx}}{\partial x} + \frac{\partial \tau_{xy}}{\partial y} = 0 \ , \tag{C.1}$$

$$\frac{\partial \tau_{xy}}{\partial x} + \frac{\partial \sigma_{yy}}{\partial y} = 0 \ . \tag{C.2}$$

For plane strain, Hooke's law relates stresses to strains in terms of the material constants μ are ν which are respectively the shear modulus and Poisson's ratio,

$$\sigma_{xx} = \frac{2\mu}{1-2\nu} \left[(1-\nu)\epsilon_x + \nu\epsilon_y\right] \ , \tag{C.3}$$

$$\sigma_{yy} = \frac{2\mu}{1-2\nu}\left[(1-\nu)\epsilon_y + \nu\epsilon_x\right] , \tag{C.4}$$

$$\tau_{xy} = \mu\gamma_{xy} . \tag{C.5}$$

The plane stress solution can be obtained by replacing ν by $\nu/(1+\nu)$. The strain-displacement relations for linear elasticity are,

$$\epsilon_x = \frac{\partial u}{\partial x} , \quad \epsilon_y = \frac{\partial v}{\partial y} , \quad \gamma_{xy} = \frac{\partial u}{\partial y}\frac{\partial v}{\partial x} , \tag{C.6}$$

where u and v are the x and y components of displacement respectively.

If the relations in Eqn. C.6 are substituted into Eqns. C.3-5 and if the resulting expressions are then substituted into Eqns. C.1,2, Navier's equations for the displacements are obtained:

$$\nabla^2 u + \frac{1}{1-2\nu}\frac{\partial}{\partial x}\left[\frac{\partial u}{\partial x} + \frac{\partial v}{\partial y}\right] = 0 , \tag{C.7}$$

$$\nabla^2 v + \frac{1}{1-2\nu}\frac{\partial}{\partial y}\left[\frac{\partial u}{\partial x} + \frac{\partial v}{\partial y}\right] = 0 . \tag{C.8}$$

The geometry of the cracked strip and the method of superposition are shown in Fig. C.1. Any field quantity on the left of this figure, say f(x,y), is given by,

$$f(x,y) = f_1(x,y) + f_2(x,y) , \tag{C.9}$$

where the subscripts correspond to the geometries on the right. Eqn. C.9 is used for all relations including the boundary conditions. The preceeding information will be used for mode 1 and for mode 2.

C.1.1 Mode 1.

The boundary conditions for the symmetric problem are:

$$\tau_{xy}(x,0) = 0 , \tag{C.10}$$

$$\tau_{xy}(0,y) = 0 ,$$

$$\tau_{xy}(h,y) = 0 \ ,$$

$$\sigma_{xx}(0,y) = 0 \ ,$$

$$\sigma_{xx}(h,y) = 0 \ , \tag{C.11}$$

$$v(x,0) = 0 \ , \ x<a \ , \ b>x \ ,$$

$$\sigma_{yy} = -p(x) \ , \ a<x<b \ . \tag{C.12}$$

To solve problem 1 of Fig. C.1 we introduce the exponential Fourier transform defined as follows,

$$f(x,y) = \frac{1}{2\pi}\int_{-\infty}^{+\infty}\bar{f}(\beta,y)e^{-i\beta x}\,d\beta \ . \tag{C.13}$$

$$\bar{f}(\beta,y) = \int_{-\infty}^{+\infty}f(x,y)e^{i\beta x}\,dx \ . \tag{C.14}$$

When the Fourier transforms of Eqns. C.7,8 are taken, the following ordinary differential equations result,

$$\frac{\partial^2\bar{u}}{\partial y^2} - \beta^2\bar{u} + \frac{1}{1-2\nu}\left[\ -\beta^2\bar{u} + i\beta\frac{\partial\bar{v}}{\partial y}\ \right] , \tag{C.15}$$

$$\frac{\partial^2\bar{v}}{\partial y^2} - \beta^2\bar{v} + \frac{1}{1-2\nu}\left[\ i\beta\frac{\partial\bar{u}}{\partial y} + \frac{\partial^2\bar{v}}{\partial y^2}\ \right] \ . \tag{C.16}$$

These equations are solved for $\bar{u}$ and $\bar{v}$, inverted according to C.13 and then substituted into Eqns. C.3-5 to obtain,

$$u_1(x,y) = \frac{1}{2\pi}\int_{-\infty}^{+\infty}\Big\{\Big[\ A_1(\beta) + yA_2(\beta)\ \Big]e^{-|\beta|y} +$$

$$\Big[\ A_3(\beta) + yA_4(\beta)\ \Big]e^{+|\beta|y}\Big\}\ e^{-i\beta x}\,d\beta \ , \tag{C.17}$$

$$v_1(x,y) = \frac{i}{2\pi}\int_{-\infty}^{+\infty}\frac{\beta}{|\beta|}\Big\{\Big[-A_1(\beta) - (\frac{\kappa}{|\beta|} + y)A_2(\beta)\Big]e^{-|\beta|y} +$$

$$\left[A_3(\beta) - \left(\frac{\kappa}{|\beta|} - y\right)A_4(\beta)\right]e^{+|\beta|y}\Big\} \; e^{-i\beta x} \, d\beta \; , \tag{C.18}$$

$$\sigma_{1xx}(x,y) = \frac{i\mu}{2\pi}\int_{-\infty}^{+\infty}\beta\Big\{\left[-2A_1(\beta) + A_2(\beta)\left(\frac{3-\kappa}{|\beta|} - 2y\right)\right] e^{-|\beta|y} +$$

$$\left[-2A_3(\beta) - A_4(\beta)\left(\frac{3-\kappa}{|\beta|} + 2y\right)\right] e^{+|\beta|y}\Big\} \; e^{-i\beta x} \, d\beta \; , \tag{C.19}$$

$$\sigma_{1yy}(x,y) = \frac{i\mu}{2\pi}\int_{-\infty}^{+\infty}\beta\Big\{\left[2A_1(\beta) + A_2(\beta)\left(\frac{1+\kappa}{|\beta|} + 2y\right)\right] e^{-|\beta|y} +$$

$$\left[2A_3(\beta) + A_4(\beta)\left(-\frac{1+\kappa}{|\beta|} + 2y\right)\right] e^{+|\beta|y}\Big\} \; e^{-i\beta x} \, d\beta \; , \tag{C.20}$$

$$\tau_{1xy}(x,y) = \frac{\mu}{2\pi}\int_{-\infty}^{+\infty}\Big\{\left[-2|\beta|A_1(\beta) + A_2(\beta)(1-\kappa-2|\beta|y)\right] e^{-|\beta|y} +$$

$$\left[2|\beta|A_3(\beta) + A_4(\beta)(1-\kappa+2|\beta|y|)\right] e^{+|\beta|y}\Big\} \; e^{-i\beta x} \, d\beta \; , \tag{C.21}$$

where $\kappa = 3-4\nu$.

For bounded behavior at infinity

$$A_3(\beta) = A_4(\beta) = 0 \; . \tag{C.22}$$

For problem 2 of Fig. C.1 there is symmetry which allows the following Fourier sine and cosine transforms to be used,

$$\bar{u}_2(x,\alpha) = \int_0^{\infty} u_2(x,y)\cos\alpha y \, dy \; , \tag{C.23}$$

$$u_2(x,y) = \frac{2}{\pi}\int_0^{\infty}\bar{u}_2(x,\alpha)\cos\alpha y \, d\alpha \; , \tag{C.24}$$

$$\bar{v}_2(x,\alpha) = \int_0^{\infty} v_2(x,y)\sin\alpha y \, dy \; , \tag{C.25}$$

$$v_2(x,y) = \frac{2}{\pi}\int_0^{\infty}\bar{v}_2(x,\alpha)\sin\alpha y \, d\alpha \; . \tag{C.26}$$

After performing an identical analysis as was done with problem 1, we obtain,

$$u_2(x,y) = \frac{2}{\pi}\int_0^\infty \Big\{\Big[\, B_1(\alpha) + B_2(\alpha)\big(\tfrac{\kappa}{\alpha} + x\big) \,\Big]e^{-\alpha x} -$$

$$\Big[\, B_3(\alpha) - B_4(\alpha)\big(\tfrac{\kappa}{\alpha} - x\big) \,\Big]e^{\alpha x}\Big\}\cos\alpha y \; d\alpha \;, \tag{C.27}$$

$$v_2(x,y) = \frac{2}{\pi}\int_0^\infty \Big\{\Big[B_1(\alpha) + xB_2(\alpha)\Big]e^{-\alpha x} +$$

$$\Big[B_3(\alpha) + xB_4(\alpha)\Big]e^{\alpha x}\Big\}\sin\alpha y \; d\alpha \;, \tag{C.28}$$

$$\sigma_{2xx}(x,y) = \frac{-2\mu}{\pi}\int_0^\infty \alpha\Big\{\Big[2B_1(\alpha) + B_2(\alpha)\big(\tfrac{1+\kappa}{\alpha} + 2x\big)\Big]\; e^{-\alpha x} +$$

$$\Big[2B_3(\alpha) + B_4(\alpha)\big(\tfrac{1+\kappa}{-\alpha} + 2x\big)\Big]\; e^{\alpha x}\Big\}\cos\alpha y \; d\alpha \;, \tag{C.29}$$

$$\sigma_{2yy}(x,y) = \frac{-2\mu}{\pi}\int_0^\infty \alpha\Big\{\Big[-2B_1(\alpha) + B_2(\alpha)\big(\tfrac{3-\kappa}{\alpha} - 2x\big)\Big]\; e^{-\alpha x} +$$

$$\Big[-2B_3(\alpha) - B_4(\alpha)\big(\tfrac{3-\kappa}{\alpha} + 2x\big)\Big]\; e^{\alpha x}\Big\}\cos\alpha y \; d\alpha \;, \tag{C.30}$$

$$\tau_{2xy}(x,y) = \frac{2\mu}{\pi}\int_0^\infty \Big\{\Big[-2\alpha B_1(\alpha) + B_2(\alpha)(1-\kappa-2\alpha x)\Big]\; e^{-\alpha x} +$$

$$\Big[2\alpha B_3(\alpha) + B_4(\alpha)(1-\kappa+2\alpha x)\Big]\; e^{\alpha x}\Big\}\sin\alpha y \; d\alpha \;. \tag{C.31}$$

Now the boundary conditions, Eqns. C.10-12 are applied making use of Eqn. C.9. First Eqn. C.10 relates $A_1(\beta)$ to $A_2(\beta)$ as follows,

$$A_1(\beta) = \frac{1-\kappa}{2|\beta|}\, A_2(\beta) \;. \tag{C.32}$$

Now introduce a new unknown,

$$v(x) = v(x,0) \;,$$

and express $A_2(\beta)$ in terms of it.

$$A_2(\beta) = \frac{2i\beta}{1+\kappa}\int_{-\infty}^{+\infty} v(t)e^{i\beta t}dt = \frac{2i\beta}{1+\kappa}\int_a^b v(t)e^{i\beta t}dt \ . \tag{C.33}$$

The unknowns in the problem are $v(x)$ and $B_i(\alpha)$, $i=1,\ldots,4$. Eqns. C.11 produce a linear system of four equations that determine $B_i(\alpha)$ as follows,

$$B_i(\alpha) = \sum_{j=1}^{4}\frac{I_j\gamma_{ij}}{\Delta} \ , \tag{C.34}$$

where

$$\Delta = e^{2\alpha h} - (4\alpha^2h^2 + 2) + e^{-2\alpha h} \ , \tag{C.35}$$

$$\gamma_{11} = -(\kappa-1)e^{2\alpha h} + [-4\alpha^2h^2 - 2\alpha h(\kappa-1) + (\kappa-1)] \ ,$$

$$\gamma_{12} = e^{\alpha h}\ [2\alpha h\kappa + \kappa - 1] + e^{-\alpha h}\ [-2\alpha h - \kappa + 1] \ ,$$

$$\gamma_{13} = -(\kappa+1)e^{2\alpha h} + [4\alpha^2h^2 + 2\alpha h(\kappa+1) + (\kappa+1)] \ ,$$

$$\gamma_{14} = e^{\alpha h}\ [-2\alpha h\kappa + \kappa + 1] + e^{-\alpha h}\ [-2\alpha h - \kappa - 1] \ ,$$

$$\gamma_{21} = 2\alpha e^{2\alpha h} + (4\alpha^2h - 2\alpha) \ ,$$

$$\gamma_{22} = e^{\alpha h}\ [-4\alpha^2h - 2\alpha] + 2\alpha e^{-\alpha h} \ ,$$

$$\gamma_{23} = 2\alpha e^{2\alpha h} - (4\alpha^2h + 2\alpha) \ ,$$

$$\gamma_{24} = e^{\alpha h}\ [4\alpha^2h - 2\alpha] + 2\alpha e^{-\alpha h} \ ,$$

$$\gamma_{31} = [-4\alpha^2h^2 + 2\alpha h(\kappa-1) + (\kappa-1)] - e^{-2\alpha h}(\kappa-1) \ ,$$

$$\gamma_{32} = e^{\alpha h}\ [2\alpha h - (\kappa-1)] + e^{-\alpha h}[-2\alpha h\kappa + (\kappa-1)] \ ,$$

$$\gamma_{33} = [-4\alpha^2h^2 + 2\alpha h(\kappa+1) - (\kappa+1)] + (\kappa+1)e^{-2\alpha h} \ ,$$

$$\gamma_{34} = e^{\alpha h}\,[-2\alpha h + (\kappa+1)] - e^{-\alpha h}\,[2\alpha h\kappa + (\kappa+1)] \ ,$$

$$\gamma_{41} = [4\alpha^2 h + 2\alpha] - 2\alpha e^{-2\alpha h} \ ,$$

$$\gamma_{42} = -2\alpha e^{\alpha h} + [-4\alpha^2 h + 2\alpha]\ e^{-\alpha h} \ ,$$

$$\gamma_{43} = [4\alpha^2 h - 2\alpha] + 2\alpha e^{-2\alpha h} \ ,$$

$$\gamma_{44} = 2\alpha e^{\alpha h} + [-4\alpha^2 h - 2\alpha]\ e^{-\alpha h} \ , \tag{C.36}$$

and

$$I_1 = \frac{-1}{2(1+\kappa)} \int_a^b (1-\alpha t) e^{-\alpha t} v(t)\ dt \ ,$$

$$I_2 = \frac{-1}{2(1+\kappa)} \int_a^b [1-\alpha(h-t)] e^{-\alpha(h-t)} v(t)\ dt \ ,$$

$$I_3 = \frac{-1}{2(1+\kappa)} \int_a^b (2-\alpha t) e^{-\alpha t} v(t)\ dt \ ,$$

$$I_4 = \frac{1}{2(1+\kappa)} \int_a^b [2-\alpha(h-t)] e^{-\alpha(h-t)} v(t)\ dt \ . \tag{C.37}$$

The mixed boundary condition gives a singular integral equation for $v(x)$, $a<x<b$.

$$\fint_a^b v(t)\left\{\frac{1}{(t-x)^2} + K_C(x,t)\right\} dt + \int_a^b K_{I1}(x,t) v(t)\ dt = \frac{-\pi(1+\kappa)}{4\mu}\ p(x) \ , \tag{C.38}$$

where

$$K_C = -\frac{1}{(t+x)^2} + \frac{12xt}{(t+x)^4} - \frac{1}{(2h-x-t)^2} + \frac{12(h-x)(h-t)}{(2h-x-t)^4} \ , \tag{C.39}$$

and

$$K_{I1}(x,t) = \int_0^\infty \Big[S_1(x,t,\alpha) + S_1(h-x,h-t,\alpha)$$

$$+ S_2(x,t,\alpha) + S_2(h-x,h-t,\alpha) \Big] d\alpha , \tag{C.40}$$

$$S_1(x,t,\alpha) = \frac{e^{-(x+t)\alpha}}{\Delta} \Big\{ e^{-2\alpha h}\Big[-2\alpha^3 xt+\alpha^2(3x+3t)-5\alpha\Big]+8\alpha^5 h^2 xt$$

$$-12\alpha^4 h^2(x+t)+\alpha^3\Big[2hx+18h^2+2xt+2ht\Big]+\alpha^2\Big[-3x-3t-6h\Big]+5\alpha\Big\} , \tag{C.41}$$

$$S_2(x,t,\alpha) = \frac{\alpha e^{(x-t)\alpha}}{\Delta} \Big\{ e^{-2\alpha h}\Big[-\alpha(x-t)-3\Big]+\alpha^3\Big[-4h^2 t+4hxt\Big]$$

$$+\alpha^2\Big[6h^2-6hx+6ht\Big]+\alpha\Big[x-t-10h\Big]+3\Big\} , \tag{C.42}$$

$$\Delta = e^{2\alpha h} - (4\alpha^2 h^2 + 2) + e^{-2\alpha h} . \tag{C.43}$$

For an edge crack a=0. The loading for tension is,

$$p(x) = \sigma_1 , \tag{C.44}$$

and for bending,

$$p(x) = \frac{2\sigma_2}{h} \left[\frac{h}{2} - x \right] . \tag{C.45}$$

C.1.2 Mode 2.

The boundary conditions for the skew-symmetric case are,

$$\sigma_{yy}(x,0) = 0 , \tag{C.46}$$

$$\tau_{xy}(0,y) = 0 ,$$

$$\tau_{xy}(h,y) = 0 ,$$

$$\sigma_{xx}(0,y) = 0 ,$$

$$\sigma_{xx}(h,y) = 0 , \tag{C.47}$$

$$u(x,0) = 0 \ , \ x<a \ , \ b>x \ ,$$

$$\tau_{xy} = -p(x) \ , \ a<x<b \ . \tag{C.48}$$

The symmetry of problem 2 in Fig. C.1 for the above boundary conditions suggests the following Fourier transforms of the displacements,

$$\bar{u}_2(x,\alpha) = \int_0^\infty u_2(x,y)\sin\alpha y \ dy \ , \tag{C.49}$$

$$u_2(x,y) = \frac{2}{\pi}\int_0^\infty \bar{u}_2(x,\alpha)\sin\alpha y \ d\alpha \ , \tag{C.50}$$

$$\bar{v}_2(x,\alpha) = \int_0^\infty v_2(x,y)\cos\alpha y \ dy \ , \tag{C.51}$$

$$v_2(x,y) = \frac{2}{\pi}\int_0^\infty \bar{v}_2(x,\alpha)\cos\alpha y \ d\alpha \ . \tag{C.52}$$

When these expressions are used to solve C.7,8 the result is,

$$u_2(x,y) = \frac{2}{\pi}\int_0^\infty \Big\{-\Big[C_1(\alpha) + C_2(\alpha)(\tfrac{\kappa}{\alpha} + x) \Big]e^{-\alpha x} +$$

$$\Big[C_3(\alpha) - C_4(\alpha)(\tfrac{\kappa}{\alpha} - x) \Big]e^{\alpha x}\Big\}\sin\alpha y \ d\alpha \ , \tag{C.53}$$

$$v_2(x,y) = \frac{2}{\pi}\int_0^\infty \Big\{\Big[C_1(\alpha) + xC_2(\alpha)\Big]e^{-\alpha x} +$$

$$\Big[C_3(\alpha) + xC_4(\alpha)\Big]e^{\alpha x}\Big\}\cos\alpha y \ d\alpha \ , \tag{C.54}$$

$$\sigma_{2xx}(x,y) = \frac{2\mu}{\pi}\int_0^\infty \alpha\Big\{\Big[2C_1(\alpha) + C_2(\alpha)(\tfrac{1+\kappa}{\alpha} + 2x)\Big] \ e^{-\alpha x} +$$

$$\Big[2C_3(\alpha) + C_4(\alpha)(\ \tfrac{1+\kappa}{-\alpha} + 2x)\Big] \ e^{\alpha x}\Big\}\sin\alpha y \ d\alpha \ , \tag{C.55}$$

$$\sigma_{2yy}(x,y) = \frac{2\mu}{\pi}\int_0^\infty \alpha\Big\{\Big[-2C_1(\alpha) + C_2(\alpha)(\frac{3-\kappa}{\alpha} - 2x)\Big]\, e^{-\alpha x} +$$

$$\Big[-2C_3(\alpha) - C_4(\alpha)(\frac{3-\kappa}{\alpha} + 2x)\Big]\, e^{\alpha x}\Big\}\sin\alpha y\, d\alpha \ , \tag{C.56}$$

$$\tau_{2xy}(x,y) = \frac{2\mu}{\pi}\int_0^\infty \Big\{\Big[-2\alpha C_1(\alpha) + C_2(\alpha)(1-\kappa-2\alpha x)\Big]\, e^{-\alpha x} +$$

$$\Big[2\alpha C_3(\alpha) + C_4(\alpha)(1-\kappa+2\alpha x)\Big]\, e^{\alpha x}\Big\}\cos\alpha y\, d\alpha \ . \tag{C.57}$$

The solution to problem 1 in the superposition of Fig. C.1 is the same as for mode 1 (Eqns. C.17-21). Eqn. C.46 gives,

$$A_1(\beta) = \frac{-(1+\kappa)}{2|\beta|}\, A_2(\beta) \ . \tag{C.58}$$

After defining

$$u(x) = u(x,0) \tag{C.59}$$

as a new unknown we can express,

$$A_2(\beta) = \frac{-2|\beta|}{(\kappa+1)}\int_{-\infty}^{+\infty} u(x)e^{i\beta x}\, dx = \frac{-2|\beta|}{(\kappa+1)}\int_a^b u(x)e^{i\beta x}\, dx \ . \tag{C.60}$$

The $C_i(\alpha)$ are determined from Eqns. C.47 to be,

$$C_i(\alpha) = \sum_{j=1}^{4}\frac{I_j\gamma_{ij}}{\Delta} \ , \tag{C.61}$$

where γ_{ij} and Δ are the same as for mode 1 (Eqns. C.35,36) and the I_j's are found to be,

$$I_1 = \frac{-1}{2(1+\kappa)}\int_a^b \alpha t e^{-\alpha t}u(t)\, dt$$

$$I_2 = \frac{1}{2(1+\kappa)}\int_a^b \alpha(h-t)]e^{-\alpha(h-t)}u(t)\, dt$$

$$I_3 = \frac{1}{2(1+\kappa)} \int_a^b (1-\alpha t)e^{-\alpha t}u(t)\ dt$$

$$I_4 = \frac{1}{2(1+\kappa)} \int_a^b [1-\alpha(h-t)]e^{-\alpha(h-t)}u(t)\ dt\ . \tag{C.62}$$

The mixed boundary condition, Eqn. C.48, gives a singular integral equation for u(x), a<x<b.

$$\fint_a^b u(t)\left\{\frac{1}{(t-x)^2} + K_C(x,t)\right\} dt + \int_a^b K_{I2}(x,t)u(t)\ dt = \frac{-\pi(1+\kappa)}{4\mu}\ p(x)\ , \tag{C.63}$$

where

$$K_C = -\frac{1}{(t+x)^2} + \frac{12xt}{(t+x)^4} - \frac{1}{(2h-x-t)^2} + \frac{12(h-x)(h-t)}{(2h-x-t)^4}\ , \tag{C.64}$$

and

$$K_{I2}(x,t) = \int_0^\infty \Big[\ S_3(x,t,\alpha) + S_3(h-x,h-t,\alpha)$$

$$+ S_4(x,t,\alpha) + S_4(h-x,h-t,\alpha)\ \Big]\ d\alpha\ , \tag{C.65}$$

$$S_3(x,t,\alpha) = \frac{e^{-(x+t)\alpha}}{\Delta}\left\{e^{-2\alpha h}\Big[-2\alpha^3xt+\alpha^2(x+t)-\alpha\Big]+8\alpha^5h^2xt\right.$$

$$\left.-4\alpha^4h^2(x+t)+\alpha^3\Big[2hx+2h^2+2xt+2ht\Big]-\alpha^2\Big[x+t+2h\Big]+\alpha\right\}\ , \tag{C.66}$$

$$S_4(x,t,\alpha) = \frac{\alpha e^{(t-x)\alpha}}{\Delta}\left\{e^{-2\alpha h}\Big[\alpha(t-x)+1\Big]+\alpha^3\Big[4h^2x-4hxt\Big]\right.$$

$$\left.+\alpha^2\Big[-2h^2-2hx+2ht\Big]+\alpha\Big[-t+x+2h\Big]-1\right\}\quad , \tag{C.67}$$

$$\Delta = e^{2\alpha h} - (4\alpha^2h^2 + 2) + e^{-2\alpha h}\ . \tag{C.68}$$

For an edge crack a=0. To obtain the mode 2 stress intensity factor for parabolic shear loading we let

$$p(x) = \sigma_3(2/h)^2 x(h-x) \ . \tag{C.69}$$

C.2 Anti-plane shear.

The governing equation for anti-plane shear is,

$$\nabla^2 w = 0 \ , \tag{C.70}$$

where w is the z-component of displacement. The stresses and strains can be written in terms of w,

$$\tau_{xz} = \mu\frac{\partial w}{\partial x} \ , \qquad \tau_{yz} = \mu\frac{\partial w}{\partial y} \ , \tag{C.71}$$

$$\gamma_{xz} = \frac{\partial w}{\partial x} \ , \qquad \gamma_{yz} = \frac{\partial w}{\partial y} \ . \tag{C.72}$$

All other components are zero. Again the superposition of Fig. C.1 together with Eqn. C.9 are used. The general solution for w(x,y) in terms of the Fourier transforms of Eqns. C.13,14 and C.25,26 is,

$$w(x,y) = \frac{1}{2\pi}\int_{-\infty}^{+\infty} A_1(\beta)e^{-|\beta|y}e^{-i\beta x}\, d\beta \ +$$

$$\frac{2}{\pi}\int_0^{\infty}\left[B_1(\alpha)e^{-\alpha x} + B_2(\alpha)e^{\alpha x}\right] \sin\alpha y \ d\alpha \ . \tag{C.73}$$

There are three unknowns in the above equation and the following conditions will determine them,

$$\tau_{xz}(0,y) = 0 \ , \tag{C.74}$$

$$\tau_{xz}(h,y) = 0 \ , \tag{C.75}$$

$$\tau_{yz}(x,0) = -p(x) \ , \ a<x<b \ ,$$

$$w(x,0) = 0 \ , \ x<a, \ x>b \ . \tag{C.76}$$

After defining

$$\phi(x) = \frac{\partial w}{\partial x}\Big|_{y=0} , \tag{C.77}$$

Eqn. C.73 becomes,

$$\phi(x) = \frac{1}{2\pi} \int_{-\infty}^{+\infty} -i\beta A_1(\beta) e^{-i\beta x} \, d\beta . \tag{C.78}$$

Inversion (Eqns. C.13,14) and Eqn. C.76 give,

$$-i\beta A_1(\beta) = \int_{-\infty}^{+\infty} \phi(t) e^{i\beta t} \, dt = \int_a^b \phi(t) e^{i\beta t} \, dt . \tag{C.79}$$

In order to apply boundary conditions C.74.75, Eqns. C.71,73 and 79 are used to express,

$$\tau_{xz}(x,y) = \frac{\mu}{2\pi} \int_a^b \frac{2\phi(t)}{y^2+(t-x)^2} \, dt$$

$$+\frac{2\mu}{\pi} \int_0^\infty \left[-\alpha B_1(\alpha) e^{-\alpha x} + \alpha B_2(\alpha) e^{\alpha x}\right] \sin\alpha y \, d\alpha . \tag{C.80}$$

Eqns. C.74,75 give the following two inverted equations,

$$B_1(\alpha) e^{-\alpha h} - B_2(\alpha) e^{\alpha h} = \frac{1}{2\alpha} \int_a^b \phi(t) \, e^{-\alpha(h-t)} dt = I_1, \tag{C.81}$$

$$B_1(\alpha) - B_2(\alpha) = \frac{1}{2\alpha} \int_a^b \phi(t) \, e^{-\alpha t} \, dt = I_2 , \tag{C.82}$$

where the following integral has been used,

$$\int_0^\infty \frac{y \sin\alpha y}{y^2+(h-t)^2} \, dy = \frac{\pi}{2} \, e^{-\alpha(h-t)} . \tag{C.83}$$

The solution is,

$$B_1(\alpha) = \frac{-I_1 e^{-\alpha y} + I_2}{-e^{-2\alpha h} + 1} , \tag{C.84}$$

$$B_2(\alpha) = \frac{-I_1 e^{-\alpha y} + I_2 e^{-2\alpha h}}{-e^{-2\alpha h} + 1} , \tag{C.85}$$

where I_1 and I_2 are defined in Eqns. C.81,82. Next we apply the mixed boundary condition C.76. Eqns. C.71 and C.73 must be used to express

$$\tau_{yz}(x,0) = -p(x) = \lim_{y\to 0} \frac{\mu}{2\pi} \int_a^b \phi(t) \int_{-\infty}^{+\infty} -i\frac{|\beta|}{\beta} e^{-|\beta| y} e^{i\beta(t-x)} d\beta \, dt +$$

$$\lim_{y\to 0} \frac{\mu}{\pi} \int_a^b \phi(t) \int_0^\infty \frac{1}{D} \left\{ -e^{-\alpha(x+2h-t)} + e^{-\alpha(x+t)} - e^{-\alpha(-x+2h-t)} + e^{-\alpha(-x+2h+t)} \right\} d\alpha , \tag{C.86}$$

where

$$D = 1 - e^{-2\alpha h} . \tag{C.87}$$

After using the following integrals,

$$\int_{-\infty}^{+\infty} -i\frac{|\beta|}{\beta} e^{-|\beta| y} e^{i\beta(t-x)} d\beta = \frac{2(t-x)}{y^2 + (t-x)^2} , \tag{C.88}$$

$$\int_0^\infty \frac{1}{D} \left\{ e^{-\alpha(x+t)} - e^{-\alpha(-x+2h-t)} \right\} d\alpha = \frac{\pi}{2h} \cot\frac{(x+t)\pi}{2h} , \tag{C.89}$$

Eqn. C.87 becomes,

$$\frac{1}{\pi} \int_a^b \phi(t) \left\{ \frac{\pi}{2h} \left[\cot\frac{(x+t)\pi}{2h} - \cot\frac{(x-t)\pi}{2h} \right] \right\} dt = \frac{-1}{\mu} p(x) . \tag{C.90}$$

This kernel is equivalent to the following,

$$\begin{aligned} \frac{\pi}{2h} \left[\cot\frac{(x+t)\pi}{2h} - \cot\frac{(x-t)\pi}{2h} \right] &= \frac{1}{t-x} && \text{(Cauchy kernel)} \\ &+ \frac{\pi}{2h} \cot\frac{(x+t)\pi}{2h} && \text{(generalized Cauchy kernel)} \\ &+ \frac{1}{x-t} - \frac{\pi}{2h} \cot\frac{(x-t)\pi}{2h} && \text{(Fredholm kernel)} . \end{aligned} \tag{C.91}$$

This same problem formulated in a different way has been solved in closed form (see [77]). The solution for an edge crack is,

$$\tau_{yz}(x,y) = \frac{\mu}{2h} \frac{\sin(\frac{\pi a}{2h})}{\sqrt{\sin^2(\frac{\pi x}{2h})-\sin^2(\frac{\pi a}{2h})}} \int_{-a}^{+a} \frac{g(\tau)\sqrt{1-k^2\sin^2(\frac{\pi\tau}{2h})}}{\sin\frac{\pi}{2h}(\tau-x)} d\tau \ , \tag{C.92}$$

where

$$g(x) = g(-x) \ , \tag{C.93}$$

and

$$k = (\sin\frac{\pi a}{2h})^{-1} \ . \tag{C.94}$$

The stress intensity factor is defined as,

$$k_3 = \lim_{x\to a} \sqrt{2(x-a)}\ \tau_{yz}(x,0) \ , \tag{C.95}$$

so

$$k_3 = \frac{\mu a}{h}\sqrt{\frac{h}{2\pi}\tan\frac{\pi a}{2h}} \int_{-1}^{+1} \frac{g(at)\sqrt{1-k^2\sin^2(\frac{\pi a}{2h}t)}}{\sin\frac{\pi}{2h}(t-1)} dt \ , \tag{C.96}$$

For in-plane shear,

$$g(x) = \sigma_4 \ , \tag{C.97}$$

so

$$\frac{k_3}{\sigma_4\sqrt{a}} = \sqrt{\frac{2}{\pi\xi}\tan(\frac{\pi}{2}\xi)} \ , \quad \xi = a/h \ . \tag{C.98}$$

Because of this simple expression α_{44} (Eqn. 2.27) can be determined in closed form,

$$\alpha_{44} = \frac{-4}{\pi(1-\nu)} \ln[\cos(\frac{\pi}{2}\xi)] \ . \tag{C.99}$$

For twisting,

$$g(x) = \frac{2\sigma_5}{h}\left[\frac{b}{2} - |x|\right] , \tag{C.100}$$

so

$$\frac{k_3}{\sigma_4\sqrt{a}} = \sqrt{\frac{2}{\pi\xi}\tan(\frac{\pi}{2}\xi)}\left\{ 1 - \frac{8}{\pi^2}\int_0^1 \frac{\sin^{-1}t/k}{\sqrt{1-t^2}}\,dt \right\} . \tag{C.101}$$

C.3 Edge Crack SIF Curve Fitting

The five solutions are listed in table C.1. In addition to the solutions required by the line-spring model, constant out-of-plane shear (σ_6) is also included.

The line-spring model requires stress intensity factors at any value of $\xi = a/h$, so a curve is fit to each solution appearing in table C.1. For mode 1 the asymptotic analysis of Benthem and Koiter, [65] suggests that as ξ approaches 1 the stress intensity factor goes to infinity with a power of 3/2. Therefore for $g_1(\xi)$ and $g_2(\xi)$ we use

$$g_i(\xi) = \frac{1}{(1-\xi)^{3/2}} \sum_{k=0}^{12} C_{ik}\xi^k , \quad i = 1,2 . \tag{C.102}$$

For all other cases a 1/2 power is used,

$$g_i(\xi) = \frac{1}{(1-\xi)^{1/2}} \sum_{k=0}^{8} C_{ik}\xi^k , \quad i = 3,4,5,6. \tag{C.103}$$

Although the singular behavior for mode 2 seems to be the same as for mode 1, (see Eqns. C.38,39 vs. 63,64), the form given in Eqn. C.103 produced a better fit than did 102. For twisting and in-plane-shear the form of 103 is correct as can be seen by Eqns. C.98,101. The C_{ij} are given in tables C.2,3. These curves reproduce the numbers in table C.1. The most difficult curves to obtain and to fit are the mode 1 curves. The limiting values for ξ approaching 1 are given in

[65] to be 1.122 and .374 for tension and for bending respectively. The curve given by Eqn. C.102 produces 1.1229 and .3735 which shows both good data and a good curve fit.

For reference the compliance curves that have been used in the literature to date are listed below. They are for tension and bending only.

1. Gross and Srawley, 1965, [61], used in Refs. [2,3].

$$\frac{k_1}{\sigma_1\sqrt{a}} = \frac{1}{\sqrt{\pi}}\left\{1.99-.41\xi+18.7\xi^2-38.48\xi^3+53.85\xi^4\right\} \quad , \qquad (C.104)$$

$$\frac{k_1}{\sigma_2\sqrt{a}} = \frac{1}{\sqrt{\pi}}\left\{1.99-2.47\xi+12.97\xi^2-23.17\xi^3+24.8\xi^4\right\} \quad . \qquad (C.105)$$

2. Tada, Paris, Irwin, 1973, [62], used in Refs. [50,51,53,55].

$$\frac{k_1}{\sigma_1\sqrt{a}} = \left\{\frac{2}{\pi\xi}\tan\frac{\pi\xi}{2}\right\}^{1/2}\left\{\frac{.752+2.02\xi+.37[1-\sin(\pi\xi/2)]^3}{\cos(\pi\xi/2)}\right\} \quad , \qquad (C.106)$$

$$\frac{k_1}{\sigma_2\sqrt{a}} = \left\{\frac{2}{\pi\xi}\tan\frac{\pi\xi}{2}\right\}^{1/2}\left\{\frac{.923+.199[1-\sin(\pi\xi/2)]^4}{\cos(\pi\xi/2)}\right\} \quad . \qquad (C.107)$$

3. Kaya and Erdogan, 1980, [63], used in Refs. [54,56-60].

$$\frac{k_1}{\sigma_1\sqrt{a}} = 1.1216+6.5200\xi^2-12.3877\xi^4+89.0554\xi^6$$

$$-188.6080\xi^8+207.3870\xi^{10}-32.0524\xi^{12} \quad , \qquad (C.108)$$

$$\frac{k_1}{\sigma_1\sqrt{a}} = 1.1202-1.8872\xi+18.0143\xi^2-87.3851\xi^3$$

$$+241.9124\xi^4-319.9402\xi^5+168.0105\xi^6 \quad . \qquad (C.109)$$

C.4 Line-Spring Model SIF Normalization

The stress intensity factor solutions for the line-spring model are normalized with respect to the corresponding plane strain value at the center of the crack. This shows how the constraining effect of the ends affects the crack driving force. The dimensional SIFs provided by the LSM are

$$K_1 = \sqrt{\pi\xi h}\,[\,\sigma_1 g_1 + \sigma_2 g_2\,]\ , \tag{C.110}$$

$$K_2 = \sqrt{\pi\xi h}\,\sigma_3 g_3\ , \tag{C.111}$$

$$K_3 = \sqrt{\pi\xi h}\,[\,\sigma_4 g_4 + \sigma_5 g_5\,]\ . \tag{C.112}$$

These are normalized with respect to

$$K_{j0} = \sqrt{\pi\xi_0 h}\,\sigma^{\infty}_k g_k(\xi_0)\ , \tag{C.113}$$

where k corresponds to the loading and j=1 when k=1,2, j=2 when k=3, and j=3 when k=4,5. Note that the primary SIF is used for all modes given in Eqns. C.110-112.

Table C.1 Stress intensity factors for an edge cracked strip for tension, bending, constant in-plane-shear, parabolic out-of-plane shear , twisting, and constant out-of-plane shear.

STRESS INTENSITY FACTORS

a/h	$\frac{k_1}{\sigma_1\sqrt{a}}$	$\frac{k_1}{\sigma_2\sqrt{a}}$	$\frac{k_2}{\sigma_3\sqrt{a}}$	$\frac{k_3}{\sigma_4\sqrt{a}}$	$\frac{k_3}{\sigma_5\sqrt{a}}$	$\frac{k_2}{\sigma_6\sqrt{a}}$
.0	1.1215	1.1215	0.	1.	1.	1.1215
.025	1.1264	1.0921	0.0670	1.0003	0.9684	1.1215
.05	1.1399	1.0708	0.1313	1.0010	0.9373	1.12155
.1	1.1892	1.0472	0.2522	1.0041	0.8765	1.1219
.15	1.2652	1.0432	0.3628	1.0094	0.8172	1.1233
.2	1.3673	1.0553	0.4638	1.0170	0.7594	1.1264
.25	1.4975	1.0822	0.5556	1.0270	0.7030	1.1323
.3	1.6599	1.1241	0.6392	1.0398	0.6477	1.1419
.35	1.8612	1.1826	0.7156	1.0558	0.5935	1.1562
.4	2.1114	1.2606	0.7859	1.0753	0.5403	1.1763
.45	2.4253	1.3630	0.8512	1.0992	0.4881	1.2034
.5	2.8246	1.4972	0.9131	1.1284	0.4368	1.2391
.55	3.3428	1.6747	0.9733	1.1642	0.3864	1.2854
.6	4.0332	1.9140	1.0339	1.2085	0.3369	1.3450
.65	4.9843	2.2459	1.0980	1.2642	0.2883	1.4221
.7	6.3549	2.7252	1.1700	1.3360	0.2408	1.5229
.725	7.2838	3.0500	1.2111	1.3801	0.2174	1.5852
.75	8.4532	3.4582	1.2572	1.4315	0.1943	1.6578
.775	9.9596	3.9830	1.3102	1.4922	0.1715	1.7435
.8	11.955	4.6764	1.3726	1.5650	0.1491	1.8459
.825	14.694	5.6248	1.4482	1.6541	0.1272	1.9708
.85	18.628	6.9817	1.5429	1.7663	0.1057	2.1269
.875	24.634	9.0444	1.6664	1.9125	0.0848	2.3289
.9	34.632	12.462	1.8368	2.1133	0.0646	2.6037
.91	40.659	14.515	1.9251			2.7448
.92	48.632	17.225	2.0304			2.9116
.925			2.0911	2.4114	0.0453	3.0074
.93	59.559	20.932	2.1584			3.1132
.94	75.23	26.236	2.3185			3.3634
.95	99.14	34.306	2.5260	2.9180	0.0273	3.6854

Table C.2 The compliance coefficients for $g_1(\xi)$ and $g_2(\xi)$ for tension and bending respectively.

COMPLIANCE COEFFICIENTS

Mode 1

k	C_{1k}	C_{2k}
0	1.12152	1.12152
1	-1.67890	-3.04507
2	8.43058	10.49184
3	-29.46644	-36.66780
4	84.43442	110.09900
5	-182.95329	-255.68184
6	274.45012	421.97167
7	-252.12029	-440.50866
8	92.30672	199.37326
9	62.66657	123.93056
10	-88.30652	-237.97164
11	37.54045	136.17068
12	-5.30201	-28.91005

Table C.3 The compliance coefficients for $g_i(\xi)$, i=3,4,5,6, for parabolic in-plane-shear, constant out-of-plane shear, twisting and constant in-plane-shear respectively.

COMPLIANCE COEFFICIENTS

Modes 2 and 3

k	C_{3k}	C_{4k}	C_{5k}	C_{6k}
0	0.0	1.0	1.0	1.12152
1	2.73069	-0.4999949	-1.773760	-0.55939
2	-3.44019	0.2860705	0.937496	-0.18069
3	0.33305	-0.2661996	-0.602894	0.39478
4	2.80514	0.2193511	1.176914	2.07787
5	-2.94406	-0.1731221	-2.183231	-5.40893
6	0.74775	0.1047768	2.906943	5.82745
7	0.63860	-0.0418068	-2.121964	-3.11784
8	-0.32028	0.0075456	0.659759	0.67088

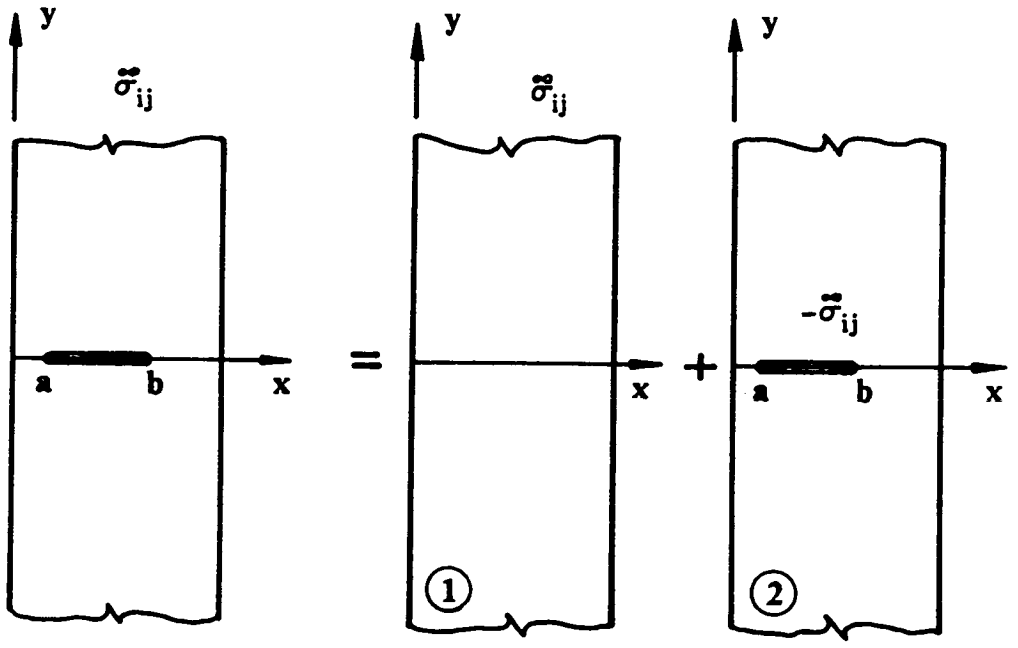

Figure C.1 The geometry and superposition for the cracked strip.

APPENDIX D

Determination of the Weight Function

The solution of a singular integral equation such as Eqn. B.5 or the strongly singular version, Eqn. B.9 involves obtaining $\phi(x)$ or $v(x)$ for $a<x<b$. Before attempting the numerical solution, the behavior or weight of the unknown at the endpoints, a and b, should be determined that will force the singular or dominant integral to be of the same order as the other terms in the equation. Without this asymptotic behavior an accurate solution near the ends is difficult to obtain, although in the central portion convergence is acceptable (at least for the integral equations studied in this dissertation). We then seek to obtain α and β defined as,

$$\phi(t) = f(t)w_1(t) = f(t)(b-t)^{\alpha-1}(t-a)^{\beta-1} , \tag{D.1}$$

$$v(t) = g(t)w_2(t) = g(t)(b-t)^{\alpha}(t-a)^{\beta} , \tag{D.2}$$

for finite

$$g(a),\ g(b),\ f(a),\ f(b) \neq 0 , \tag{D.3}$$

where $w_i(x)$ are known as weight functions for the integral equation.

The typical integral equation studied in fracture mechanics has a right-hand side ($p(x)$ in Eqns. B.5,9) that is of order one. Here the weight function must be such that the singular term in these equations is finite. All through crack problems are in this category. However for the part-through crack case, only when the crack shape, $\xi(x)$ is of the form,

$$\xi(x) = \xi_0(1-x^2)^\gamma \ , \ \gamma \le 1/4 \ , \tag{D.4}$$

is this condition met. If $\gamma > 1/4$ the line-spring terms will be unbounded and for $\gamma < 1/4$ they will be zero (see Chapter 2). If $\gamma > 1/4$, such as for a semi-ellipse ($\gamma = 1/2$), a solution for $a<x<b$ can only be obtained if a weight is chosen that will duplicate this unbounded behavior. For the special case where $K(x,t)$ is zero (see Eqn. B.5,9) and $\gamma < 1/4$, the weight function should be chosen such that the singular integral matches the γ dependent zero behavior of the line-spring contribution. In both of these cases the weight function will be such that the displacement profile will be physically unacceptable. If this matching is ignored and the through crack weight is used for all γ, a convergent solution to the part-through crack problem can still be obtained for about 98% of the domain, $a<x<b$ without too much extra computer time. Of course this is well beyond the expected range of validity of the line-spring model, and therefore all crack shapes will be treated as though the resulting line-spring terms are of order one. One way to deal with this problem, shown in Chapter 2, is to force $\gamma = 1/4$ behavior at the endpoints.

First consider the internal crack case of an equation of the form of B.5. From the basic theory of Muskhelishvili [78], and from Eqn. B.22 to extend this theory to finite-part integrals (see Kaya [67]), we have,

$$\lim_{x\to a} \frac{1}{\pi} \fint_a^b \frac{v(t)}{(t-x)^2}\, dt \simeq -\beta\cot\pi\beta \lim_{x\to a} \frac{v(x)}{x-a} + O(1) \ , \tag{D.5}$$

$$\lim_{x\to b} \frac{1}{\pi} \fint_a^b \frac{v(t)}{(t-x)^2}\, dt \simeq -\alpha\cot\pi\alpha \lim_{x\to b} \frac{v(x)}{b-x} + O(1) \ , \tag{D.6}$$

where

$$v(t) = g(t)(b-t)^{\alpha}(t-a)^{\beta} \ , \qquad g(a),g(b) \neq 0 \ . \tag{D.7}$$

For Eqns. D.5,6 to be of order one,

$$\cot\pi\beta = \cot\pi\alpha = 0 \ . \tag{D.8}$$

This gives,

$$\beta = \alpha = 1/2, 3/2, \ldots . \tag{D.9}$$

As a rule for deciding what form to take for finite-part integrals, Kaya [79] states that all roots should be used such that g(x) and its derivatives remain bounded at x approaching a and b. Therefore we take,

$$\alpha = \beta = 1/2 \ , \tag{D.10}$$

and

$$v(t) = g(t)(b-t)^{1/2}(t-a)^{1/2} \ . \tag{D.11}$$

In order to obtain the compliance functions used in the line-spring model, the edge cracked strip (Appendix C) must be solved. The crack opening displacement, v(x) will have a different weight function than Eqn. D.11. From Eqn. C.39 note that there are integrals which become singular when both t and x go to zero simultaneously, so these terms must be included in the limit as $x\to 0$.

$$\frac{1}{\pi} \fint_0^b \frac{v(t)}{(t-x)^2}\, dt + \frac{1}{\pi} \int_0^b \frac{-v(t)}{(t+x)^2}\, dt + \frac{1}{\pi} \int_0^b \frac{12xt}{(t+x)^4}\, v(t)\, dt \sim O(1) \ , \tag{D.12}$$

for

$$v(t) = g(t)(b-t)^{\alpha}t^{\beta} \ , \qquad g(0),g(b) \neq 0 \ . \tag{D.13}$$

The analysis for x at b is the same as for the internal crack. From Ref. [67] we have,

$$\lim_{x\to 0} \frac{1}{\pi} \fint_0^b \frac{v(t)}{(t-x)^2}\, dt = -\beta\cot\pi\beta \lim_{x\to 0} \frac{v(x)}{x} + O(1) \ , \tag{D.14}$$

$$\lim_{x\to 0} \frac{1}{\pi} \int_0^b \frac{v(t)}{(t+x)^2}\, dt = \frac{\beta}{\sin\pi\beta} \lim_{x\to 0} \frac{v(x)}{x} + O(1) \ , \tag{D.15}$$

$$\frac{1}{\pi} \int_0^b \frac{12xt}{(t+x)^4}\, v(t)\, dt = \frac{12(\beta+1)\beta(\beta-1)}{3!\sin\pi(\beta+1)} \lim_{x\to 0} \frac{v(x)}{x} + O(1) \ . \tag{D.16}$$

Therefore the characteristic equation for β is,

$$-\beta\cot\pi\beta - \frac{\beta}{\sin\pi\beta} + \frac{2(\beta+1)\beta(\beta-1)}{\sin\pi(\beta+1)} = 0 \ , \tag{D.17}$$

which reduces to,

$$\frac{-\beta}{\sin\pi\beta} \left[\cos\pi\beta - 1 + 2\beta^2\right] = 0 \ , \tag{D.18}$$

which has the root $\beta = 0$. Therefore for an edge crack,

$$v(t) = g(t)(b-t)^{1/2} \ . \tag{D.19}$$

APPENDIX E

Numerical Methods for the Solution of Singular Integral Equations

In this section the two most common numerical methods for solving singular integral equations of the following form will be considered:

$$\fint_a^b \frac{\phi(t)}{t-x}\, dt + \int_a^b \phi(t)K(x,t)\, dt = p(x) \ , \quad a<x<b \ , \tag{E.1}$$

$$\fint_a^b \frac{v(t)}{(t-x)^2}\, dt - \int_a^b v(t)\frac{\partial K}{\partial t}\, dt = p(x) \ , \quad a<x<b \ . \tag{E.2}$$

These two equations are equivalent for

$$v(t) = v^+(t) - v^-(t) \ , \quad \phi(t) = \frac{\partial v}{\partial t} \ , \tag{E.3}$$

with the condition

$$v(a) = v(b) = 0 \ , \tag{E.4}$$

which for Eqn. E.1 is expressed as,

$$\int_a^b \phi(t)\, dt = 0 \ . \tag{E.5}$$

Both solution methods can easily be generalized to include multiple unknowns and multiple cracks, so for simplicity will be left out.

E.1 Quadrature.

Here we consider the solution of Eqn. E.1 for the case of an internal crack. The first step is to express the unknown in terms of its weight function given in Eqn. D.11. We have,

$$\phi(t) = \frac{f(t)}{(t-a)^{1/2}(b-t)^{1/2}} \ . \tag{E.6}$$

This is substituted into Eqn. E.1 using the following definitions:

$$t = \frac{b-a}{2}r + \frac{b+a}{2} , \tag{E.7}$$

$$x = \frac{b-a}{2}s + \frac{b+a}{2} , \tag{E.8}$$

$$p(x) = \bar{p}(s) , \tag{E.9}$$

$$\phi(t) = \frac{\bar{f}(r)}{(1-t^2)^{1/2}} , \quad f(t) = \frac{b-a}{2}\bar{f}(r) , \tag{E.10}$$

$$L(r,s) = \frac{b-a}{2}K(x,t) , \tag{E.11}$$

to obtain,

$$\int_{-1}^{+1} \frac{\bar{f}(r)\,dr}{(1-r^2)^{1/2}(r-s)} + \int_{-1}^{+1} \frac{\bar{f}(r)}{(1-r^2)^{1/2}} L(r,s)\,dr = \bar{p}(s) , \quad -1<s<1 . \tag{E.12}$$

We now make use of the quadrature formula

$$\int_{-1}^{+1} \frac{h(r)}{(1-r^2)^{1/2}}\,dr = \sum_{j=1}^{N} w_j h(r_j) , \tag{E.13}$$

where

$$r_j = \cos\frac{j-1}{N-1}\pi , \quad j = 1,\ldots,N , \tag{E.14}$$

which are roots of the Chebychev polynomial $T_N(r)$, and

$$w_j = \frac{\pi}{N-1} , \quad j = 2,\ldots,N-1 ,$$

$$w_1 = w_N = \frac{\pi}{2(N-1)} . \tag{E.15}$$

This quadrature is exact when the function h(t) is a polynomial of degree (2N-1) or less and therefore has good convergence when integrating the well behaved Fredholm kernel L(r,s) in Eqn. E.12 as N is increased. However the integration of the singular term in this

equation introduces a relatively large error which has been found to be proportional to the Chebychev polynomial $U_N(r)$. Therefore when values of s are chosen to make U_N zero, the error is reduced and the integration is exact for polynomials of degree 2N or less. The s values are,

$$s_i = \cos\frac{2i-1}{N-1}\frac{\pi}{2} \quad , \quad i = 1,\ldots,N-1 \quad . \tag{E.16}$$

It is this information that makes the method work. Applying the quadrature formula to Eqn. E.11, we obtain,

$$\sum_{j=1}^{N} w_j f(r_j)\left[\frac{1}{r_j-s_i} + L(r_j,s_i)\right] = p(s_i) \quad , \quad i = 1,\ldots,N-1 \quad , \tag{E.17}$$

which is a system of N unknowns ($g(r_j)$, $j=1,\ldots,N$) and N-1 equations. Recalling Eqn. E.5 we supplement Eqn. E.17 with

$$\sum_{j=1}^{N} w_j f(r_j) = 0 \quad , \tag{E.18}$$

which can then be solved as a system of linear algebraic equations. Convergence is obtained as N is increased.

In the case of an edge crack where a = 0, the weight function changes (see Eqn. D.19) and $\phi(t)$ becomes,

$$\phi(t) = \frac{f(t)}{(b-t)^{1/2}} \quad . \tag{E.19}$$

After substitution using Eqns. E.7-11 with a=0, the singular integral equation, E.1 becomes,

$$\int_{-1}^{+1} \frac{\bar{f}(r)\,dr}{(1-r)^{1/2}(r-s)} + \int_{-1}^{+1} \frac{\bar{f}(r)}{(1-r)^{1/2}} L(r,s)\,dr = \bar{p}(s) \quad , \quad -1<s<1 \quad . \tag{E.20}$$

The necessary quadrature for this weight function is,

$$\int_{-1}^{+1} \frac{h(r)}{\sqrt{1-r}}\, dr = \sum_{j=1}^{N} w_j h(r_j) \quad , \tag{E.21}$$

where now the values of w_j and r_j must be obtained numerically as roots of the following Jacobi polynomials:

$$P_N^{(-1/2,-1)}(t_j) = 0 \quad , \quad j = 1,\ldots,N \quad . \tag{E.22}$$

$$P_{N-1}^{(1/2,1)}(s_i) = 0 \quad , \quad i = 1,\ldots,N-1 \quad . \tag{E.23}$$

It is easier to use Eqns. E.12-16 and include $(1+t)^{1/2}$ in the function $\bar{f}(r)$. For the edge crack however, Eqn. E.18 is replaced with

$$h(-1) = h(t_N) = 0 \quad . \tag{E.24}$$

The quadrature method is not a good choice for the solution of strongly singular integral equations such as Eqn. E.2 because the existing quadrature formulas for finite-part integrals involve operations that make solving the integral equations far more complicated than solving the equivalent equation with a Cauchy singularity, (see [67]). Perhaps in time a more convenient quadrature will be developed. A better and simpler approach to solving Eqn. E.2 is the expansion method, or more specifically, the collocation method.

E.2 Collocation.

First consider the internal crack where the unknown is expressed as

$$v(t) = g(t)(t-a)^{1/2}(b-t)^{1/2} \quad . \tag{E.25}$$

Note that Eqn. E.4 is satisfied which shows an advantage of using the displacement as the unknown which leads to a strongly singular integral equation. Again use Eqns. E.7-9 with

$$v(t) = \frac{b-a}{2}\,\bar{v}(r)\,(1-r^2)^{1/2} \ , \tag{E.26}$$

$$L(r,s) = \left(\frac{b-a}{2}\right)^2 \frac{\partial K}{\partial t} \ . \tag{E.27}$$

Substituting into Eqn. E.2 we obtain,

$$\fint_{-1}^{+1} \frac{\bar{v}(r)\sqrt{1-r^2}}{(r-s)^2}\,dr + \int_{-1}^{+1} \bar{v}(r)\,(1-r^2)^{1/2} L(r,s)\,dr = \bar{p}(s) \ , \qquad -1<s<1 \ . \tag{E.28}$$

Next we choose

$$\bar{v}(r) = \sum_{j=1}^{N} a_j f_{j-1}(r) \ , \tag{E.29}$$

where $f_j(r)$ are linearly independent functions chosen to "fit the curve" and the a_j are coefficients to be determined. I believe that it is best to choose orthoganol polynomials so that the coefficients show convergence as N is increased. The proper choice for the weight of Eqn. E.28, is the Chebychev polynomial of the second kind, $U_{j-1}(r)$. With other functions such as a simple power series r^{j-1}, convergence can only be seen by calculating the sum (Eqn. E.29) as the coefficients themselves do not converge. Also as N gets large the coefficients of r^{j-1} can get large enough to cause round off error as was experienced with the thin plate limit in Chapter 3. This problem is avoided when using orthoganol polynomials. These convergence characteristics are shown in table E.1 where the coefficients, a_j are

listed for N = 10 and 20, using both $U_{(2j-2)}(r)$ and $r^{(2j-2)}$ for the fitting function, $f_{(2j-2)}(r)$ (see Eqn. 29). The problem is symmetric in r so only even functions have non-zero coefficients. This shows slow convergence typical of part-through crack problems. Although the numbers for N = 20 and $r^{(2j-2)}$ are large, they give the same result as the Chebychev polynomials. Mostly all problems can be solved with power series, but the orthoganol polynomials, I believe, are better.

Next substitute Eqn. E.29 into Eqn. E.28 to obtain,

$$\sum_{j=1}^{N} a_j \left\{ \fint_{-1}^{+1} \frac{f_j(r)(1-r^2)^{1/2}}{(r-s)^2}\, dr + \int_{-1}^{+1} f_j(r)(1-r^2)^{1/2} L(r,s)\, dr \right\} = \bar{p}(s) \qquad -1<s<1 \ . \quad (E.30)$$

With this method there is no restriction on the choice of s as long as it does not coincide with r in Eqn. E.30. Roots of Chebychev polynomials which concentrate points near -1 and +1 are a good choice when information near the endpoints is needed such as the determination of stress intensity factors for through cracks. Table E.2 lists the coefficients for N = 3 and 6 and the resulting stress intensity factor to show how good convergence is for this type of integral equation.

A more uniform spacing of points has been found to be a better choice for convergence of the line-spring model where information in the central portion is more important (see Table E.3). In this table equally spaced points improve convergence by about one order of magnitude. Another reason to prefer this choice of s_j is that the solution is most accurate there (recall that the collocation method gives the solution for all s) and it is more convenient to know the

solution at these points than at the roots of an orthoganol polynomial.

For a given value of s there are two integrations to perform in Eqn. E.30. Any standard technique can be used, for example Gauss-Chebychev quadrature which takes advantage of the weight,

$$\int_{-1}^{+1} h(r)(1-r^2)^{1/2}\, dr = \sum_{k=1}^{M} w_k h(r_k) \ , \tag{E.31}$$

where

$$w_k = \frac{\pi}{M+1}\left(\sin\frac{k\pi}{M+1}\right)^2 , \tag{E.32}$$

$$r_k = \cos\frac{k\pi}{M+1} \ . \tag{E.33}$$

The first integral can be determined by using Eqn. B.27 or for certain expansion functions $f_j(r)$ such as $U_j(r)$, there are closed form expressions. For example,

$$\fint_{-1}^{+1} \frac{U_j(r)(1-r^2)^{1/2}}{(r-s)^2}\, dr = -\pi(j+1)U_j(s) \ . \tag{E.34}$$

See Appendix A or Ref. [67] for similar formulas for other functions and other weights. Therefore if Eqn. E.30 is evaluated at N different points, the coefficients, a_j , j=1,...,N can be determined. Also a least squares technique can be applied if more than N values of s are selected.

Both numerical methods have been used in this dissertation, and the collocation method has been found to be better. One important advantage of this method is that the number of unknowns is unrelated to the way in which the integrations are performed. This makes for

better efficiency. Another advantage is that the function is given at all points instead of at discrete values of s as in the quadrature method (Eqns. E.16,24). This makes convergence easier to check because with quadrature, as N is increased, the stations at which the function is given, shift. The only common points from one value of N to another are the endpoint, the most difficult to converge, and the midpoint which is the easiest. With collocation either the same values of s can be used for successive N values, or the function can simply be evaluated at any point according to Eqn. E.29. I have found the collocation method to be most accurate when N unknowns and N equations are used as opposed to using the before mentioned least squares method. This is similar in principle to curve fitting.

For the edge crack the technique is similar except the singular integral in Eqn. E.30 must be solved numerically because expressions such as Eqn. E.34 are not available for a $(1-r)^{1/2}$ weight. Kaya [67] has developed a scheme which gets around this. Instead of normalizing from -1 to +1, he normalizes from 0 to +1 as follows,

$$t = br \ , \tag{E.35}$$

$$x = bs \ , \tag{E.36}$$

$$v(t) = b\bar{v}(r) \ , \tag{E.37}$$

$$L(r,s) = b^2 \frac{\partial K}{\partial t} \ . \tag{E.38}$$

Then Eqn. E.2 becomes,

$$\fint_0^1 \frac{\bar{v}(r)}{(r-s)^2}\, dr - \int_0^1 \bar{v}(r) L(r,s)\, dr = \bar{p}(\sigma) \ , \quad 0<s<1 \ . \tag{E.39}$$

Now we can use

$$\bar{v}(r) = g(r)(1-r^2)^{1/2} \ . \tag{E.40}$$

Also if

$$\int_{-1}^{0} \frac{\bar{v}(r)}{(r-s)^2}\, dr \ , \tag{E.41}$$

is added and subtracted from Eqn. E.39 we have,

$$\fint_{-1}^{+1} \frac{g(r)(1-r^2)^{1/2}}{(r-s)^2}\, dr + \int_{0}^{+1} g(r)(1-r^2)^{1/2} L(r,s)\, dr -$$

$$\int_{-1}^{0} \frac{g(r)(1-r^2)^{1/2}}{(r-s)^2}\, dr = \bar{p}(s) \ , \quad 0<s<1 \ . \tag{E.42}$$

Now the singular term can be evaluated in closed form.

Table E.1 Coefficients for expansion functions, $U_{j-1}(r)$ and r^{j-1} for a part-through crack to show convergence for coefficients of U for increasing N and to show how power series coefficients get large.

$\xi = .6(1-s^2)^{1/4}$, tension.

		$U_{(2j-2)}(r)$		$r^{(2j-2)}$	
	j	a_{1j}	a_{2j}	a_{1j}	a_{2j}
N = 10					
	1	.602954e00	.201102e01	.633626e00	.197755e01
	2	-.353661e-1	.357367e-1	-.995538e-1	.124094e00
	3	-.633608e-2	.297401e-2	.991316e-1	-.204339e00
	4	-.238970e-2	.120856e-2	-.223967e01	.373660e01
	5	-.115589e-2	.878486e-3	.170071e02	-.275699e02
	6	-.672035e-3	.658983e-3	-.676896e02	.107146e03
	7	-.448539e-3	.514599e-3	.150545e03	-.234331e03
	8	-.336133e-3	.429394e-3	-.188716e03	.289774e03
	9	-.280330e-3	.389471e-3	.124487e03	-.188933e03
	10	-.128226e-3	.192492e-3	-.336138e02	.504607e02
N = 20					
	1	.602962e00	.201104e01	.633599e00	.197746e01
	2	-.353528e-1	.357469e-1	-.981042e-1	.124878e00
	3	-.631705e-2	.297507e-2	.127104e00	-.752523e00
	4	-.236433e-2	.119822e-2	-.116577e02	.472852e02
	5	-.112297e-2	.854624e-3	.413200e03	-.145520e04
	6	-.629824e-3	.618609e-3	-.841220e04	.265618e05
	7	-.394573e-3	.453260e-3	.109143e06	-.315897e06
	8	-.266935e-3	.340355e-3	-.963774e06	.259884e07
	9	-.191184e-3	.262485e-3	.605181e07	-.153958e08
	10	-.143206e-3	.207703e-3	-.278436e08	.674988e08
	11	-.111307e-3	.168386e-3	.957704e08	-.223025e09
	12	-.893108e-4	.139685e-3	-.249352e09	.561471e09
	13	-.737318e-4	.118478e-3	.494303e09	-.108197e10
	14	-.624979e-4	.102717e-3	-.745521e09	.159325e10
	15	-.543247e-4	.910346e-4	.848642e09	-.177709e10
	16	-.483900e-4	.825134e-4	-.716454e09	.147440e10
	17	-.441540e-4	.765362e-4	.434607e09	-.881107e09
	18	-.412504e-4	.726940e-4	-.179004e09	.358246e09
	19	-.393969e-4	.706965e-4	.448065e08	-.886709e08
	20	-.190835e-4	.349693e-4	-.514322e07	.100789e08

Table E.2 Convergence of expansion function coefficients a_j and normalized stress intensity factor $k_1/(\sigma_2\sqrt{a})$ for a through crack, a/h=1, ν=.3

	j	s_j	a_j	$k_1/(\sigma_2\sqrt{a})$
N = 3				
	1	.00000	.255900e01	
	2	.58779	.126237e00	
	3	.95106	.103953e-1	.74742
N = 6				
	1	.00000	.255883e01	
	2	.28173	.125167e00	
	3	.54064	.103724e-1	
	4	.75575	.508637e-3	
	5	.90963	.159547e-4	
	6	.98982	.334089e-6	.74748

Table E.3 The effect of the choice of the collocation points, s_j on convergence for a part-through crack loaded in tension.

		$\xi = .6(1-s^2)^{1/2}$		$\xi = .6(1-s^2)^{1/4}$	
j	s_j	a_{1j}	a_{2j}	a_{1j}	a_{2j}
N = 12					
1	.0	.517675e00	.179305e01	.602986e00	.201108e01
2	.1	-.826466e-1	-.932252e-1	-.353093e-1	.357855e-1
3	.2	-.862004e-2	-.478427e-1	-.625598e-2	.298601e-2
4	.3	-.320951e-2	-.163700e-1	-.228765e-2	.117540e-2
5	.4	-.154063e-2	-.772860e-2	-.103516e-2	.799027e-3
6	.5	-.816275e-3	-.413912e-2	-.535729e-3	.535892e-3
7	.6	-.454261e-3	-.232331e-2	-.296962e-3	.349407e-3
8	.7	-.249781e-3	-.128652e-2	-.165651e-3	.218096e-3
9	.8	-.125213e-3	-.650011e-3	-.858241e-4	.123060e-3
10	.9	-.514386e-4	-.269770e-3	-.372392e-4	.571948e-4
11	.95	-.148252e-4	-.787855e-4	-.116721e-4	.189765e-4
12	.98	-.217783e-5	-.117624e-4	-.192020e-5	.327248e-5
1	.0	.517492e00	.179224e01	.602958e00	.201103e01
2	.13617	-.828914e-1	-.945347e-1	-.353590e-1	.357420e-1
3	.26980	-.891617e-2	-.494622e-1	-.632578e-2	.297444e-2
4	.39840	-.353796e-2	-.181809e-1	-.237578e-2	.120271e-2
5	.51958	-.188429e-2	-.963221e-2	-.113751e-2	.864942e-3
6	.63109	-.116178e-2	-.605954e-2	-.647982e-3	.635656e-3
7	.73084	-.796345e-3	-.422672e-2	-.417042e-3	.478286e-3
8	.81697	-.590135e-3	-.317589e-2	-.294652e-3	.375106e-3
9	.88789	-.465276e-3	-.253009e-2	-.225401e-3	.309416e-3
10	.94226	-.386326e-3	-.211617e-2	-.185580e-3	.270293e-3
11	.97908	-.334534e-3	-.184705e-2	-.163903e-3	.251536e-3
12	.99767	-.149021e-3	-.840827e-3	-.767395e-4	.124182e-3

APPENDIX F

Short Crack Analysis of the Compliance Functions

For small ξ (small crack depths) we write,

$$g_1(\xi) = c_0 + c_{11}\xi + c_{12}\xi^2 + c_{13}\xi^3 + c_{14}\xi^4 + c_{15}\xi^5 + \dots , \quad (F.1)$$

$$g_2(\xi) = c_0 + c_{21}\xi + c_{22}\xi^2 + c_{23}\xi^3 + c_{24}\xi^4 + c_{25}\xi^5 + \dots , \quad (F.2)$$

where

$$c_{i0} = C_{i0} \ , \ C_{10} = C_{20}$$

$$c_{i1} = 3/2C_{i0} + C_{i1} \ ,$$

$$c_{i2} = 15/8C_{i0} + 3/2C_{i1} + C_{i2} \ ,$$

$$c_{i3} = 35/16C_{i0} + 15/8C_{i1} + 3/2C_{i2} + C_{i3} \ ,$$

$$c_{i4} = 315/128C_{i0} + 35/16C_{i1} + 15/8C_{i2} + 3/2C_{i3} + C_{i4} \ ,$$

$$c_{i5} = 693/256C_{i0} + 315/128C_{i1} + 35/16C_{i2} + 15/8C_{i3} + 3/2C_{i4} + C_{i5} \ , \quad (F.3)$$

where C_{ij} are listed in table C.2. From Eqn. 2.26,

$$\alpha_{11} = \pi\Big\{ 1/2c_0^2\xi^2 + 2/3c_0c_{11}\xi^3 + 1/4\xi^4[c_{11}^2 + 2c_0c_{12}] + 1/5\xi^5[2c_0c_{13} + 2c_{11}c_{12}] + 1/6\xi^6[2c_0c_{14} + c_{12}^2 + 2c_{11}c_{13}] + 1/7\xi^7[2c_0c_{15} + 2c_{11}c_{14} + 2c_{12}c_{13}] + 0(\xi^8)\Big\} \ , \quad (F.4)$$

$$\alpha_{22} = \pi\Big\{ 1/2c_0^2\xi^2 + 2/3c_0c_{21}\xi^3 + 1/4\xi^4[c_{21}^2 + 2c_0c_{22}] + 1/5\xi^5[2c_0c_{23} + 2c_{21}c_{22}] + 1/6\xi^6[2c_0c_{24} + c_{22}^2 + 2c_{21}c_{23}] + 1/7\xi^7[2c_0c_{25} + 2c_{21}c_{24} + 2c_{22}c_{23}] + 0(\xi^8)\Big\} \ , \quad (F.5)$$

$$\alpha_{12} = \alpha_{21} = \pi\Big\{ 1/2c_0^2\xi^2 + 1/3\xi^3[c_0c_{11} + c_0c_{21}] +$$

$$1/4\xi^4[c_{11}c_{21} + c_0c_{22} + c_0c_{12}] +$$

$$1/5\xi^5[c_0c_{23} + c_0c_{13} + c_{11}c_{22} + c_{21}c_{12}] +$$

$$1/6\xi^6[c_0c_{24} + c_0c_{14} + c_{11}c_{23} + c_{21}c_{13} + c_{12}c_{22}] +$$

$$1/7\xi^7[c_0c_{25} + c_0c_{15} + c_{11}c_{24} + c_{21}c_{14} + c_{12}c_{23} + c_{22}c_{13}]\Big\}. \tag{F.6}$$

Eqn. 2.33 relates γ_{ij} to α_{ij} as follows

$$(1-\nu^2)\gamma_{11} = \pi\Big\{ \xi^{-4}1/2c_0^2\delta_1 + \xi^{-3}[2/3c_0c_{21}\delta_1 + 1/2c_0^2\delta_2] +$$

$$\xi^{-2}[1/4(c_{21}^2 + 2c_0c_{22})\delta_1 + 2/3c_0c_{21}\delta_2 + 1/2c_0^2\delta_3] +$$

$$\xi^{-1}[2/5(c_0c_{23} + c_{21}c_{22})\delta_1 + 1/4(c_{21}^2 + 2c_0c_{22})\delta_2 +$$

$$2/3c_0c_{21}\delta_3 + 1/2c_0^2\delta_4] + 0(1)\Big\}, \tag{F.7}$$

$$36(1-\nu^2)\gamma_{22} = \pi\Big\{ \xi^{-4}1/2c_0^2\delta_1 + \xi^{-3}[2/3c_0c_{11}\delta_1 + 1/2c_0^2\delta_2] +$$

$$\xi^{-2}[1/4(c_{11}^2 + 2c_0c_{12})\delta_1 + 2/3c_0c_{11}\delta_2 + 1/2c_0^2\delta_3] +$$

$$\xi^{-1}[2/5(c_0c_{13} + c_{11}c_{12})\delta_1 + 1/4(c_{11}^2 + 2c_0c_{12})\delta_2 +$$

$$2/3c_0c_{11}\delta_3 + 1/2c_0^2\delta_4] + 0(1)\Big\}, \tag{F.8}$$

$$-6(1-\nu^2)\gamma_{12} = -6(1-\nu^2)\gamma_{12} = \pi\Big\{\xi^{-4}1/2c_0^2\delta_1 + \xi^{-3}[1/3c_0(c_{11} + c_{21})\delta_1$$

$$+ 1/2c_0^2\delta_2] + \xi^{-2}[1/4(c_{11}c_{21} + c_0c_{22} + c_0c_{12})\delta_1 +$$

$$1/3c_0(c_{11} + c_{21})\delta_2 + 1/2c_0^2\delta_3] + \xi^{-1}[1/5(c_0c_{23} + c_0c_{13} +$$

$$c_{11}c_{22} + c_{21}c_{12})\delta_1 + 1/4(c_{11}c_{21} + c_0c_{22} + c_0c_{12})\delta_2 +$$

$$1/3c_0(c_{11} + c_{21})\delta_3 + 1/2c_0^2\delta_4] + 0(1)\Big\} , \qquad (F.9)$$

where

$$\delta_1 = \frac{1}{\Delta_1} ,$$

$$\delta_2 = -\frac{\Delta_2}{\Delta_1^2} ,$$

$$\delta_3 = \frac{\Delta_2^2-\Delta_1\Delta_3}{\Delta_1^3} ,$$

$$\delta_4 = \frac{\Delta_2^3-2\Delta_1\Delta_2\Delta_3+\Delta_1^2\Delta_4}{\Delta_1^4} , \qquad (F.10)$$

and

$$\Delta_1 = \pi^2\Big\{1/8c_0^2(c_{21}^2+2c_0c_{22}+c_{11}^2+2c_0c_{12}) + 4/9c_0^2c_{11}c_{21} -$$

$$1/9c_0^2(c_{11}+c_{21})^2 - 1/4c_0^2(c_{11}c_{21}+c_0c_{22}+c_0c_{12})\Big\} ,$$

$$\Delta_2 = \pi^2\Big\{1/5c_0^2(c_0c_{13}+c_{11}c_{12}+c_0c_{23}+c_{21}c_{22}) -$$

$$1/6c_0(c_{11}c_{21}^2+2c_0c_{11}c_{22}+c_{21}c_{11}^2+2c_0c_{21}c_{12}) - 1/5c_0^2(c_0c_{23}+c_0c_{13}+$$

$$c_{11}c_{22}+c_{21}c_{12}) - 1/6c_0(c_{11}+c_{21})(c_{11}c_{21}+c_0c_{22}+c_0c_{12})\Big\} ,$$

$$\Delta_3 = \pi^2\Big\{1/12c_0^2(2c_0c_{24}+c_{22}^2+2c_{21}c_{23}+2c_0c_{14}+c_{12}^2+2c_{11}c_{13}) +$$

$$4/15c_0(c_0c_{11}c_{23}+c_{11}c_{21}c_{22}+c_0c_{21}c_{13}+c_{21}c_{11}c_{12}) +$$

$$1/16(c_{11}^2+2c_0c_{12})(c_{21}^2+2c_0c_{22}) - 1/6c_0^2(c_0c_{24}+c_0c_{14}+c_{21}c_{13}+c_{12}c_{22}+$$

$$c_{11}c_{23}) - 1/16(c_{11}c_{21}+c_0c_{22}+c_0c_{12})^2 -$$

$$2/15c_0(c_{11}+c_{21})(c_0c_{23}+c_0c_{13}+c_{11}c_{22}+c_{21}c_{12})\Big\} ,$$

$$\Delta_4 = \pi^2\Big\{2/14c_0^2(c_0c_{25}+c_{21}c_{24}+c_{22}c_{23}+c_0c_{15}+c_{11}c_{14}+c_{12}c_{13}) +$$

$$1/9c_0(2c_0c_{11}c_{24}+c_{11}c_{22}^2+2c_{21}c_{11}c_{23}+2c_0c_{21}c_{14}+c_{21}c_{12}^2+2c_{11}c_{21}c_{13}) +$$

$$1/20(c_{11}^2+2c_0c_{12})(2c_0c_{23}+2c_{21}c_{22}) +$$

$$1/20(c_{21}^2+2c_0c_{22})(2c_0c_{13}+2c_{11}c_{12}) - 1/7c_0^2(c_0c_{25}+c_0c_{15}+c_{11}c_{24}+$$

$$c_{21}c_{14}+c_{12}c_{23}+c_{22}c_{13}) - 1/9c_0(c_{11}+c_{21})(c_0c_{24}+c_0c_{14}+c_{11}c_{23}+$$

$$c_{21}c_{13}+c_{12}c_{22}) - 1/10(c_{11}c_{21}+c_0c_{22}+c_0c_{12})(c_0c_{23}+c_0c_{13}+$$

$$c_{11}c_{22}+c_{21}c_{12})\Big\} . \tag{F.11}$$

Now I have

$$\gamma_{11} = s_1\xi^{-4} + s_2\xi^{-3} + s_3\xi^{-2} + s_4\xi^{-1} + 0(1) , \tag{F.12}$$

$$\gamma_{22} = q_1\xi^{-4} + q_2\xi^{-3} + q_3\xi^{-2} + q_4\xi^{-1} + 0(1) , \tag{F.13}$$

$$\gamma_{12} = \gamma_{21} = t_1\xi^{-4} + t_2\xi^{-3} + t_3\xi^{-2} + t_4\xi^{-1} + 0(1) , \tag{F.14}$$

where s_i, t_i and q_i, i=1,2,3,4 can be obtained from Eqns. F.7-9. Now consider the stresses (recall Eqn. 2.31),

$$\sigma_1 = u(s)\gamma_{11}(\xi) + \beta(s)\gamma_{12}(\xi) , \tag{F.15}$$

$$\sigma_2 = u(s)\gamma_{21}(\xi) + \beta(s)\gamma_{22}(\xi) , \tag{F.16}$$

where for the remaining analysis,

$$\xi = \xi_0(1-s^2)^{1/2} . \tag{F.17}$$

I will also assume that the loading is symmetric in s, so the following expressions for u(s) and $\beta(s)$ are used,

$$u(s) = (1-s^2)^{1/2} \sum_{j=1}^{N} a_{1j} U_{(2j-2)}(s) \ , \tag{F.18}$$

$$\beta(s) = (1-s^2)^{1/2} \sum_{j=1}^{N} a_{2j} U_{(2j-2)}(s) \ . \tag{F.19}$$

For small ξ or for s near 1,

$$u(s) = \frac{\xi}{\xi_0} \sum_{j=1}^{N} a_{1j} \left\{ b_j + \xi^2 c_j \right\} + 0(\xi^4) \ , \tag{F.20}$$

$$\beta(s) = \frac{\xi}{\xi_0} \sum_{j=1}^{N} a_{2j} \left\{ b_j + \xi^2 c_j \right\} + 0(\xi^4) \ , \tag{F.21}$$

where

$$b_j = (2j-1) \ , \tag{F.22}$$

$$c_j = \frac{-4}{\xi_0^2} \sum_{i=1}^{j-1} i^2 \ . \tag{F.23}$$

The following expressions result for Eqns. F.15,16,

$$\begin{aligned} \sigma_1(\xi) = \frac{1}{\xi_0} \sum_{j=1}^{N} a_{1j} \Big\{ & \xi^{-3} b_j s_1 + \xi^{-2} b_j s_2 + \xi^{-1} (b_j s_3 + c_j s_1) + \\ & (b_j s_4 + c_j s_2) \Big\} + \\ + \frac{1}{\xi_0} \sum_{j=1}^{N} a_{2j} \Big\{ & \xi^{-3} b_j t_1 + \xi^{-2} b_j t_2 + \xi^{-1} (b_j t_3 + c_j t_1) + \\ & (b_j t_4 + c_j t_2) \Big\} + 0(\xi) \ , \end{aligned} \tag{F.24}$$

$$\sigma_2(\xi) = \frac{1}{\xi_0} \sum_{j=1}^{N} a_{1j} \Big\{ \xi^{-3} b_j t_1 + \xi^{-2} b_j t_2 + \xi^{-1} (b_j t_3 + c_j t_1) +$$

$$(b_j t_4 + c_j t_2)\Big\} +$$

$$+ \frac{1}{\xi_0} \sum_{j=1}^{N} a_{2j}\Big\{\xi^{-3} b_j q_1 + \xi^{-2} b_j q_2 + \xi^{-1}(b_j q_3 + c_j q_1) +$$

$$(b_j q_4 + c_j q_2)\Big\} + 0(\xi) \ . \quad \text{(F.25)}$$

Using the prediction of Chapter 2 that the stresses must have a square root singularity at the ends, i.e. ξ^{-1}, we must have,

$$\frac{1}{\xi_0} \sum_{j=1}^{N} a_{1j}\Big\{\xi^{-3} b_j s_1 + \xi^{-2} b_j s_2\Big\} +$$

$$\frac{1}{\xi_0} \sum_{j=1}^{N} a_{2j}\Big\{\xi^{-3} b_j t_1 + \xi^{-2} b_j t_2\Big\} = 0 \ , \quad \text{(F.26)}$$

$$\frac{1}{\xi_0} \sum_{j=1}^{N} a_{1j}\Big\{\xi^{-3} b_j t_1 + \xi^{-2} b_j t_2\Big\} +$$

$$\frac{1}{\xi_0} \sum_{j=1}^{N} a_{2j}\Big\{\xi^{-3} b_j q_1 + \xi^{-2} b_j q_2\Big\} = 0 \ , \quad \text{(F.27)}$$

which is true if

$$\sum_{j=1}^{N} a_{1j} b_j = 0 \ , \quad \text{(F.28)}$$

and

$$\sum_{j=1}^{N} a_{2j} b_j = 0 \ . \quad \text{(F.29)}$$

This is equivalent to saying that the <u>through crack stress intensity factor</u> is zero, because

$$\frac{k_1}{\sigma\sqrt{a}} \propto \sum_{j=1}^{N} a_{ij} b_j \ , \ i=1,2 \ . \quad \text{(F.30)}$$

APPENDIX G

Stress Intensity Factors

G.1 Elasticity Theory.

The study of the static stress distribution near the tip of a crack in a linear, elastic solid has been reduced to the determination of constants called stress intensity factors (see Irwin [68,69]). To illustrate this consider the two-dimensional plane geometry where Williams [4] and Sih [80] have given the asymptotic form of the stresses of in-plane and anti-plane loading, respectively. These solutions, presented below, are obtained by use of eigenfunction expansions which satisfy the crack surface boundary conditions. The coordinate system is chosen to duplicate the through crack geometry used in this dissertation where the crack lies in the yz-plane with z tangent to the crack front. The polar coordinates r,θ are measured from the crack tip and lie in the xy-plane.

$$\sigma_y \simeq \frac{k_1}{\sqrt{2r}} \cos\frac{\theta}{2} \left[1-\sin\frac{\theta}{2} \sin\frac{3\theta}{2}\right] - \frac{k_2}{\sqrt{2r}} \sin\frac{\theta}{2} \left[2 + \cos\frac{\theta}{2} \cos\frac{3\theta}{2}\right] +$$

$$+ \sum_{n=1}^{\infty} \left[b_{1n} r^{\frac{2n-1}{2}} f_{1n}(\theta) + b_{2n} r^n f_{2n}(\theta)\right] , \qquad (G.1)$$

$$\sigma_x \simeq \frac{k_1}{\sqrt{2r}} \cos\frac{\theta}{2} \left[1+\sin\frac{\theta}{2} \sin\frac{3\theta}{2}\right] + \frac{k_2}{\sqrt{2r}} \sin\frac{\theta}{2} \cos\frac{\theta}{2} \cos\frac{3\theta}{2} +$$

$$+ \sigma_{0x} + \sum_{n=1}^{\infty} \left[b_{3n} r^{\frac{2n-1}{2}} f_{3n}(\theta) + b_{4n} r^n f_{4n}(\theta)\right] , \qquad (G.2)$$

$$\sigma_z \simeq 2\nu \left[\frac{k_1}{\sqrt{2r}} \cos\frac{\theta}{2} - \frac{k_2}{\sqrt{2r}} \sin\frac{\theta}{2} \right] + \nu\sigma_{0x} +$$

$$+ \sum_{n=1}^{\infty} \left[b_{5n} r^{\frac{2n-1}{2}} f_{5n}(\theta) + b_{6n} r^n f_{6n}(\theta) \right] , \qquad (G.3)$$

$$\tau_{xy} \simeq \frac{k_1}{\sqrt{2r}} \sin\frac{\theta}{2} \cos\frac{\theta}{2} \cos\frac{3\theta}{2} + \frac{k_2}{\sqrt{2r}} \cos\frac{\theta}{2} \left[1-\sin\frac{\theta}{2} \sin\frac{3\theta}{2}\right] +$$

$$+ \sum_{n=1}^{\infty} \left[b_{7n} r^{\frac{2n-1}{2}} f_{7n}(\theta) + b_{8n} r^n f_{8n}(\theta) \right] , \qquad (G.4)$$

$$\tau_{yz} \simeq \frac{k_3}{\sqrt{2r}} \sin\frac{\theta}{2} + \sum_{n=1}^{\infty} \left[b_{9n} r^{\frac{2n-1}{2}} f_{9n}(\theta) + b_{10n} r^n f_{10n}(\theta) \right] , \qquad (G.5)$$

$$\tau_{xz} \simeq \frac{k_3}{\sqrt{2r}} \cos\frac{\theta}{2} + \sum_{n=1}^{\infty} \left[b_{11n} r^{\frac{2n-1}{2}} f_{11n}(\theta) + b_{12n} r^n f_{12n}(\theta) \right] . \qquad (G.6)$$

The stress intensity factors are k_1, k_2, and k_3 which correspond to the opening (symmetric), sliding (skew-symmetric) and tearing (anti-plane) modes of fracture shown in figure G.1. Equations similar to G.1-6 exist for displacement as follows,

$$v(r,\theta) \simeq \frac{k_1}{8\mu} \sqrt{2r} \left[(2\kappa-1)\cos\frac{\theta}{2} - \cos\frac{3\theta}{2} \right]$$

$$+ \frac{k_2}{8\mu} \sqrt{2r} \left[(2\kappa+3)\sin\frac{\theta}{2} + \sin\frac{3\theta}{2} \right] , \qquad (G.7)$$

$$u(r,\theta) \simeq \frac{k_1}{8\mu} \sqrt{2r} \left[(2\kappa+1)\sin\frac{\theta}{2} - \sin\frac{3\theta}{2} \right]$$

$$- \frac{k_2}{8\mu} \sqrt{2r} \left[(2\kappa-3)\cos\frac{\theta}{2} + \cos\frac{3\theta}{2} \right] , \qquad (G.8)$$

$$w(r,\theta) \simeq \frac{k_3}{\mu}\sqrt{2r}\,\sin\frac{\theta}{2} \quad , \tag{G.9}$$

where μ is the shear modulus, ν is Poisson's ratio, and $\kappa=4-3\nu$ for plane strain and $\kappa=(3-\nu)/(1+\nu)$ for plane stress. Clearly the stress intensity factors play the important role in the expansion near the crack tip and have been shown to play an important role in fracture [68] or more recently [70].

The singular terms in the stresses have also been shown to apply to geometries other than plane strain. Irwin [68] examined Sneddon's solution [81] of a circular shaped crack in an infinite solid under mode 1 loading and found that in a plane normal to the crack front the definition of k_1 is the same as for the straight crack front of plane strain. Since then Kassir and Sih [82] have proven this to apply for a plane elliptical crack under general, or mixed-mode loading conditions. It may be assumed that this result will hold for any plane crack with a smooth crack front, see Ref. [83].

From Eqns. G.1-9 we define the stress intensity factors in terms of stress and displacement below.

$$k_1 = \lim_{y\to b} \sqrt{2(y-b)}\;\sigma_x(0\;y,z) \quad , \tag{G.10}$$

$$= \frac{2\mu}{\kappa+1}\lim_{y\to b}\frac{1}{\sqrt{2(y-b)}}\left[\;u(0^+,y,z) - u(0^-,y,z)\;\right] \quad , \tag{G.11}$$

$$k_2 = \lim_{y\to b} \sqrt{2(y-b)}\;\tau_{xy}(0,y,z) \quad , \tag{G.12}$$

$$= \frac{2\mu}{\kappa+1}\lim_{y\to b}\frac{1}{\sqrt{2(y-b)}}\left[\;v(0^+,y,z) - v(0^-,y,z)\;\right] \quad , \tag{G.13}$$

$$k_3 = \lim_{y\to b} \sqrt{2(y-b)}\;\tau_{yz}(0,y,z) \quad , \tag{G.14}$$

$$= \frac{\mu}{2} \lim_{y \to b} \frac{1}{\sqrt{2(y-b)}} \left[w(0^+,y,z) - w(0^-,y,z) \right] . \qquad (G.15)$$

These expressions are not valid at the point where a crack front meets a free surface. Benthem [1] has found that the stress singularity at this point is dependent on Poisson's ratio and is not equal to .5. The values for the order of the singularity are given in table G.1. For mode 1 the exponent is less than .5 and for modes 2 and 3 it is greater than .5. In most theoretical work a singularity of .5 is assumed along the entire crack front, see for example Ref. [33].

G.2 Plate and Shell Theory.

The typical expression for stress resultants in either plates or shells is of the non-dimensional form

$$F_i(0,y) = \frac{c_i}{\pi} \int_a^b \frac{u_i(t)}{(t-y)^2} dt + O(1) \ , \ y<a, \ b<y \ , \ i=1,\ldots,5 \ , \qquad (G.16)$$

from which the singular integral equations are obtained

$$-F_k \delta_{ik} = \frac{c_i}{\pi} \fint_a^b \frac{u_i(t)}{(t-y)^2} dt +$$

$$\sum_{j=1}^{5} \int_a^b u_j(t) K_{ij}(y,t) \, dt \ , \ a<y<b \ , \ i=1,\ldots,5 \ , \qquad (G.17)$$

where k corresponds to the loading where δ_{ik} is zero for $i \neq k$ and one for $i=k$. F_i, c_i, and u_i are defined in the following equations where "a" represents the dimensional form, and "b" the non-dimensional.

$$\{ F \} = \{ N_{11}/hE, \ M_{11}/h^2E, \ V_1 12(1+\nu)/5hE, \ N_{12}/hE, \ M_{12}/h^2E \}$$

$$= \{ N_{xx}, M_{xx}, V_x, N_{xy}, M_{xy} \} \quad , \tag{G.18a,b}$$

$$\{ N_{11}, M_{11}, V_1, N_{12}, M_{12} \} =$$

$$\{ h\sigma_{1D}, h^2/(6)\sigma_{2D}, 2h/(3)\sigma_{3D}, h\sigma_{4D}, h^2/(6)\sigma_{5D} \}$$

$$\{ N_{xx}, M_{xx}, V_x, N_{xy}, M_{xy} \} =$$

$$\{ \sigma_1, \sigma_2/6, \sigma_3 8(1+\nu)/5, \sigma_4, \sigma_5/6 \} \quad , \tag{G.19a,b}$$

$$\sigma_i = \sigma_{iD}/E \quad , \tag{G.20}$$

$$\{ c \} = \{ 1/2, 1/24, 1, 1/2, 1/24 \} \ , \tag{G.21}$$

$$\{ u \} = \{ u_x/h, \beta_x, u_z/h, u_y/h, \beta_y \}$$

$$= \{ u_1, u_2, u_3, u_4, u_5 \} \quad , \tag{G.22a,b}$$

with only one exception for the shell,

$$u_y(t) = hu_4(t) + (\lambda_2/\lambda)^2 t u_3(t) \quad , \tag{G.23}$$

where λ_2 and λ are shell parameters defined in Appendix A. To obtain the stress intensity factors (both primary and secondary) from G.17 using G.10-15 we first convert G.17 to

$$-1/P_k\delta_{ik} = \frac{1}{\pi} \fint_{-1}^{+1} \frac{f_i(r)(1-t^2)^{1/2}}{(r-s)^2} dr$$

$$+\sum_{j=1}^{5} \frac{1}{c_j} \int_{-1}^{+1} f_j(r)(1-r^2)^{1/2} L_{ij}(s,r)\, dr \quad ,-1<s<1,\ i=1,\ldots,5 \ , \tag{G.24}$$

where

$$t = \frac{b-a}{2} r + \frac{b+a}{2} \quad , \ y = \frac{b-a}{2} s + \frac{b+a}{2} \quad , \tag{G.25}$$

$$L_{ij}(s,r) = ((b-a)/2)^2 K_{ij}(y,t) \quad , \tag{G.26}$$

$$u_j(t) = (b-t)^{1/2}(t-a)^{1/2} g_j(t)$$

$$= \frac{b-a}{2} \bar{g}_j(r)(1-r^2)^{1/2}$$

$$= \frac{1}{c_j} \overset{\infty}{\sigma}_k \frac{b-a}{2} f_j(r)(1-r^2)^{1/2} \quad , \tag{G.27}$$

$$\sigma_k = P_k F_k \ , \tag{G.28}$$

$$\{ P \} = \{ 1,\ 6,\ 5/(8(1+\nu)),\ 1,\ 6 \} \ . \tag{G.29}$$

To calculate stress intensity factors we require the three-dimensional stress in dimensional form. From Eqn. G.16 with substitutions from G.25-27,

$$\frac{\bar{F}_i(0,s)}{\overset{\infty}{\sigma}_k} = \frac{1}{\pi} \int_{-1}^{+1} \frac{f_i(r)(1-t^2)^{1/2}}{(r-s)^2} dr + O(1) \quad , \ i=1,\ldots,5 \ . \tag{G.30}$$

From Eqn. G.28, using G.25 to convert functions of y to s denoted as such by a bar, we obtain,

$$\frac{\bar{\sigma}_i(0,s)}{\overset{\infty}{\sigma}_k} = \frac{\bar{F}_i(0,s)}{\overset{\infty}{\sigma}_k} P_i \quad . \tag{G.31}$$

In terms of this stress ratio, (dimensional and non-dimensional are equivalent, see Eqn. G.20), the stress expressions needed for Eqns. G.10,12,14 are,

$$\sigma_x(0,y,z) = \overset{\infty}{\sigma}_{kD}\ h_1(z) \left(\frac{\bar{\sigma}_1(0,s)}{\overset{\infty}{\sigma}_k} \right) \quad \text{for tension, (mode 1),}$$

$$= \overset{\infty}{\sigma}_{kD}\ h_2(z) \left(\frac{\bar{\sigma}_2(0,s)}{\overset{\infty}{\sigma}_k} \right) \quad \text{for bending, (mode 1),}$$

$$\tau_{yz}(0,y,z) = \overset{\infty}{\sigma}_{kD}\, h_3(z) \left[\frac{\bar{\sigma}_3(0,s)}{\overset{\infty}{\sigma}_k} \right] \quad \text{for out-of-plane shear, (mode 3),}$$

$$\tau_{xy}(0,y,z) = \overset{\infty}{\sigma}_{kD}\, h_4(z) \left[\frac{\bar{\sigma}_4(0,s)}{\overset{\infty}{\sigma}_k} \right] \quad \text{for in-plane shear, (mode 2),}$$

$$= \overset{\infty}{\sigma}_{kD}\, h_5(z) \left[\frac{\bar{\sigma}_5(0,s)}{\overset{\infty}{\sigma}_k} \right] \quad \text{for twisting, (mode 2),} \qquad (G.32)$$

where $h_i(z)$ are

$$\{ h_1(z),\ h_2(z),\ h_3(z),\ h_4(z),\ h_5(z) \} =$$

$$= \{ 1,\ 2z/h,\ [1-(2z/h)^2],\ 1,\ 2z/h \} \ . \qquad (G.33)$$

Next we use the following result from the asymptotic analysis of singular integrals,

$$\lim_{s\to 1} \frac{1}{\pi} \int_{-1}^{+1} \frac{f_i(r)(1-t^2)^{1/2}}{(r-s)^2}\, dr \sim \lim_{s\to 1} \frac{f_i(s)}{\sqrt{2(s-1)}} + O(1) \ , |s|>1 \ . \qquad (G.34)$$

From Eqns. G.10,12,14 we can write

$$k_j = \lim_{y\to b} \sqrt{2(y-b)}\ \sigma(0\ y,z) \ . \qquad (G.35)$$

which becomes after using G.25,30,31,32,34,

$$k_j = \lim_{s\to 1} \left(\frac{b-a}{2}\right)^{1/2} \sqrt{2(s-1)}\ \overset{\infty}{\sigma}_{kD} h_i(z) P_i \frac{f_i(s)}{\sqrt{2(s-1)}} \ , \qquad (G.36)$$

$$= \left(\frac{b-a}{2}\right)^{1/2} \overset{\infty}{\sigma}_{kD} h_i(z) P_i f_i(1) \ , \qquad (G.37)$$

where j=1 for i=1,2, j=2 for i=4,5 and j=3 for i=3. Because the functional z dependence is known for each of the loading cases, it is sufficient to use the maximum value of $h_i(z)$ which is one. After

normalizing,

$$\frac{k_j}{\overset{\infty}{\sigma}_{kD}\left(\frac{b-a}{2}\right)^{1/2}} = P_i f_i(1) \quad , \tag{G.38}$$

for the crack tip at y=b and similarly for y=a

$$\frac{k_j}{\overset{\infty}{\sigma}_{kD}\left(\frac{b-a}{2}\right)^{1/2}} = P_i f_i(-1) \quad . \tag{G.39}$$

In solving the integral equation, the function $f_i(r)$ is determined on the interval $-1 \le r \le 1$. It is therefore a simple matter to determine the value at the endpoints for substitution into G.38,39.

Next the stress intensity factors will be calculated in terms of the displacement. From Eqns. G.19a,b

$$u(0,y,z) = hu_1(0,y) + (2z/h)h/2u_2(0,y) \ ,$$

$$v(0,y,z) = hu_4(0,y) + (2z/h)h/2u_5(0,y) \ . \tag{G.40}$$

The expression for the out-of-plane displacement w, is not known as a function of z and will be dealt with later. For modes 1 and 2 we proceed as follows. Eqn. G.27 is substituted into the above displacement expressions and then Eqns. G.11,13,15 are used to write,

$$k_j = \frac{hE}{\gamma_j \delta_i} \lim_{y \to b} \frac{1}{\sqrt{2(y-b)}} h_i(z) \frac{1}{c_i} \overset{\infty}{\sigma}_k \frac{b-a}{2h} f_i(s) \sqrt{1-s^2}$$

$$= \frac{h_i(z)\overset{\infty}{\sigma}_{kD}}{\gamma_j \delta_i c_i} \left(\frac{b-a}{2}\right)^{1/2} f_i(1) \ , \quad i \neq 3 \ , \tag{G.41}$$

where

$$u_i = u_i^+ = -u_i^- , \quad 2\mu = \frac{E}{1+\nu} \ , \quad \kappa = \frac{3-\nu}{1+\nu} \ ,$$

$$\gamma_j = 2,\ j=1,2\ (\text{i.e. } i=1,2,4,5)\ ,\ \gamma_3 = 2(1+\nu)\ ,$$

$$\delta_i = 1,\ i=1,3,4 \text{ and } \delta_i = 2,\ i=2,5\ . \tag{G.42}$$

Therefore the normalized stress intensity factors calculated from displacement are,

$$\frac{k_j}{\overset{\infty}{\sigma}_{kD}\left(\frac{b-a}{2}\right)^{1/2}} = \frac{f_i(1)}{\gamma_j \delta_i c_i} \tag{G.43}$$

and

$$\frac{k_j}{\overset{\infty}{\sigma}_{kD}\left(\frac{b-a}{2}\right)^{1/2}} = \frac{f_i(-1)}{\gamma_j \delta_i c_i}\ . \tag{G.44}$$

From Eqns. G.38,39 and 43,44 we should have,

$$1/P_i = \gamma_j \delta_i c_i\ . \tag{G.45}$$

First note that if the primary stress intensity factors for both stress and displacement are the same, the secondary SIFs will also be. The four cases (i=1,2,4,5), are shown below to be equivalent when defined in terms of stress or displacement indicating a compatibility between this plate theory, which includes transverse shear deformation, and elasticity theory for modes 1 and 2:

$\underline{i=1}$, $1/P_1 = 1$

$$\gamma_1 \delta_1 c_1 = (2)(1)(1/2) = 1\ , \tag{G.46}$$

$\underline{i=2}$, $1/P_2 = 1/6$

$$\gamma_1 \delta_2 c_2 = (2)(2)(1/24) = 1/6\ , \tag{G.47}$$

$\underline{i=4}$, $1/P_4 = 1$

$$\gamma_2\delta_4 c_4 = (2)(1)(1/2) = 1 \ , \tag{G.48}$$

<u>i=5</u>, $1/P_5 = 1/6$

$$\gamma_2\delta_5 c_5 = (2)(2)(1/24) = 1/6 \ . \tag{G.49}$$

As mentioned above, for out-of-plane shear which represents mode 3 loading, there is a problem. The displacement plate variable u_z, is an average quantity defined in terms of the actual displacement w as follows, see Timoshenko [84],

$$u_z(x,y) = \frac{3}{2h}\int_{-h/2}^{+h/2} w(x,y,z)\left[1 - (2z/h)^2\right] dz \ . \tag{G.50}$$

The z dependence of u_z cannot be determined because of the plate assumption concerning ϵ_z, i.e. $\sigma_z = 0$. Therefore the stress intensity factor cannot be defined in terms of displacement. It can only be shown that the stress intensity factor obtained from u_z is equal to the weighted average using G.50.

First assume that the actual out-of-plane displacement can be expressed as,

$$w(x,y,z) \sim \bar{w}(x,y) = hu_z(x,y) \ . \tag{G.51}$$

Then by an analysis similar to that used for i=1 and 4 above,

$$\frac{k_{3avg}}{\overset{\infty}{\sigma}_{kD}\left(\frac{b-a}{2}\right)^{1/2}} = \frac{f_3(1)}{\gamma_3\delta_3 c_3} = \frac{f_3(1)}{2(1+\nu)} \ . \tag{G.52}$$

The stress intensity factor from stress is given by G.37 to be,

$$\frac{k_3(z)}{\overset{\infty}{\sigma}_{kD}\left(\frac{b-a}{2}\right)^{1/2}} = \frac{5f_3(1)}{8(1+\nu)}\left[1 - (2z/h)^2\right] \ . \tag{G.53}$$

When this is substituted into Eqn. G.50, we obtain,

$$k_{3avg} = \frac{3}{2h} \int_{-h/2}^{+h/2} k_3(z) \left[1 - (2z/h)^2\right] dz \quad ,$$

$$= \left(\frac{b-a}{2}\right)^{1/2} \sigma_{kD}^{\infty} f_3(1) \frac{1}{2(1+\nu)} \quad , \tag{G.54}$$

which is the same as predicted by Eqn. G.52.

The shell displacement component of Eqn. G.23 also is only known as an average quantity because of its association with u_z. Here

$$v(0,y,z) = hu_4(0,y) + (\lambda_2/\lambda)^2 (y/h) hu_3(0,y) +$$

$$+ (2z/h) h/2 u_5(0,y) \quad . \tag{G.55}$$

Again only in the average sense does this form comply with the theory of elasticity so stress is used for the SIF calculation.

It should be noted that a stress singularity of .5 is assumed at the free surface for all fracture modes. In mode 3 the parabolic shear assumption forces k_3 equal to zero at the plate surface when in fact Benthem [1] predicts it to be infinite. However the surface effects are not believed to greatly influence the value of the SIF away from the surface and in most work a singularity of .5 is assumed, see for example Refs. [33,43].

Table G.1 Strength of stress singularity for the intersection of a straight crack front with a free surface in a half-space, Refs. [1,85].

Poisson's ratio	Stress Singularity mode 1	modes 2 and 3
0.	→-.5	→-.5
.15	-.4836	-.5668
.3	-.4523	-.6073
.4	-.4132	-.6286
.5	-.3318	-.6462

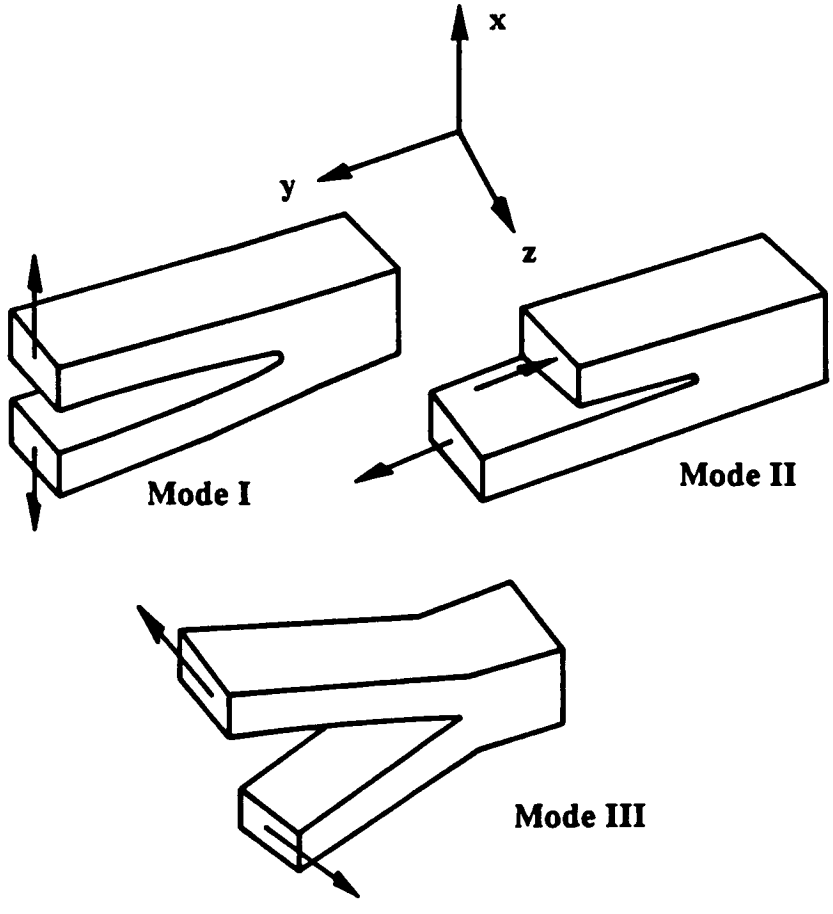

Figure G.1 Crack surface displacement for the different modes of loading.

APPENDIX H

Thin Plate Bending Limit of Fredholm Kernel

We consider the behavior of the Fredholm kernel of Eqn. 3.130 for a/h approaching infinity. Define

$$I(y,a/h) = \frac{5}{\pi(1+\nu)} (a/h)^2 \int_{-1}^{+1} K(z)g(t)\ dt \quad , \tag{H.1}$$

where

$$K(z) = \frac{-48}{z^4} + \frac{4}{z^2} - 4K_0(z) + 4K_2(z) + \frac{24}{z^2}K_2(z) \quad , \tag{H.2}$$

$$z = \rho|t-y| \ , \ \rho = (10)^{1/2}(a/h) = \beta(a/h) \quad . \tag{H.3}$$

First consider the limit for y outside of the crack. This case is simple because as a/h gets large, z gets large. The only contribution from K(z) comes from the $4/z^2$ term. For $|y|>1$,

$$\lim_{a/h\to\infty} I(y,a/h) = \frac{2}{\pi(1+\nu)} \int_{-1}^{+1} \frac{g(t)}{(t-y)^2}\ dt \quad . \tag{H.4}$$

For y inside of the crack domain the variable z can be of order one at t near y so it is not clear that these terms are negligible even for large a/h. Rewrite I(y,a/h) as follows,

$$I(y,a/h) = \frac{5(a/h)^2}{\pi(1+\nu)} \int_{-1}^{+1} K(z)g(t)\ dt = \frac{\rho^2}{2\pi(1+\nu)} \int_{-1}^{+1} K(z)g(t)\ dt \quad , \tag{H.5}$$

$$= \frac{\rho^2}{2\pi(1+\nu)} \left\{ \int_{-1}^{y} K(z)g(t)\ dt + \int_{y}^{+1} K(z)g(t)\ dt \right\} \quad , \tag{H.6}$$

$$= \frac{\rho}{2\pi(1+\nu)} \left\{ \int_{0}^{\rho(1+y)} K(u)g(y-u/\rho)\ du + \int_{0}^{\rho(1-y)} K(u)g(y+u/\rho)\ du \right\} \tag{H.7}$$

$$= \frac{\rho}{2\pi(1+\nu)} \left\{ \int_{\rho(1-y)}^{\rho(1+y)} K(u)g(y-u/\rho)\ du + \right.$$

$$\left. \int_{0}^{\rho(1-y)} K(u)\,[g(y+u/\rho)+g(y-u/\rho)]\ du \right\} \tag{H.8}$$

Next write Taylor expansions for g(t) as follows,

$$g(y-u/\rho) = \sum_{n=0}^{\infty}(-1)^n\frac{1}{n!}\ (u/\rho)^n g^n(y) \quad , \tag{H.9}$$

$$g(y+u/\rho) = \sum_{n=0}^{\infty}\frac{1}{n!}\ (u/\rho)^n g^n(y) \quad , \tag{H.10}$$

where $g^n(y)$ denotes the nth derivative of g(y). These expressions are substituted into the second integral of Eqn. H.8. Because of symmetry only y>0 will be considered. After rewriting the first integral using a simple substitution, Eqn. H.8 becomes,

$$I(y,a/h) = \frac{\rho^2}{2\pi(1+\nu)} \int_{-1}^{-1+2y} K[\rho(y-t)]g(t)\ dt +$$

$$+ \frac{\rho}{\pi(1+\nu)} \sum_{n=0}^{\infty} \frac{1}{(2n)!}\ g^{2n}(y)\ \rho^{-2n} \int_{0}^{\rho(1-y)} u^{2n}K(u)\ du \quad . \tag{H.11}$$

Now consider the limit of these two terms separately. Since the first integral is not singular for y<1, as ρ gets large all terms of K(z) go to zero except the $4/z^2$ term. Therefore we have,

$$\lim_{a/h\to\infty} \frac{\rho^2}{2\pi(1+\nu)} \int_{-1}^{-1+2y} K[\rho(y-t)]g(t)\ dt = \frac{2}{\pi(1+\nu)} \int_{-1}^{-1+2y} \frac{g(t)}{(t-y)^2}\ dt \quad . \tag{H.12}$$

Now for the second integral of Eqn. H.11. For large u

$$K_n(u) \sim [\pi/(2u)]^{1/2} e^{-u}(1+\alpha/u+\ldots) \quad , \tag{H.13}$$

where $K_n(u)$ is a Bessel function and α is a constant. The important

feature is the exponential decay. It can be shown that,

$$\int_u^\infty \frac{u^n}{\sqrt{u}} e^{-u} \, du \sim e^{-u} \quad . \tag{H.14}$$

Now divide the second integral in Eqn. H.11 into two integrals,

$$\int_0^{\rho(1-y)} u^{2n} K(u) \, du = \int_0^{\epsilon} u^{2n} K(u) \, du + \int_{\epsilon}^{\rho(1-y)} u^{2n} K(u) \, du \quad , \tag{H.15}$$

where ϵ is sufficiently large such that the exponentially decaying Bessel functions may be neglected when integrated from ϵ to infinity, (here we assume that $\epsilon<\rho(1-y)$). The first term in the series, (n=0) requires special treatment.

$$\int_0^{\rho(1-y)} K(u) \, du = \int_0^\infty K(u) \, du - \int_{\rho(1-y)}^\infty K(u) \, du \quad , \tag{H.16}$$

where

$$\int_0^\infty K(u) \, du = \left[\frac{-16}{u^3} + \frac{4}{u} + \frac{8}{u} K_2(u)\right|_0^\infty = 0 \quad . \tag{H.17}$$

Now we make use of Eqn. H.14 to evaluate

$$\int_{\rho(1-y)}^\infty K(u) \, du \simeq \int_{\rho(1-y)}^\infty (4/u^2) \, du \simeq \frac{4}{\rho(1-y)} \quad , \tag{H.18}$$

to leading order. The second integral in Eqn. H.15 for n≥1 including the coefficient of ρ^{-2n} from Eqn. H.11 becomes,

$$\rho^{-2n} \int_{\epsilon}^{\rho(1-y)} u^{2n} K(u) \, du \simeq \rho^{-2n} \int_{\epsilon}^{\rho(1-y)} u^{2n} (4/u^2) \, du \simeq$$

$$\frac{4}{2n-1} \left\{ \frac{1}{\rho}(1-y)^{2n-1} - \epsilon^{2n-1}/\rho^{2n} \right\} \simeq \frac{4}{2n-1} \frac{1}{\rho}(1-y)^{2n-1} \quad . \tag{H.19}$$

Now for the first integral in Eqn. H.15. For n≥1 this integral with the ρ^{-2n} coefficient from Eqn. H.11 is,

$$\rho^{-2n} \int_0^{\epsilon} u^{2n} K(u)\, du < O(\rho^{-1}) \quad . \tag{H.20}$$

In the limit as ρ gets large, this term will not have an order one contribution to $I(y,a/h)$ because $\epsilon \ll \rho$ and therefore it is neglected.

Now we substitute Eqns. H.12,16,18,19,20 into H.11 and obtain,

$$\underset{a/h\to\infty}{\text{limit}} I(y,a/h) = \frac{2}{\pi(1+\nu)} \left\{ \int_{-1}^{-1+2y} \frac{g(t)}{(t-y)^2}\, dt + \right.$$

$$\left. + \frac{-2}{1-y} g(y) + 2 \sum_{n=1}^{\infty} \frac{1}{(2n)!}\, g^{2n}(y) \frac{(1-y)^{2n-1}}{2n-1} \right\} \quad . \tag{H.21}$$

Now look at the first integral of Eqn. H.21.

$$\int_{-1}^{-1+2y} \frac{g(t)}{(t-y)^2}\, dt = \fint_{-1}^{+1} \frac{g(t)}{(t-y)^2}\, dt - \fint_{1}^{-1+2y} \frac{g(t)}{(t-y)^2}\, dt \ . \tag{H.22}$$

Substitute the expansion,

$$g(t) = \sum_{n=0}^{\infty} (-1)^n \frac{1}{n!}\, (t-y)^n g^n(y) \quad , \tag{H.23}$$

into the second integral of H.22 and after some algebra,

$$\fint_{1}^{-1+2y} \frac{g(t)}{(t-y)^2}\, dt = \fint_{1}^{-1+2y} \sum_{n=0}^{\infty} (-1)^n \frac{1}{n!}\, (t-y)^{n-2} g^n(y)\, dt =$$

$$= -2 \sum_{n=0}^{\infty} \frac{1}{(2n)!} g^{2n}(y) \frac{(1-y)^{2n-1}}{2n-1} \quad . \tag{H.24}$$

When this is combined with Eqns. H.21 and 22 we obtain,

$$\underset{a/h\to\infty}{\text{limit}} I(y,a/h) = \frac{2}{\pi(1+\nu)} \fint_{+1}^{-1} \frac{g(t)}{(t-y)^2}\, dt \quad , \tag{H.25}$$

which is perhaps the expected result considering Eqn. H.4. The reason for going through this algebra (and there is probably a better way),

is to show that this derivation fails for y sufficiently close to one. Eqns. H.12,18 and 19 are valid only for,

$$\frac{1}{\rho(1-y)} = o(1) \quad . \tag{H.26}$$

In the limit as ρ goes to infinity, the quantity (1-y) must be such that the product $\rho(1-y)$ still goes to infinity. Otherwise Eqn. H.25 is not valid. For more information, see Chapter 3.

APPENDIX I

Log integrals

The major expense in solving an integral equation on the computer is in the evaluation and the integration of the Fredholm kernels. In the shell problem for each point used to integrate the Fredholm kernel an infinite integral must be determined. The plate kernels are known in closed form but involve evaluation of Bessel functions.

Log integrals and integrals of the form,

$$\int_{-1}^{+1} (t-y)^n \ln|t-y| (1-t^2)^{1/2}\, dt \quad , \quad -1<y<+1 \quad , \tag{I.1}$$

which appear in both the plate and the shell equations, (and in many other problems) may be the determining factor for convergence of the integration of the Fredholm kernels. Gauss-Chebychev integration (see Eqns. E.31-33) is used to show this difficulty for small n in table I.1. The number of points used to integrate Eqn. I.1 is N. The closed form expression used may be found in Appendix A. The value of y does not have a significant effect on these results. Because of this slow convergence log terms were separated from the kernels for $n \leq 3$ with the option of doing them in closed form. The following asymptotic analysis of the log terms for $z = \beta(t-y)$ approaching zero is given for the plate kernels where the subscripts 2,3 and 5 respectively correspond to bending (M_{xx}), out-of-plane shear (V_x), and twisting (M_{xy}).

$$K_{22}(z) \sim \frac{\gamma}{\kappa} \ln(z) + c_1 + \frac{\gamma}{\kappa} \left(\frac{z}{2}\right)^2 \ln(z) + O(z^4 \ln(z)) \quad , \tag{I.2}$$

$$K_{33}(z) \sim -\beta^2 \ln(z) + c_2 - \frac{3}{2}\beta^2 (\frac{z}{2})^2 \ln(z) + O(z^4 \ln(z)) \quad , \tag{I.3}$$

$$K_{35}(z) \sim -\beta(\frac{z}{2}) \ln(z) + c_3 z - \frac{2}{3}\beta\ (\frac{z}{2})^3 \ln(z) + O(z^5 \ln(z)) \quad , \tag{I.4}$$

$$K_{53}(z) \sim \beta^3 \gamma (1-\nu) \left[\frac{1}{2}(\frac{z}{2}) \ln(z) + c_4 z + \frac{1}{3}(\frac{z}{2})^3 \ln(z) + O(z^5 \ln(z)) \right] , \tag{I.5}$$

$$K_{55}(z) \sim \frac{\gamma}{\kappa} \ln(z) + c_5 + \frac{\gamma}{\kappa} (\frac{z}{2})^2 \ln(z) + O(z^4 \ln(z)) \quad , \tag{I.6}$$

where the c_i's are constants. In the shell problem these types of terms come from the large α behavior of the infinite integrals, see section J.4 of Appendix J.

To show how these terms affect the convergence of the stress intensity factors, table I.2 lists results for the plate bending problem solved in three different ways. First both log(t-y) and $(t-y)^2 \log(t-y)$ terms of Eqn. I.2 are evaluated in closed form. Then only the log term is evaluated in closed form. Finally both terms are integrated numerically. In the case where the log term was integrated numerically, convergence was unstable for increasing N . The table shows improved convergence when the $z^2 \ln z$ term is evaluated in closed form. It should be noted however, that as a/h gets large the coefficient of this term is proportional to $(a/h)^2$, and it becomes unwise to separate it from the rest of the Fredholm kernel. This is generally the case when doing part of the Fredholm kernel in closed form. For certain parameters the two separate terms become increasingly equal and opposite and consequently big numbers are added to small numbers and accuracy is lost. This typically occurs for the most interesting/difficult geometries. Table I.3 is similar to I.2

but for out-of-plane shear and for twisting. Here there are five different cases as can be seen from Eqns. I.3-6. Again it is necessary to factor out the log term. The other terms are not so important. My conclusion is that for other than the log term, a closed form solution should only be used when repeated calculations are necessary for an "expensive" problem.

Table I.1 - Convergence of log integrals (see Eqn. I.1) using Gauss-Chebychev integration . N=∞ corresponds to closed form.

Convergence of Log Integrals

y=.49

N	n=0	n=1	n=2
20	-.1578327285023e01	.8493750878678e-1	-.4311621931347e-1
40	-.1492930970972e01	.8768209651665e-1	-.4319761807491e-1
60	-.1470627952900e01	.8713681420222e-1	-.4320566456916e-1
80	-.1482919042609e01	.8693758759624e-1	-.4320296083838e-1
100	-.1531715634235e01	.8700300152495e-1	-.4320130620737e-1
200	-.1492468021175e01	.8708543360460e-1	-.4320230905703e-1
300	-.1491702663902e01	.8705949644705e-1	-.4320231744712e-1
∞	-.1497043010486e01	.8706261970927e-1	-.4320228921493e-1

N	n=3	n=4	n=5
20	-.5934890759307e-1	.1070779572998e00	-.1692569091885e00
40	-.5935358973931e-1	.1070783355533e00	-.1692568662971e00
60	-.5935323791180e-1	.1070783468198e00	-.1692568670579e00
80	-.5935318085722e-1	.1070783448821e00	-.1692568671124e00
100	-.5935320220412e-1	.1070783444628e00	-.1692568670990e00
200	-.5935320644195e-1	.1070783446586e00	-.1692568670976e00
300	-.5935320568158e-1	.1070783446588e00	-.1692568670977e00
∞	-.5935320573115e-1	.1070783446580e00	-.1692568670977e00

Table I.2 The effect of log terms on convergence of SIF's for a cracked plate, ν=.3, a/h=1 subjected to bending.

N	closed form $\ln z$ & $z^2 \ln z$	closed form $\ln z$	numerical $\ln z$ & $z^2 \ln z$
10	.747480	.747002	.803520
20	.747475	.747434	.764523
30	.747475	.747473	.748220
40	.747475	.747475	.748087

Table I.3 The effect of log terms on convergence of SIF's for a cracked plate, ν=.3, a/h=1 subjected to out-of-plane shear and twisting.

	out-of-plane shear		twisting	
Closed form $(t-y)^n \ln(t-y)$, $n \leq 3$.				
N	mode 3	mode 2	mode 3	mode 2
10	1.676091	.4656783	-.06969634	.5218047
20	1.675977	.4656280	-.06969737	.5218052
30	1.675978	.4656283	-.06969736	.5218053
40	1.675978	.4656283	-.06969736	.5218053
Closed form $(t-y)^n \ln(t-y)$, $n \leq 2$.				
N	mode 3	mode 2	mode 3	mode 2
10	1.676091	.4657690	-.06972434	.5218006
20	1.675977	.4656276	-.06969702	.5218053
30	1.675977	.4656284	-.06969738	.5218052
40	1.675978	.4656283	-.06969735	.5218053
Closed form $(t-y)^n \ln(t-y)$, $n \leq 1$.				
N	mode 3	mode 2	mode 3	mode 2
10	1.668236	.4622265	-.06976822	.5218403
20	1.676051	.4656858	-.06969392	.5218064
30	1.675995	.4656386	-.06969702	.5218054
40	1.675984	.4656324	-.06969720	.5218053
Closed form $\ln(t-y)$ only.				
N	mode 3	mode 2	mode 3	mode 2
10	1.668817	.4554824	-.06769097	.5221562
20	1.676039	.4655730	-.06971322	.5218015
30	1.676022	.4655065	-.06965142	.5218123
40	1.675970	.4655034	-.06972230	.5218015
All numerical.				
N	mode 3	mode 2	mode 3	mode 2
10	2.846719	1.020734	-.06166954	.5240765
20	1.594647	.4349318	-.07014928	.5244262
30	1.654414	.4506305	-.07051167	.5214280
40	1.660155	.4547331	-.07034780	.5215313
100	1.662201	.4583573	-.06995209	.5216891
200	1.666864	.4626725	-.06966782	.5220058

APPENDIX J

Asymptotic Analysis of the Shell Infinite Integrals

There are two reasons why the large α behavior of the infinite integrals must be determined. First the singular behavior of the integral equation comes from the leading order term in the large α expansion of the integrand. The second reason is simply for numerical simplification. The numerical technique used divides the integral into two parts, $0 < \alpha < A$ performed numerically, and $\alpha > A$ which is evaluated in closed form. The more terms in the expansion, the smaller need be A.

The complication in the integrand is its dependence on the roots of the quartic polynomial,

$$p^4 - \kappa\lambda_2^4 p^3 + \left\{\left[(\lambda_1^2-\lambda_2^2)\alpha^2\right]2\kappa\lambda_2^2 + \lambda_2^4\right\}p^2 -$$

$$- \left\{\left[(\lambda_1^2-\lambda_2^2)\alpha^2\right]^2\kappa + \left[(\lambda_1^2-\lambda_2^2)\alpha^2\right]2\lambda_2^2\right\}p + \left[(\lambda_1^2-\lambda_2^2)\alpha^2\right]^2 . \qquad (J.1)$$

One need only trace through Chapter 5 to see that the kernels in question are heavily dependent on these roots.

J.1 Asymptotic Expansions for the Roots of the Characteristic Equation

A straightforward asymptotic analysis of the integrands of the infinite integrals of Chapter 5 would start with the large α expansion of the roots of Eqn. J.1. They have been found to be

$$p_1 = \frac{1}{\kappa} + \frac{1}{\alpha^4}\frac{1}{\kappa^5(\lambda_1^2-\lambda_2^2)^2} + \frac{1}{\alpha^6}\frac{2\lambda_2^2}{\kappa^6(\lambda_1^2-\lambda_2^2)^3} + \frac{1}{\alpha^8}\frac{4+3\kappa^2\lambda_2^4}{\kappa^9} + \dots , \quad (J.2)$$

$$p_j = \alpha^{4/3}p_{1j} + \alpha^{2/3}p_{2j} + p_{3j} + \dots \quad , \quad j = 2,3,4 \quad , \quad (J.3)$$

where

$$p_{12} = (\kappa f)^{1/3}, \; p_{13} = p_{12}\left(-\frac{1}{2} + i\frac{\sqrt{3}}{2}\right) , \; p_{14} = p_{12}\left(-\frac{1}{2} - i\frac{\sqrt{3}}{2}\right)$$

$$p_{2j} = \frac{-bp_{1j}^2}{4p_{1j}^3 + d} \quad , \quad j=2,3,4 \quad ,$$

$$p_{3j} = -\frac{6p_{1j}^2p_{2j}^2 + ap_{1j}^3 + 2bp_{1j}p_{2j} + f}{4p_{1j}^3 + d} \quad , \quad j=2,3,4 \quad , \quad (J.4)$$

$$a = -\kappa\lambda_2^4 \quad , \quad b = 2\kappa\lambda_2^2(\lambda_1^2 - \lambda_2^2) \quad , \quad c = \lambda_2^4 \quad , \quad d = -\kappa(\lambda_1^2 - \lambda_2^2)^2 \quad ,$$

$$e = -2\lambda_2^2(\lambda_1^2 - \lambda_2^2) \quad , \quad f = (\lambda_1^2 - \lambda_2^2)^2 \quad . \quad (J.5)$$

By using these roots one can obtain all the quantities found in the various kernels, for example for large α

$$D(\alpha) = \alpha^4 3i\sqrt{3}\lambda^4\kappa^2(\lambda_1^2 - \lambda_2^2)^2 + O(\alpha^2) \quad . \quad (J.6)$$

This method is good enough to determine the leading order term but there is a better way which is shown in section J.2. It is also useful to have the small $\alpha^2(\lambda_1^2-\lambda_2^2)$ expansion of the roots of Eqn. J.1. They are:

$$p_{1,2} = \eta_0 + z\eta_1 + z^2\eta_2 + z^3\eta_3 + O(z^4) \quad , \quad (J.7)$$

$$p_3 = \frac{z}{\lambda_2^2} + i\frac{z^2}{\lambda_2^6} + \frac{-4+\kappa i}{2\lambda_2^8}z^3 + O(z^4) \quad ,$$

$$p_4 = \frac{z}{\lambda_2^2} - i\frac{z^2}{\lambda_2^6} + \frac{-4-\kappa i}{2\lambda_2^8}z^3 + O(z^4) \quad , \tag{J.8}$$

$$\eta_0 = \frac{\kappa\lambda_2^4}{2} \pm \frac{1}{2}(\kappa^2\lambda_2^8-4\lambda_2^4)^{1/2} \quad , \quad \eta_1 = -\frac{\bar{b}\eta_0^2+\bar{e}\eta_0}{4\eta_0^3+3a\eta_0^2+2c\eta_0} \quad ,$$

$$\eta_2 = -\frac{6\eta_0^2\eta_1^2+3a\eta_0\eta_1^2+c\eta_1^2+2\bar{b}\eta_0\eta_1+\bar{d}\eta_0+\bar{e}\eta_1+1}{4\eta_0^3+3a\eta_0^2+2c\eta_0} \quad ,$$

$$\eta_3 = -\frac{12\eta_0^2\eta_1\eta_2+4\eta_0\eta_1^3+6a\eta_0\eta_1\eta_2+a\eta_1^3+\bar{b}\eta_1^2+2\bar{b}\eta_0\eta_2+2c\eta_1\eta_2+\bar{d}\eta_1+\bar{e}\eta_2}{4\eta_0^3+3a\eta_0^2+2c\eta_0} \quad , \tag{J.9}$$

$$z = \alpha^2(\lambda_1^2-\lambda_2^2) \quad , \tag{J.10}$$

$$\bar{b} = 2\kappa\lambda_2^2 \ , \quad \bar{d} = -\kappa \ , \quad \bar{e} = -2\lambda_2^2 \quad , \tag{J.11}$$

where p_1 is obtained from using the plus sign for η_0 and p_2 corresponds to the minus sign.

J.2 Symmetric Asymptotic Analysis

First recall Eqns. 5.39,65,66,67,68,80,81 from Chapter 5.

$$m_j = -(p_j+\alpha^2)^{1/2} \quad , \quad j=1,2,3,4 \quad , \tag{J.12}$$

$$\sum_{j=1}^{4} m_j K_j R_j \left\{ \left[\kappa(1-\nu)\alpha^2+1\right]p_j - \alpha^2(1-\nu)\right\} = 0 \quad , \tag{J.13}$$

$$\sum_{j=1}^{4} m_j K_j R_j \left\{ \kappa p_j - 1 \right\} = \frac{-1}{\alpha}\, q_2(\alpha) \quad , \tag{J.14}$$

$$\sum_{j=1}^{4} m_j R_j = 0 \quad , \tag{J.15}$$

$$\sum_{j=1}^{4} m_j R_j \left\{ \lambda_2^2 K_j \frac{\kappa p_j - 1}{\lambda^2} - m_j^2 \right\} = -\alpha q_1(\alpha) \quad , \tag{J.16}$$

$$-f_1(y) = -\frac{1}{\pi} \lim_{x \to 0} \int_0^{+\infty} \alpha^2 \sum_{j=1}^{4} R_j e^{m_j x} \cos\alpha(t-y)\, d\alpha \quad , \tag{J.17}$$

$$\frac{-\lambda^4}{1-\nu} f_2(y) = \frac{1+\nu}{\pi} \lim_{x \to 0} \int_0^{+\infty} \left\{ -\kappa r e^{rx} \sum_{j=1}^{4} m_j p_j K_j R_j + \right.$$

$$\left. + \frac{1}{1-\nu} \sum_{j=1}^{4} p_j K_j R_j e^{m_j x} + \alpha^2 \sum_{j=1}^{4} K_j R_j e^{m_j x} \right\} \cos\alpha(t-y)\, d\alpha \quad . \tag{J.18}$$

Instead of determining the behavior of the individual quantities of Eqns. J.17,18, Eqns. J.13-16 are used to determine the behavior of the entire sum. First Eqn. J.12 is expanded for large α.

$$m_j = -(p_j + \alpha^2)^{1/2} \simeq -\alpha\left[1 + \frac{1}{2}\frac{p_j}{\alpha^2} - \frac{1}{8}\frac{p_j^2}{\alpha^4} + \ldots \right] \quad ,$$

$$\simeq -\alpha \sum_{n=0}^{\infty} a_n (-1)^{n+1} \left(\frac{p_j}{\alpha^2} \right)^n \quad , \quad a_n = \binom{1/2}{n} \text{ (binomial coef.)} \quad . \tag{J.19}$$

This expansion is valid because $(p_j/\alpha^2) \sim \alpha^{-2/3}$ which goes to zero for large α. Also the following expression will be needed,

$$r = -\left[\alpha^2 + \frac{2}{\kappa(1-\nu)} \right]^{1/2} \quad ,$$

$$r \simeq -\alpha \sum_{n=0}^{\infty} b_n (-1)^{n+1} \left(\frac{\rho}{\alpha^2} \right)^n \quad , \quad \rho = \frac{2}{\kappa(1-\nu)} \quad . \tag{J.20}$$

Note that for either r or m_j, the large α and small x behavior of the exponentials may be simplified as follows,

$$e^{rx} \sim \exp\left[-\alpha x \left\{ 1 + \frac{1}{2}\frac{\rho}{\alpha^2} - \frac{1}{8}\frac{\rho^2}{\alpha^4} + \ldots \right\} \right] \sim e^{-\alpha x} \quad , \tag{J.21}$$

$$e^{m_j x} \sim \exp\left[-\alpha x\left\{1 + \frac{1}{2}\frac{p_j}{\alpha^2} - \frac{1}{8}\frac{p_j^2}{\alpha^4} + \ldots\right\}\right] \sim e^{-\alpha x} \quad . \tag{J.22}$$

The kernels of Eqns. J.17,18 are defined for large α:

$$I_1 = I_{11}q_1(\alpha)/\alpha + I_{12}q_2(\alpha)/\alpha = \alpha^2\sum_{j=1}^{4}R_j \quad , \tag{J.23}$$

$$I_2 = I_{12}q_1(\alpha)/\alpha + I_{22}q_2(\alpha)/\alpha = -\kappa r\sum_{j=1}^{4}m_j p_j K_j R_j +$$

$$+ \frac{1}{1-\nu}\sum_{j=1}^{4}p_j K_j R_j + \alpha^2\sum_{j=1}^{4}K_j R_j \quad . \tag{J.24}$$

Therefore the following expressions are needed,

$$\sum_{j=1}^{4}R_j \quad , \tag{J.25}$$

$$\sum_{j=1}^{4}K_j R_j \quad , \tag{J.26}$$

$$\sum_{j=1}^{4}p_j K_j R_j \quad , \tag{J.27}$$

$$\sum_{j=1}^{4}m_j p_j K_j R_j \quad . \tag{J.28}$$

From Eqns. J.13-16, Eqn. J.28 can be easily determined,

$$\sum_{j=1}^{4}m_j p_j K_j R_j = i\alpha(1-\nu)q_2(\alpha) \quad . \tag{J.29}$$

Also from these equations we can write

$$\sum_{j=1}^{4}m_j K_j R_j = i\alpha\kappa(1-\nu)q_2(\alpha) + \frac{i}{\alpha}q_2(\alpha) \quad , \tag{J.30}$$

$$\sum_{j=1}^{4} m_j p_j R_j = -i\frac{\lambda_2^2}{\lambda^2}\frac{1}{\alpha}q_2(\alpha) + i\alpha q_1(\alpha) \quad . \tag{J.31}$$

Next express K_j in terms of p_j. The characteristic equation, J.1 is first used to write

$$\frac{1}{\kappa p_j - 1} = \frac{\lambda_2^4}{p_j^2} + \frac{2\lambda_2^2(\lambda_2^2-\lambda_1^2)\alpha^2}{p_j^3} + \frac{(\lambda_2^2-\lambda_1^2)^2\alpha^4}{p_j^4} \quad . \tag{J.32}$$

K_j can then be written as

$$K_j = \frac{p_j^2\lambda^2}{(m_j^2\lambda_2^2-\lambda_1^2\alpha^2)(\kappa p_j-1)} =$$

$$= \frac{\lambda^2}{\alpha^2(\lambda_2^2-\lambda_1^2)}\left\{\lambda_2^4 + \frac{2\lambda_2^2(\lambda_2^2-\lambda_1^2)\alpha^2}{p_j} + \frac{(\lambda_2^2-\lambda_1^2)^2\alpha^4}{p_j^2}\right\} \times$$

$$\times \sum_{n=0}^{\infty}(-1)^n\left(\frac{p_j}{\alpha^2}\right)^n\delta^n \quad , \quad \delta = \frac{\lambda_2^2}{\lambda_2^2-\lambda_1^2} \quad . \tag{J.33}$$

This expression is used to obtain

$$\sum_{j=1}^{4} K_j R_j = \alpha^2\lambda^2(\lambda_2^2-\lambda_1^2)\sum_{j=1}^{4} p_j^{-2}R_j + \lambda^2\lambda_2^2\sum_{j=1}^{4} p_j^{-1}R_j \quad , \tag{J.34}$$

$$\sum_{j=1}^{4} p_j K_j R_j = \alpha^2\lambda^2(\lambda_2^2-\lambda_1^2)\sum_{j=1}^{4} p_j^{-1}R_j + \lambda^2\lambda_2^2\sum_{j=1}^{4} R_j \quad . \tag{J.35}$$

Therefore we can find all that is needed (Eqns. J.25-27), if the following three sums are known,

$$\sum_{j=1}^{4} p_j^{-i}R_j \quad , \quad i=0,1,2 \quad . \tag{J.36}$$

In a similar way in which Eqns. J.34,35 were found, it may also be shown that

$$\sum_{j=1}^{4} p_j^{-1} m_j R_j = \frac{i(1-\nu)}{\alpha\lambda^2(\lambda_2^2-\lambda_1^2)} q_2(\alpha) \quad , \tag{J.37}$$

$$\sum_{j=1}^{4} p_j^{-2} m_j R_j = iq_2(\alpha)\left\{ \frac{1}{\alpha} \frac{\kappa(1-\nu)}{\lambda^2(\lambda_2^2-\lambda_1^2)} + \right.$$

$$\left. + \frac{1}{\alpha^3}\left[\frac{1}{\lambda^2(\lambda_2^2-\lambda_1^2)} - \frac{(1-\nu)\lambda_2^2}{\lambda^2(\lambda_2^2-\lambda_1^2)^2} \right] \right\} \quad . \tag{J.38}$$

From Eqns. J.15,31,37,38, the characteristic equation, J.1 can be used to determine

$$\sum_{j=1}^{4} p_j^n m_j R_j \quad , \tag{J.39}$$

for any n because these four equations represent four consecutive values of the integer n. By making use of Eqn. J.19, Eqn. J.39 can be converted into

$$\sum_{j=1}^{4} p_j^n R_j \quad , \tag{J.40}$$

for any n, in particular n = 0,-1,-2, see Eqn. J.36. This involves algebra, the amount of which is determined by how many terms in the expansion are desired. The result is

$$I_{11} \simeq \frac{\alpha}{2} + \sum_{k=1}^{5} \beta_{2k-1}^{11} \alpha^{-(2k-1)} + 0(\alpha^{-11}) \quad , \tag{J.41}$$

$$I_{12} \simeq \sum_{k=1}^{5} \beta_{2k-1}^{12} \alpha^{-(2k-1)} + 0(\alpha^{-11}) \quad , \tag{J.42}$$

$$I_{21} \simeq \sum_{k=1}^{6} \beta_{2k-1}^{21} \alpha^{-(2k-1)} + 0(\alpha^{-13}) \quad , \tag{J.43}$$

$$I_{22} \simeq \frac{-\alpha}{2}(1+\nu) + \sum_{k=1}^{6} \beta_{2k-1}^{22} \alpha^{-(2k-1)} +$$

$$+ \sum_{k=7}^{\infty} \alpha^{-(2k-1)} \kappa(1-\nu) a_{k+1} (-1)^k \rho^{k+1} + 0(\alpha^{-13}) \quad , \tag{J.44}$$

where,

$$\beta_1^{11} = \left[-\kappa\gamma^2 \frac{35}{128} + \frac{5}{8}\kappa\gamma\lambda_2^2 - \frac{3}{8}\kappa\lambda_2^4\right] ,$$

$$\beta_{2k-1}^{11} = \sum_{j=1}^{2k+1} (-1)^{k+j-1} \gamma^{2k+1-j} Q_1(k,j) c(3k+2-j) \quad , \; k = 1,\ldots,5 \quad ,$$

$$\beta_1^{12} = \frac{1}{\lambda^2} \left[-\gamma\left(\frac{5}{16}(1-\nu) - \frac{3}{8}\right) + \lambda_2^2\left(\frac{3}{8}(1-\nu) - \frac{1}{2}\right)\right] ,$$

$$\beta_{2k-1}^{12} = \frac{1}{\lambda^2} \sum_{j=1}^{2k} (-1)^{k+j+1} \gamma^{2k-j} Q_2(k,j) d(3k+1-j) \quad , \; k = 1,\ldots,5 \; ,$$

$$\beta_1^{21} = \lambda^2 \left[\frac{1}{1-\nu}\left(\frac{1}{2}\lambda_2^2 - \frac{3}{8}\gamma\right) + \frac{5}{16}\gamma - \frac{3}{8}\lambda_2^2\right] ,$$

$$\beta_{2k+1}^{21} = \lambda^2 \sum_{j=1}^{2k+1} (-1)^{k+j} \gamma^{2k+1-j} Q_1(k,j) \left[\left(\frac{\gamma}{1-\nu} + \lambda_2^2\right) c(3k+3-j) -\right.$$

$$\left. - \frac{\lambda_2^2}{1-\nu} c(3k+2-j) - \gamma c(3k+4-j)\right] \quad , \; k = 1,\ldots,5 \quad ,$$

$$\beta_1^{22} = \frac{-1}{2\kappa(1-\nu)} \quad ,$$

$$\beta_{2k+1}^{22} = \left\{\kappa(1-\nu) a_{k+2} (-1)^{k+1} \rho^{k+2} + \sum_{j=1}^{2k} (-1)^{k+j} \gamma^{2k-j} Q_2(k,j) \; \times\right.$$

$$\left. \times \left[\left(\frac{\gamma}{1-\nu} + \lambda_2^2\right) d(3k+2-j) - \frac{\lambda_2^2}{1-\nu} d(3k+1-j) - \gamma d(3k+3-j)\right]\right\} \; , \; k=1,\ldots,5 \; , \tag{J.45}$$

where

$$\gamma = (\lambda_2^2-\lambda_1^2) \ , \tag{J.46}$$

$$c_0 = 1 \quad , \quad c_1 = a_1 \quad , \quad c_n = a_n + \sum_{i=1}^{n-1} a_{n-i}c_i \quad , \tag{J.47}$$

$$d_0 = (1-\nu) \quad , \quad d_n = c_n(1-\nu) - c_{n-1} \quad , \tag{J.48}$$

$Q_1(1,1)=\kappa,\ Q_1(1,2)=2\kappa\lambda_2^2,\ Q_1(1,3)=\kappa\lambda_2^4,$

$Q_1(2,1)=\kappa^2,\ Q_1(2,2)=4\kappa^2\lambda_2^2,\ Q_1(2,3)=6\kappa^2\lambda_2^4-1,\ Q_1(2,4)=\lambda_2^2(4\kappa^2\lambda_2^4-2),$

$Q_1(2,5)=\lambda_2^4(\kappa^2\lambda_2^4-1),$

$Q_1(3,1)=\kappa^3,\ Q_1(3,2)=6\kappa^3\lambda_2^2,\ Q_1(3,3)=\kappa(15\kappa^2\lambda_2^4-2),$

$Q_1(3,4)=\kappa\lambda_2^2(20\kappa^2\lambda_2^4-8),\ Q_1(3,5)=\kappa\lambda_2^4(15\kappa^2\lambda_2^4-12),$

$Q_1(3,6)=\kappa\lambda_2^6(6\kappa^2\lambda_2^4-8),\ Q_1(3,7)=\kappa\lambda_2^8(\kappa^2\lambda_2^4-2),$

$Q_1(4,1)=\kappa^4,\ Q_1(4,2)=8\kappa^4\lambda_2^2,\ Q_1(4,3)=\kappa^2(28\kappa^2\lambda_2^4-3),$

$Q_1(4,4)=\kappa^2\lambda_2^2(56\kappa^2\lambda_2^4-18),\ Q_1(4,5)=(70\kappa^4\lambda_2^8-45\kappa^2\lambda_2^4+1),$

$Q_1(4,6)=\lambda_2^2(56\kappa^4\lambda_2^8-60\kappa^2\lambda_2^4+4),\ Q_1(4,7)=\lambda_2^4(28\kappa^4\lambda_2^8-45\kappa^2\lambda_2^4+6),$

$Q_1(4,8)=\lambda_2^6(8\kappa^4\lambda_2^8-18\kappa^2\lambda_2^4+4),\ Q_1(4,9)=\lambda_2^8(\kappa^4\lambda_2^8-3\kappa^2\lambda_2^4+1),$

$Q_1(5,1)=\kappa^5,\ Q_1(5,2)=10\kappa^5\lambda_2^2,\ Q_1(5,3)=\kappa^3(45\kappa^2\lambda_2^4-4),$

$Q_1(5,4)=\kappa^3\lambda_2^2(120\kappa^2\lambda_2^4-32),\ Q_1(5,5)=\kappa(210\kappa^4\lambda_2^8-112\kappa^2\lambda_2^4+3),$

$Q_1(5,6)=\kappa\lambda_2^2(252\kappa^4\lambda_2^8-224\kappa^2\lambda_2^4+18),$

$$Q_1(5,7)=\kappa\lambda_2^4(210\kappa^4\lambda_2^8-280\kappa^2\lambda_2^4+45),$$

$$Q_1(5,8)=\kappa\lambda_2^6(120\kappa^4\lambda_2^8-224\kappa^2\lambda_2^4+60),$$

$$Q_1(5,9)=\kappa\lambda_2^8(45\kappa^4\lambda_2^8-112\kappa^2\lambda_2^4+45),$$

$$Q_1(5,10)=\kappa\lambda_2^{10}(10\kappa^4\lambda_2^8-32\kappa^2\lambda_2^4+18),$$

$$Q_1(5,11)=\kappa\lambda_2^{12}(\kappa^4\lambda_2^8-4\kappa^2\lambda_2^4+3),$$

$$Q_2(1,1)=1,\ Q_2(1,2)=\lambda_2^2,$$

$$Q_2(2,1)=\kappa,\ Q_2(2,2)=3\kappa\lambda_2^2,\ Q_2(2,3)=3\kappa\lambda_2^4,\ Q_2(2,4)=\kappa\lambda_2^6,$$

$$Q_2(3,1)=\kappa^2,\ Q_2(3,2)=5\kappa^2\lambda_2^2,\ Q_2(3,3)=(10\kappa^2\lambda_2^4-1),$$

$$Q_2(3,4)=\lambda_2^2(10\kappa^2\lambda_2^4-3),\ Q_2(3,5)=\lambda_2^4(5\kappa^2\lambda_2^4-3),$$

$$Q_2(3,6)=\lambda_2^6(\kappa^2\lambda_2^4-1),$$

$$Q_2(4,1)=\kappa^3,\ Q_2(4,2)=7\kappa^3\lambda_2^2,\ Q_2(4,3)=\kappa(21\kappa^2\lambda_2^4-2),$$

$$Q_2(4,4)=\kappa\lambda_2^2(35\kappa^2\lambda_2^4-10),\ Q_2(4,5)=\kappa\lambda_2^4(35\kappa^2\lambda_2^4-20),$$

$$Q_2(4,6)=\kappa\lambda_2^6(21\kappa^2\lambda_2^4-20),\ Q_2(4,7)=\kappa\lambda_2^8(7\kappa^2\lambda_2^4-10),$$

$$Q_2(4,8)=\kappa\lambda_2^{10}(\kappa^2\lambda_2^4-2),$$

$$Q_2(5,1)=\kappa^4,\ Q_2(5,2)=9\kappa^4\lambda_2^2,\ Q_2(5,3)=\kappa^2(36\kappa^2\lambda_2^4-3),$$

$$Q_2(5,4)=\kappa^2\lambda_2^2(84\kappa^2\lambda_2^4-21),\ Q_2(5,5)=(126\kappa^4\lambda_2^8-63\kappa^2\lambda_2^4+1),$$

$$Q_2(5,6)=\lambda_2^2(126\kappa^4\lambda_2^8-105\kappa^2\lambda_2^4+5),$$

$$Q_2(5,7)=\lambda_2^4(84\kappa^4\lambda_2^8-105\kappa^2\lambda_2^4+10),$$

$$Q_2(5,8)=\lambda_2^6(36\kappa^4\lambda_2^8-63\kappa^2\lambda_2^4+10),$$

$$Q_2(5,9)=\lambda_2^8(9\kappa^4\lambda_2^8-21\kappa^2\lambda_2^4+5),$$

$$Q_2(5,10)=\lambda_2^{10}(\kappa^4\lambda_2^8-3\kappa^2\lambda_2^4+1) \quad . \tag{J.49}$$

As mentioned at the beginning of this appendix, the infinite integrals are divided into two parts. The portion from A to infinity is integrated in closed form. This part can be written as,

$$\int_A^\infty I_{ij}\cos\alpha(t-y)d\alpha \quad , \quad i,j=1,2 \quad . \tag{J.50}$$

This integral for I_{ij} of the form given by Eqns. J.41-44 is evaluated in section J.4 of this appendix. The following expressions are used in Eqns. 5.84,85.

$$\bar{I}_{1j} = \sum_{n=2}^{5}\beta_{2n-1}^{1j}(-1)^n\frac{(t-y)^{2n-2}}{(2n-2)!}\ln|t-y| +$$

$$+\sum_{n=1}^{5}\beta_{2n-1}^{1j}(-1)^{n+1}\frac{(t-y)^{2n-2}}{(2n-2)!}F_c(1)+\sum_{n=2}^{5}\beta_{2n-1}^{1j}\bar{F}_c(2n-1) \quad , \quad j=1,2 \quad , \tag{J.51}$$

$$\bar{I}_{21} = \sum_{n=2}^{6}\beta_{2n-1}^{21}(-1)^n\frac{(t-y)^{2n-2}}{(2n-2)!}\ln|t-y| +$$

$$+\sum_{n=1}^{6}\beta_{2n-1}^{21}(-1)^{n+1}\frac{(t-y)^{2n-2}}{(2n-2)!}F_c(1)+\sum_{n=2}^{6}\beta_{2n-1}^{21}\bar{F}_c(2n-1) \quad , \tag{J.52}$$

$$\bar{I}_{22} = \left\{\sum_{n=2}^{6}\beta_{2n-1}^{22}+\kappa(1-\nu)\sum_{n=7}^{\infty}\rho^{n+1}(-1)^n a_{n+1}\right\}(-1)^n\frac{(t-y)^{2n-2}}{(2n-2)!}\ln|t-y| +$$

$$+\left\{\sum_{n=1}^{6}\beta_{2n-1}^{22}+\kappa(1-\nu)\sum_{n=7}^{\infty}\rho^{n+1}(-1)^n a_{n+1}\right\}(-1)^{n+1}\frac{(t-y)^{2n-2}}{(2n-2)!}F_c(1) +$$

$$+ \left\{\sum_{n=2}^{6}\beta_{2n-1}^{22}+\kappa(1-\nu)\sum_{n=7}^{\infty}\rho^{n+1}(-1)^n a_{n+1}\right\}\bar{F}_c(2n-1) \quad . \tag{J.53}$$

J.3 Skew-Symmetric Asymptotic Analysis

The same procedure that was used in section J.2 is used here. The necessary equations are 5.93-96,106-108, which are repeated below,

$$\frac{1}{1-\nu}\sum_{j=1}^{4}p_jK_jR_j = q_5(\alpha) \quad , \tag{J.54}$$

$$\sum_{j=1}^{4}R_j = 0 \quad , \tag{J.55}$$

$$\sum_{j=1}^{4}m_j^2R_j = q_4(\alpha) \quad , \tag{J.56}$$

$$\sum_{j=1}^{4}R_jK_j(\kappa p_j-1) = \frac{i}{\alpha}q_3(\alpha) \quad , \tag{J.57}$$

$$-f_3(y) = \frac{1}{2\pi}\lim_{x\to 0}\int_{-\infty}^{+\infty}\left\{\frac{-1}{r(1-\nu)}\sum_{j=1}^{4}(m_j^2-\nu\alpha^2)K_jR_je^{rx} + \right.$$

$$\left. + \kappa\sum_{j=1}^{4}m_jp_jK_jR_j(\alpha)e^{m_jx}\right\} e^{-i\alpha y}\, d\alpha \quad , \tag{J.58}$$

$$-f_4(y) = \frac{i}{2\pi}\lim_{x\to 0}\int_{-\infty}^{+\infty}\alpha\sum_{j=1}^{4}m_jR_j(\alpha)e^{m_jx}e^{-i\alpha y}\, d\alpha \quad , \tag{J.59}$$

$$-\frac{2\lambda^4}{1-\nu}f_5(y) = \frac{1+\nu}{2\pi}\lim_{x\to 0}\int_{-\infty}^{+\infty}\left\{\sum_{j=1}^{4}K_jR_j\left[\frac{-e^{rx}(\alpha^2+r^2)}{i\alpha r(1-\nu)}(m_j^2-\nu\alpha^2) - \right.\right.$$

$$\left.\left. - 2i\alpha m_je^{m_jx}\right]\right\} e^{-i\alpha y}\, d\alpha \quad . \tag{J.60}$$

Eqns. J.19-22 are again used. The kernels in Eqns. J.58-60 are defined as follows for large α,

$$I_3 = I_{33}q_3(\alpha)/\alpha + I_{34}q_4(\alpha)/\alpha + I_{35}q_5(\alpha)/\alpha =$$

$$= \frac{-1}{r(1-\nu)}\sum_{j=1}^{4}p_jK_jR_j - \frac{\alpha^2}{r}\sum_{j=1}^{4}K_jR_j + \kappa\sum_{j=1}^{4}m_jp_jK_jR_j(\alpha) \quad , \tag{J.61}$$

$$I_4 = I_{43}q_3(\alpha)/\alpha + I_{44}q_4(\alpha)/\alpha + I_{45}q_5(\alpha)/\alpha =$$

$$= i\alpha\sum_{j=1}^{4}m_jR_j(\alpha) \quad , \tag{J.62}$$

$$I_5 = I_{53}q_3(\alpha)/\alpha + I_{54}q_4(\alpha)/\alpha + I_{55}q_5(\alpha)/\alpha =$$

$$= \sum_{j=1}^{4}K_jR_j\left[\frac{-(\alpha^2+r^2)}{i\alpha r(1-\nu)}p_j - \frac{\alpha(\alpha^2+r^2)}{ir} - 2i\alpha m_j\right] \quad . \tag{J.63}$$

From Eqns. J.54-57 we find:

$$\sum_{j=1}^{4}p_j^{-2}R_j = q_5(\alpha)\left\{\frac{\kappa(1-\nu)}{\alpha^2\lambda^2(\lambda_2^2-\lambda_1^2)} - \frac{\lambda_2^2(1-\nu)}{\alpha^4\lambda^2(\lambda_2^2-\lambda_1^2)^2}\right\} -$$

$$- q_3(\alpha)\frac{i}{\alpha^3\lambda^2(\lambda_2^2-\lambda_1^2)} \quad , \tag{J.64}$$

$$\sum_{j=1}^{4}p_j^{-1}R_j = \frac{(1-\nu)q_5(\alpha)}{\alpha^2\lambda^2(\lambda_2^2-\lambda_1^2)} \quad , \tag{J.65}$$

$$\sum_{j=1}^{4}R_j = 0 \quad , \tag{J.66}$$

$$\sum_{j=1}^{4}p_jR_j = q_4(\alpha) \quad . \tag{J.67}$$

Combined with Eqn. J.1 the following may be determined,

$$\sum_{j=1}^{4}p_j^nR_j \quad , \tag{J.68}$$

for any n from which all of the expressions in Eqns. J.61-63 may be obtained to any order of α. The result is:

$$I_{33} \simeq -i\alpha + i\sum_{k=1}^{4}\beta_{2k-1}^{33}\alpha^{-(2k-1)} - i\alpha\sum_{k=5}^{\infty}(-1)^k(\rho/\alpha^2)^k e_k + 0(\alpha^{-9}) \tag{J.69}$$

$$I_{34} \simeq \kappa\lambda^2\left[\tfrac{1}{8}(\lambda_2^2-\lambda_1^2) - \tfrac{1}{2}\lambda_2^2\right] + \sum_{k=1}^{4}\beta_{2k}^{34}\alpha^{-(2k)} + 0(\alpha^{-10}) \quad , \tag{J.70}$$

$$I_{35} \simeq \sum_{k=1}^{4}\beta_{2k}^{35}\alpha^{-(2k)} + \sum_{k=5}^{\infty}(-1)^k(\rho/\alpha^2)^k[e_k-2e_{k+1}] + 0(\alpha^{-10}) \quad , \tag{J.71}$$

$$I_{43} \simeq i\frac{(\lambda_2^2-\lambda_1^2)}{8\lambda^2} + i\sum_{k=1}^{3}\beta_{2k}^{34}\alpha^{-(2k)} + 0(\alpha^{-8}) \quad , \tag{J.72}$$

$$I_{44} \simeq \frac{-\alpha}{2} + \sum_{k=1}^{4}\beta_{2k-1}^{44}\alpha^{-(2k-1)} + 0(\alpha^{-9}) \quad , \tag{J.73}$$

$$I_{45} \simeq \sum_{k=1}^{4}\beta_{2k-1}^{45}\alpha^{-(2k-1)} + 0(\alpha^{-9}) \quad , \tag{J.74}$$

$$I_{53} \simeq \sum_{k=1}^{3}\beta_{2k}^{53}\alpha^{-(2k)} + \alpha^2\sum_{k=5}^{\infty}(-1)^k(\rho/\alpha^2)^k[e_{k-1}-2e_k] + 0(\alpha^{-8}) \quad , \tag{J.75}$$

$$I_{54} \simeq i\sum_{k=1}^{4}\beta_{2k-1}^{54}\alpha^{-(2k-1)} + 0(\alpha^{-9}) \quad , \tag{J.76}$$

$$I_{55} \simeq -i\alpha(1+\nu) + i\sum_{k=1}^{4}\beta_{2k-1}^{55}\alpha^{-(2k-1)} -$$

$$- i\alpha\sum_{k=5}^{\infty}(-1)^{k+1}(\rho/\alpha^2)^k[e_{k-1}-4e_k+4e_{k+1}] + 0(\alpha^{-9}) \quad , \tag{J.77}$$

where

$$\beta_1^{33} = \frac{1}{\kappa(1-\nu)} + \frac{\kappa}{16}(\lambda_2^4-\lambda_1^4) \quad ,$$

$$\beta_3^{33} = -\rho^2 e_2 + \kappa\gamma\left[-a_3\kappa\lambda_2^6 + a_4 3\kappa\lambda_2^4\gamma - a_5 3\kappa\lambda_2^2\gamma^2 + a_6\kappa\gamma^3\right] ,$$

$$\beta_5^{33} = \rho^3 e_3 + \kappa\gamma\left[a_4\lambda_2^6(\kappa^2\lambda_2^4-1) - a_5\lambda_2^4\gamma(5\kappa^2\lambda_2^4-3) + a_6\lambda_2^2\gamma^2(10\kappa^2\lambda_2^4-3) - \right.$$

$$\left. -a_7\gamma^3(10\kappa^2\lambda_2^4-1) + a_8 5\kappa^2\lambda_2^2\gamma^4 - a_9\kappa^2\gamma^5\right] ,$$

$$\beta_7^{33} = -\rho^4 e_4 + \kappa\gamma\left[-a_5\kappa\lambda_2^{10}(\kappa^2\lambda_2^4-2) + a_6\kappa\lambda_2^8\gamma(7\kappa^2\lambda_2^4-10) - \right.$$

$$-a_7\kappa\lambda_2^6\gamma^2(21\kappa^2\lambda_2^4-20) + a_8\kappa\lambda_2^4\gamma^3(35\kappa^2\lambda_2^4-20) - a_9\kappa\lambda_2^2\gamma^4(35\kappa^2\lambda_2^4-10) +$$

$$\left. +a_{10}\kappa\gamma^5(21\kappa^2\lambda_2^4-2) - a_{11}7\kappa^3\lambda_2^2\gamma^6 + a_{12}\kappa^3\gamma^7\right] ,$$

$$\beta_2^{34} = \kappa\lambda^2\left[a_2\kappa\lambda_2^6 - a_3 3\kappa\gamma\lambda_2^4 + a_4 3\kappa\lambda_2^2\gamma^2 - a_5\kappa\gamma^3\right] ,$$

$$\beta_4^{34} = \kappa\lambda^2\left[-a_3\lambda_2^6(\kappa^2\lambda_2^4-1) + a_4\gamma\lambda_2^4(5\kappa^2\lambda_2^4-3) - a_5\lambda_2^2\gamma^2(10\kappa^2\lambda_2^4-3) + \right.$$

$$\left. +a_6\gamma^3(10\kappa^2\lambda_2^4-1) - a_7 5\kappa^2\lambda_2^2\gamma^4 + a_8\kappa^2\gamma^5\right] ,$$

$$\beta_6^{34} = \kappa\lambda^2\left[a_4\kappa\lambda_2^{10}(\kappa^2\lambda_2^4-2) - a_5\kappa\lambda_2^8\gamma(7\kappa^2\lambda_2^4-10) + a_6\kappa\lambda_2^6\gamma^2(21\kappa^2\lambda_2^4-20) - \right.$$

$$-a_7\kappa\lambda_2^4\gamma^3(35\kappa^2\lambda_2^4-20) + a_8\kappa\lambda_2^2\gamma^4(35\kappa^2\lambda_2^4-10) - a_9\kappa\gamma^5(21\kappa^2\lambda_2^4-2) +$$

$$\left. +a_{10}7\kappa^3\lambda_2^2\gamma^6 - a_{11}\kappa^3\gamma^7\right] ,$$

$$\beta_8^{34} = \kappa\lambda^2\left[-a_5\lambda_2^{10}(\kappa^4\lambda_2^8 - 3\kappa^2\lambda_2^4 + 1) + a_6\gamma\lambda_2^8(9\kappa^4\lambda_2^8 - 21\kappa^2\lambda_2^4 + 5) - \right.$$

$$-a_7\lambda_2^6\gamma^2(36\kappa^4\lambda_2^8 - 63\kappa^2\lambda_2^4 + 10) + a_8\gamma^3\lambda_2^4(84\kappa^4\lambda_2^8 - 105\kappa^2\lambda_2^4 + 10) -$$

$$-a_9\lambda_2^4\gamma^4(126\kappa^4\lambda_2^8 - 105\kappa^2\lambda_2^4 + 5) + a_{10}\gamma^5(126\kappa^4\lambda_2^8 - 63\kappa^2\lambda_2^4 + 1) -$$

$$\left. -a_{11}\kappa^2\lambda_2^2\gamma^6(84\kappa^2\lambda_2^4 - 21) + a_{12}\kappa^2\gamma^7(36\kappa^2\lambda_2^4 - 3) - a_{13}9\kappa^4\lambda_2^2\gamma^8 + a_{14}\kappa^4\gamma^9\right] ,$$

$$\beta_2^{35} = -\rho(e_1-2e_2)+\kappa(1-\nu)\left[-a_2\lambda_2^4+a_3 2\lambda_2^2\gamma-a_4\gamma^2\right] ,$$

$$\beta_4^{35} = \rho^2(e_2-2e_3)+\kappa(1-\nu)\left[a_3\kappa\lambda_2^8-a_4 4\kappa\lambda_2^6\gamma+a_5 6\kappa\lambda_2^4\gamma^2-a_6 4\kappa\lambda_2^2\gamma^3+a_7\kappa\gamma^4\right],$$

$$\beta_6^{35} = -\rho^3(e_3-2e_4)+\kappa(1-\nu)\left[-a_4\lambda_2^8(\kappa^2\lambda_2^4-1)+a_5\lambda_2^6\gamma(6\kappa^2\lambda_2^4-4)-\right.$$

$$-a_6\lambda_2^4\gamma^2(15\kappa^2\lambda_2^4-6)+a_7\lambda_2^2\gamma^3(20\kappa^2\lambda_2^4-4)-a_8\gamma^4(15\kappa^2\lambda_2^4-1)+$$

$$\left.+a_9 6\kappa^2\lambda_2^2\gamma^5-a_{10}\kappa^2\gamma^6\right] ,$$

$$\beta_8^{35} = \rho^4(e_4-2e_5)+\kappa(1-\nu)\left[a_5\kappa\lambda_2^{12}(\kappa^2\lambda_2^4-2)-a_6\kappa\lambda_2^{10}\gamma(8\kappa^2\lambda_2^4-12)+\right.$$

$$+a_7\kappa\lambda_2^8\gamma^2(28\kappa^2\lambda_2^4-30)-a_8\kappa\lambda_2^6\gamma^3(56\kappa^2\lambda_2^4-40)+a_9\kappa\lambda_2^4\gamma^4(70\kappa^2\lambda_2^4-30)-$$

$$\left.-a_{10}\kappa\lambda_2^2\gamma^5(56\kappa^2\lambda_2^4-12)+a_{11}\kappa\gamma^6(28\kappa^2\lambda_2^4-2)-a_{12}8\kappa^3\lambda_2^2\gamma^7+a_{13}\kappa^3\gamma^8\right] ,$$

$$\beta_2^{43} = (\gamma/\lambda^2)\left[-a_3\kappa\lambda_2^4+a_4 2\kappa\lambda_2^2\gamma-a_5\kappa\gamma^2\right] ,$$

$$\beta_4^{43} = (\gamma/\lambda^2)\left[a_4\lambda_2^4(\kappa^2\lambda_2^4-1)-a_5 2\lambda_2^2\gamma(2\kappa^2\lambda_2^4-1)+a_6\gamma^2(6\kappa^2\lambda_2^4-1)-\right.$$

$$\left.-a_7 4\kappa^2\lambda_2^2\gamma^3+a_8\kappa^2\gamma^4\right] ,$$

$$\beta_6^{43} = (\gamma/\lambda^2)\left[-a_5\kappa\lambda_2^8(\kappa^2\lambda_2^4-2)+a_6 2\kappa\lambda_2^6\gamma(3\kappa^2\lambda_2^4-4)-a_7\kappa\lambda_2^4\gamma^2(15\kappa^2\lambda_2^4-12)+\right.$$

$$\left.+a_8\kappa\lambda_2^2\gamma^3(20\kappa^2\lambda_2^4-8)-a_9\kappa\gamma^4(15\kappa^2\lambda_2^4-2)+a_{10}6\kappa^3\lambda_2^2\gamma^5-a_{11}\kappa^3\gamma^6\right] ,$$

$$\beta_1^{44} = \kappa\left[\frac{5}{128}(\lambda_2^2-\lambda_1^2)^2+\frac{1}{8}\lambda_1^2\lambda_2^2\right] ,$$

$$\beta_3^{44} = -a_3\lambda_2^4(\kappa^2\lambda_2^4-1)+a_4\lambda_2^2\gamma(4\kappa^2\lambda_2^4-2)-a_5\gamma^2(6\kappa^2\lambda_2^4-1)+$$

$$+a_6 4\kappa^2\lambda_2^2\gamma^3-a_7\kappa^2\gamma^4 ,$$

$$\beta_5^{44} = a_4\kappa\lambda_2^8(\kappa^2\lambda_2^4-2)-a_5\kappa\lambda_2^6\gamma(6\kappa^2\lambda_2^4-8)+a_6\kappa\lambda_2^4\gamma^2(15\kappa^2\lambda_2^4-12)-$$

$$-a_7 2\kappa\lambda_2^2\gamma^3(10\kappa^2\lambda_2^4-4)+a_8\kappa\gamma^4(15\kappa^2\lambda_2^4-2)-a_9 6\kappa^3\lambda_2^2\gamma^5+a_{10}\kappa^3\gamma^6 \quad ,$$

$$\beta_7^{44} = -a_5\lambda_2^8(\kappa^4\lambda_2^8-3\kappa^2\lambda_2^4+1)+a_6\lambda_2^6\gamma(8\kappa^4\lambda_2^8-18\kappa^2\lambda_2^4+4)-$$

$$-a_7\lambda_2^4\gamma^2(28\kappa^4\lambda_2^8-45\kappa^2\lambda_2^4+6)+a_8\lambda_2^2\gamma^3(56\kappa^4\lambda_2^8-60\kappa^2\lambda_2^4+4)-$$

$$-a_9\gamma^4(70\kappa^4\lambda_2^8-45\kappa^2\lambda_2^4+1)+a_{10}\kappa^2\lambda_2^2\gamma^5(56\kappa^2\lambda_2^4-18)-$$

$$-a_{11}\kappa^2\gamma^6(28\kappa^2\lambda_2^4-3)+a_{12}8\kappa^4\lambda_2^2\gamma^7-a_{13}\kappa^4\gamma^8 \quad ,$$

$$\beta_1^{45} = -(1-\nu)\frac{\lambda_2^2+\lambda_1^2}{16\lambda^2} \quad ,$$

$$\beta_3^{45} = (1-\nu)/\lambda^2\left[a_3\kappa\lambda_2^6-a_4 3\kappa\lambda_2^4\gamma+a_5 3\kappa\lambda_2^2\gamma^2-a_6\kappa\gamma^3\right] \quad ,$$

$$\beta_5^{45} = (1-\nu)/\lambda^2\left[-a_4\lambda_2^6(\kappa^2\lambda_2^4-1)+a_5\lambda_2^4\gamma(5\kappa^2\lambda_2^4-3)-a_6\lambda_2^2\gamma^2(10\kappa^2\lambda_2^4-3)+\right.$$

$$\left.+a_7\gamma^3(10\kappa^2\lambda_2^4-1)-a_8 5\kappa^2\lambda_2^2\gamma^4+a_9\kappa^2\gamma^5\right] \quad ,$$

$$\beta_7^{45}=(1-\nu)/\lambda^2\left[a_5\kappa\lambda_2^{10}(\kappa^2\lambda_2^4-2)-a_6\lambda_2^8\kappa\gamma(7\kappa^2\lambda_2^4-10)+a_7\kappa\lambda_2^6\gamma^2(21\kappa^2\lambda_2^4-20)-\right.$$

$$-a_8\lambda_2^4\kappa\gamma^3(35\kappa^2\lambda_2^4-20)+a_9\kappa\lambda_2^2\gamma^4(35\kappa^2\lambda_2^4-10)-a_{10}\kappa\gamma^5(21\kappa^2\lambda_2^4-2)+$$

$$\left.+a_{11}7\kappa^3\lambda_2^2\gamma^6-a_{12}\kappa^3\gamma^7\right] \quad ,$$

$$\beta_2^{53} = \rho^2(e_1-2e_2)-2\gamma\left[a_3\lambda_2^2-a_4\gamma\right] \quad ,$$

$$\beta_4^{53} = -\rho^3(e_2-2e_3)-2\gamma\left[-a_4\kappa\lambda_2^6+a_5 3\kappa\lambda_2^4\gamma-a_6 3\kappa\lambda_2^2\gamma^2+a_7\kappa\gamma^3\right] \quad ,$$

$$\beta_6^{53} = \rho^4(e_3-2e_4)-2\gamma\Big[a_5\lambda_2^6(\kappa^2\lambda_2^4-1)-a_6\lambda_2^4\gamma(5\kappa^2\lambda_2^4-3)+a_7\lambda_2^2\gamma^2(10\kappa^2\lambda_2^4-3)-$$

$$-a_8\gamma^3(10\kappa^2\lambda_2^4-1)+a_9 5\kappa^2\lambda_2^2\gamma^4-a_{10}\kappa^2\gamma^5\Big] \ ,$$

$$\beta_8^{53} = -\rho^5(e_4-2e_5)-2\gamma\Big[-a_6\kappa\lambda_2^{10}(\kappa^2\lambda_2^4-2)+a_7\kappa\lambda_2^8\gamma(7\kappa^2\lambda_2^4-10)-$$

$$-a_8\kappa\lambda_2^6\gamma^2(21\kappa^2\lambda_2^4-20)+a_9\kappa\lambda_2^4\gamma^3(35\kappa^2\lambda_2^4-20)-a_{10}\kappa\lambda_2^2\gamma^4(35\kappa^2\lambda_2^4-10)+$$

$$+a_{11}\kappa\gamma^5(21\kappa^2\lambda_2^4-2)-a_{12}7\kappa^3\lambda_2^2\gamma^6+a_{13}\kappa^3\gamma^7\Big] \ ,$$

$$\beta_1^{54} = -\lambda^2\,\frac{\lambda_2^2+\lambda_1^2}{8} \ ,$$

$$\beta_3^{54} = 2\lambda^2\Big[a_3\kappa\lambda_2^6-a_4 3\kappa\lambda_2^4\gamma+a_5 3\kappa\lambda_2^2\gamma^2-a_6\kappa\gamma^3\Big] \ ,$$

$$\beta_5^{54} = 2\lambda^2\Big[-a_4\lambda_2^6(\kappa^2\lambda_2^4-1)+a_5\lambda_2^4\gamma(5\kappa^2\lambda_2^4-3)-a_6\lambda_2^2\gamma^2(10\kappa^2\lambda_2^4-3)+$$

$$+a_7\gamma^3(10\kappa^2\lambda_2^4-1)-a_8 5\kappa^2\lambda_2^2\gamma^4+a_9\kappa^2\gamma^5\Big] \ ,$$

$$\beta_7^{54} = 2\lambda^2\Big[a_5\kappa\lambda_2^{10}(\kappa^2\lambda_2^4-2)-a_6\kappa\lambda_2^8\gamma(7\kappa^2\lambda_2^4-10)+a_7\kappa\lambda_2^6\gamma^2(21\kappa^2\lambda_2^4-20)-$$

$$-a_8\kappa\lambda_2^4\gamma^3(35\kappa^2\lambda_2^4-20)+a_9\kappa\lambda_2^2\gamma^4(35\kappa^2\lambda_2^4-10)-a_{10}\kappa\gamma^5(21\kappa^2\lambda_2^4-2)+$$

$$+a_{11}7\kappa^3\lambda_2^2\gamma^6-a_{12}\kappa^3\gamma^7\Big] \ ,$$

$$\beta_1^{55} = \frac{-1}{\kappa(1-\nu)} \ ,$$

$$\beta_3^{55} = \rho^2(e_1-4e_2+4e_3)+2(1-\nu)\Big[-a_3\lambda_2^4+a_4 2\lambda_2^2\gamma-a_5\gamma^2\Big] \ ,$$

$$\beta_5^{55} = -\rho^3(e_2-4e_3+4e_4)+2(1-\nu)\Big[a_4\kappa\lambda_2^8-a_5 4\kappa\lambda_2^6\gamma+a_6 6\kappa\lambda_2^4\gamma^2-$$

$$-a_7 4\kappa\lambda_2^2\gamma^3+a_8\kappa\gamma^4\Big] \ ,$$

$$\beta_7^{55} = \rho^4(e_3-4e_4+4e_5)+2(1-\nu)\Big[-a_5\lambda_2^8(\kappa^2\lambda_2^4-1)+a_6\lambda_2^6\gamma(6\kappa^2\lambda_2^4-4)-$$

$$-a_7\lambda_2^4\gamma^2(15\kappa^2\lambda_2^4-6)+a_8\lambda_2^2\gamma^3(20\kappa^2\lambda_2^4-4)-a_9\gamma^4(15\kappa^2\lambda_2^4-1)+$$

$$+a_{10}6\kappa^2\lambda_2^2\gamma^5-a_{11}\kappa^2\gamma^6\Big] \ . \qquad (J.78)$$

The constants defined in section J.2 also apply to this section. Other constants that are introduced are:

$$r^{-1} = -\left[\alpha^2+\frac{2}{\kappa(1-\nu)}\right]^{-1/2} \ ,$$

$$r^{-1} \simeq -\alpha^{-1}\sum_{n=0}^{\infty}e_n(-1)^n\left(\frac{\rho}{\alpha^2}\right)^n \ , \ \rho = \frac{2}{\kappa(1-\nu)} \ . \qquad (J.79)$$

As mentioned at the beginning of this appendix, the infinite integrals are divided into two parts. The portion from A to infinity is integrated in closed form. This part can be written as,

$$\int_A^{\infty} I_{ij}\cos\alpha(t-y)d\alpha \ , \quad i=3,\ j=3;\ i=4,5,\ j=4,5 \ ,$$

$$\int_A^{\infty} I_{ij}\sin\alpha(t-y)d\alpha \ , \quad i=3,\ j=4,5;\ i=4,5,\ j=3 \ . \qquad (J.80)$$

This integral for I_{ij} of the form given by Eqns. J.61-63 is evaluated in section J.4. The following expressions are used in Eqns. 5.109-111.

$$\bar{I}_{33} = \left\{\sum_{n=2}^{4}\left[\beta_{2n-1}^{33}+(\lambda_2/\lambda)^2\beta_{2n-2}^{34}\right]+\sum_{n=5}^{\infty}-e_n(-1)^n\rho^n\right\} \times$$

$$\times\left\{(-1)^n\frac{(t-y)^{2n-2}}{(2n-2)!}\ln|t-y| + \bar{F}_c(2n-1)\right\} +$$

$$+\left\{\sum_{n=1}^{4}\left[\beta_{2n-1}^{33}+(\lambda_2/\lambda)^2\beta_{2n-2}^{34}\right]+\sum_{n=5}^{\infty}-e_n(-1)^n\rho^n\right\}\times$$

$$\times(-1)^{n+1}\frac{(t-y)^{2n-2}}{(2n-2)!}F_c(1)\ , \tag{J.81}$$

$$\bar{I}_{34}=\sum_{n=1}^{4}\beta_{2n}^{34}\left\{(-1)^{n+1}\frac{(t-y)^{2n-1}}{(2n-1)!}F_c(1)+\bar{F}_s(2n)+(-1)^n\frac{(t-y)^{2n-1}}{(2n-1)!}\ln|t-y|\right\}, \tag{J.82}$$

$$\bar{I}_{35}=\left\{\sum_{n=1}^{4}\beta_{2n}^{35}+\sum_{n=5}^{\infty}n(-1)^n\rho^n[e_n-2e_{n+1}]\right\}\times$$

$$\times\left\{(-1)^n\frac{(t-y)^{2n-1}}{(2n-1)!}\ln|t-y|+\bar{F}_s(2n)+(-1)^{n+1}\frac{(t-y)^{2n-1}}{(2n-1)!}F_c(1)\right\}\ , \tag{J.83}$$

$$\bar{I}_{43}=-\left\{\sum_{n=1}^{3}\left[\beta_{2n}^{43}+(\lambda_2/\lambda)^2\beta_{2n-1}^{44}\right]\right\}\times$$

$$\times\left\{(-1)^n\frac{(t-y)^{2n-1}}{(2n-1)!}\ln|t-y|+\bar{F}_s(2n)+(-1)^{n+1}\frac{(t-y)^{2n-1}}{(2n-1)!}F_c(1)\right\} \tag{J.84}$$

$$\bar{I}_{4j}=\sum_{n=2}^{4}\beta_{2n-1}^{4j}\left\{(-1)^n\frac{(t-y)^{2n-2}}{(2n-2)!}\ln|t-y|+\bar{F}_c(2n-1)\right\}+$$

$$+\sum_{n=1}^{4}\beta_{2n-1}^{4j}(-1)^{n+1}\frac{(t-y)^{2n-2}}{(2n-2)!}F_c(1)\ ,\quad j=4,5\ , \tag{J.85}$$

$$\bar{I}_{53}=\left\{\sum_{n=1}^{4}\left[\beta_{2n}^{53}-(\lambda_2/\lambda)^2\beta_{2n-1}^{54}\right]+\sum_{n=5}^{\infty}(-1)^n\rho^n(e_{n-1}-2e_n)\right\}\times$$

$$\times\left\{(-1)^n\frac{(t-y)^{2n-1}}{(2n-1)!}\ln|t-y|+\bar{F}_s(2n)+(-1)^{n+1}\frac{(t-y)^{2n-1}}{(2n-1)!}F_c(1)\right\}\ , \tag{J.86}$$

$$\bar{I}_{54}=\sum_{n=2}^{4}\beta_{2n-1}^{54}\left\{\bar{F}_c(2n-1)+(-1)^n\frac{(t-y)^{2n-2}}{(2n-2)!}\ln|t-y|\right\}+$$

$$+ \sum_{n=1}^{4} \beta_{2n-1}^{54} (-1)^{n+1} \frac{(t-y)^{2n-2}}{(2n-2)!} F_c(1) \quad , \tag{J.87}$$

$$\bar{I}_{55} = \left\{ \sum_{n=2}^{4} \beta_{2n-1}^{55} + \sum_{n=5}^{\infty} (-1)^n \rho^n (e_{n-1} - 4e_n + 4e_{n+1}) \right\} \times$$

$$\times \left\{ \bar{F}_c(2n-1) + (-1)^n \frac{(t-y)^{2n-2}}{(2n-2)!} \ln|t-y| \right\} +$$

$$+ \left\{ \sum_{n=1}^{4} \beta_{2n-1}^{55} + \sum_{n=5}^{\infty} (-1)^n \rho^n (e_{n-1} - 4e_n + 4e_{n+1}) \right\} (-1)^{n+1} \frac{(t-y)^{2n-2}}{(2n-2)!} F_c(1) \quad . \tag{J.88}$$

J.4 Integrals From A to Infinity

We need expressions for

$$\int_A^{\infty} \frac{\cos\alpha(t-y)}{\alpha^{2n-1}} \, d\alpha \quad , \tag{J.89}$$

$$\int_A^{\infty} \frac{\sin\alpha(t-y)}{\alpha^{2n}} \, d\alpha \quad , \quad A>0, \; n>0 \quad . \tag{J.90}$$

These integrals come from the large α expansion of the Fredholm kernels. Note that for n>0 the limit for x→0 has been taken under the integral sign. The n=0 cases of Eqns. J.89,90, for which the limit must be taken after integration, are respectively demonstrated below,

$$\lim_{x \to 0} \int_0^{\infty} \alpha e^{-\alpha x} \cos\alpha(t-y) \, d\alpha = \frac{-1}{(t-y)^2} \quad , \tag{J.91}$$

$$\lim_{x \to 0} \int_0^{\infty} e^{-\alpha x} \sin\alpha(t-y) \, d\alpha = \frac{1}{t-y} \quad . \tag{J.92}$$

The $1/\alpha$ case of Eqn. J.89 has a log singularity, the $1/\alpha^2$ term of J.90 becomes $(t-y)\ln|t-y|$ and so on. This is shown in the general expressions presented below:

$$\int_A^\infty \frac{\cos\alpha(t-y)}{\alpha^{2n-1}}\,d\alpha = \bar{F}_c(2n-1) + (-1)^{n+1}\frac{(t-y)^{2n-2}}{(2n-2)!}F_c(1) +$$

$$+ (-1)^n \frac{(t-y)^{2n-2}}{(2n-2)!}\ln|t-y| \quad , \tag{J.93}$$

$$\int_A^\infty \frac{\sin\alpha(t-y)}{\alpha^{2n}}\,d\alpha = \bar{F}_s(2n) + (-1)^{n+1}\frac{(t-y)^{2n-1}}{(2n-1)!}F_c(1) +$$

$$+ (-1)^n \frac{(t-y)^{2n-1}}{(2n-1)!}\ln|t-y| \quad , \tag{J.94}$$

where

$$F_c(1) = -\gamma_e - \ln(A) - \int_0^{A|t-y|}\frac{\cos x - 1}{x}\,dx \quad , \tag{J.95}$$

$$\bar{F}_c(2n-1) = \sum_{j=1}^{n-1}(-1)^{j+1}\frac{(t-y)^{2j-2}(2n-1-2j)!}{(2n-2)!A^{2n-2j}}\cos A(t-y) +$$

$$+ \sum_{j=1}^{n-1}(-1)^{j}\frac{(t-y)^{2j-1}(2n-2-2j)!}{(2n-2)!A^{2n-2j-1}}\sin A(t-y) \quad , \tag{J.96}$$

$$\bar{F}_s(2n) = \sum_{j=1}^{n}(-1)^{j+1}\frac{(t-y)^{2j-2}(2n-2j)!}{(2n-1)!A^{2n-2j+1}}\sin A(t-y) +$$

$$+ \sum_{j=1}^{n-1}(-1)^{j+1}\frac{(t-y)^{2j-1}(2n-1-2j)!}{(2n-1)!A^{2n-2j}}\cos A(t-y) \quad . \tag{J.97}$$

The constant in Eqn. J.95 is Euler's constant, γ_e =.57721566490153. This expression is a cosine integral, $Ci[A|t-y|]$, with the log term taken out.